Solar cooling with absorption chillers: Control strategies and transient chiller performance

vorgelegt von

Diplom-Ingenieur
Paul Kohlenbach

Von der Fakultät III – Prozesswissenschaften
der Technischen Universität Berlin
zur Erlangung des akademischen Grades

Doktor der Ingenieurwissenschaften
- Dr.-Ing. -

genehmigte Dissertation.

Promotionsausschuss:

Vorsitzender:	Prof. Dr.-Ing. G. Tsatsaronis
Berichter:	Prof. Dr.-Ing. F. Ziegler
Berichter:	Prof. Dr.-Ing. A. Luzzi

Tag der wissenschaftlichen Aussprache: 13.01.2006

Berlin 2006
D83

Acknowledgements

This thesis has been conducted on the solar cooling system and its components at Phönix SonnenWärme AG in Berlin, Germany, during the author's employment as director of the research and development department. Part of the work on this thesis has been co-financed by the European Union and the federal state of Berlin within the UEP-programme (contract. No. 10530 UEP OÜ2).

First and foremost I would like to thank my supervisor, Prof. Dr.-Ing. Felix Ziegler, for his constant support and help throughout this work. His competence combined with the skill to always ask the right questions has fuelled my scientific curiosity and inspired me a lot of times. It was extremely enjoyable and beneficial to work with him, especially during the last months of this thesis work. I also would like to thank Prof. Ziegler for providing me with an office room for part of the thesis work.

A special thanks goes to Raoul von der Heydt from Phönix SonnenWärme AG for his generous support during my employment there. His interest and open attitude towards this thesis has been a base of my work.

I would like to thank Volker Clauss, Oliver Tamm and Enno Wiegand for contributing to this thesis.

Niels Braunschweig is gratefully acknowledged for his intensive proof-reading and comments.

Abstract

This thesis reports on improvements of the state of the art in controlling solar cooling systems with absorption chillers. In this context, two main approaches are being presented.

In the first approach, control strategies for the system circuits are being presented and discussed. Various possibilities of temperature and mass flow control for the external circuits of hot, cooling and chilled water are being described in this thesis in a state of the art overview. Guidelines for the incorporation of the storage tank in the system control are being given with regard to reference layer and hysteresis temperature. The solar circuit as the most complex circuit is being investigated deeper. A differential, a temperature-based and an insolation-based mass flow control strategy for the heat carrier fluid in this circuit are being tested in TRNSYS simulations and experiments with regard to the overall system performance. There, the focus of attention are the key figures of cooling capacity and power consumption which are being integrated and combined in a daily yield factor. The yield factor is being used for the comparison of the individual strategies in simulation and experiment. The ambition is to find the strategy with the lowest power consumption and simultaneously biggest cooling effect. In the comparison of simulation and experiment, good agreement has been found for both the dynamic course of the variables as well as the integrated energy balance expressed in the yield factor. From the simulations, the insolation-based strategy (INSOL) has been found to perform best at cloudless conditions regarding the yield factor. An improvement of 6% in the yield factor for the insolation-based strategy compared to the other strategies has been found in simulations. From the experimental comparison of the dynamic behaviour, the temperature-difference based control strategy (TDIFF) has been found to yield the best performance. However, from the experimental comparison of the integrated energy balances for all three control strategies a clear tendency towards one strategy cannot be seen. Several improvements on the experimental methodology have been derived from this result.

The second approach describes investigations on the main system component, the absorption chiller. Two different methods of determining the thermal transfer behaviour are being presented, an experimental identification and a theoretical simulation method. For both methods, the transfer function between hot water input and chilled water output is being determined as necessary for a chilled water temperature control. Using the experimental method, transfer functions for the three-way valve in the hot water circuit and the absorption chiller have been determined using the system identification method of Ljung. With the combined transfer functions of valve and chiller a chilled water temperature controller has been designed and successfully tested on a solar cooling system. The theoretical simulation method includes the development of a mathematical model of the transient internal heat and mass transfer of the chiller. A dynamic simulation model with transient behaviour implemented via thermal and mass storage terms as well as delay times is being presented in this thesis. General functionality and internal consistency of

the model have been demonstrated and the thermodynamic calculations of the model have been found to reproduce the real chiller with sufficient accuracy. The focus of attention has been laid on the dynamic model performance. Using experimental data for verification, it has been proven that dynamic effects are being accounted for in a very satisfying way. Maximum dynamic deviations between vessel temperatures in simulation and reality are in the magnitude of approximately 2%. The model developed in this thesis has been designed for the Phönix 10 kW absorption chiller but can easily be adapted to other LiBr/water absorption chillers. It can be used for the development of a temperature control strategy or as a useful tool in the overall design process of absorption chillers.

This thesis work extends the knowledge-base on control strategies of solar cooling systems using absorption chillers. A foundation for energy-saving operation of such systems has been laid by the research on solar circuit control and further research paths towards this goal have been paved. A helpful tool for controller design and general performance analysis of absorption chillers has been made available with the dynamic model presented. The model is a significant improvement of present steady-state simulations of absorption chillers.

Kurzzusammenfassung

In der vorliegenden Dissertation werden neueste Erkenntnisse und Methoden zur Regelung solarer Kühlsysteme mit Absorptionskälteanlagen vorgestellt. Schwerpunkte werden dabei auf die Untersuchung von Regelungsvarianten für den solarthermischen Teil eines solchen Systems sowie die Ermittlung des transienten Übertragungsverhaltens der Absorptionskälteanlage mit dem Ziel der Entwicklung einer Kaltwasserregelung gelegt. Die Arbeit kann in zwei hauptsächliche Teile aufgeteilt werden.

Im ersten Teil wird zunächst ein allgemeiner Stand der Technik zu Regelstrategien für die Systemkreise von Heiss-, Kühl- und Kaltwasser vorgestellt. Die Einbindung eines Heisswasserspeichers wird diskutiert hinsichtlich der Wahl der Speicherreferenzschicht für eine Temperaturdifferenzregelung. Weiterhin werden vertiefende Untersuchungen zu Regelstrategien des Solarkreises präsentiert. Ziel dabei ist, eine möglichst stromsparende und gleichzeitig thermisch ergiebige Regelstrategie zu finden. Zu diesem Zwecke werden drei verschiedene Varianten einer Massenstromregelung des Wärmeträgers im Solarkreis verglichen. Diese beinhalten eine Konstantmassenstromregelung sowie zwei variable Massenstromregelungen, abhängig von Temperaturdifferenz bzw. solarer Einstrahlung. Alle drei Regelvarianten werden sowohl experimentell als auch mittels TRNSYS-Simulationen getestet und verglichen. Als Vergleichsgröße wird der Quotient aus gelieferter Kälteenergie und Stromverbrauch, die sogenannte Arbeitszahl, verwendet. Im simulierten Vergleich liefert die einstrahlungsgeführte Massenstromregelung eine um 6 % größere Arbeitszahl als die beiden anderen Strategien. Aus den experimentellen Ergebnissen läßt sich eine solch klare Tendenz jedoch nicht ablesen. Aufgrund eines relativ hohen Meßfehlers sowie verschiedener anderer Einflüsse liegen die sich experimentell ergebenden Unterschiede zwischen den Strategien im Bereich des Fehlerbalkens. Als Konsequenz werden in dieser Arbeit Verbesserungen der experimentellen Methodik abgeleitet und diskutiert.

Im zweiten Teil der Arbeit wird die Absorptionskälteanlage als Hauptkomponente eines solaren Kühlsystems hinsichtlich ihres thermischen Übertragungsverhaltens untersucht. Hauptziel dabei ist die Bestimmung der anlagenbedingten Abhängigkeit der Kaltwasseraustrittstemperatur von der Heisswassereintrittstemperatur, ausgedrückt durch die Übertragungsfunktion. Es werden zwei verschiedene Methoden zur Bestimmung der Übertragungsfunktion für eine Kaltwassertemperaturregelung angewendet: eine experimentelle Identifikation sowie eine theoretische Simulation. Die experimentelle Methode beinhaltet die Ermittlung der Übertragungsfunktion aus Messdaten der Kälteanlage nach einem von Ljung vorgestellten Verfahren. Dabei werden einzelne Übertragungsfunktionen für alle in die Regelung involvierten Komponenten ermittelt und in einer Gesamtübertragungsfunktion zusammengefasst. Mit dieser wurde für das vorgestellte System eine Kaltwasserregelung entwickelt und erfolgreich getestet. Nachteil der experimentellen Methode ist ihr eingeschränkter Anwendungsbereich durch die

Festlegung auf bestimmte Parameter. Dieses Manko kann durch eine theoretische Simulation behoben werden. Im Rahmen dieser Dissertation wird ein theoretisches Modell einer LiBr/Wasser Absorptionskälteanlage vorgestellt, welches das transiente Verhalten einer solchen Anlage abbildet. Dazu wurden Wärme- und Massenspeicher sowie zeitliche Verzögerungsglieder in die Energie- und Stoffbilanzen der Kälteanlage integriert und das Modell auf allgemeine Funktionalität und einwandfreie Wiedergabe der internen Prozesse getestet. Dabei wurde der Schwerpunkt auf korrektes dynamisches Verhalten gelegt, stationäre Übereinstimmung war nur sekundäres Ziel der Arbeit. Das Modell wurde mittels experimentellen Daten getestet und eine sehr gute dynamische Übereinstimmung zwischen Simulation und Realität festgestellt. Maximale zeitliche Verschiebungen zwischen gemessenen und simulierten Daten von 25 s wurden ermittelt. Verglichen mit der Gesamtzeit zum Erreichen eines stationären Zustandes liegt diese Verschiebung in der Größenordnung von 2 % und kann vernachlässigt werden. Das vorgestellte Modell bildet die 10 kW Absorptionskälteanlage der Phönix SonnenWärme AG ab, kann aber problemlos an andere Kälteanlagen angepasst werden. Es kann zum einen zur Bestimmung der Übertragungsfunktion und somit zur Entwicklung von Reglern verwendet werden, bietet zum anderen aber auch die Möglichkeit, konstruktive Veränderungen an bestehenden Kälteanlagen ohne großen apparativen Aufwand zu testen. Dies gilt auch für die Neuentwicklung von Absorptionskälteanlagen. Insbesondere für transiente Simulationen von solaren Kühlsystemen bietet das entwickelte dynamische Modell eine interessante Alternative. Die stark instationäre Betriebscharakteristik von solaren Kühlsystemen kann durch die Verwendung des dynamischen Modells wesentlich besser reproduziert werden als durch die bisher verwendeten stationären Modelle.

Nomenclature

Variables

Symbol	Definition	Unit
a	Yield factor	kW_{th}/kW_{el}
A	Area	m^2
B	Duehring factor	-
c	Specific heat capacity	kJ/kgK
D	Density	kg/m^3
G	Transfer function	-
h	Specific enthalpy	kJ/kg
H	Enthalpy	kJ
k_1	collector loss coefficient	W/m^2K
k_2	collector loss coefficient	W/m^2K^2
K	Gain of controlled system	-
l	Solution enthalpy	kJ/kg
$\dot{m}$	Mass flow	kg/s
m, M	Mass	kg
n	Fan speed	1/min
N	Digital on/off signal	-
p	Pressure	Pa
P	Power	W
$\dot{q}$	Specific heat flow	kW/kg
q	Specific heat	kJ/kg
$\dot{Q}$	Heat flow	kW
Q	Heat	kJ
r	Evaporation enthalpy	kJ/kg
s	Gradient in characteristic equation, mean error	kW/K, -
t	External temperature of chiller	°C/K
$\hat{t}$	time	s
T	Internal temperature of chiller	°C/K
U	Voltage	V
$\dot{V}$	Volume flow rate	m^3/s
x	Concentration of LiBr/water solution	kgLiBr/kgSolution
y	Control signal	V

Greek

Symbol	Definition	Unit
α	Heat transfer coefficient	W/m²K
η	Efficiency	-
ρ	Density	kg/m³
Δ	Temperature Difference	°C or K
$\Delta\Delta t$	Characteristic temperature difference	°C or K

Subscripts

Symbol	Definition	Symbol	Definition
1, 2, 3,…	State points, circuit numbers	meas	Measured value
a	Air	min	Minimum value
abs	Absorber (collectors)	MAG	Membrane expansion tank
av	Average	o	Output
amb	Ambient	op	Operating
A	Absorber (chiller)	pc	At constant pressure
AC	Cooling water circuit	PS	Storage tank sensor position
B	Storage circuit	req	Required
c	Cold, corrected	rp	Refrigerant pump
cal	Calibrated	sol,s	Strong solution leaving generator
C	Condenser (chiller)	sol,w	Weak solution leaving absorber
el	Electrical	set	Set point for control
ext	External	sim	Simulated
E	Evaporator (chiller) or evaporator circuit	sp	Solution pump
f	Fan	st	Storage tank
F	Heat transfer fluid	stg	Storage circuit to generator
FK	Flat plate collectors	S	Solution or solar circuit
g	Generator (chiller)	th	Thermal
gt	Global tilted (insolation)	tot	Total
G, Ge	Generator circuit	ts	Time step
h	Hot	UR	U-shaped tube
i	Input	v	Vapour
K	Collector field circuit	VE	Valve
KT	Cooling tower	VK	Evacuated tube collectors
l	Layer of storage tank	w	Water
max	Maximum value	wb	Wet bulb

Table of contents

1 Introduction

Today's intensive use of fossil fuels for power generation, transport and heating has severe consequences for the earth's ecosystem. The effects of global warming have already started to affect our daily lives and will do so even stronger in the future. Climate experts expect an average global temperature rise between 1.5K and 6K until the end of this century [Lebert 2005]. As a result, climate-related natural disasters are expected to take place more often and with more drastic consequences. The hurricanes 'Katrina' and 'Rita' which devastated the U.S. states of Louisiana and Texas in September 2005 give an idea about the power of such impacts. Apart from the local ecological damage caused by the hurricanes, surprisingly strong global economic consequences could be observed. With almost no delay, oil prices reached the same level as during the oil crisis in the late seventies, namely over US$ 65 per barrel. Figure 1.1 shows the spot price development of Brent Crude oil between Sept. 1st 2004 and Sept. 24th 2005. The peak price caused by the hurricanes is clearly visible.

Figure 1.1. Spot price development of Brent Crude oil between September 1st 2004 and September 24th 2005 [WTRG 2005].

The hurricane experience shows how sensitive the current global system of energy supply reacts on external disturbances. It can be expected that the naturally occurring shortage of the fossil fuel sources in combination with an increased number of such climate-related incidents will increase the cost for energy even further. However, despite rising energy prices the global primary energy

consumption still increases by approximately 2% per year. A large contributor to this worldwide rise is China with an average energy consumption rise of 7% p.a. between 1999 and 2004 [BP 2004].

A significant contribution to the primary energy consumption of first and second world countries is being made by the rapidly increasing use of electrical air-conditioning units worldwide. Worldwide sales of room air-conditioners of all types amount to approximately 50 Mio. units p.a., with the U.S., China and Japan being the three main markets [BSRIA 2002]. In the U.S., air-conditioning accounts for 180 billion kWh or 14% of the total electricity consumption, resulting in CO_2 emissions of 110.000 Mio tons per year. In the OECD countries, the electrical energy consumption for residential space cooling accounts for 6% of the total consumption. In Europe, commercial air-conditioning has a share of 4% of the total annual electricity consumption while residential air-conditioning accounts only for 0.4%. Although the latter number is still comparatively low, Europe has seen a seven-fold increase of residential air-conditioning sales between 1990 and 2004 [EIA 2005], [Harrington 2003].

The reasons for the growing use of air-conditioning are twofold. First, the comfort demands from both building users and owners have increased. The standard of living of the present generation is higher than in the past, especially in private buildings. In the U.S., the share of households with central air-conditioning has risen from 23% of all households in 1978 to 55% in 2001[EIA 2005], [Harrington 2003]. Second, the trend towards commercial buildings with large glazed facades has increased the internal heat load to be removed by air-conditioning. Third, electricity prices are comparatively low. The additional cost caused by the use of air-conditioning units is not in the order of magnitude to influence the consumer behaviour significantly.

The obvious consequence of this growing air-conditioning use is increased power consumption. Recently, Europe has seen a number of power grid breakdowns in summer caused by a seasonal peak use of air-conditioners in combination with reduced power plant output. Outside Europe, another consequence of excessive air-conditioning are locally higher temperatures in metropolitan areas, commonly referred to as heat islands. As a part, these inner-city temperature peaks are the result of heat conveyed from building inside to outside, released at a temperature level above ambient temperature. Both these consequences are strong arguments for alternative air-conditioning or cooling methods.

The latest development of absorption chillers with small cooling capacities around 10 kW now provides such an alternative. Solar cooling systems using these chillers can provide cooling comfort with reduced power consumption and CO_2 emissions. However, despite their ecological advantages, solar cooling systems also have to yield an economic advantage for the customer. At present, investment costs are higher for solar cooling systems than for comparable compressor-based cooling units. Thus, the full potential of solar cooling is far from being realised, however building owners, occupants and architects are becoming more and more sensitive towards energy issues. The economic advantage of solar cooling systems results from much lower operation costs which include the costs for power, water and maintenance. Especially the electrical power consumption of a solar cooling system influences the economics strongly. The main idea of such a system is to use thermal energy for most of the process work, thus the remaining power consumption should be kept as low as possible. The power consuming components of a solar

cooling system include pumps, fans and control units. The latter can usually be neglected, but pumps and especially cooling tower fans can have a power consumption in the range of few hundred Watts. Their operation time and speed are relevant parameters for the total power consumption of the system.

The first part of this thesis approaches the problem of controlling the system circuits in a way to minimize power consumption while maintaining the desired operating conditions of the chiller. The need for such a control arises from the influence of the insolation which is the most transient input parameter of a solar cooling system. Insolation variations can be accounted for by adjusting the mass flows of the heat carrier fluid in the relevant system circuits. In this context, three different control strategies for the hot water mass flow in solar and storage circuit are being presented and discussed regarding power consumption, thermal output and operation time. The control strategies are implemented in a TRNSYS simulation model of the solar cooling system and simulation results are being presented. Also, results from the experimental operation of a solar cooling system using the same control strategies are presented and compared to the simulations. Furthermore, control strategies of the cooling and chilled water circuit are presented and discussed as well.

The second part of this thesis investigates further into the main component of a solar cooling system, the absorption chiller. Embedded in a solar cooling system, its operation is highly non-constant due to the transient system inputs. Varying hot or cooling water inlet temperatures will result in varying chilled water outlet temperatures as well. For applications where a constant chilled water temperature is desired, a control algorithm has to be implemented which maintains a set temperature value or adapts the chilled water temperature to the actual cooling demand. This temperature control can be realised using an industrial controller with the respective parameters which are determined by the transfer behaviour of the chiller. The second thesis part presents two different methodologies of identifying the transfer behaviour of an absorption chiller with regard to the transfer function: an experimental identification as well as a theoretical simulation of the chiller. Both methods are being applied to a 10kW water/LiBr absorption chiller and a comparison of simulated and experimental transfer functions is presented.

If not otherwise stated, the work presented in this thesis has been conducted on the solar cooling system and its components at Phönix SonnenWärme AG in Berlin, Germany, as part of the author's work for the company. Phönix SonnenWärme AG started investigating into solar cooling technology in 2001. A joint research project has been conducted from 2002 to 2004 together with partners Technical University of Berlin, Bavarian Centre for Applied Energy Research (ZAE Bayern) and the Institute for Rehabilitation and Modernization of Buildings Berlin (IEMB). Two prototype generations of a 10 kW Li/Br-water absorption chiller have been built and tested during the project. The experiments conducted in this thesis have been performed on the first prototype generation of the chiller. From 2005 to 2006, the third chiller generation will be undergoing intensive field testing at locations in Germany and Switzerland. Commercial market entry is scheduled for the second half of 2006.

The thesis comprises of the following chapters:

Chapter 2 contains an overview on solar cooling technologies with regard to the design options. Fundamentals, a historical retrospective and an overview on present research are being presented. The solar cooling system used for the experiments in this thesis is described in detail in this chapter. This includes a comprehensive description of each system circuit and all its components. The energy balance calculations applied for the experiments are presented.

Chapter 3 describes the functionality of control strategies for subsystems and components of a solar cooling system. General fundamentals and the state of the art are being presented for control strategies of hot, cooling and chilled water circuit. This includes mass flow control in solar and storage circuit using three different control strategies, fan speed control of an open wet cooling tower with regard to the cooling water temperature and temperature control of the chilled water outlet temperature.

Chapter 4 presents a closer look on the different control strategies for the hot water mass flow in solar and storage circuit. The experimental application of the control strategies introduced in chapter 3 is being described and experimental results are being presented. Also, simulations of the solar cooling system using the same control strategies are being described and the simulation results are being compared to the experimental results.

Chapter 5 reports two different methods of determining the transfer function of an absorption chiller. The first method is an experimental system identification which has been performed on the absorption chiller. The functionality of this method as well as the identification results are being presented. The second method is a theoretical simulation of the transfer behaviour based on a mathematical model of the chiller. The model development, its verification, a parameter analysis and simulation results are being presented and discussed. The transfer functions determined from experiments and simulations are being compared to each other.

Chapter 6 presents a summary and the conclusions of this thesis, discusses open problems and gives recommendations for future research.

2 Solar cooling

The sun's energy reaching the earth has an abundant energy potential. More than 3000 times of the annual world energy demand reaches the earth every year in form of solar radiation on the earth's surface. In theory, an area of 700*700 km, i.e. the size of Spain, equipped with photovoltaic cells with a net efficiency of 10% would be enough to supply the total world electricity demand. With upcoming shortages of oil and gas supplies, the solar energy potential will have to be used more intensively than at present. This applies to both solar power and heat generation. However, the sun's energy is also a major cause for the use of air-conditioning systems worldwide. A significant portion of the total heat load of buildings is caused by solar radiation entering through windows or other transparent building openings. The peak electricity demand during the summer months already causes power supply systems to work to maximum capacity.

It seems that cooling is only an electricity problem. However, there is an interesting linkage to solar thermal plants. Normally, just at the times of peaking cooling demand, large solar thermal plants are experiencing long standstill periods as the heat demand of buildings is low. The available thermal energy potential due to high solar irradiation is mostly unused during the hot season of the year. Due to the same reason, cogeneration plants and district heating power stations have to reduce their power output in summer. A large amount of thermal energy is being unused during the hot period of the year. An ideal solution is therefore the use of this surplus heat for building air-conditioning using a heat-driven - in our special case solar-driven - refrigeration process. This can be done in various ways, using solar-generated heat to drive a suitable refrigeration process. This chapter describes the varieties and application possibilities of solar cooling systems.

2.1 Historical context and present work

To improve the living conditions inside buildings, passive technologies have already been used by the ancient Greeks. The philosopher Socrates describes the correct orientation of buildings to achieve best comfort conditions in summer and winter, as recorded by the greek historian Xenophon in his "Memorabilia". Also the Iraqis built their houses traditionally in a way to use the wind as a cooling means by orienting their houses in the prevailing wind direction. The wind was channelled through ducts underneath the house and to the roof, thus cooling the building [Florides *et al.* 2002].

Active installations of solar cooling systems date back until the 19th century. Albel Pifre is reported to be the first to have produced ice in 1872 by means of a solar boiler with a steam-regenerated absorbing solution [Ziegler and Lamp 1998]. An open LiCl system was realised before 1940 in Catalania. Several solar-driven chillers were installed and operated in the 1950's throughout the world, e.g. in 1953 in Tashkent, UdSSR, with a parabolic mirror as heat source. Other examples are a water/LiBr chiller installed in 1958 in Brisbane, Australia and a complete solar house with a

solar-assisted chiller in Queensland, Australia, in 1966. Due to the energy crisis in the 1970's the interest in solar cooling applications grew rapidly, resulting in approx. 500 solar-driven air-conditioners being installed in the U.S.A. in 1976. National and international research programmes were released then, some of which still exist today, such as the IEA Solar Heating and Cooling Programme. The Task 25 of this programme, "Solar Assisted Air Conditioning of Buildings", contained active research on solar cooling demonstration applications and the development of a simulation design tool. It was conducted from June 1st 1999 until May 31st 2004 [IEA 2002].

Today, the focus of research in solar cooling is on the development of small chillers with cooling capacities around 10 kW or below. In Germany, four companies are currently involved into the commercial development of small-scale absorption. A 15 kW LiBr/water absorption chiller is being commercially sold by the company EAW in Westenfeldt. In Berlin, Phönix SonnenWärme AG has developed a 10kW LiBr/water absorption chiller for which commercial distribution is scheduled to start in 2006. The company Solarcool in Johannesberg is the commercial spin-off from a research project at the University for Applied Sciences Stuttgart. They are developing a 2.5 kW diffusion absorption chiller using water/ammonia. The Sortech AG in Halle is developing the only commercial adsorption chiller at present, a 6kW unit using advanced zeolithe technology.
Further research is being performed in Germany by the Technical University of Berlin, Institute for Energy Technology (ETA), the Bavarian Centre for Applied Energy Research (ZAE Bayern), the Fraunhofer Institute for Solar Energy Systems (ISE), the University for Applied Sciences Stuttgart, Faculty of Building Physics and the Institute for Air and Cold Technology Dresden (ILK).
Throughout Europe, small-scale chillers are under commercial development in Austria by the Joanneum Research Centre and in Sweden by the company Climatewell. Research is being performed in France by the Centre Scientifique et Technique du Bâtiment (CSTB), in Portugal by the Instituto Nacional de Engenharia, Tecnologia et Inovação (INETI) and in Sweden by the University of Goteborg. Worldwide, a small-scale chiller with 10kW cooling capacity is being developed by the Indian company Thermomax. A slightly bigger absorption chiller model with 35 kW cooling capacity is being sold by the Japanese company Yazaki.

2.2 Fundamentals

In theory, the design options for a solar-driven cooling system are manifold. A variety of solar collectors can be used as a heat source for thermally-driven refrigeration processes; photovoltaic cells or solar concentrating power generation systems can yield electricity for mechanically-driven refrigeration applications or thermo-electric cooling processes. Also, the shaft power of a solar-driven Rankine process can be used to power the compressor of a vapour compression process. Yet in this thesis only solar cooling systems using heat sources will be discussed. An output classification of solar technologies usable for heat-driven solar cooling can be made by comparing the operating temperatures as shown in Table 2.1.

Table 2.1. Temperature, concentration ratio, and tracking requirement of solar thermal collectors. Modified from [Kreetz 2001]

Technology	Operating temperature [°C]	Concentration ratio	Tracking
Solar chimney	20-80	1	-
Volumetric air collectors	50-80	1	-
Solar pond	70-90	1	-
Flat plate collectors	30-100	1	-
Evacuated tube collectors	90-200	1	-
Non-imaging concentrating collectors	100-150	1-2	-
Trough concentrators	260-400	8-80	One-axis
Dish concentrators	500-1200	800-8000	Two-axis

The operating temperature of a solar heat source determines its usability for a heat-driven refrigeration process. Such processes run at different driving temperature levels starting from approximately 50 °C, depending on working pairs and thermodynamic cycle parameters. There are some heat-driven processes which depend on a high temperature level and thus a specific heat source, otherwise their functionality is limited or the efficiency decreased. The most common combinations of solar energy source and refrigeration process used for building cooling applications are solar thermal collectors using ab- or adsorption chillers and desiccant evaporative (DEC) systems. Ab- and adsorption chillers use a heat transfer medium (usually water) in a closed loop for the extraction of the building heat, DEC systems use ambient air in an open loop as the heat transfer medium. Consequently, ab- and adsorption cooling systems are called closed systems, DEC plants are referred to as open systems.

The function principle of an absorption chiller is based on different boiling temperatures of refrigerant and a liquid sorption medium, the absorbent. External heat input causes a refrigerant to evaporate. The refrigerant steam is absorbed by the absorbent, thus diluting it. Pumped to a higher pressure level, external heat input evaporates the refrigerant steam again while the concentrated absorbent stays liquid. It flows back to the absorber, whereas the refrigerant steam condenses, passes an expansion device and evaporates again, closing the cycle.
Adsorption chillers have a similar working principle, although the sorption component is solid. Also, the cycle is not a continuous one but consists of two phases. In the evaporation phase, refrigerant steam is adsorbed by the adsorbent, thus saturating it. The adsorbent has to be cooled during this phase. In the condensation phase, the adsorbent is heated and the refrigerant evaporates again. It condenses in the same unit where it evaporated before, thus closing the cycle. In an adsorption chiller two such cycles run simultaneously with opposite operation modes. This ensures a continuous chilled water supply with fluctuating chilled water temperature.
In a DEC cycle, the evaporative cooling effect of water is being used for air-conditioning by selective humidifying and dehumidifying of the building supply air. DEC cycles allow controlled air cooling and humidifying at the same time using a rotating sorption wheel connected to both supply and return air flow. In the supply flow, fresh ambient air is being dehumidified and chilled by evaporation of water. In the return flow, the exhaust air from the building is being heated and used for the regeneration of the sorption wheel.

A differentiation between heat-driven sorption processes can also be made by the individual working pairs. For absorption processes using water as the refrigerant, sorption components include LiBr, LiCl and sulphuric acid. For ammonia as the refrigerant, water is used as sorption component. Other absorption working pairs include CO_2 as refrigerant and acetone as sorption component or R12 as refrigerant and oil as sorption component. However, the most popular working pair is LiBr/water. It has a high ratio of cooling to driving energy, is non-toxic, available in large amounts and has been industrially used for over 50 years. Nevertheless, it cannot be used for cooling applications below zero degrees and is therefore widely used for air-conditioning purposes.

Adsorption working pairs incorporate zeolithe or silicagel as sorption component and water as refrigerant. Ammonia can also be used as refrigerant for special zeolithes and activated carbon. Other combinations include activated carbon with methanol, ethanol, acetone or water as refrigerant as well as hydrogen as refrigerant in combination with metal hydroxides. Also, CO_2 as refrigerant in combination with zeolithes can be used [Ziegler 1997].

In practice, the number of combinations of solar heat source and refrigeration process to be used in a commercial application is limited due to economic and availability reasons. Not all of the solar technologies are technically mature; some of them are still in the prototype stadium. While technically a lot of combinations are possible, the cost for realising a commercial system would be too high for most of them. For example, concentrating systems still have high investment cost and are not being used frequently for solar cooling. However, due to their high output temperatures such systems can be well suited for driving a double-effect absorption process. Recent developments on fibre-optic mini-dish receivers may be an option for the future [Feuermann *et al.* 2002]. Solar chimneys are in the prototype stage and there is no application of a solar chimney being used for cooling purposes. To the author's knowledge also no application of a solar pond for cooling purposes exists. Volumetric air collectors are normally being used for open DEC processes due to their low temperature level. There, they can be a cost-effective and simple alternative.
This reduces the usable solar technologies for closed solar cooling systems to non-concentrating solar thermal collectors, such as flat plate and evacuated tube collectors. On the cooling side, the choice is limited to the commercial availability of suitable plants that have appropriate driving temperatures and cooling capacities.

In this thesis, the combination of flat plate collectors and an absorption chiller will be discussed in detail. All applications using adsorption chillers or DEC systems will not be further discussed. For a solar cooling system using adsorption technology see [Glaser 2005], for a DEC system see [Hindenburg and Henning 1999] or [Henning 2004].

2.3 Solar cooling system description

The solar cooling system used for experiments in this thesis is installed at the Phönix SonnenWärme AG in Berlin, Germany. There, it fulfils two tasks. First, it serves as a test stand for the scientific investigation of different aspects of a solar cooling system, such as different hot water sources (solar and gas heater), different collector types (flat plate and evacuated tubes) and various control strategies. Second, it is a room cooling system in everyday use for the office rooms of the company. It has been installed in 2002/2003 and is in operation since August 2003. The system was co-financed by the European Union and the federal state of Berlin within the UEP-programme (contract. No. 10530 UEP OÜ2). It consists of two solar thermal collector fields, a water/LiBr absorption chiller, a hot water storage tank, an auxiliary heating system, a wet cooling tower; chilled ceiling panels and the necessary peripheral equipment, such as pumps, valves, piping, measurement instrumentation etc. For the investigations presented in this thesis, the total system has been sub-divided into six circuits which will be described individually as follows. Figure 2.3.1 shows the circuit definition.

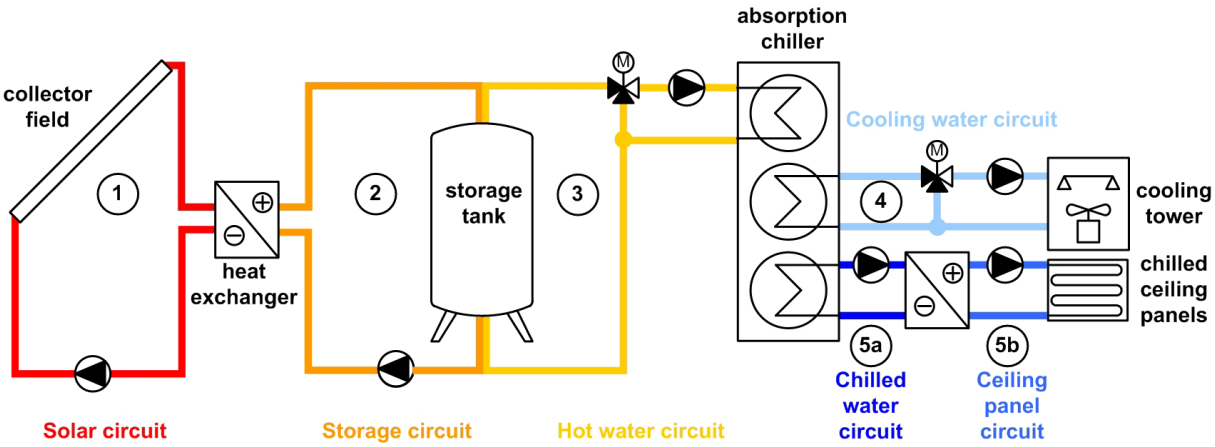

Figure 2.3.1. Circuit definition of solar cooling system.

The system is shown in detail in Figure 2.3.2. Although in everyday use, the system has been equipped with more sensors than necessary for normal operation. Temperature, flow, pressure and insolation sensors have been installed in order to calculate energy balances of the system. Also, the absorption chiller has been equipped with sufficient pressure, temperature and flow sensors in order to allow a detailed analysis of the chiller performance and detect possible optimization potentials. Figure 2.3.2 shows the hydraulic setup and the measurement sensors of the system. All details on technical data of the individual system components can be found in Appendix 8.1.

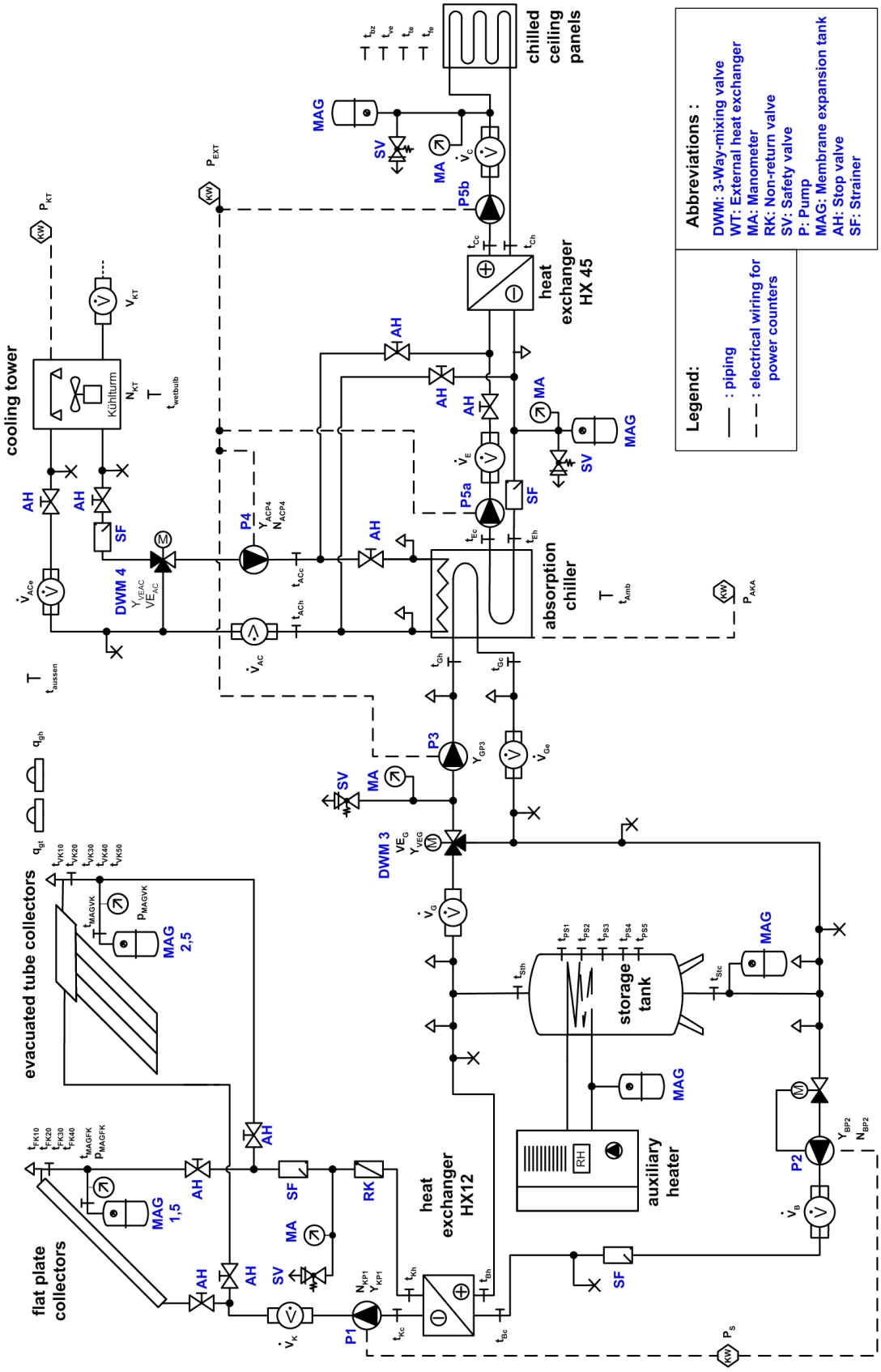

Figure 2.3.2. Hydraulic setup and component denomination of the Phönix solar cooling system (solid line: piping, dashed line: electrical wiring for power counters).

2.3.1 System circuits and components

2.3.1.1 Solar thermal circuit

Solar thermally heated hot water can be taken from either a 42 m² flat plate collector field or a 25 m² evacuated tubes collector field. Each collector field is able to supply the nominal heat flow of approximately 14 kW to the absorption chiller. Two collector fields have been installed for scientific reasons, i.e. to allow a comparison of operation performance, thermal inertia and long time behaviour of both collector types. The collectors are installed on the roof of the office building of the Phönix SonnenWärme AG in Berlin. Both the flat plate collectors and the evacuated tubes have an absorber slope of 35° and a southwest orientation of 217°.

Figure 2.3.3 shows the two collector fields mounted on the roof of the Phönix SonnenWärme AG.

Figure 2.3.3. Collector fields on steel support mounted on the roof. In the foreground the wet cooling tower can be seen. Picture by E. Wiegand.

The solar pump P1 in Figure 2.3.2 is a frequency-controlled, variable speed pump operating between 0 and 1.4 m³/h. Furthermore, the collector field loop contains a security pressure release valve, a strainer, air release valves and a non-return-valve to prevent backward flow during night time. A counter-flow plate heat exchanger HX 12 separates the antifreeze water-glycol mixture in the collector fields from pure water in the storage. It was included in order to avoid a storage tank completely filled with anti-freeze mixture which would have increased the investment cost significantly. However, this also results in a temperature drop across the heat exchanger which has to be taken into account during the system planning. In the solar circuit the glycol-water mixture Tyfocor LS is being used.

The global insolation on absorber area and horizontal plane is being measured with two pyranometers which are mounted at angles of 35° and 0° to the horizontal, respectively. The supply and return temperatures of the heat transfer fluid are being measured using PT 100 resistance temperature sensors located directly at the in- and outlet of the heat exchanger HX12. They are mounted in immersion sleeves with the sensor tip pointing against the flow direction to ensure the whole sensor length being immersed in the fluid. The volume flow $\dot{V}_K$ is being measured using a magnetic-inductive flow meter that is located in the return part of the solar circuit next to the heat exchanger HX12.

2.3.1.2 Storage and hot water circuit

From the solar heat exchanger, energy is either being transferred directly to the absorption chiller or temporarily being stored in a non-pressurized 750 litre hot water storage tank. Five tank layer temperatures are being measured with Pt 1000 resistance temperature sensors, positioned on the outside of the tank and clamped to the surface. Figure 2.3.4 shows a picture of the storage tank as well as the sensor positions.

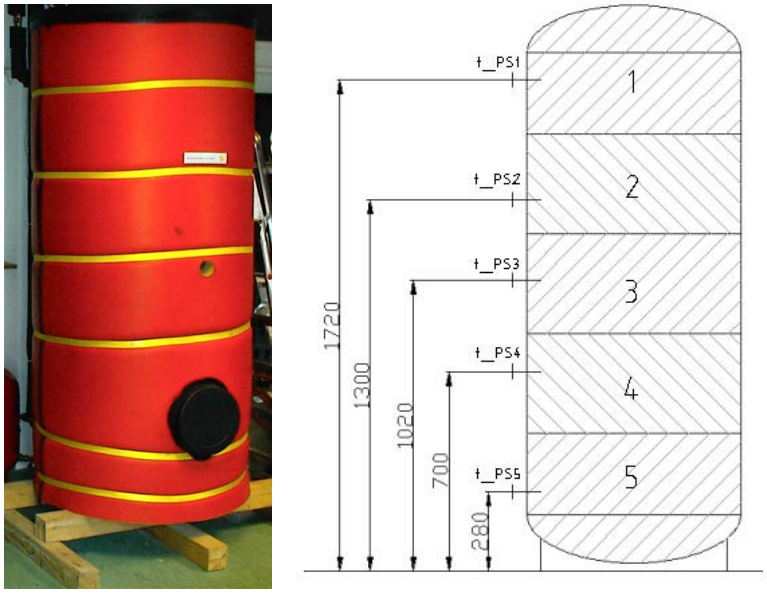

Figure 2.3.4. 750 Liter storage tank and temperature sensor positions [mm]

The storage pump P2 in Figure 2.3.2 is a frequency-controlled, variable speed pump pumping between 0.6 m³/h and 1.6 m³/h. To control the hot water inlet temperature of the absorption chiller, a three-way mixing valve has been installed. It is motor-driven and runs between 0% and 100% recirculation of the hot water return. The hot water supply pump P3 is frequency-controlled and pumps at variable speed between 0.6 and 1.5 m³/h in a closed loop. A strainer and air release valves have been installed in the piping.

Temperature measurements for this circuit are being taken at the secondary side of the heat exchanger HX12 and at the generator inlet of the absorption chiller using PT100 temperature sensors. They are mounted the same way as in the solar circuit. Flow measurements are being taken next to the pump P2 in the storage charge circuit ($\dot{V}_B$), before the three-way valve in the hot water circuit ($\dot{V}_G$) and in the return leg of the hot water circuit before the generator ($\dot{V}_{Ge}$), using magnetic-inductive flow meter.

For experimental chiller operation on days with low solar insolation, a backup heating system has been installed. It consists of a gas-fired condensing boiler with a maximum heating capacity of 28 kW at hot water feed temperatures of 85°C. It is a commercial household heating appliance and connected to the hot water storage via an internal heat exchanger, as shown in Figure 2.3.2. The boiler has an internal pump providing the mass flow.

Note: Such a backup heater is not needed in a commercial system. It has only been installed to increase the experimental period of the cooling system for scientific purposes.

2.3.1.3 Absorption chiller

The absorption chiller is a water/LiBr single-effect chiller with a nominal cooling power of 10 kW_{th} at inlet conditions of 75°C hot water, 27°C cooling water and 18°C chilled water temperature. It is the latest step in the development of a chiller which has been designed and developed at the Bavarian Centre for Applied Energy Research (ZAE Bayern). The step before was done within the course of the EU Joule-project JOR3 CT97 0181 in 1999 [Michel *et al.* 2001]. The present chiller design is the result of a follow-up joint collaboration project between Phönix SonnenWärme AG, the Institute of Energy Engineering at the Technical University of Berlin, the ZAE Bayern and the Institute for Rehabilitation and Modernization of Buildings (IEMB).

With respect to the low cooling capacity and low driving temperature a single-stage process allowing for both a straight-forward plant design and a reliable and durable plant operation was chosen [Kohlenbach *et al.* 2004a]. Key aspects of the design were

- low driving hot water temperatures between 55°C and 95°C allowing solar and trigeneration operation
- high cooling water temperatures between 27°C and 40°C allowing wet and dry cooling tower use
- COP of 0.78 at nominal conditions, not lower than 0.72 over the total operation range
- efficient part-load behaviour with a range of 40% to 160% of nominal load
- compact design matching standard door size, small footprint
- automatic cycle control (crystallization and anti-freeze guard)
- use of standard hermetic centrifugal pumps for solution and refrigerant cycle

The chiller is a compact construction, using falling film tube bundle heat exchangers in rectangular vessels. Generator and condenser are integrated in the upper vessel, separated by steam louvers to allow mass transfer of the refrigerant steam with minimized pressure loss. Absorber and evaporator have been integrated into the lower vessel for the same reasons. The vertical arrangement of the two vessels allows the backflow of the weak solution from generator to the absorber without the need for a second solution pump. Figure 2.3.5 shows the chiller.

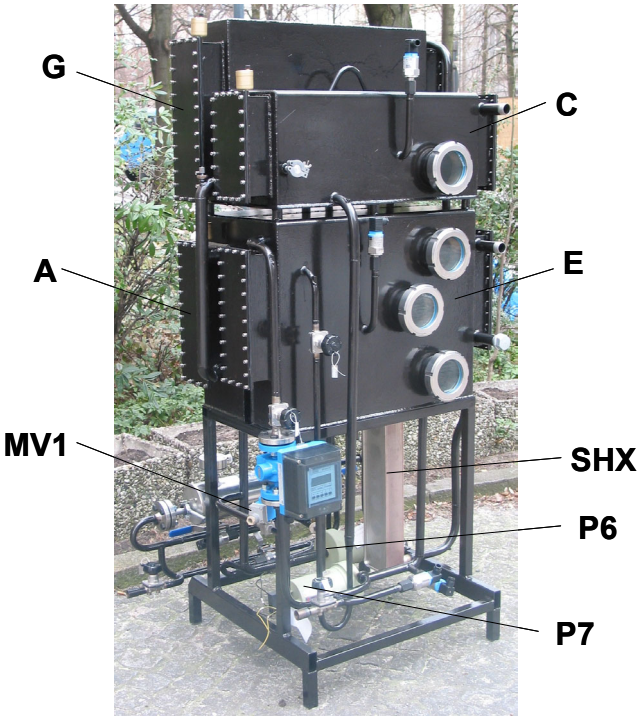

Figure 2.3.5. Phönix 10 kW absorption chiller.
Picture by A. Kühn.

The chiller mainly consists of four heat exchangers between internal and external streams (G: generator, A: absorber, C: condenser, E: evaporator), an internal solution heat exchanger (SHX), a solution distribution pump (P6), a refrigerant circulation pump (P7) and a magnetic valve (MV1). The piping and instrumentation diagram (PID) is shown in Figure 2.3.6.

Refrigerant steam from the evaporator is being absorbed by concentrated solution in the absorber. The resulting diluted solution is being pumped into the generator, where external heat evaporates the refrigerant. The steam condenses in the condensator and flows back to the evaporator whereas the concentrated solution returns to the absorber. A solution heat exchanger provides the energy exchange between hot solution from the generator and cold solution from the absorber, thus minimizing temperature differences between solution inlet temperature and the respective equilibrium temperature of generator/absorber. For increased heat exchange in the evaporator the refrigerant is circulated by means of a circulation pump. A bypass connection between refrigerant and solution loop can be opened for controlled solution dilution, e.g. in case of crystallization danger. The magnetic valve MV 1 shuts the bypass in normal operation.

To maintain the refrigerant pressure difference between evaporator and condenser, a u-shaped tube is being used. The pressure drop of the refrigerant is achieved by the level difference of the refrigerant liquid column in the two communicating parts of the u-shaped tube. Another u-shaped tube is being used between generator and absorber to prevent possible pump damage in case of crystallization. In case of crystallization the solution mass flow from generator to absorber will be blocked. Solution is however still able to flow from absorber to generator, resulting in a solution level increase in the generator sump. In worst case all solution will be pumped into the generator, resulting in dry operation of the solution pump due to an empty absorber sump. To prevent pump damage, the u-shaped tube allows a solution overflow from the generator sump straight into the absorber sump, thus maintaining a steady flow.

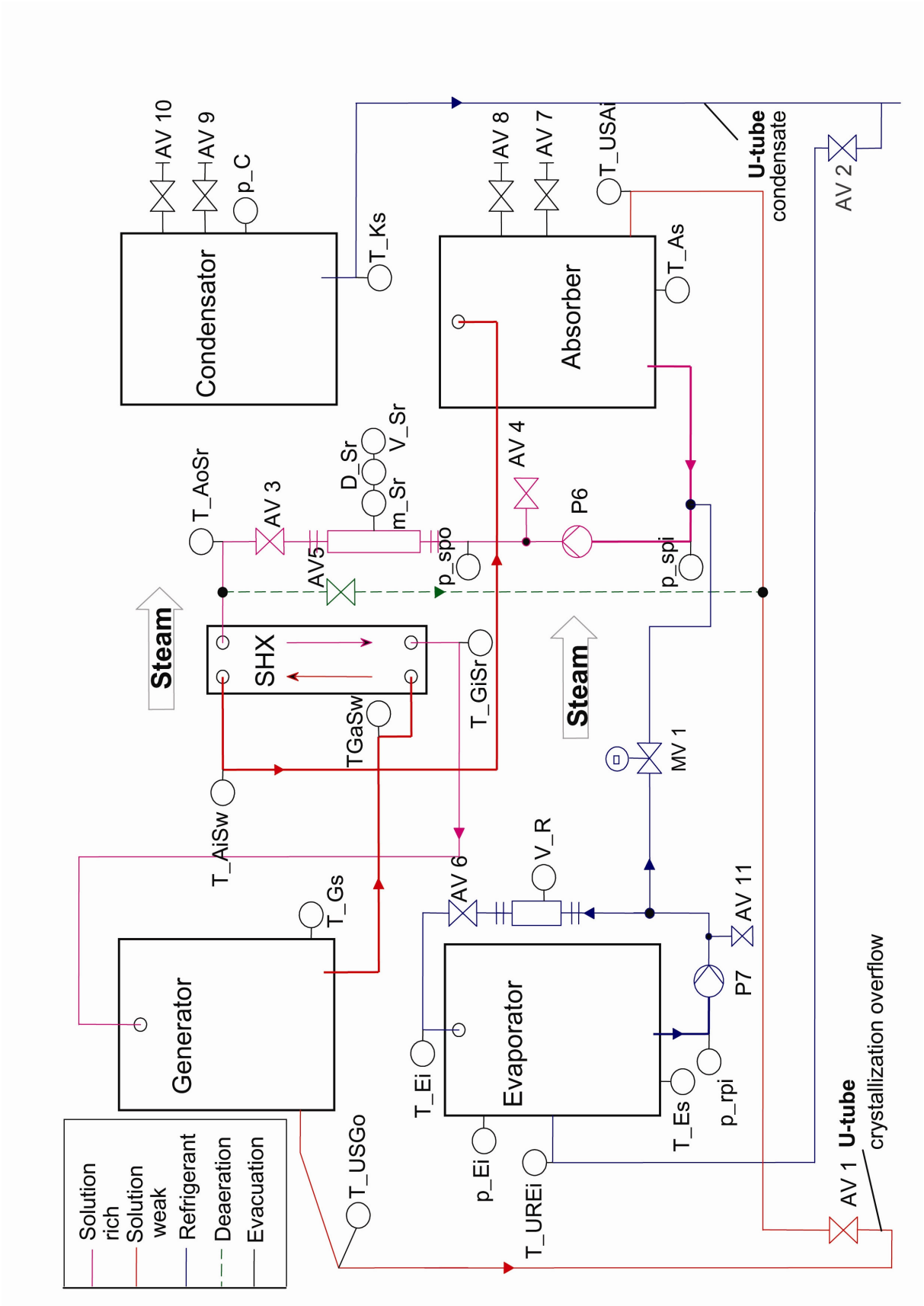

Figure 2.3.6. Piping and instrumentation diagram (PID) of the Phönix absorption chiller (second generation model). Figure modified from M. Harm.

2.3.1.4 Cooling water circuit

The cooling water for the absorption chiller is being provided by an open wet cooling tower of 23kW$_{th}$ cooling power at nominal conditions of 21°C wet bulb temperature and supply/return temperatures of 35/27°C. The cooling tower has a frequency-controlled fan which can be operated between 10 and 50 Hz. The cooling water pump P4 is a frequency-controlled, variable speed pump pumping between 0 and 2.8 m³/h. The three-way mixing valve DWM4 can be used for the control of the cooling water inlet temperature of the chiller by recirculation of the return flow. It is motor-driven and runs between 0% and 100% recirculation. The cooling water loop is open, thus water constantly evaporates during operation of the cooling tower and has to be made up to the cooling tower sump. This is being done via a flotation valve in the tower sump connected to the fresh water grid. A strainer has been installed in the loop to filter particles from ambient. Figure 2.3.3 shows the cooling tower.

The cooling tower can also be used in free-cooling mode. Cooling water from the cooling tower can be pumped directly through the heat exchanger HX45 in the chilled water circuit. It can thus directly be used for the operation of the chilled ceiling panels without absorption chiller operation. Free cooling is generally only possible when the ambient wet bulb temperature is sufficiently low. For this purpose, the wet bulb temperature of the ambient air has been measured continuously using a custom-made device. It consists of a PT100 resistance temperature sensor enclosed by a piece of wet cotton cloth. Figure 2.3.7 shows the construction of the device. The cloth (2) is wrapped around the temperature sensor (1). Its lower part is immersed in a reservoir with demineralised water (3) to keep it wet. A small fan (4) provides the necessary air flow across the cloth to establish continuous evaporation. It sucks ambient air through an air duct (5) which prevents the circulating of saturated air within the housing.

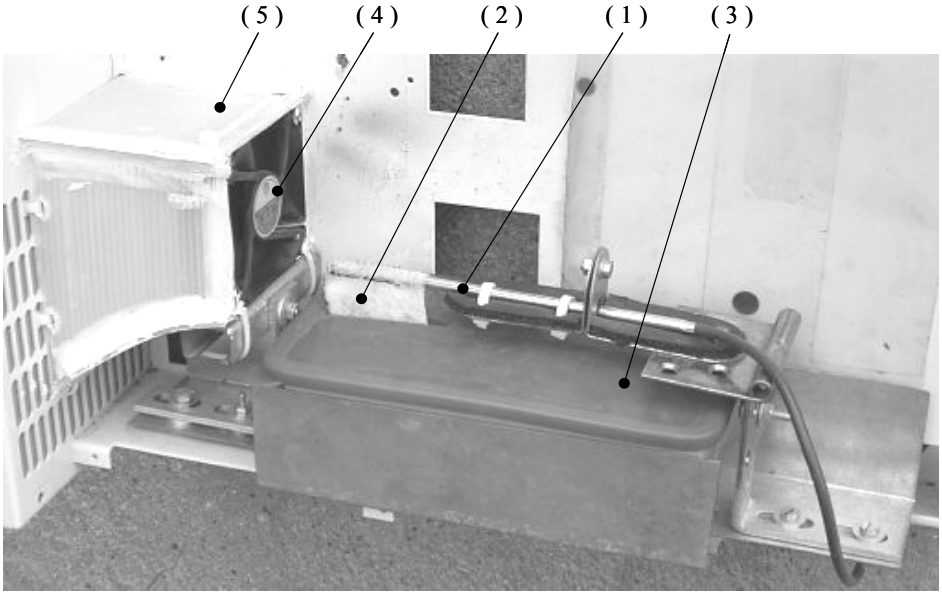

Figure 2.3.7. View of wet bulb temperature measurement device with open housing. Picture by E. Wiegand.

2.3.1.5 Chilled water and ceiling panel circuit

Figure 2.3.8. View of a chilled ceiling panel used for cooling load distribution. The picture was taken during maintenance work. During normal operation the panels are mounted in horizontal position with the copper meander facing upwards.

The chilled water from the absorption chiller circulates through a plate heat exchanger and is being heated by water from the ceiling panels. The heat exchanger HX45 has been installed to allow the free cooling mode without polluting the ceiling panels. The cooling water circuit is an open circuit and dust or particles can enter the system. The heat exchanger separates cooling water and chilled water circuits and thus prevents the introduction of dirt into the ceiling panel tubes. It also allows the operation of chilled water and ceiling panel circuit with different flow rates.

Pump P5a in Figure 2.3.2 provides the circulation through the evaporator of the chiller and the heat exchanger at a constant flow rate of 2.6 m^3/h. Pump P5b circulates the water through the chilled ceiling panels at a constant flow rate of 2.3 m^3/h.

Four office rooms of the Phönix SonnenWärme AG with a total room area of 152m^2 have been retrofitted with varying panel areas to cover the cooling load, yielding a total ceiling panel area of 91m^2. The nominal supply/return temperatures of the panels are 16°C/19°C at a constant flow rate of 2.6 m^3/h. Each room is equipped with a dew point sensor and a temperature control thermostat, both connected to a motor-driven valve that shuts in case of a trigger signal from either. Figure 2.3.8 shows a chilled ceiling panel.

2.3.2 Data acquisition and control equipment

The system is equipped with eight different types of sensors as shown in Table 2.3.1. All sensors are connected to a Mahöle Symbiscan K2 data acquisition unit, consisting of a Keithley Multimeter in combination with a 128 channel multiplexer card. A temperature module is included on the multiplexer card allowing a direct connection of two- and four-wire resistance temperature sensors. All analogue sensor signals are being converted into digital signals in the K2 data acquisition unit which is connected to a personal computer. There, measurement data is being recorded and visualized in an interval of approx. 12-14 seconds. Visualization is done using LabVIEW software. A complete list of all measurement variables can be found in Appendix 8.3.

Table 2.3.1. Overview on sensor equipment of the solar cooling system. Measurement uncertainties can be found in Appendix 8.3.

Sensor equipment	Measurement purpose system	Measurement purpose chiller
Pt 100 1/3 Class B resistance temperature sensors	All temperatures involved in energy balance calculations and control	All internal chiller temperatures
Pt 1000 Class B resistance temperature sensors	All temperatures for monitoring purposes	-
Contactless magnetic-inductive flow sensors	All system volume flows	Refrigerant volume flow
Coriolis mass flow sensor	-	Solution mass flow
Coriolis density sensor	-	Solution density
Piezo-electric pressure transducers	Expansion tank pressures of both collector fields	Evaporator/condenser pressure, hydrostatic and delivery head of solution pump
Electricity meter	Electricity consumption of all system pumps and cooling tower fan	Electric energy consumption of solution and refrigerant pump
Water meter	Water consumption of cooling tower	-
Pyranometer insolation sensors	Total global irradiation on horizontal and absorber plane of collector field	-

The absorption chiller and the system are being controlled via a software-based control. The measurement data necessary for controlling purposes (controlled variables) is taken from the data acquisition unit and used as input for into a PID control module included in LabVIEW. The control output data (set variables) is then calculated by the PID controllers, set by a pair of digital output cards and distributed to the individual actuators in the chiller or system. In order to keep the control simple and reliable, only few actuators have been installed. Table 2.3.2 shows the individual actuators, their control purpose, parameters and digital output card output.

Table 2.3.2. Overview of actuators, control parameters and output. Refer to Figure 2.3.2 and Figure 2.3.6 for denotations.

	Control purpose	Actuator	Control parameter	Output
System	Hot water supply temperature	Valve DWM3	position	0-10 VDC
	Cooling water supply temperature	Valve DWM4 Cooling tower fan	position on/off, r.p.m.	0-10VDC Relay, 0-10VDC
	Heat transfer fluid circulation	Pump P_i	on/off (i=1,2,3,4,5a,5b)	Relay
	Heat transfer fluid circulation	Pump P_i	r.p.m. (i=1,2,3,4)	0-10VDC
Chiller	Solution circulation	Solution pump P6	on/off, r.p.m.	0-10VDC, Relay
	Refrigerant circulation	Refrigerant pump P7	on/off	Relay
	Solution dilution	Magnetic valve MV1	open/shut	Relay

2.4 System energy balance calculation

For the experiments presented in this thesis, the solar cooling system at Phönix SonnenWärme AG has been monitored during operation of the cooling period 2004 in Berlin. The factors of interest for a system energy balance are the absolute amounts of energy transferred through the system boundaries from solar input to chilled water output. This includes both thermal and electrical energy.
In operation, the system almost never reaches steady-state conditions. This is due to several facts. First, the solar insolation is a transient parameter, fluctuating constantly. Second, the chiller has a thermal inertia, resulting in time lags between a change of input temperatures and the corresponding output temperature change. Also, the solar thermal collectors have a thermal inertia that cannot be neglected. Steady-state calculations are therefore almost impossible. Thus only energy amounts integrated over a definite time period have been used for energy balance calculations instead of energy flows. If not otherwise stated, the time period over which energy amounts have been integrated was the period of chiller operation, i.e. the time between chiller start-up and shutdown. This time period was chosen to allow the comparison of different control strategies with least disturbance influence. Using the chiller operation time instead of the total measurement time excludes the influence of the storage tank status at the beginning of each measurement day on the chiller start-up time and thus the integrated cooling energy per day.

For the energy balance calculations the solar cooling system described in Figure 2.3.2 has been partitioned into different sub-systems. Each sub-system was individually balanced. Figure 2.4.1 shows the partition of the solar cooling system into subsystems for energy balance calculations.

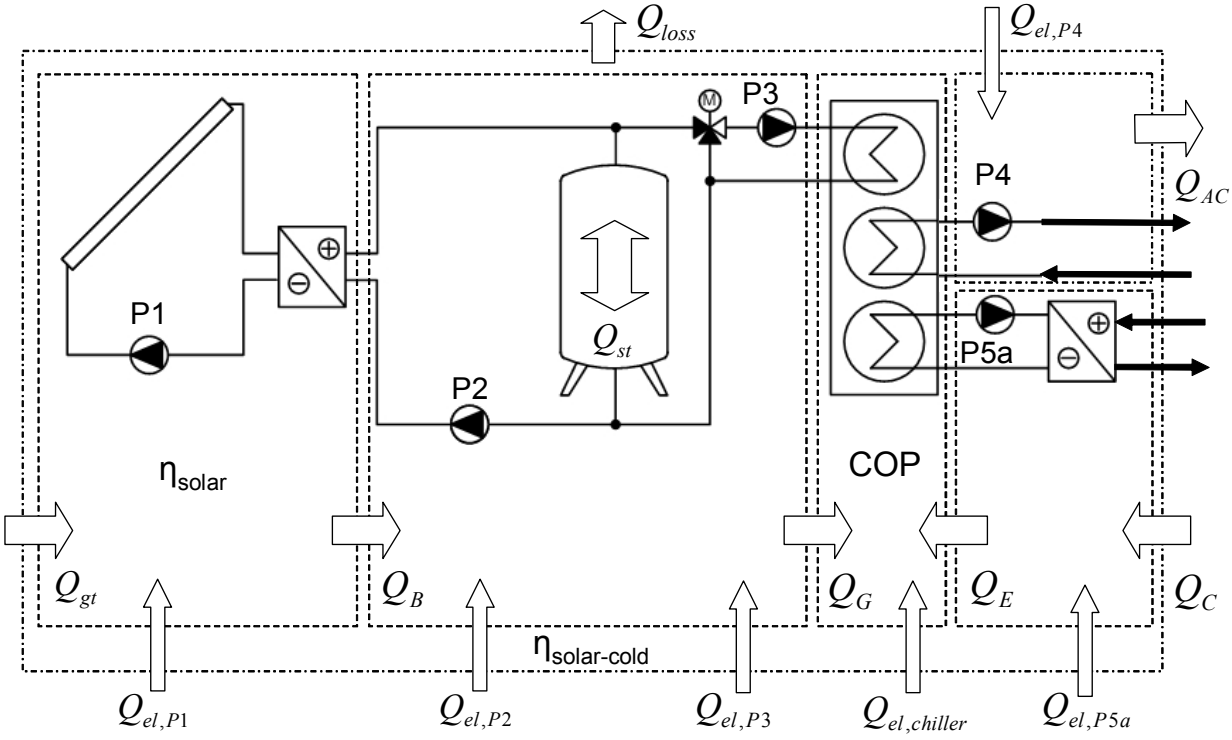

Figure 2.4.1. Partition of solar cooling system into different subsystems for energy balance calculations (⇨: heat flow, ➡: mass flow)

The first subsystem is the collector field. It consists of the solar thermal collector fields, piping, solar pump P1 and heat exchanger HX12 between solar and storage circuit. The storage circuit is defined as the second subsystem, consisting of storage pump P2, storage tank, three-way valve, piping and generator pump P3. The third subsystem is the absorption chiller itself. The fourth subsystem is the cooling water circuit with pump P4. The last subsystem consists of heat exchanger 45, piping and pump P5a in the chilled water circuit, separating the evaporator from the ceiling panel circuit. The ceiling panels are not considered as a subsystem, as the cooling load is being introduced into the system by the heat exchanger HX45.

The positions of the sensors for the energy balance calculations do not allow the balancing of each individual component. For example, the solar pump P1 and the storage tank pump P2 cannot be balanced separately although they are in two different subsystems. Due to the electricity meter setup only the total balance of both pumps can be made. The same holds true for pumps P3, P4, P5a and P5b.

During the time period of chiller operation, all measurement data has been recorded at variable time intervals $\hat{t}_{ts,i}$ with an average of 13 s. It was assumed for the energy balance calculations that each measured value was constant for the time interval between two measurements. In the following energy balances of the individual subsystems, index *i* refers to a single time interval, *n* is the number of all time intervals per time period $\hat{t}_{tot}$ over which the energy balances were calculated.

$$\hat{t}_{tot} = \sum_{i=1}^{n} \hat{t}_{ts,i} \qquad (2.4.1)$$

Property data of specific heat capacity and density of water in the following energy balance calculations has been used as given in [VDI 1997]. Property data of Tyfocor LS has been used as given by the manufacturer in Appendix 8.5. All variable names used in the following energy balance calculations refer to Figure 2.3.2.

The calculation of the solar energy input on the tilted absorber area per time step Q_{gt} is made as follows

$$Q_{gt} = A_{abs,tot} \cdot \sum_{i=1}^{n} q_{gt,i} \cdot \hat{t}_{ts,i} \qquad (2.4.2)$$

All calculations of energy amounts transferred through the system per time step *i* follow the main equation

$$Q_{x,i} = \sum_{i=1}^{n} \dot{V}_{x,i} \cdot \rho_{x,i} \cdot c_{p,x,i} \cdot \left(t_{x,in,i} - t_{x,out,i}\right) \cdot \hat{t}_{ts,i} \qquad (2.4.3)$$

where subscript x symbolizes a system circuit according to Figure 2.3.2 (x = B, G, AC, E, C). $Q_{x,i}$ is the energy amount transferred per time step $t_{ts,i}$.
The thermal efficiency of the solar circuit can be calculated as

$$\eta_{solar} = \frac{Q_B}{Q_{gt}} \qquad (2.4.4)$$

For the absorption chiller, a daily mean coefficient of performance (COP_{th}) based on thermal energy is calculated as

$$COP_{th} = \frac{Q_E}{Q_G} \qquad (2.4.5)$$

The total solar cooling system is marked by the dash-dotted line in Figure 2.4.1. It has the energy inputs of global radiation on absorber plane Q_{gt} and heat input on chilled ceiling panels Q_C. The total electrical energy for all pumps is also an input. The only energy output of the system to ambient is the reject heat Q_{AC}. The storage tank can however buffer energy from one day to the following one. The overall thermal system efficiency 'solar-to-cold' reads

$$\eta_{solar-cold} = \frac{Q_E}{Q_{gt}} \qquad (2.4.6)$$

Equation (2.4.6) is the daily net efficiency for the transformation from solar to cooling energy. It is being calculated using the input of the evaporator instead of the heat exchanger HX45 to allow a later comparison to simulated data.

So far, the electricity consumption of the pumps has been neglected. For the total energy balance of the system it has to be taken into account. The same holds true for the total thermal system loss. The system energy balance reads

$$Q_{gt} + Q_C + Q_{el,P,tot} - Q_{AC} - Q_{loss} = 0\,, \qquad (2.4.7)$$

where $Q_{el,P,tot}$ is the sum of the electricity consumption of all system pumps.

An error analysis on the measurement parameters of the system can be found in Appendix 8.2.

3 Control strategies of solar cooling systems

Controlling a solar cooling system means simultaneously controlling its system parts in order to fulfil one or more given tasks. With regard to the main system purpose of cooling, various operational modes can be defined. The system can operate under the premise of potentially low electricity consumption of the system components for a given cooling demand. It can also be operated with the task of a potentially high cooling effect at all times. Both operation possibilities contradict each other if used solely, combinations of both can however be used in specific applications. Hence the user of a solar cooling system has to specify his interest and the system has to be planned, built and operated accordingly. Due to the variety of operation and design possibilities of solar cooling systems it is not recommendable to use just one specific design for all application purposes. Instead, system design and control have to be adapted to the given characteristics of the user location. Amongst others, these include annual weather and insolation profile, building type, cold demand profile, desired chilled water temperature, user preferences and possibly existing components that are to be included. It is the planners' duty to consider all relevant characteristics in the design process in order to create a system fulfilling the given tasks.
The main component in a solar cooling system is the chiller. Its relevant controlled parameters are:

- hot water inlet temperature and mass flow
- cooling water inlet temperature and mass flow
- chilled water outlet temperature and mass flow

The hot water inlet temperature is a result of the control of the solar thermal system while the outlet temperature depends on the momentary heat flow in the generator. The cooling water inlet temperature depends on the cooling tower type and performance, the outlet temperature is the result of the heat flows in absorber and condenser. The chilled water inlet temperature of the chiller depends on the type of chilled water distribution system and cannot be influenced. The chilled water outlet temperature is the result of the chiller operating at given inlet conditions and usually has to be kept within certain limits to allow satisfactory operation of the chilled water distribution system.

In the following two general modes for controlling solar cooling systems will be presented.

a) Solar-guided mode

The basic idea of this mode is to use the simultaneity of solar gain and cooling load during days with high solar irradiation and high ambient temperature. It is a control mode characterised by a direct transformation of the available solar gain into cold without regard to building conditions. Cold is produced whenever the solar capacity is sufficient to drive the chiller, regardless of the momentary cooling load. The chilled water outlet temperature is the result of chiller operation at given hot, cooling and chilled water inlet conditions. There is no active control of the chilled water temperature respectively cooling capacity, as well as there are no temporal limits for cold demand. It is assumed that cold is demanded as long as there is sufficient solar irradiation to drive the chiller. Any available amount of solar energy is transformed into cold. There is no back-up heating system, therefore the strict meeting of defined cooling conditions can not be guaranteed.

In a variation of this mode the system operates without a storage tank [Grassie and Sheridan 1977]. Without a storage tank, a direct link is established between solar field and chiller, creating a fast connection between solar offer and cooling supply. Only the thermal inertia of chiller and building causes temporal delays. The cooling capacity can be provided fast but unlimited in its quantity. The latter can be a disadvantage. Too low chilled water inlet temperatures in combination with high solar insolation can result in freezing of the evaporator. Also, the lack of a storage tank causes transient load operation and unstable chilled water outlet temperatures as each variation in the solar input results in a direct response of the cooling load.

Using a storage tank in the system the cooling capacity can be limited. Excess solar energy can be stored in the tank, thus decreasing the cooling capacity. The stored energy can be used at a later time to balance periods with low solar irradiation.

With or without a storage tank, the solar-guided control mode is not suitable for cooling purposes with a steady demand of cold, such as food storage or server room cooling. It will most likely be used in building applications where the strict meeting of room temperatures at all times is not demanded.

b) Cold-guided mode

This mode can be regarded as the transformation of the classic control strategy of air conditioning systems onto a solar cooling system. The user sets a desired room temperature (or alternatively a desired chilled water temperature) and the chiller produces exactly the chilled water temperature to fulfil the cooling demand, almost independent from the momentary solar offer. This requires a hot water storage tank of sufficient size which is an important element for system performance, solar fraction and therefore primary energy consumption. Only the amount of solar heat needed for the momentary cooling load is being used. The rest is stored in the storage tank. Due to the use of a chilled water temperature control the cooling capacity is limited. The chilled water temperature is controlled by adjusting either hot or cooling water inlet temperature into the chiller. In this thesis, only the hot water adjustment will be discussed.

To achieve a constant chilled water outlet temperature, the storage tank has always to be charged to a certain capacity to allow hot water temperature control with a constant hot water flow. Before the chiller can be started, the storage tank has to be charged until the temperature of a reference layer exceeds the start-up temperature of the chiller. The layers above the reference layer then have a higher temperature than the start-up temperature of the chiller due to the thermal stratification in the storage. This allows a temperature control of the hot water. After reaching the necessary temperatures and chiller start-up, the chilled water temperature can be controlled via a three-way valve in the hot water circuit. Cooling water temperature and flow are kept constant to avoid disturbances and noise on the control. If the solar field yields a higher hot water temperature than needed to keep the set chilled water temperature, the hot water return flow is mixed with the supply flow to achieve the necessary temperature level. The effective flow to the chiller decreases and the difference between solar circuit flow and generator flow is pumped through the storage, thus charging it. If the solar circuit yields a lower temperature than needed to keep the set chilled water temperature, the storage tank is discharged in order to keep the hot water temperature. If the reference temperature in the storage falls below the minimum driving temperature of the chiller, the generator pump is being switched off. The storage is now empty and the chiller can only be started again after charging the storage as described above. Usually this is typical for the end of the day. A restart does not happen until the following morning.
This mode can be extended to maintaining a given cooling load at all times. In this case the installation of a backup heating or cooling system is necessary.

The two modes described above can be used for the control of solar cooling systems. In the following context of this thesis, the cold-guided mode has been further investigated regarding control issues. The solar-guided mode will not be further discussed.

3.1 Literature review and operational experience

The controlling of components or parts of solar cooling systems has been investigated in multiple publications. The focus of research in this area lies on the control of absorption chillers, i.e. the control of internal chiller processes. Another large field of research addresses the control of large solar thermal systems and their performance with regard to solar fraction and power consumption. However, only little research is being conducted on comprehensive control strategies for the total solar cooling system. One possible reason for the lack of research on this subject could be the small number of existing solar cooling installations that are suitable for experimental testing. There are currently approximately 53 solar cooling systems operating in Europe but almost all of them are in daily use at fixed conditions and the range of possible parameter variations of the control of these systems is very small [Paar and Heunemann 2004]. This prohibits extensive experimental research that is being needed in order to find suitable control strategies. In addition, the number of available simulation models for absorption chiller simulation is low which limits a theoretical approach to the subject. The following literature references were chosen to give an impression of precedent and contemporary research on the control of solar cooling systems and their components.

Bong et.al. describe the control strategy of a solar cooling system with chilled water storage in Singapore. The authors have made an attempt to reduce the fluctuation of the hot water temperature in the top part of the storage tank. The system is divided into three main control circuits: one circuit from solar collectors to storage tank, another one from storage tank to absorption chiller and one from chiller to fan-coil units. The solar circuit is connected directly to the storage tank and there is no storage pump in the system. The solar circuit pump is controlled using a two-point control via the temperature difference between collector field and bottom layer of storage tank. The storage tank in the system can be bypassed via an on-off three-way valve which is controlled according to the difference between exit temperature of the collector field and top layer temperature of the storage tank. Thus only water hot enough to charge the storage is fed into the tank, otherwise the water re-circulates through the valve to the collector field again. This setup was installed in order to prevent frequent pump cycling and fluctuating inlet temperature into the chiller. Real-time controlled operation of the absorption chiller for the time period from 8am to 5pm each day is used in the system. Outside this time period chiller and system pumps do not operate. The circuit control from chiller to fan-coils uses the level in the chilled water tank for controlling the chiller operation. If the level falls below a threshold the chiller is restarted. The chilled water distribution pump in the fan-coil circuit is operated as long as the monitored room temperature is above 20 °C. The system performance has been compared to two other solar cooling systems and the authors report lower collector efficiencies and higher power consumption for the Singapore system. They relate this to the chosen storage tank charging and chilled water distribution strategies [Bong *et al.* 1987].

Yeung et.al. describe a simple control mechanism for chilled and cooling water temperature in a solar air-conditioning system in Hong Kong. The chilled water temperature is being monitored and

if it drops below a setpoint, the hot water supply to the chiller is cut off. The cooling water temperature is controlled with a differential controller in on-off mode. The fan of the wet cooling tower is being switched on if the cooling tower sump temperature exceeds 29.5 °C and switched off at temperatures below. These control strategies result in a fluctuating operation of the chiller with increased thermal losses due to a higher number of start-up and shut-down procedures. No information is given about the influence of this control strategy on the overall system [Yeung *et al.* 1992].

Wolkenhauer and Albers provide qualitative instructions on solar cooling control, based on the minimization of primary energy consumption and effective part load operation. The solar cooling system is divided into three modules: a solar module including collectors, heat exchanger and hot water storage tank; a cold generation module including chiller, cooling tower and cold water storage tank and a cold distribution module including fan-coils or chilled ceiling panels. The main parameters for the control of each module are the corresponding storage tank temperatures. An insolation-based control strategy for the solar pump in combination with a temperature-difference (hysteresis) two-point control for the storage pump is recommended. The storage tank in the solar module is to be charged to a minimum temperature before the chiller can be started. To control the heating capacity of the chiller a combination of temperature- and mass flow based control strategy for the generator pump is proposed. The cooling water temperature is recommended to be kept as low as possible in order to allow the most effective chiller [Wolkenhauer and Albers 2001].

Li and Sumathy report on the performance of a solar powered absorption air conditioning system with a partitioned hot water storage tank. They use an active control of the hot water feed-in position into the storage tank, depending on available solar and tank temperatures. The goal of this setup was an earlier chiller start-up in the morning due to a reduced storage tank volume. The system employs a flat-plate collector array with a surface area of 38 m² to drive a LiBr-H_2O absorption chiller of 4.7 kW cooling capacity. The solar pump has no variable flow control and is operated only in differential on-off mode. The cooling tower is a wet cooling tower with a differential on-off controller for the fan. The storage tank has a volume of 2.75 m³ which is partitioned into two parts. The upper part has a volume of about one-fourth of the entire tank. It is being used only during the morning; during the afternoon the whole tank is employed. The performance of the system is presented and compared with the conventional system design in whole-tank mode. Their investigations show that the solar cooling effect can be realized nearly two hours earlier for the system operating in partitioned mode. The total solar cooling COP could be increased by approx. 15% higher compared to the traditional whole-tank mode. Experimental results also show that during cloudy days, the conventional system could not provide a cooling effect, however in the partitioned mode-driven system the chiller could be operated [Li and Sumathy 2001].

Improved control strategies for a solar-driven adsorption chiller system in Freiburg, Germany, are presented by Glaser. The system consists of a 50 kW NAK 20/70 adsorption chiller model by the Japanese manufacturer Nishiyodo. It is driven by 171 m² of evacuated tube collectors as heat

source. The system supplies cold water for the air-conditioning of laboratory rooms of a hospital. The control is divided into four modules: solar circuit, storage charging circuit, storage discharging circuit and cold/chilled water circuit. The solar circuit supplies heat to the storage charging circuit via a heat exchanger. The outlet temperature of the solar circuit is being controlled via a mass flow control of the solar pump using a PI-controller. The outlet temperature setpoint depends on the temperature of either the storage tank (for solar cooling operation) or the hot water tank (for building hot water supply). The storage charging circuit distributes the heat from the heat exchanger to the hot water tank or directly to the adsorption chiller. Its pump is also mass flow controlled and the flow in the storage charging circuit is adjusted to the flow in the solar circuit in order to achieve matching heat capacity rates. The storage discharging circuit supplies heat to the adsorption chiller. Its pump is mass flow controlled in a way that flow rate and temperature level into the generator of the chiller can be adjusted. The control is based on the cooling capacity demanded by the chilled water cooling load. Chilled and cooling water pump run with a constant mass flow whenever the chiller is in operation. The speed of the cooling tower fan is controlled depending on the outlet temperature of the cooling tower. A reliable operation of the system was achieved using the control strategies above. However, during operation, the adsorption chiller model did not reach the COP and cooling capacity given by the manufacturer. The problem could be identified and related to the internal chiller control, especially the number and length of ad- and desorption cycles. The control was re-designed and a capacity-depending cycle control using variable hot water temperature and flow was installed. This resulted in an increase of the COP from 0.35 to 0.5, although even after the control improvement the nominal manufacturer data could not be reached [Glaser 2005].

Concluding from Yeung and Bong it can be stated that a differential on/off operation of the main external circuit pumps should be avoided. Although such a control is simple to operate and install, the system performance decrease due to frequent on/off operation of the chiller does not seem to justify the simplicity. It can be understood that a mass flow and/or temperature control should be installed in the external circuits. This has been done in the system reported by Glaser where the variation of mass flow and temperature in all external circuits seems to yield good system performance. The continuous fan speed control in this system avoids disturbances in the cooling water temperature. From the work of Li and Sumathy it can be concluded that a small storage volume before and during the start-up phase of the chiller can increase the mean system COP. Also, due to a faster charging procedure an earlier chiller start-up can be realized. The design-engineering and control effort is however higher as additional valves are required for the partition of the tank.

The experience with solar cooling systems shows that a large fraction of currently operating systems does not perform in the way they were designed to. Lower COP's and cooling capacities as well as high standstill time are reported from system operators. The causes for this can be manifold. Insufficient planning and system design, incompatible system components, inexperienced operation, wrong hydraulic setup or technical defects, to name only a few. However, repeatedly insufficient control strategies have been the cause for the system faults. This was

reported by Glaser for the adsorption chiller in Freiburg, Germany. The following two references also describe flawed control behaviour and/or design.

The Bavarian Centre for Applied Energy Research (ZAE Bayern) has investigated the operational performance of six solar cooling or solar air-conditioning systems in Germany in the course of a federal FIA (research-information-exchange) project. They report an insufficient control strategy in the solar circuit of a solar cooling system in the Bavarian State Office for Environmental Protection (LFU) in Augsburg, Germany. There the solar pump was originally designed for constant pump speed operation which led to hot water temperatures up to 95°C. The adsorption chiller used in the system was designed for nominal temperatures of 75°C. As a consequence of the higher hot water temperatures, the thermal loss of the collector field was rather high. The installation of variable speed pumps reduced the thermal loss and improved the overall system performance [Kaelke *et al.* 2003].

During the move of the German capital from Bonn to Berlin, federal building measures included the installation of two solar assisted air-conditioning systems using absorption chillers. One system has been installed in the federal public relation office, the other in the federal ministry of transport, building and housing. Albers reports on technical difficulties during the operation of the latter system. In the federal ministry, unexpected on/off operation of the absorption chiller was recorded during periods with sufficient insolation. The reason for the pulsing was that a compression chiller back-up system was activated before the chilled water setpoint had been reached by the absorption chiller. After the start-up of an absorption chiller it takes a certain the time for the chilled water to reach the temperature setpoint. The control in the federal ministry was programmed in a way that the back-up system was activated if the chilled water setpoint was not reached after a certain dead time. As both absorption and compression chiller are connected to the same flow header, an operating compression chiller decreases the inlet and outlet temperatures of the absorption chiller. If after a while too low chilled water outlet temperatures were detected by the control, the valve controlling the hot water inlet temperature was completely shut. This in consequence led to a chiller shutdown although there was sufficient insolation and cold demand. The frequent on/off operation reduced the overall COP of the system in the federal ministry significantly [Albers 2003], [Albers 2004a].

The three examples above show that the control of a solar cooling system has to be carefully designed in order to achieve good operational results. All aspects relevant for the optimum system performance have to be considered. All components that can be controlled actively should be included in the system control. The choice of the right control strategies is essential for the system performance.

For the work presented here, the controlled system parts include solar thermal system, absorption chiller and cooling tower of the design described in the previous chapter. The control of the chilled water distribution will not be discussed in this thesis. Also, during all experiments performed in the course of this thesis the back-up heater was not in use; the solar cooling system was operated purely on solar energy.

3.2 Hot water temperature control

This chapter describes three control strategies for the mass flow in the solar circuit of a solar cooling system. The strategies include constant mass flow as well as variable mass flow, the latter depending on either temperature difference or insolation. Furthermore, a literature review is being given with regard to the application of these strategies in solar thermal systems. The influence of the storage layer temperature used as reference for a circuit control is being discussed and guidelines for the appropriate choice of the reference layer are being given.

3.2.1 Fundamentals and state of the art

The desired effect of operating a solar cooling system is to provide comfort air-conditioning or industrial cooling at given conditions with reduced operational costs, compared to conventional compressor-driven equipment. The overall performance of such a system is influenced by the individual operation of its internal circuits. The solar circuit couples the sun's driving energy to the storage tank and/or the absorption chiller. Its control strategy has to provide the desired operating conditions for the hot water input of the chiller. For the Phönix solar cooling system, the solar circuit control has to perform under the following requirements:

- Driving temperature between 55 °C and 95 °C
- Power consumption as low as possible
- Storage tank charging/discharging adapted to chiller operation
- Adaptable for both cooling and heating operation (summer/winter mode)
- Only two controlled components (pumps P1 and P2)

An inappropriate control strategy for the solar circuit can result in bad system behaviour. For example, a long charging time of the storage tank delays the start-up time of the chiller. A late chiller start-up results in less cooling capacity per day. The charging time of the storage tank can be influenced by the control strategy as explained later in this chapter.

The components of the solar circuit in a solar cooling system are similar to those of a conventional solar thermal hot water system used for tap water or space heating. However, its control is more complex than the control of a conventional solar thermal hot water system. For the purpose of domestic solar hot water generation it is usually sufficient to provide storage tank charging above the minimum desired hot water temperature. Variations in the hot water feed temperature due to on/off operation of the solar circuit pump do not influence the tap or heating water temperature, since the storage tank buffers these variations. The solar energy is transferred into the storage tank and stored completely before being used for heating purposes.

As far as a solar cooling system according to Figure 2.3.2 is concerned, the criteria applied are different. The solar energy does not have to be stored completely in the storage tank before being

used. It can bypass the storage and drive the absorption chiller directly. In order to reach a sufficient performance of the chiller it is necessary to control the hot water feed temperature and mass flow into the chiller. The storage tank charge status is another parameter influencing the performance of a solar cooling system. Since the chiller start-up depends on a minimum temperature of approx. 56 °C, it is not reasonable to start the generator circuit pump (P3, Figure 2.3.2) before a certain minimum temperature in the storage tank of approx. 58-60 °C has been reached. The storage layer that is chosen for this temperature monitoring also influences the dynamic behaviour of the whole system. If the top storage layer temperature is being used, the chiller can start up earlier during the day but has only a small buffer potential for covering periods of low insolation. Using the bottom storage layer results in a later daily start-up but provides a sufficient buffer volume for periods of low insolation. Controlled alternation between top and bottom layer during system operation can increase the operating time of the chiller.

Furthermore, the total power consumption of both solar and storage circuit pumps of such a system is a main parameter for economic comparisons between solar and conventional cooling systems. The minimization of the power consumption is a goal which can be achieved by carefully choosing the right components and by applying an effective control strategy for the main components, which include all pumps of the external circuits in the system plus the absorption chiller. Such a control system can be subdivided into various sub-controls, one controlling the solar pump and the storage circuit pump, one controlling the absorption chiller operation and its external pumps for hot, cooling and chilled water, another one controlling the cooling tower performance.

The three most common control strategies of solar thermal systems include differential on/off, radiation-based and temperature-difference-based strategies. Usually the mass flow of the heat transfer medium in the solar circuit is the controlled variable and the outlet temperature of the solar field is the measured variable. These control strategies will be presented and discussed in the following chapter. The setup used for this is shown in Figure 3.2.1.

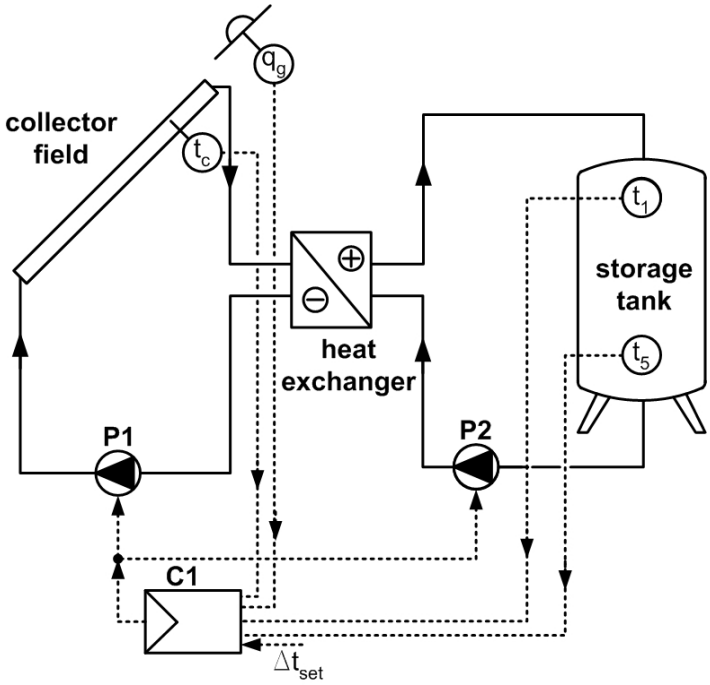

Figure 3.2.1. Hydraulic scheme of solar and storage circuit with controller. (solid line: fluid flow, dotted line: sensor or control signal)

For practical reasons, Figure 3.2.1 displays the hydraulic setup and sensor equipment necessary to realize all three control strategies mentioned above. The solar pump P1 is controlled by the controller C1 which has either the collector temperature t_c or the insolation q_g as input variable. The other input variable into C1 is the bottom or top layer storage tank temperature t_5 or t_1. The storage pump P2 is activated simultaneously with P1 and operates with the same mass flow, if the heat transfer media in both circuits are equal. If not, the mass flow of P2 has to be adjusted according to the heat capacities of both media.

3.2.1.1 Different mass flow control strategies

a) Differential on/off control (STAN)

In the simplest variation of a solar circuit control, C1 is a differential controller that switches pumps P1 and P2 only on and off. The control command is made by comparing the temperature of a collector field sensor t_C with the temperature of a storage tank temperature sensor t_1 or t_5. If the collector temperature is bigger than the tank temperature plus a hysteresis difference the pump is being switched on. If the temperature difference between both sensors falls below a given value the pump is switched off. The hysteresis accounts for losses and prevents frequent pump pulsations. If in operation, P1 and P2 always run at constant mass flow with maximum pump speed.
The result is a changing collector field outlet temperature according to the insolation gradient. After each pump switch-off the water in the piping between collector field and absorption chiller

decreases in temperature due to the thermal loss. In parallel the collector field heats up until the upper hysteresis temperature has been reached. If the pumps switch on again, cooler water from the piping is followed by hot water from the collector field which has a bigger temperature.

For small domestic hot water systems this strategy is the most common one and used frequently in commercial applications. Its advantages are obviously: a low number of components and thus low investment cost. Only two temperature sensors are being needed, the pump can be a single-phase constant speed pump and there is no need for a PID-type controller. The disadvantage of this strategy is a higher thermal loss of the collectors due to frequent periods of standstill time. The pulsating operation of the pump causes the thermal mass of collector and heat transfer medium to frequently heat up and cool down again. This results in lower solar gains. The outlet temperature of the collector field fluctuates quite strongly. The full speed operation of both pumps at all times results in a high electrical power consumption.

b) Temperature-difference based control (TDIFF)

An advanced control strategy has been developed in order to avoid the pulsating on/off operation of the pumps in the STAN strategy and thus to guarantee a continuous heat flow from the collector field. The TDIFF strategy also uses a temperature sensor each in collector and storage tank. Here, C1 is a proportional controller and controls the mass flow of P1 and P2 in proportion to the momentary temperature difference between collector field and storage tank measured by t_C and t_1 or t_5. A similar temperature hysteresis as in a) is used to determine the pump on/off operation. If in operation, the pump speed for each time step *t* is being calculated via the difference between the set temperature difference Δt_{set} and the actual temperature difference between solar collector and storage tank $\Delta t_{real,t}$. The bigger the value of ($\Delta t_{real,t}$ - Δt_{set}), the bigger the change in pump speed and vice versa. This way the TDIFF strategy is capable to hold a temperature level which -within certain limits- does not depend on the day's insolation gradient.

For this strategy also single-phase constant speed pumps can be used. The electronic speed control of a single-phase pump can be realized in two variations, either using wave packet control or phase-angle modulated power control. A three-phase pump in combination with a frequency inverter can also be used but has higher investment cost. The advantages of this strategy are reduced thermal losses of the collector due to less standstill time during operation. The outlet temperature of the collector field is quite stable, although still coupled to the storage tank temperature. A disadvantage of the strategy is the need for a proportional controller and the electronic pump speed control which results in higher investment cost. For small domestic solar thermal systems this control strategy is also commercially available in pre-programmed control units using a single-phase pump.

c) Radiation-based control (INSOL)

A third variation of controlling the mass flow through the collector is a radiation-based control. Instead of measuring the collector temperature, the momentary global radiation on the collector

plane is being measured. The mass flow is being increased with rising insolation and vice versa, resulting in a quite stable collector field outlet temperature. Again, a temperature hysteresis as in a) is used to determine the pump on/off operation. For the INSOL strategy, C1 is also a proportional controller but controls the mass flow value of P1 and P2 in proportion to the momentary insolation measured by q_g. An empirical correlation between insolation and pump speed is being needed for this strategy. This correlation depends on pressure loss, piping length and system components and is different for each system. Usually, a mean value of insolation is used to avoid rapid changes in mass flow due to e.g. single clouds. This mean value is being calculated over a time period depending on the thermal inertia of the solar field and has also to be determined empirically. The same variations for electronic pump speed control as in b) can be used. The outlet temperature of the collector field is not coupled to the storage tank anymore.

The advantage of this strategy is a very constant outlet temperature of the collector. The disadvantage is a higher control and measurement effort, especially with regard to the insolation sensor. This also results in higher investment cost. Commercial units for this strategy are not available yet. The radiation-based strategy is mainly used for larger solar thermal systems where stable outlet temperatures are being demanded.

The solar circuit of a solar cooling system is a main part for successful overall system performance. Generally, its output temperature level needs to be higher than in conventional solar thermal hot water systems. However, control strategies of conventional and solar cooling systems regarding the solar pump can still be compared. Research on control strategies of domestic or large solar hot water systems has been extensively performed. Especially strategies for achieving maximum solar gain have been developed. In the following, an overview of literature on the control of large solar thermal systems with collector areas above 30m² is presented. Research on domestic-size systems with collector areas below 30 m² has been left out as these are too small for the operation in a solar cooling system.

Streicher et.al. have investigated the influence of different hystereses on solar pump operating hours and system gain for large solar thermal hot water systems with a collector field size of more than 100 m². They describe a simulative comparison using TRNSYS for a reference case solar hot water system according to the European norm EN 12977-2 and variations of on/off temperature for solar pumps with constant mass flow. A bigger on/off temperature with a smaller hysteresis leads to maximized solar gains and minimized pump operating time. An optimum configuration for the investigated specific configuration has been found at 10/11 K [Streicher *et al.* 2003].

Klingenberger also presents a comparative simulation using TRNSYS for a reference case solar hot water system and various control strategies. In addition to Streicher et.al. the control strategies investigated here also include an insolation-based strategy with constant mass flow and a temperature-difference-based strategy with variable (matched) mass flow. An optimum combination of high solar gain and low pump power consumption has been found for a temperature-difference based strategy with constant mass flow and an on/off hysteresis of 20/14K [Klingenberger 2000].

Wittwer et.al. have analysed different control strategies for an existing solar hot water system as part of the German program “Solarthermie 2000”. A validated system model of a solar system has been used as reference and simulations with various control strategies for solar and storage discharge pump have been conducted. Also the influence of the feed-in position of the solar hot water into the storage has been investigated. The additional system gain compared to the reference system was found to be highest for a combination of a hysteresis-control of the solar and discharge pump together with stratified storage charging. An insolation-based control strategy led to slightly lower system gains than a temperature-difference based one [Wittwer *et al.* 2002].

Krause et.al. have performed different optimization procedures on existing large solar thermal systems using genetic and evolutionary algorithms. The solar gain less the pump power consumption was defined as an objective function and performance improvements have been simulated using TRNSYS for varying input parameters and algorithms. They conclude that the influence of pump flow rates on solar gain is significantly higher than of control parameters [Krause *et al.* 2002].

Interpreting the work of Klingenberger and Streicher, it can be concluded that solar gain and electrical power consumption are mainly determined by the on/off temperature difference and hysteresis of the solar pump. Both authors state that a rather high upper hysteresis temperature together with a small difference between upper and lower hysteresis yields a high solar gain and low power consumption. Also, a constant mass flow in the solar circuit is recommended by both. In addition, Klingenberger and Wittwer conclude that an insolation-based control strategy does not perform better than a temperature-based one, although this could be expected.

3.2.1.2 Choice of reference layer in storage tank

The position of the temperature sensor in the storage tank which is used for the differential comparison between collector field and storage tank temperature is an important parameter for the performance of solar thermal systems. In both domestic and solar cooling systems, this sensor position determines the available hot water volume. In domestic systems, the temperature level of this volume is of secondary interest as long as the minimum water temperature for domestic use is being exceeded. For solar cooling however, the temperature level is of importance. The outlet temperature of the storage top layer influences the chiller input temperature if a parallel connection of heat exchanger, storage tank and chiller is used as shown in Figure 3.2.2. The controller C2 compares the storage layer temperatures to a the set minimum start-up temperature of the chiller (here: 60°C). If this temperature is exceeded, the chiller and its external pumps P3, P4 and P5 are being switched on.

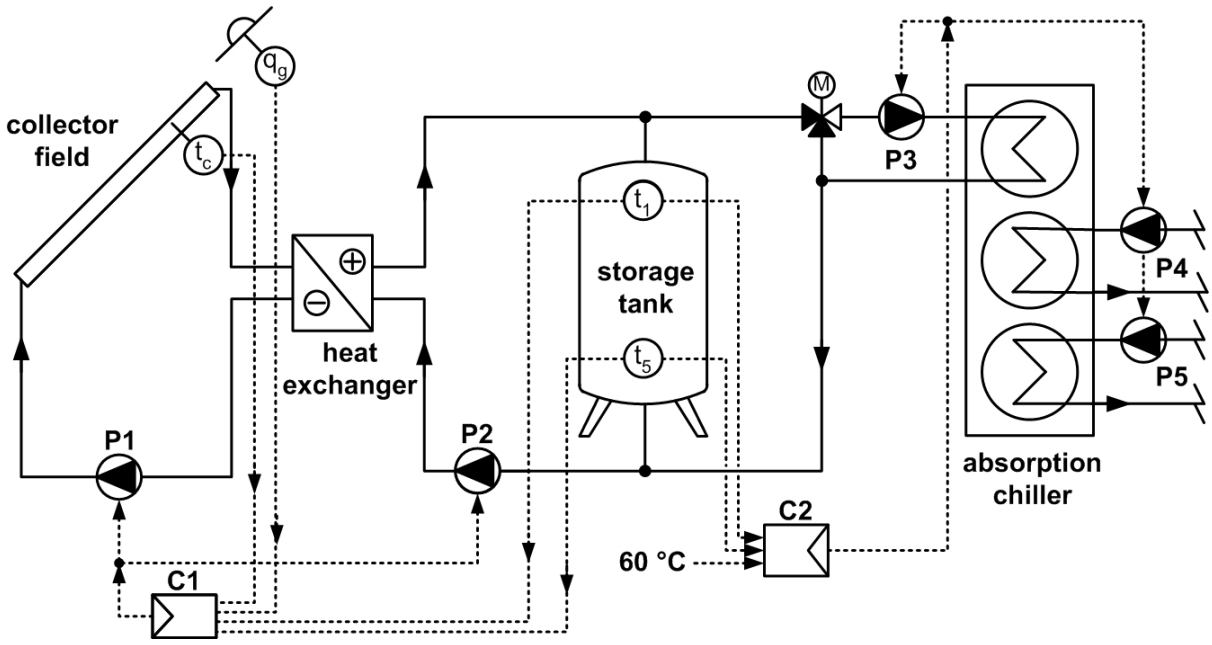

Figure 3.2.2. Hydraulic scheme of solar, storage and hot water circuit with controllers.

The available hot water volume also determines the charging time, i.e. the time period until a specified temperature in this volume has been reached. Again, in domestic solar systems this time period is not important, yet in solar cooling systems it strongly influences the daily operating time of the chiller. A lower sensor position results in a bigger hot water volume and a later start of the chiller during the morning and vice versa. Apart from the start time, the sensor position (or the reference layer) has more effects on the performance of the whole system. A difference can be made for three operation modes: before, during and after chiller operation.

Before the chiller is being started, the storage tank has to be charged to a minimum temperature level. Here, using the bottom layer is of advantage because then the whole tank is being charged to a set temperature; most likely the minimum start-up temperature of the chiller plus a 1-2K difference accounting for piping loss. The total tank volume is then available for chiller operation which results in a buffer volume sufficient to bridge shorter periods of low insolation. If the top layer temperature is being used, the tank will be charged earlier but the available buffer volume will be much smaller, resulting in more frequent chiller shutdown and start-up.

During chiller operation it makes a difference whether top or bottom layer are being used as reference layers. If the reference temperature is set at the bottom layer of the storage the system temperature decreases. The lower temperature of the bottom storage layer causes an earlier start of P1 and P2 due to the lower temperature difference to the collector field, resulting in a lower collector field outlet (and thus chiller inlet) temperature. Therefore the return temperature from the chiller also decreases, causing the bottom storage layer temperature to decrease further. The system temperature is drawn towards a lower level. If the reference temperature is taken at the top layer of the storage, the hot water temperature from the solar field is being kept on a high

level. The top temperature of the storage tank is higher than the bottom temperature and using it as hysteresis reference leads to higher collector outlet temperatures. Also, the temperature level of the storage top part and the absorption chiller inlet is about the same due to the direct coupling of solar field and chiller. Having a hot water volume in the top of the storage tank is of advantage during short periods of low insolation, e.g. caused by intermittent clouds. If pumps P1 and P2 stop working, the chiller is being driven with hot water from the storage top layer that has the same temperature as the hot water taken from the solar field previous to the switch-off of P1 and P2. During chiller operation, using the top layer as reference avoids rapid changes of hot water input temperature in the chiller and dampens the resulting oscillation of the chilled water outlet temperature. The latter is of importance if a chilled water temperature control is active. In this operation mode, a smaller difference between upper and lower hysteresis temperature is useful. This increases the pump pulsations and reduces the temperature fluctuations in the collector field outlet temperature due to shorter standstill time.

If the chiller inlet temperature falls beneath the minimum temperature during operation the chiller will shut down. If this happens during the day and cold demand exists in the building it is desirable to re-start the chiller as soon as possible. After a chiller shutdown with cold demand still existing it is therefore useful to charge the top layer of the storage tank instead of the bottom layer until the minimum start-up temperature of the chiller has been reached again. This way the buffer volume is small but charging can be achieved fast.

Control guidelines for the storage tank have been derived from experiments performed by Clauss for Phönix SonnenWärme AG [Clauss 2003]. The general relationship between storage reference layer and system performance was investigated as described above. The goal of these guidelines is to avoid a temperature decrease of the storage tank during chiller operation, to couple the temperatures of storage and solar field and to optimize the frequency of operation of the two-point controller for pumps P1 and P2 during chiller operation. Three operational modes for the storage tank have been defined. Table 3.2.1 gives an overview.

Table 3.2.1 Operational modes for the storage tank.

Mode	Task	Hysteresis (on/off) [K]	Storage reference layer	Cold demand
before chiller operation	charge storage tank for chiller start-up in the morning	7/3	Bottom	No
during chiller operation	provide buffer volume of hot water during chiller operation	7/5	Top	Yes
after chiller operation	prepare chiller start-up after unexpected chiller shutdown	7/3	Top	Yes

3.3 Cooling water temperature control

In this chapter, an overview on control possibilities for the cooling water temperature in a solar cooling system is being given. This chapter provides practical information for the application in solar cooling systems, reports experiences with a cooling water control strategy used in the Phönix solar cooling system and contains guidelines for optimized cooling water control. Different control strategies of the cooling water temperature have not been further investigated in this thesis. However, this chapter has been included in this thesis to complement the overview of all three external circuits of an absorption chiller regarding control strategies.

3.3.1 Fundamentals and state of the art

The cooling tower is an important component for the thermal behaviour of any cooling system. The absorption and condensation heat of the absorption chiller have to be dissipated at an average temperature level of approx. 30 °C. Such low temperatures usually exclude a further economical use of the reject heat, although there are applications in which the reject heat of the chiller is being used e.g. for the heating of outdoor swimming pools. However for most solar cooling systems a cooling tower in an open or closed configuration will be the simplest way to dissipate the reject heat to ambient.

3.3.1.1 Cooling tower design

The heat transfer from chiller to ambient air can be realised with various cooling tower configurations. In a dry cooling tower, only sensible heat is transferred to an ambient air flow. Dry cooling towers are called closed or indirect systems, as there is no direct contact between the cooling heat transfer fluid and the ambient air. The cooling fluid passes a tube bundle heat exchanger that is forced air-cooled by a motor-driven fan. A temperature difference between the cooling fluid and the ambient air of typically 10-15 K is necessary to reach sufficient heat transfer [Cube *et al.* 1997]. Dry cooling towers cannot provide cooling fluid outlet temperatures below ambient temperature but operate without any water consumption.

Wet cooling towers use mostly latent heat transfer to lower the temperature of the cooling fluid. They are called open or direct systems when there is a direct contact between cooling fluid and ambient air. For an open cooling tower, the cooling fluid has to be water. It is distributed over a package which is forced air-cooled by a motor-driven fan. Partial evaporation of approx. 2-3 % of the water as well as convection heat transfer between water and ambient air result in the cooling effect [Henning 2004]. A higher heat transfer rate due to evaporation allows lower temperature differences between water and air, however limited by the wet bulb temperature.
Wet cooling towers can provide water outlet temperatures below ambient temperature but they depend on the availability of water for operation. They also have significantly lower electricity

consumption due to smaller fans and are available at much lower investment cost. In the Phönix solar cooling system, a wet cooling tower of the construction displayed in Figure 3.3.1 is being used. It is a MITA PMS 4/65 model of the German producer Balcke-Dürr and will be further discussed in this chapter with regard to control issues.

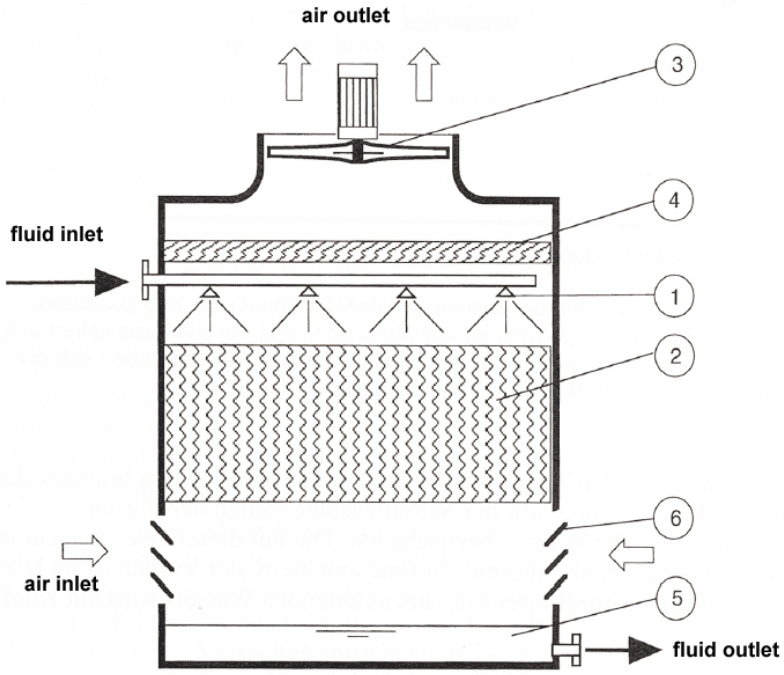

Figure 3.3.1 Typical cross section of open wet cooling tower [Cube *et al.* 1997]

Figure 3.3.1 shows a typical cross section of an open wet cooling tower. The warm water enters the cooling tower at the top and is distributed via a spray nozzle (1). After passing the exchange package (2) and cooling down it is collected in the cold water sump (5) from where it leaves the tower again. Air is drawn through the tower from bottom to top by a motor-driven fan (3). Louvers at the air inlet (6) prevent excessive water losses by splashing. A droplet separator (4) catches water droplets carried in the air stream. A flotation valve (not shown) controls the water level in the cold water sump and equalizes the water loss due to evaporation by adding fresh water from the grid.

The heat transfer in such a cooling tower is a function of the water inlet temperature, the water and air mass flows and the ambient air conditions. For the ambient air conditions, the wet bulb temperature is the dominating parameter. The relationship between cooling capacity, water inlet temperature and wet bulb temperature can be displayed in a characteristic diagram of the cooling tower. Wiegand has performed steady-state experimental measurements for the cooling tower used in the solar cooling system at Phönix. The characteristic diagram as calculated from these measurements is displayed over the full operation range in Figure 3.3.2 [Wiegand 2004].

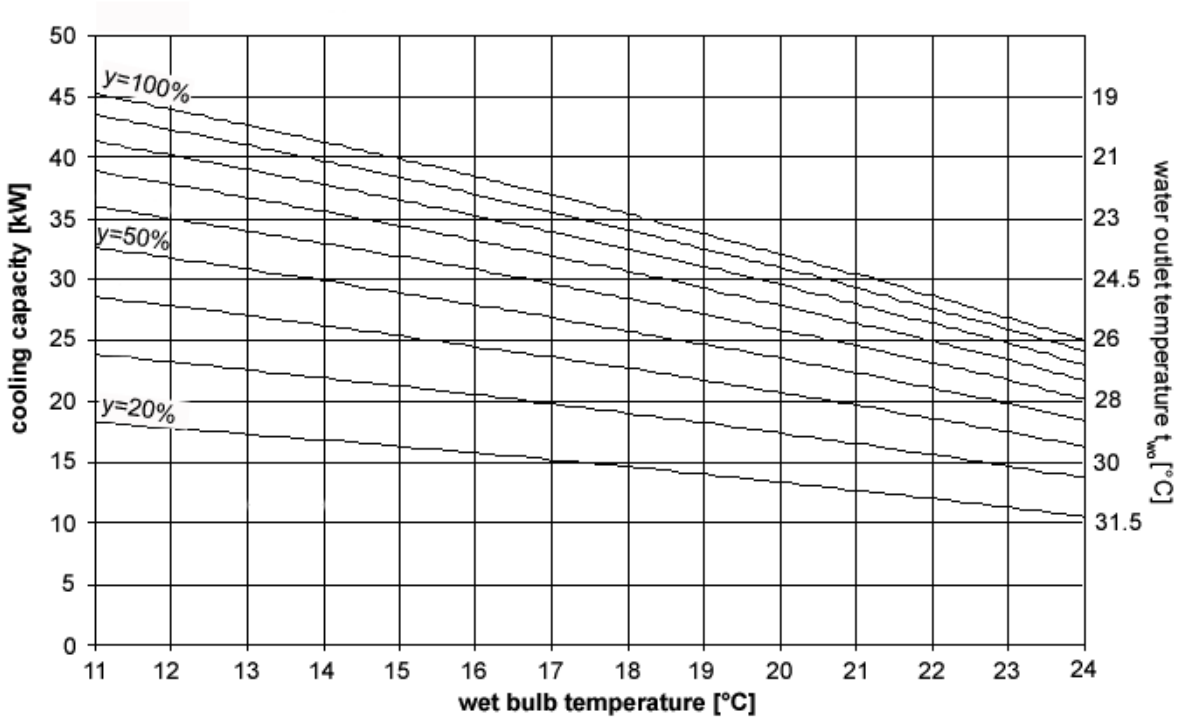

Figure 3.3.2 Characteristic diagram of the wet cooling tower for variations of the fan speed *y* between 20% and 100% of maximum speed. The inlet water temperature was 35 °C and the water mass flow was 0.69 kg/s for all steady-state calculations. Graph modified from Wiegand.

In Figure 3.3.2, the water mass flow as well as the water inlet temperature have been constant for all steady-states. The inlet water temperature into the cooling tower was 35 °C for all operation points, the mass flow was 0.69 kg/s. These values represent nominal operation of the absorption chiller. The air mass flow is being expressed by the fan speed *y*. It has been varied between 20% and 100% of the maximum fan speed. The cooling capacity is displayed versus the wet bulb temperature for various values of water outlet temperature.

Reading example: For a wet bulb temperature of 15 °C and maximum fan speed, a cooling water flow of 0.69 kg/s can be cooled from 35 to 21 °C, resulting in a cooling capacity of 40 kW. It can be seen that for constant water inlet temperature and mass flow there is a quasi-linear relationship between wet bulb temperature and cooling capacity.

3.3.1.2 Influence on absorption chiller performance

The cooling tower performance in a solar cooling system is influenced by a number of general conditions. Changes of the ambient air conditions influence the cooling power directly. Transient insolation as well as changing cooling loads influences the thermal performance of the absorption chiller and thus indirectly the return temperature of the cooling water. None of these general conditions can be influenced or changed by the user and the cooling tower control has to be able to equalize these external changes in order to provide cooling water at given parameters for all load conditions.

An important factor for the steady operation of an absorption chiller is a constant cooling water inlet temperature and a constant mass flow. For constant hot and chilled water inlet temperatures as well as mass flows, a change in cooling water temperature influences directly the absorber capacity and therefore the amount of water vapour flowing from evaporator to absorber. The heat flow in the evaporator changes and thus the chilled water outlet temperature. If a chilled water temperature control is active, any variation of cooling water temperature is a disturbance that has to be equalized by the chilled water control, thus lowering the control accuracy. A varying cooling water mass flow influences the heat transfer in the heat exchangers of absorber and condenser. The flow through the heat exchangers is designed to be turbulent at nominal conditions but can get laminar at lower mass flows, then resulting in lower heat transfer rates. This also influences the chilled water control.
The general demand on the cooling water control is to maintain a constant cooling water temperature as set by the user (or by a superior control) over the whole operation range of the absorption chiller.

3.3.1.3 Hydraulic setups and control

The control of temperature and mass flow can be realized in various ways by combining the respective hydraulic arrangement of the cooling water circuit with a suitable control strategy. Influence on the cooling water inlet temperature and the mass flow into the chiller can be taken via controllable components such as three-way valves, pumps and fans. An overview on common ways of controlling the cooling water temperature is given in Figure 3.3.3.

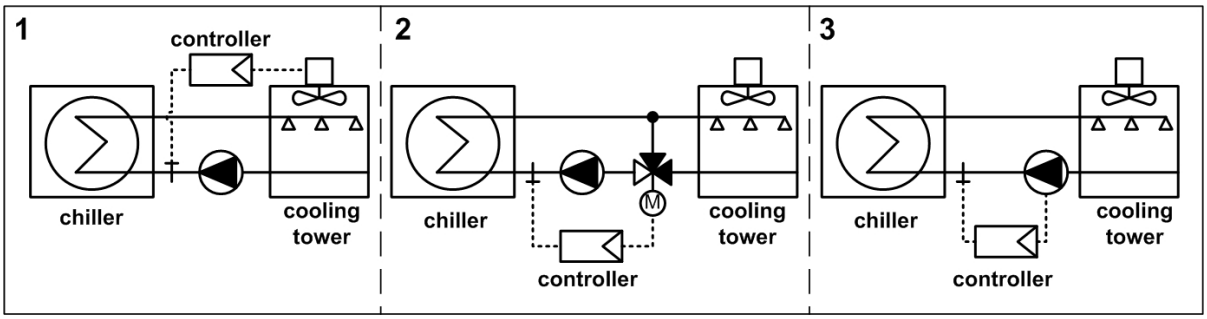

Figure 3.3.3 Overview on cooling water temperature control possibilities

In configuration (1), the cooling water inlet temperature into the chiller is being controlled via the speed of the cooling tower fan using a frequency inverter. The cooling water mass flow is kept constant. The water inlet temperature is being measured before the chiller and the fan speed is adjusted. An increased fan speed results in higher air mass flows, increased evaporation of water and thus lower cooling water temperatures; a decreased fan speed lowers the evaporation rate and results in a higher cooling water temperature. The fan is always operated at the speed that is being needed to provide the momentary cooling power. The electrical power consumption of the fan increases with the third power of the fan speed, hence one advantage of this configuration is rather low electricity consumption.

Furthermore, the constant mass flow of the pump ensures operation at nominal conditions of the chiller. A disadvantage of the system is the rather slow response to a control signal change due to thermal inertia of cooling water sump and piping. After changing the fan speed, the amount of water left in the sump has to pass the chiller first until water with the new temperature can follow.

Configuration (1) can also be operated in a simplified version without a frequency inverter. The fan is then operated by a two-point controller that switches the fan on if the inlet temperature lies outside a specified temperature range and off if it is within this range. If switched on, the fan runs always at full speed. The advantage of this configuration is a simple controller; the disadvantages are a high electricity consumption of the fan and periodically changing cooling water temperatures which influence absorption chiller performance.

In configuration (2), the cooling water inlet temperature into the chiller is being controlled via a three-way valve that mixes warm return water from the chiller with cold feed water from the cooling tower. The water inlet temperature is being measured at chiller inlet and the position of the valve is adjusted accordingly by the controller. The cooling water mass flow and the cooling tower fan speed are kept constant. The proximity of the three-way valve to the chiller allows a fast response of the cooling water temperature to a control signal change. However, this control strategy has a disadvantage in part load operation of the chiller. The cooling tower has to be designed in order to meet the full load at the highest existing wet bulb temperature for the chosen location. For lower wet bulb temperatures this results in a constant admixture of warm return water as otherwise the cooling water temperatures would be too low. At a constant fan speed, a high electricity consumption is the result.

In configuration (3), the cooling water inlet temperature into the chiller is being controlled via the pump speed of the cooling water pump using a frequency inverter. The cooling tower fan speed is kept constant. Again, the water inlet temperature is being measured before the chiller and the pump speed is adjusted accordingly by the controller. An increased pump speed results in lower temperature differences between warm and cold cooling water and vice versa. Although this configuration is quite simple, it has the disadvantage of changing mass flow through the chiller. This strongly influences the thermal performance of the chiller and increases the control activity of the chilled water controller. In analogy to (1) there is also a slow response to a control signal change due to thermal inertia of cold water sump and piping.

Of course combinations of (2) and (3) with (1) are possible. A fan speed control can be integrated in (2) and (3) as well, then solving the problem of high electricity consumption but also increasing the complexity of the control. However, the most energy-efficient cooling tower operation can be achieved using a frequency inverter for the speed control of the fan motor. The fan speed can be adjusted according to the momentary load and ambient conditions, resulting in constant fluid outlet temperatures over the full load range and significantly reduced power consumption. This is a significant advantage of configuration (1) compared to (2) and (3).

The control of the fan speed with regard to the outlet temperature of the cooling tower can be realised using a standard industrial PID-controller in a closed-loop.

Only few strategies have been published for the control of cooling tower parameters. A reason for this could be that cooling towers in industrial applications are usually operated at very constant conditions. In this case the control is reduced to on/off operation of the fan. Two advanced models suitable for fan speed control are presented as follows.

Fisenko and Petruchik present a mathematical model for the heat transfer between the water film on the packing and the air stream in a wet cooling tower based on heat transfer coefficients determined from experiments. For assumed steady-state operation they calculate the minimum air velocity that is necessary to achieve given water temperature drop at constant flow rates and changing ambient air conditions. Three different options for achieving bigger cooling capacities with a given cooling tower are described [Fisenko *et al.* 2004]. In another publication by the same authors a mathematical model is presented that takes the radii distribution of water droplets into account. The authors have established a correlation between the number of droplets and their velocity on the parameters of humid air. It was found that the distribution of the droplets in the cooling tower influences the evaporation rate. The smaller the droplets, the bigger the evaporative heat transfer. The model has been used for the calculation of the necessary air velocity for given inlet and outlet temperatures of water and changing air conditions [Fisenko and Petruchik 2004].

Although the above models for differ from each other in the fundamental heat transfer mechanisms, they have in common that the ambient air conditions have to be known for the heat transfer calculation. The authors did not provide information on the practical application of the models.

3.3.2 Fan speed control

For closed–loop control, the heat transfer characteristics of the cooling tower have to be known. They can be determined by a system identification of the cooling tower according to the methodology described in chapter 5.1. Then, a correlation between fan speed and cooling water outlet temperature can be calculated and used for the development of a controller. In operation, the measurement of the cooling water outlet temperature yields the deviation to a given setpoint and the fan speed can be adjusted accordingly.
However, the correlation between fan speed and cooling water outlet temperature is valid only for the conditions during which the identification of the cooling tower has been performed. If the operating conditions deviate from the identification conditions, the accuracy of the control decreases. Of all operating conditions, the water inlet temperature and the wet bulb temperature of the ambient air have the biggest influence on the cooling tower capacity (Figure 3.3.2). They have to be constant during the identification but will most likely change during normal operation.

Experiences with a closed-loop control of the cooling water temperature have been made in the Phönix solar cooling system in 2004 and in two other field test projects using the same chiller in 2005. There, a closed-loop strategy as in configuration (1) has been used for the cooling water temperature control. Although the underlying system identification has been carried out only for

specific water inlet and wet bulb temperatures, the control performs with very good accuracy, even for different inlet and air conditions. This comes as a surprise at first, but can be explained with the cooling tower design expressed by the characteristic diagram.

For the absorption chiller, the cooling water parameters required for nominal operation are an outlet temperature of 35°C, an inlet temperature of 27°C and a mass flow of 0.69 kg/s. The highest mean wet bulb temperature is 22°C for a system location in Germany. From the characteristic diagram in Figure 3.3.2 it can be seen that for a wet bulb temperature of 22°C and an inlet temperature in the cooling tower of 35°C a minimum outlet temperature of approximately 25°C can be achieved. The cooling tower has a surplus capacity due to its design which provides a degree of freedom sufficient for the control to maintain a setpoint of 27°C even at conditions other than it has been identified for.

Of course, this surplus capacity is not necessary. In fact, it increases the average electricity consumption of the cooling tower. During the cooling period, maximum wet bulb temperatures occur only very rarely. The average wet bulb temperature will be at least 3K lower than the maximum. A cooling tower with a fan and package designed for a cooling capacity that is bigger than the maximum required capacity has an electricity consumption which is also bigger, even in part-load operation. To reduce the electricity consumption, an optimum would be a tailor-made cooling tower for each absorption chiller, designed to provide just the maximum cooling capacity needed for the chiller, not more. Such a cooling tower can provide cooling capacity at lower electrical consumption of the fan speed. For the Phönix absorption chiller, such a tailor-made cooling tower has been developed as a consequence of the oversize of other commercially available cooling tower models. Further information on this model can be found in [Wiegand *et al.* 2005].

Of course a tailor-made cooling tower is not available for each absorption chiller model. Nevertheless, the application of a fan speed control strategy contributes significantly to the reduction of the electricity consumption. If a frequency-inverter is being used, such a fan speed control can easily be retrofitted to existing oversized cooling towers. For the oversized cooling tower in the Phönix system the control has been retrofitted in 2004. During the cooling period of 2003, the cooling tower has operated always at maximum fan speed with a power consumption of 0.55 kW. Then, the cooling water temperature was controlled via the three-way valve DWM 4 in Figure 2.3.2. During 2004, cooling water temperature was controlled via variable fan speed and the average power consumption was 0.23 kW. In daily balances, a peak power consumption of 0.49 kW and a minimum power consumption of 0.12 kW have been recorded in 2004. This shows that the cooling tower did not even operate once with maximum fan speed in 2004! The distribution of the electrical energy consumption in 2003 and 2004 can be seen in Figure 3.3.4 and Figure 3.3.5.

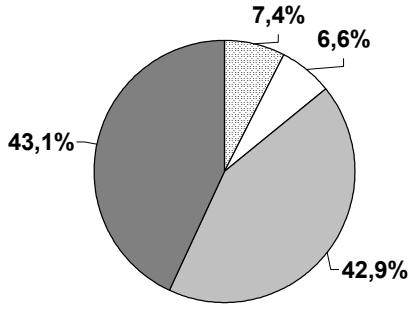

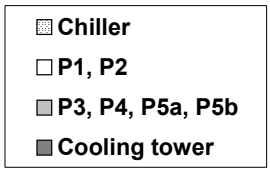

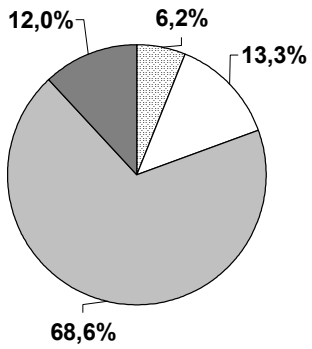

Figure 3.3.4. Electrical energy consumption of system components in 2003.

Figure 3.3.5. Electrical energy consumption of system components in 2004.

It is visible that the electrical energy consumption of the cooling tower has been drastically reduced from 2003 to 2004. Its share from the total power consumption was 43% in 2003 and only 12% in 2004.

3.3.3 Cooling water temperature setpoint

In this chapter, a general overview on cooling tower technology and possible control strategies for the cooling water temperature has been given. For the Phönix solar cooling system, experimental results with and without a fan speed control of the cooling tower have shown that the adaptation of the fan speed to the momentary cooling load of the absorption chiller is highly recommendable to reduce the parasitic power consumption of a solar cooling system. In such a control, the set point of the cooling water temperature is an important parameter. Two possibilities for choosing the set point can be formulated.

(1) If the purpose of a solar cooling system is to provide a defined cooling capacity at preferably low electrical energy consumption, then the cooling water temperature set point should be kept as high as possible. Under the condition that ample solar driving energy is available and the designated cooling load can be achieved, a high cooling water temperature reduces the electrical power consumption of the cooling tower fan. In cold-guided mode, a control hierarchy is recommended. First, the driving energy of the hot water should be used to achieve a desired chilled water temperature. Only if the available driving energy is not sufficient to maintain a constant chilled water temperature, the cooling water temperature should be lowered.

(2) If the purpose of a solar cooling system is to provide maximum cooling capacity and if the electrical power consumption is of secondary importance, then the cooling water temperature set point should be kept as low as possible. This increases the electrical power consumption of the cooling tower fan to maximum capacity but also increases the

cooling capacity of the evaporator. Also, higher solar fractions can be achieved due to the lower return temperature of the hot water into the collector field.

The combination of the two possibilities above provides a contribution to the problem of oversized system design for maximum cooling loads. Still, the majority of air-conditioning and cooling systems is being designed in order to handle the maximum annual cooling load. This however occurs only on very few days per year. During the rest of the time, the oversized system operates in part load with reduced efficiency and thus high electricity consumption. This applies to both conventional and solar cooling systems. Applied to the latter, a combination of (1) and (2) in combination with a thorough system design can help to solve this problem. A system can be designed for dissipating not the maximum but an average specific cooling load from a building, operating most of the time as described in (1) with a relatively high cooling water setpoint. During the few days where the cooling load in the building rises, combination (2) can be used. Additional cooling capacity can then be provided due to lower cooling water temperature, however at higher power consumption. Using this method, the solar cooling system does not have to be oversized to handle the maximum annual cooling load, however the cooling tower needs to have surplus capacity. Nevertheless, the investment cost for a cooling tower with surplus capacity will be much lower than for a complete oversized system.

3.4 Chilled water temperature control

In this chapter, only the fundamentals of chilled water temperature control will be presented. Such a control can be designed quite easily if the transfer behaviour of the chiller is known. Controller design is a standard procedure and shall not be discussed further in this thesis. In contrast, the determination of the transfer behaviour is the interesting part of the control design. The focus in this thesis will therefore be laid on the identification of the transfer behaviour, expressed by the transfer function of the chiller. Two methods for this will be described in detail in chapter 5.

3.4.1 Fundamentals and state of the art

For most cooling applications a constant chilled water temperature has to be maintained. The desired temperature level of chilled water depends on the cold distribution system, for which several variations exist. The most common systems are fan-coils, chilled ceiling or wall panels and thermo-activated building parts (slab cooling). Fan-coils usually operate with inlet temperatures around 6-8 °C, chilled ceiling panels with inlet temperatures of 15-16 °C and thermo-activated building parts can have inlet temperatures up to 20 °C. A fixed inlet temperature value is usually required for each cold distribution system. For fan-coils, the temperature has to be below the dew point to ensure sufficient dehumidification of the air. For chilled ceiling panels, the temperature should be above the dew point to prevent condensation of water on the panels.

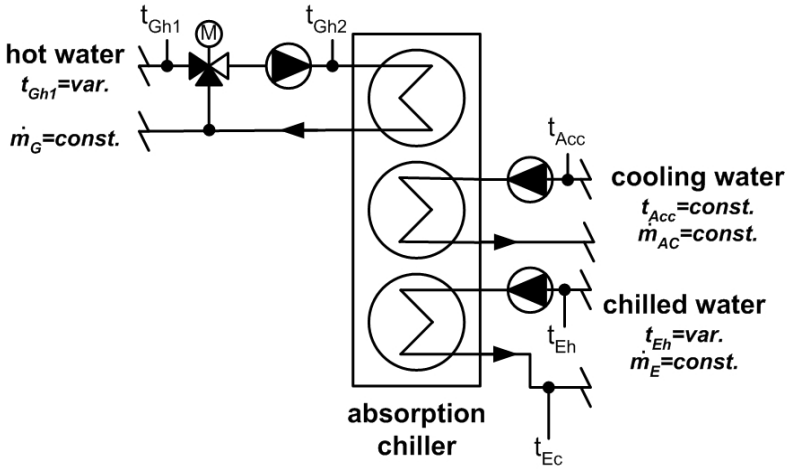

Figure 3.4.1. Chilled water control via hot water temperature

The chilled water temperature of an absorption chiller can be controlled using different strategies. The most common strategy is the control of the hot water inlet temperature during chiller operation with constant cooling water inlet temperature as shown in Figure 3.4.1. A three-way valve is being used to mix the cold return flow from the generator with the supply flow of temperature t_{Gh1} from the hot water source. The valve recirculation is controlled in such a way that the hot water temperature t_{Gh2} entering the chiller in combination with inlet temperatures of cooling

water t_{Acc} and chilled water t_{Eh} results in the desired chilled water outlet temperature t_{Ec}. At constant cooling and chilled water input temperature, the reduction of the external heat input into the generator results in a decrease of vapour mass flow to the condenser and thus a lower concentration of the solution leaving the generator. The lower solution concentration reduces the capacity of the absorber and less vapour mass flow can be absorbed. This results in a decrease of the evaporator heat flow and a rising chilled water outlet temperature.

$$t_{Ec} = f(t_{Gh2}, t_{Acc}); \textit{ constant mass flows through all heat exchangers assumed}$$

The dependency of t_{Ec} on t_{Gh2} and t_{Acc} at constant mass flows depends on the thermal behaviour and the chiller construction and is different for each chiller. The characteristic of the controlled system, i.e. valve, piping and chiller, needs to be known for this control strategy. The hot water based control will be chosen most likely for applications with a variable hot water temperature such as solar cooling systems. In such systems, large variations in hot water temperature have to be equalized by the control.

A second possibility is the control of the cooling water inlet temperature during chiller operation with constant hot water inlet temperature as shown in Figure 3.4.2. A three-way valve is being used to mix the warm return flow from the condenser with the cold supply flow of temperature t_{Acc1} from the cooling water source. The valve recirculation is controlled in such way that the cooling water temperature t_{Acc2} entering the chiller in combination with inlet temperatures of hot water t_{Gh} and chilled water t_{Eh} results in the desired chilled water outlet temperature t_{Ec}. For constant hot and chilled water inlet temperatures as well as mass flows, an increase in cooling water temperature decreases the absorber capacity, therefore less water vapour can be evaporated in the evaporator. The heat flow decreases and the chilled water outlet temperature rises.

$$t_{Ec} = f(t_{Acc2}, t_{Gh}); \textit{ constant mass flows through all heat exchangers assumed}$$

Using a three-way valve as in Figure 3.4.2 does not allow the reduction of t_{Ec} as the re-circulated return cooling water has always a higher temperature than the supply flow. This hydraulic setup can therefore only be used to prevent the chilled water temperature from too low values. Again, the characteristic of the controlled system needs to be known.

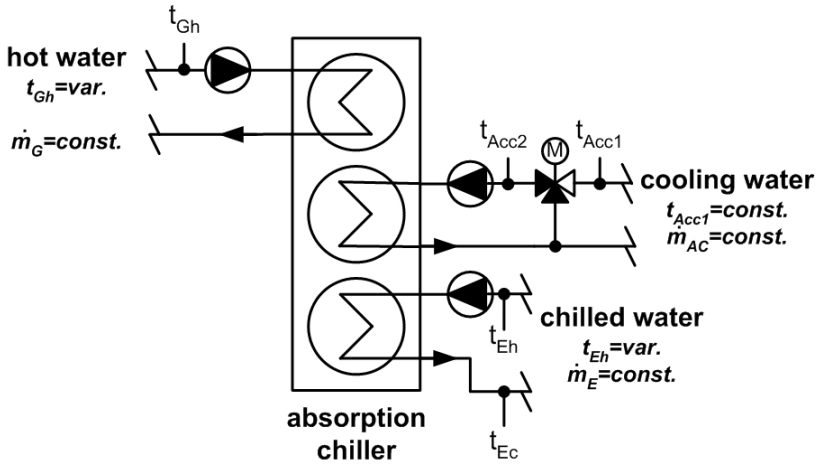

Figure 3.4.2. Chilled water control via cooling water temperature

The setup of Figure 3.4.2 will most likely be used for applications with very constant operating parameters. A constant hot water source of sufficient temperature level is necessary. For example, this could be a system with district heating as heat source. District heat yields very constant supply temperatures and a chilled water control only has to maintain the set temperature at part load operation (i.e. limit it from getting too low). Of course strategies for controlling the cooling water temperature other than using a three-way valve can be applied here. Using a frequency-inverter for fan speed control of a dry or wet cooling tower allows the adjustment of t_{Acc2} over a wider temperature range. The cooling water control using a three-way valve is rarely being used due to the fact that t_{Ec} can only be increased, not reduced as well.

A combination of both hot and cooling water based strategies can also be used. If the hot water inlet temperature is not sufficient for a given cooling load the cooling water temperature can be lowered in order to reach the desired chilled water temperature. The optimum combination of hot and cooling water control depends on the user-specified conditions as discussed in chapter 3.3.3.

The realization of any of the two control strategies described in this chapter requires a controller for maintaining the set temperature. In a practical application, the correct parameters of such a controller have to be identified for stable system operation. This can be done by determining the transfer function of the system using either experimental or theoretical methods. In chapter 5, one experimental and one theoretical identification method will be presented and compared to each other. The controller development itself is a standard procedure and will not be discussed in this thesis.

4 Solar circuit control

Solar cooling is a highly transient system operation. The naturally fluctuating input parameters in a solar cooling system result in output fluctuations as well. However, the influence of each input parameter on the system behaviour is not the same. For a solar cooling system, the insolation is usually the most transient input parameter and has the greatest influence on the overall system performance. Consequently, solar and storage circuit are the most complex system circuits due to their control strategy and number of components. As described in chapter 3, all system circuits are equally important for successful overall system operation, however solar and storage circuit have the largest input variations and thus the highest control demand. They also contribute considerably to the total power consumption of the system. Their operational behaviour will therefore be investigated more profound in this thesis with regard to thermal performance and power consumption.

The control task for these circuits is twofold: Firstly, the transient influence of the insolation has to be equalized, at least partially, to provide constant input conditions for the chiller. Secondly, a certain storage volume has to be charged to sufficient temperature level to buffer low insolation periods. The latter can be achieved by applying the storage tank operation modes as given in Table 3.2.1. It will not be further discussed in this thesis. Instead, solar and storage circuit are being further investigated in this chapter with regard to different ways of controlling the mass flow as introduced in Chapter 3.2.1.1.

The experimental application of the mass flow control strategies to the Phönix solar cooling system will be described as follows. As each experimental day is different regarding insolation and weather conditions a simulation of the total system has been performed in addition. It will be described and discussed as well in this chapter.

Note: In the following, the combination of solar and storage circuit will be referred to simply as solar circuit.

4.1 Experimental application of mass flow control strategies

In addition to the control setup of Figure 3.2.2, another controller has been used for maintaining a steady outlet temperature of the chilled water. Figure 4.1.1 shows the final control setup.

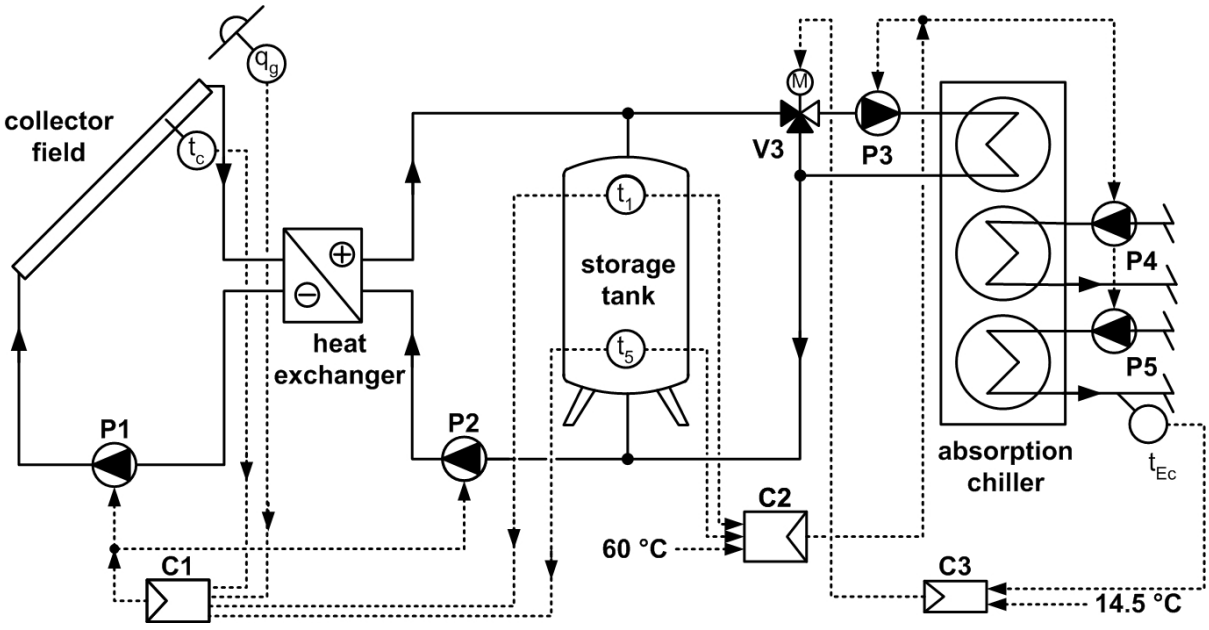

Figure 4.1.1. Hydraulic scheme with chilled water control.

During chiller operation the controller C3 compares the chilled water outlet temperature t_{Ec} to a given setpoint (for the Phönix system this setpoint is 14.5 K) and controls the position of valve V3 accordingly. There, the return hot water mass flow is mixed with the supply hot water mass flow to achieve the necessary input temperature for the set chilled water temperature. A constant hot water mass flow input including a stable hot water temperature level is necessary to achieve stable control behaviour of C3 as well. The chilled water control strategy used in the experiments was hot-water-based as discussed in chapter 3.4.

The three control strategies described in chapter 3.2 and the storage tank modes described in chapter 3.2.1.2 have been used during the operation of the Phönix solar cooling system in the cooling period of 2004. All strategies have in common that the on/off commands for solar and storage circuit pumps P1 and P2 are determined via a hysteresis between collector field temperature and storage temperature. The storage reference temperature is determined according to the operational modes in Table 3.2.1. The only difference between the control strategies is the mass flow of pumps P1 and P2 during operation. It is either constant, temperature-dependent or insolation-dependent. For the latter two strategies the control parameter describing the correlations between mass flow and temperature difference respectively insolation had to be determined empirically. This procedure was not an analytical one. Engineering knowledge combined with experience from previous work led to the correlations presented. The control strategies used for experiments in 2004 have thus not been optimized for best

performance using e.g. parameter studies or simulations. They represent only a part of the possible solutions.

The experimental data recorded is not too suitable for comparing the three strategies. Each experimental day has different insolation and different ambient and building conditions. This results in a different chiller runtime and operating condition for every day. For example, a cloudless day in summer with an integrated insolation of 240 kWh per day yields a chiller runtime of 7.5 hours and a cooling energy of 61 kWh per day. A day with medium cloud coverage and transient insolation of 160 kWh yields a chiller runtime of 5 hours and a cooling energy of 26 kWh per day. The fluctuation of the insolation has a strong influence on the system performance. For an objective comparison of control strategies, equal input data would be preferable. Therefore the system has been modelled in a theoretical simulation using TRNSYS. Each strategy has been implemented and simulation runs with equal input conditions have been performed. The goal was to determine the differences between the strategies and to find the most suitable one for system operation with minimised power consumption. The next chapter describes the simulation methodology.

4.2 Solar system simulation

The control strategies described in the previous chapter need to be compared to each other with regard to their electrical energy consumption, solar gain and cooling effect. To perform such a comparison it is necessary to design a software model that allows the simulation of all control strategies with multiple variations of input parameters. For this reason, a TRNSYS simulation of the solar cooling system has been modelled. It includes the main components like collector field, heat exchanger, pumps, storage tank, three-way valve, absorption chiller and piping. The hydraulic and control setup of the simulations is similar to Figure 4.1.1. Except for the absorption chiller and the collector type, all TRNSYS types being used in the model are standard types included in the TRNSYS component library [Klein *et al.* 1996]. The collector type being used is a non-standard type which models the thermal performance of a flat plate collector, accounting for the heat capacity of collector and fluid and the transport time of the fluid through the collector [Isakson and Eriksson 1993]. The heat transfer fluid being used in all circuits of the system is water. The absorption chiller is being simulated using an absorption chiller model developed by Albers [Albers 2004b]. The cooling tower and chilled water circuits have been left out of the model to keep the simulation simple and avoid additional disturbances. Instead, cooling and chilled water are kept at constant inlet temperature and mass flow without being modelled as components. Due to the complexity of the file it is not possible to display a one-page figure of it. Each simulation has been performed over a time period of 12 hours.

To investigate the performance behaviour of each control strategy for different insolation characteristics, two different insolation patterns have been used for simulations. This allows the testing of each control strategy with various degrees of controller action and allows a comparative rating of each strategy. Figure 4.2.1 shows the different insolation variations.

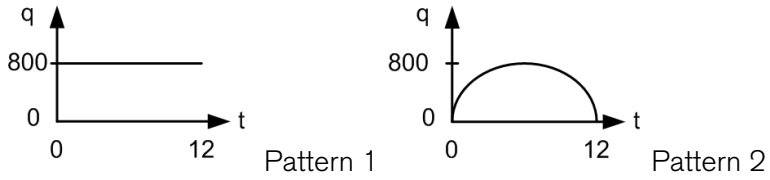

Figure 4.2.1. Insolation patterns used for simulation (units: y-axis: W/m², x-axis: h)

A constant insolation (pattern 1) does not require a high degree of controller action. The constant insolation leads to a fast storage charge and an early start-up of the absorption chiller. Hot water of sufficient temperature can be provided from the solar thermal system for almost the whole simulation time. In order to test a more realistic insolation pattern as well, the bell curve-type (pattern 2) was chosen. It models the insolation of a typical cloudless day in central Europe with increasing and decreasing radiation and has thus the highest demand on the control. Hot water from the solar thermal system can only be provided for a certain time during the simulation due to the decreasing insolation at the end. The storage tank is thus being discharged towards the simulation end.

The simulation results for the combination of a certain control strategy and a certain insolation pattern can only be compared to the results for the other control strategies using the same insolation pattern. In order to allow a comparison of the results, key figures have been calculated.

4.2.1 Key figures and control parameters

The attempt of this chapter is to compare different control strategies with regard to their primary energy consumption and thermal performance. The primary energy consumption can be expressed in terms of the power consumption Q_{el} of the system pumps P1, P2 and P3. Pumps P1 and P2 express the electrical energy being needed in the solar and storage circuit, P3 represents the electrical energy being needed for chiller operation. The electrical energy needed for the external pumps of cooling and chilled water is independent from the solar control strategy and not considered here. The internal electricity consumption of the chiller due to solution and refrigerant pump does not depend on the solar control strategy and is also not considered. The total power consumption per simulation interval i reads

$$Q_{el} = \sum_{i=0}^{12} (P_{1,i} + P_{2,i} + P_{3,i}) \cdot \Delta\hat{t} \qquad (4.2.1)$$

The thermal performance of the solar circuit can be described by the energy input from the solar field Q_S achieved during a simulation run (i.e. the energy used for chiller operation plus the amount of energy stored in the tank). Q_S is being calculated on the secondary side of the solar heat exchanger HX12 in Figure 2.3.2 and includes therefore the thermal loss of the heat exchanger to ambient as well as its effectiveness.

$$Q_S = \sum_{i=0}^{12} \dot{m}_{B,i} \cdot cp_i \cdot \left(t_{Bh,i} - t_{Bc,i}\right) \cdot \Delta\hat{t} \qquad (4.2.2)$$

The thermal performance of the solar cooling system can be described by the integrated energy input into the evaporator of the absorption chiller Q_E achieved during a simulation run (i.e. the cooling effect). Q_E is being calculated on the evaporator inlet/outlet of the absorption chiller.

$$Q_E = \sum_{i=0}^{12} \dot{m}_{E,i} \cdot cp_i \cdot \left(t_{Eh,i} - t_{Ec,i}\right) \cdot \Delta\hat{t} \qquad (4.2.3)$$

The heat capacity in equation (*4.2.2*) and (*4.2.3*) is calculated using the arithmetic mean temperature of fluid inlet and outlet temperature.

Another key figure is the time it takes to charge the bottom layer of the storage tank from the temperature of 38 °C at simulation start to the minimum temperature of 60°C that is necessary for chiller start-up. The start-up time t_{start} thus indicates whether a control strategy is able to charge the storage tank as fast as possible, allowing an early chiller start during daily operation. t_{start} is being measured in hours from the simulation start.

The runtime of the chiller t_{op} is also a key figure for each strategy. It depends on the control strategy and is being measured by integrating the simulation time steps with the chiller in operation.

As a measure for comparing the control strategies, the individual values described above are only partially suitable. The interesting fact is the electricity consumption that is necessary to achieve the cooling effect. To combine this information in a single parameter, the yield factor a is defined as

$$a = \frac{Q_E}{Q_{el}} \ [\mathrm{kWh_{th}}/\mathrm{kWh_{el}}]. \qquad (4.2.4)$$

The quotient of Q_E and Q_{el} gives information about the energy ratio of cooling effect to electricity consumption and allows the comparison of the control strategies with regard to the thermal performance of the solar cooling system.

The open-loop control parameters for the TDIFF and INSOL strategy have been set as follows for the simulations. The mass flow in solar and storage circuit of TDIFF per time step *i* is calculated in percent of the value of the previous time step *i-1*.

$$\dot{m}_{K,i} = \dot{m}_{K,i-1} \cdot (0{,}005 \cdot x_i + 1) \qquad (4.2.5)$$

$$x_i = \Delta_{real,i} - \Delta_{set}$$

$$\Delta_{real,i} = t_{c,i} - t_{1/5,i}$$

$$\Delta_{set} = 10\,K$$

The temperature of the storage layer $t_{1/5,i}$ is chosen according to the current storage operation mode as described in chapter 3.2.1.2. The mass flow per time step *i* is limited by the controller to maximum and minimum values in order to avoid a wind-up behaviour. The coefficient of 0.005 1/K in *(4.2.5)* has been determined empirically as described in chapter 4.2. It is valid for the collector field size and hydraulic setup of the Phönix solar cooling system described in chapter 2.3. The set-point temperature difference Δ_{set} was 10 K for all simulations and experiments.

For the INSOL strategy, the calculation of the mass flow is different over the insolation range. Until a threshold of 450 W/m² the mass flow is kept constant at minimum pump speed. For the insolation range between 450 and 800 W/m², equation (4.2.6) is being used to calculate the mass flow depending on the momentary insolation *q*,

$$\dot{m}_{K,i} = 0{,}001 \cdot q_i \qquad (4.2.6)$$

Above an insolation of 800 W/m² the mass flow is kept constant at maximum pump speed. The slope of 0.001 was found experimentally. It is valid for the collector field size and hydraulic setup of the experimental system described in chapter 2.3.

4.2.2 Simulation performance analysis

Three different simulation runs with varying solar insolation have been performed for each control strategy described in chapter 3.2.1.1. Every simulation run has a time range of 12 hours with a simulation interval of 0.1 hours, thus simulating half a day at six-minute time steps. At the start of every simulation run the storage tank has always the same stratification and temperature distribution with an average temperature of approx. 38 °C, collector field and piping components are at ambient temperature of 22 °C. The controllers C2 and C3 in Figure 4.1.1 work the same way for all control strategies.

An analysis of the consistency of the simulation can be done by comparing the results of the three control strategies at constant insolation. There, the least controller action is required and the results of the different strategies are most comparable. The integrated values for constant insolation can be estimated beforehand. With an average collector field efficiency of 45 %, a 12-hour insolation of 800 W/m² on the absorber area of 42 m² should yield a solar gain of approximately 181 kWh or an average heat flow of 15 kW. With this heat flow, the storage tank temperature should increase from 38°C to 60°C within approximately 1.3 hours. For an operation

time of 12 hours (P1, P2) and 10.7 hours (P3), the total electrical power consumption can be estimated to 4.6 kWh.

The simulation graphs for constant insolation are presented in Figure 4.2.2 to Figure 4.2.4.

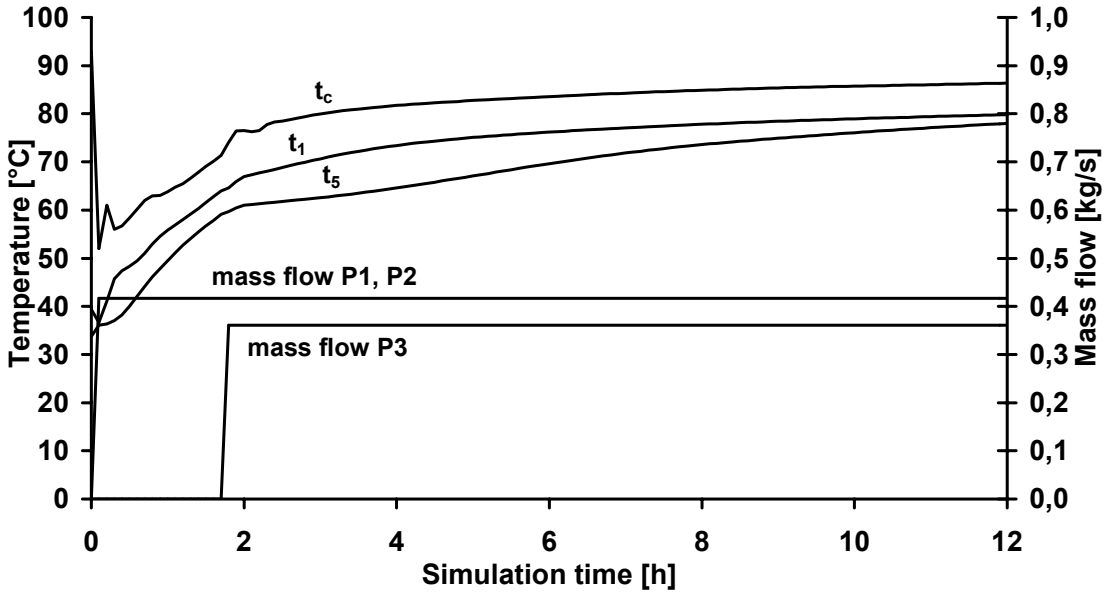

Figure 4.2.2. Simulation results for STAN at constant insolation.

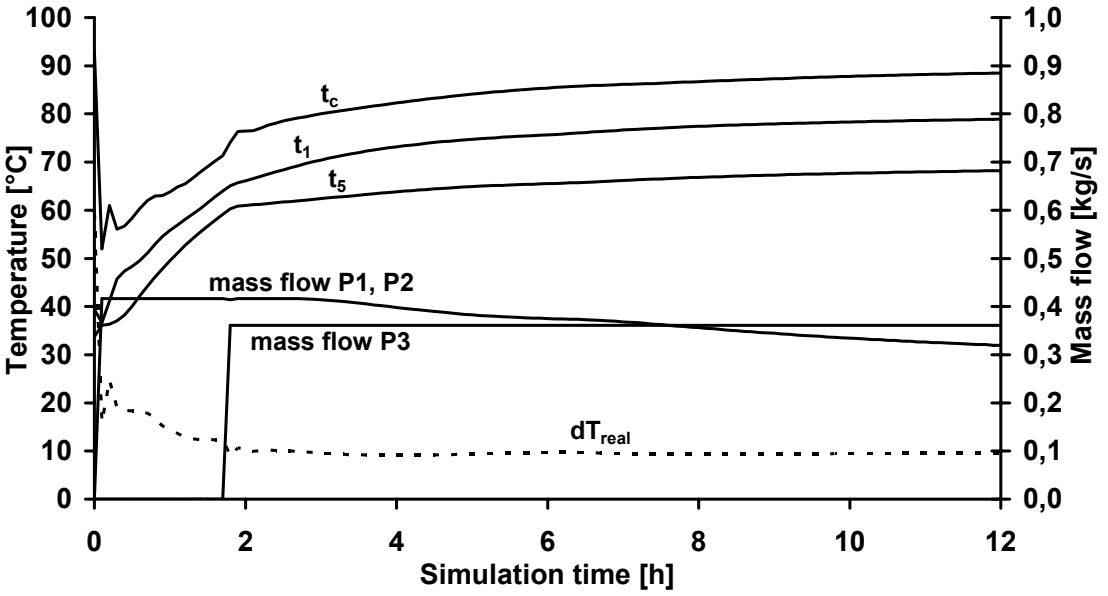

Figure 4.2.3. Simulation results for TDIFF at constant insolation.

Note: The high initial collector temperature t_c in Figures 4.2.2 to 4.2.4 is the result of software limitations in TRNSYS 15. There, a six minute period is the smallest possible simulation interval. Irradiating the collector with 800 W/m^2 over the first six minutes of the simulation leads to the high collector temperature of approx. 90 °C. With the pump start-up in the next simulation interval this temperature then rapidly decreases.

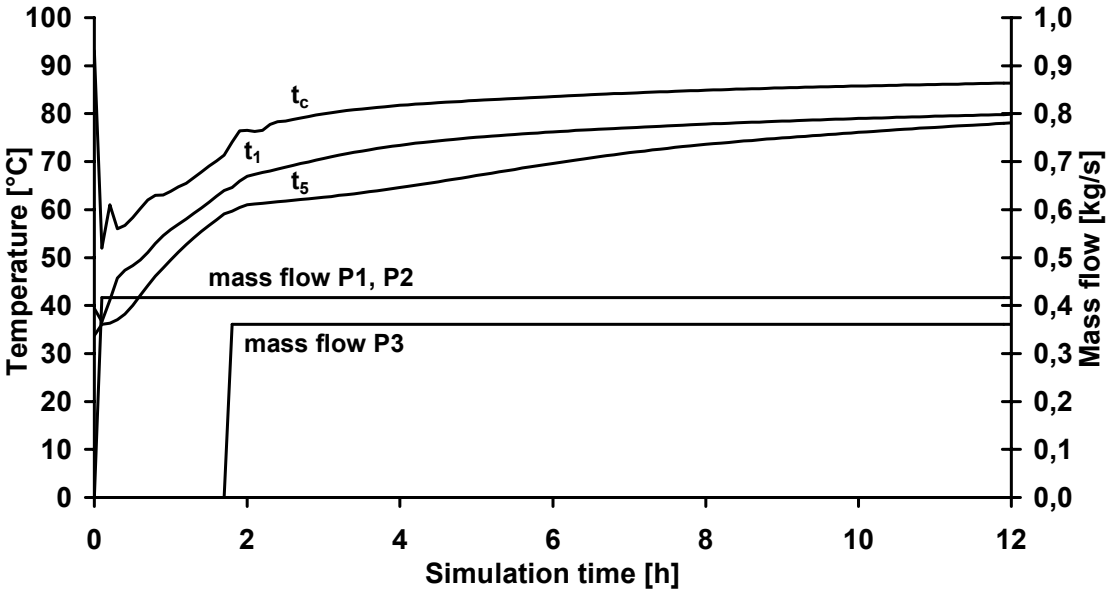

Figure 4.2.4. Simulation results for INSOL at constant insolation.

It is visible that the simulation course until chiller start-up is equal for all three strategies. Solar and storage pump P1 and P2 operate immediately after simulation start as soon as the upper hysteresis temperature has been reached. The storage tank is then being charged and after 1.8 h of simulation time pump P3 starts operating. The mass flow in solar and storage circuit is the same for all three strategies until chiller start-up and has then a maximum value of 1500 kg/h or 0.42 kg/s. For the STAN strategy, the mass flow equals the maximum mass flow of pumps P1 and P2. For the INSOL strategy, the mass flow is calculated according to (4.2.6) and has also the maximum value of 0.42 kg/s. Compared to the other two strategies, the mass flow of the TDIFF strategy is the same for the first 2.8 hours of the simulation as long as the set temperature difference Δ_{real}=10 K (Figure 4.2.3) is exceeded. After that, the mass flow decreases to maintain the set temperature difference of 10K.

The integrated simulation results for the control strategies in combination with constant insolation are presented as follows. The electrical power consumption Q_{el}, the solar gain Q_S, the cooling effect Q_E, the yield factor a, the chiller operation time t_{op} and the start-up time t_{start} are displayed in Table 4.2.1. The maximum values of Q_s, Q_E, t_{op} and a as well as the minimum values of Q_{el} and t_{start} are shown in bold numbers.

Table 4.2.1. Key figures for different solar control strategies and constant insolation.

(units: Q_{el} [kWh_{el}], Q_S, Q_E [kWh_{th}], a [kWh_{th}/kWh_{el}], t_{start}, t_{op} [hours])

	Q_{el}	Q_S	Q_E	a	t_{op}	t_{start}
STAN	4.6	176.1	128.9	28.0	10.2	1.8
TDIFF	**4.2**	176.1	**130.9**	**31.2**	10.2	1.8
INSOL	4.6	176.1	128.9	28.0	10.2	1.8

The solar energy heat flow Q_s integrated over the simulation time is equal for all three strategies, as visible in Table 4.2.1. STAN and INSOL have exactly the same mass flow and storage tank temperatures, thus equal values of Q_s are reasonable for these strategies. As visible in Figure 4.2.3, the consequences of the lower mass flow of TDIFF are slightly higher collector temperatures and a bigger temperature difference between top and bottom of the storage tank. This also yields a bigger temperature difference between inlet and outlet of the collector field, as the bottom temperature of the storage tank influences the return temperature of the solar circuit. The lower mass flow of TDIFF is thus compensated by a bigger temperature spread, yielding a heat flow value equal to STAN and INSOL. With an equal mass flow of P3 for all strategies, the bigger temperature spread in the storage tank also yields a bigger heat flow into the generator and therefore a bigger value of Q_E.
The electricity consumption Q_{el} is equal for STAN and INSOL but lower for TDIFF. This can be explained with a lower mass flow of P1 and P2 and thus lower pump power consumption of TDIFF. The start-up time of the chiller is the same for all three strategies due to the same conditions for heating up the storage tank at simulation start. The same values of operation time result from equal start-up times and sufficient insolation afterwards.
At constant insolation, the TDIFF strategy has an advantage compared to STAN and INSOL due to its mass flow control via temperature difference, not insolation. The INSOL strategy performs like STAN if the insolation is absolutely constant and has therefore no advantage.

The numeric values of the simulated integrated heat flows for constant insolation in Table 4.2.1 prove the estimations made earlier. The slightly smaller simulated value of Q_s can be explained with the heat exchanger effectiveness and the thermal loss in storage tank and piping which is assumed in the model. The longer start-up time is due to a smaller average heat flow into the storage tank than assumed. For constant insolation conditions, the TRNSYS model performs internally consistent with expected numeric results and will be used for further simulations.

4.3 Results and discussion

The Phönix solar cooling system is in operation since August 2003. During the time period of September and October 2003 the system has been operated in solar-guided mode only. From October 2003 until May 2004 the system was out of operation. During this period, no cooling load existed in the building. In the cooling period between May and October 2004, the system has been operated in cold-guided mode. In this time period, experimental results using the solar circuit control strategies STAN, TDIFF and INSOL in combination with the storage modes described in chapter 3.2.1.2 were achieved.. In this chapter, the experimental results are presented and compared to simulation results. To allow a comparison, only experimental days with bell-curve-like insolation using flat plate collectors have been chosen. All variable names in the following figures refer to Figure 2.3.2.

4.3.1 STAN strategy

Results from simulation and experiment are presented for the STAN strategy as follows. The simulation has been performed with the bell-curve insolation pattern. It is being compared to an experimental run from a cloudless day with bell-curve insolation. The flat plate collector field has been used for this run. Cooling water and chilled water temperature were controlled as described in chapters 3.3 and 3.4, respectively. Figure 4.3.1 shows the simulation, Figure 4.3.2 to Figure 4.3.4 show the experiment. Unfortunately the data acquisition has been started late on this experimental run so data is only available from 11:30 am onwards.

Note: In the following simulation graphs, the mass flow into the generator, m_{P3}, is constant and thus displayed as one tenth of its value for the reason of better visibility of the other parameters.

4.3.1.1 Simulation results

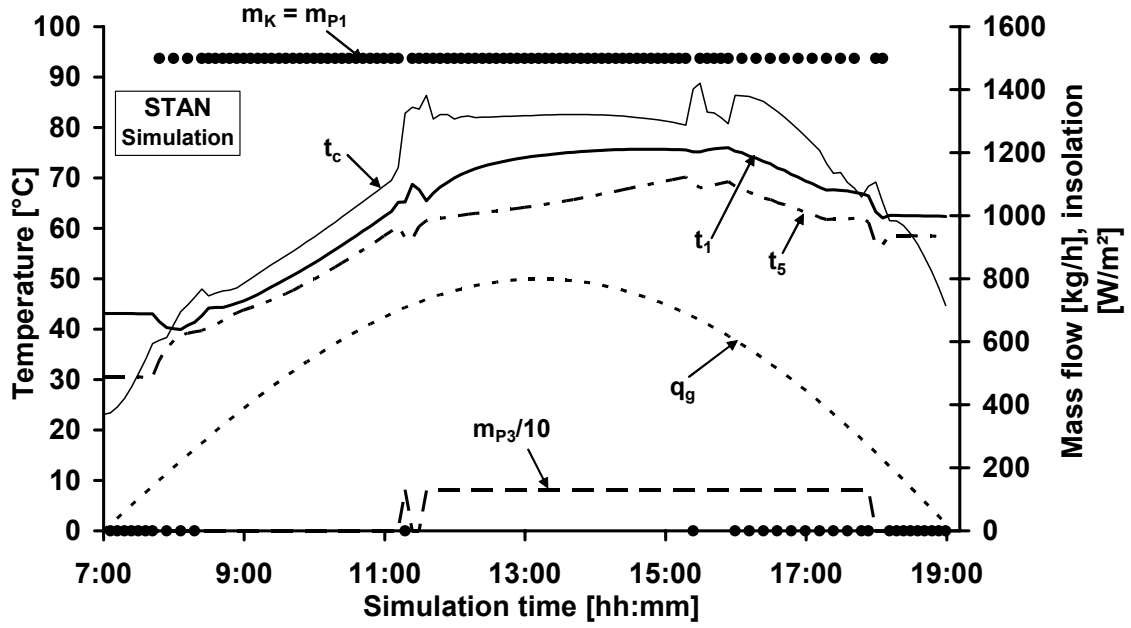

Figure 4.3.1. Simulation results for STAN at bell-curve insolation. Collector and storage tank temperatures are shown on the left ordinate, mass flow and insolation are shown on the right ordinate.

4.3.1.2 Experimental results

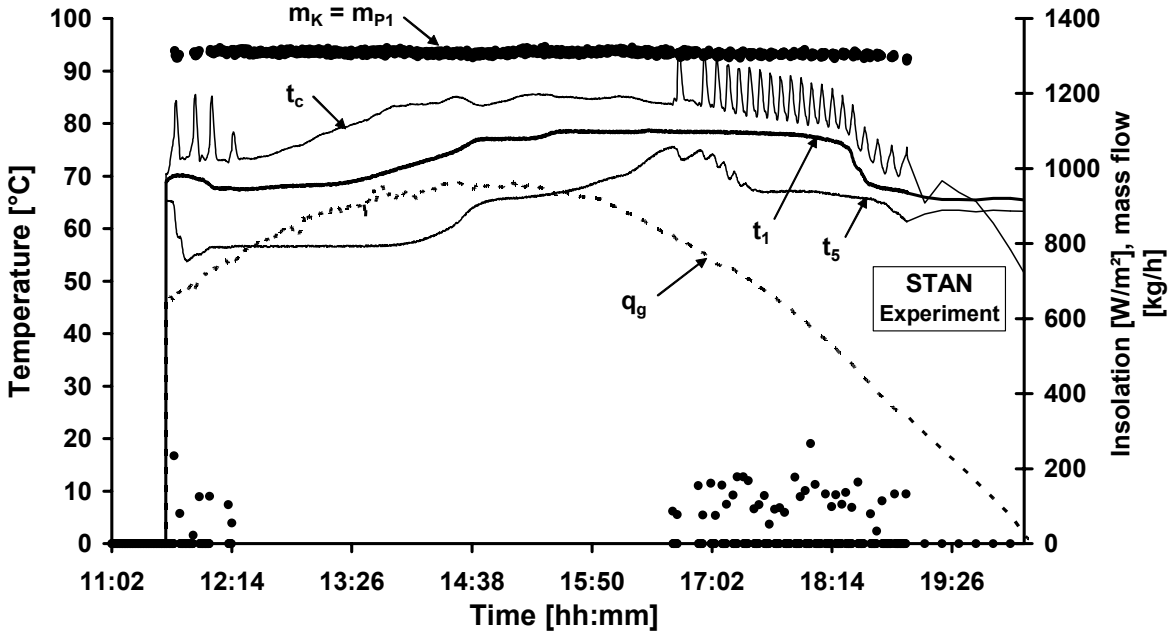

Figure 4.3.2. Experimental results for STAN with bell-curve insolation. Collector and storage tank temperatures are shown on the left ordinate, mass flow and insolation are shown on the right ordinate.

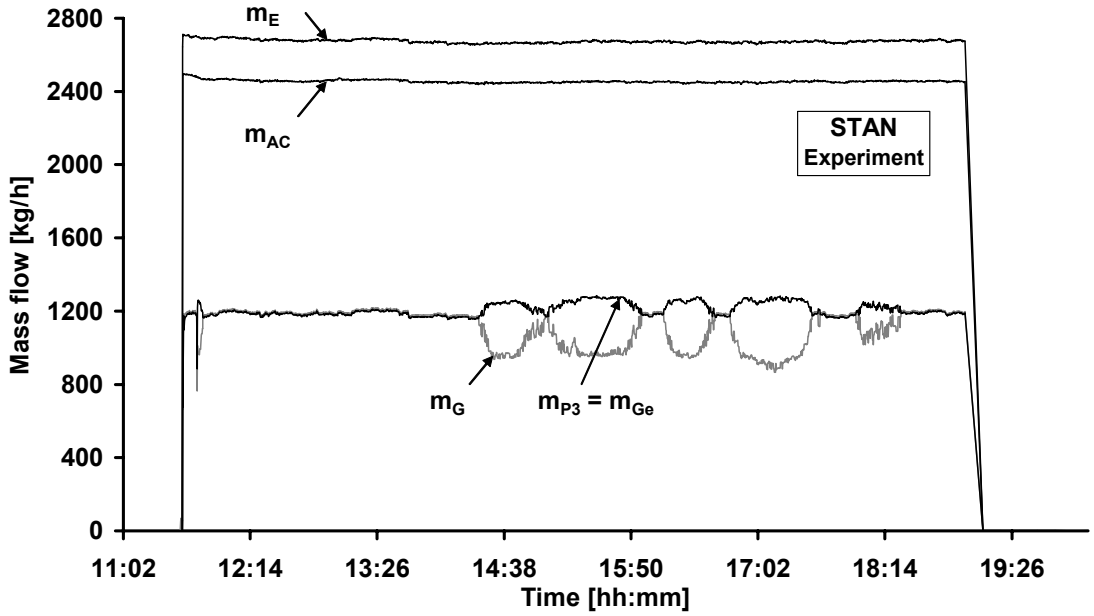

Figure 4.3.3. Experimental mass flows for the STAN with bell-curve insolation.

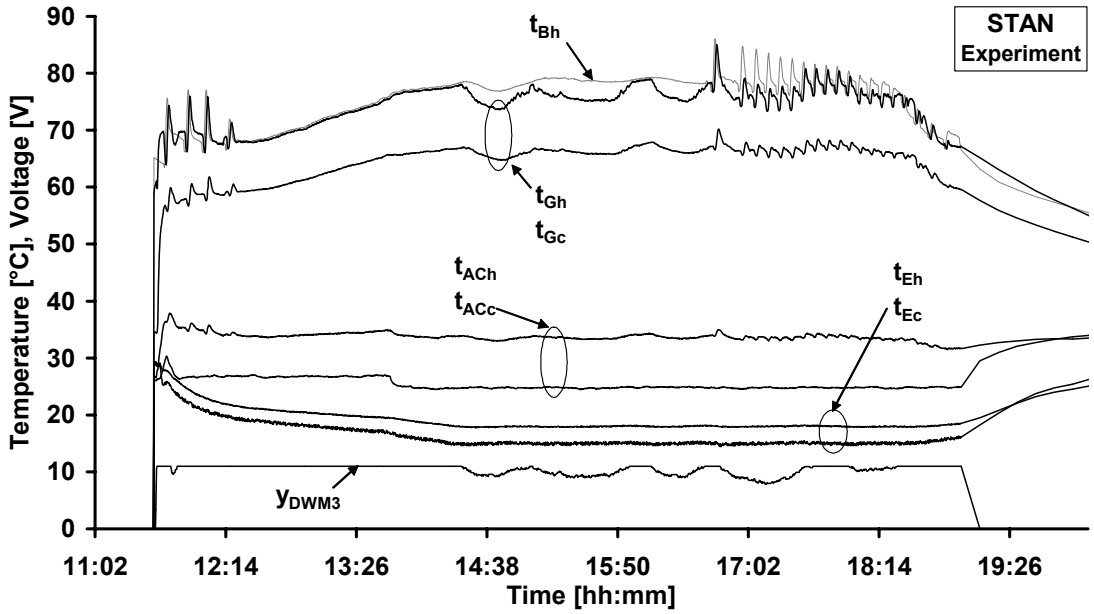

Figure 4.3.4. Experimental external temperatures of the chiller for STAN with bell-curve insolation. Also shown is the control voltage of the valve DWM3.

The comparison of Figure 4.3.1 to Figure 4.3.2 shows a good dynamic agreement between simulation and experiment. The typical characteristic features of the STAN strategy can be seen in both figures. The solar mass flow m_{P1} is constant at all times. At low insolation between 800 and 400 W/m², mass flow pulsations which translate into temperature fluctuations and hot water temperature peaks can be seen. These peaks are better visible in the experiment due to the smaller measurement interval. The simulation has a time step of six minutes; the real data acquisition of 13s.

Figure 4.3.2 shows that the real insolation resembles very much the bell-curve used for the simulations with a maximum insolation of 960 W/m² at 2:26 pm. The storage tank has an average temperature of approx. 67 °C at chiller start which increases to a maximum value of approx. 77 °C at 4:37 pm. It decreases again to approx. 64°C at the end of the run. The collector temperature has peaks of approx. 10 K around noon and 4:30 pm which are due to the on/off pulsations of the solar circuit pump. For decreasing insolation between 800-600 W/m², 20 pulses of the solar pump occur. The mass flow of the solar circuit $\dot{m}_K$ has been constant at 1310 kg/h, if pump P1 has been operating. The mass flow data points around and below 200 kg/h have been sampled after the pump has just been switched on or off.

Figure 4.3.3 shows the other mass flows of the system. It can be seen that cooling and chilled water flows have been constant at values of 2400 and 2700 kg/h, respectively. The mass flow $\dot{m}_{Ge}$ through the generator of the chiller varies between 1210 and 1280 kg/h, depending on the position of the valve DWM 3. Ideally, there should be no variation of $\dot{m}_{Ge}$, but due to an unequal hydraulic balance there have been slight variations. Also shown is the mass flow entering the valve DWM 3, $\dot{m}_G$. The difference between $\dot{m}_{Ge}$ and $\dot{m}_G$ is the recirculation of the return flow of the chiller through the valve.

Figure 4.3.4 shows the temperatures of the external circuits of the absorption chiller. Also shown is the hot water outlet temperature of the heat exchanger HX 12, i.e. the temperature t_{Bh} of the mass flow $\dot{m}_G$. The control voltage of the valve DWM 3 is shown as well. It can be seen that cooling water inlet as well as chilled water inlet and outlet temperature are constant. The setpoint of the cooling water inlet temperature was changed from 27°C to 25°C at 1:44 pm. The hot water inlet temperature into the chiller fluctuates according to the position of DWM 3 and the respective flow recirculation. The decrease of hot water temperature due to the recirculation is the difference between t_{Bh} and t_{Gh}. The recirculation and thus the control of t_{Ec} started at 2:20 pm. The setpoint for the chilled water outlet temperature was 15 °C. It was reached at 2:20 pm and t_{Ec} was kept constant until 6:40 pm with maximum deviations around the set point of +0.4 °C and -0.6 °C.

4.3.2 TDIFF strategy

For the TDIFF strategy no experimental run with absolutely cloud-free insolation has been recorded. The run with the closest approximation of the insolation to a bell-curve is shown in Figure 4.3.6 to Figure 4.3.8.

4.3.2.1 Simulation results

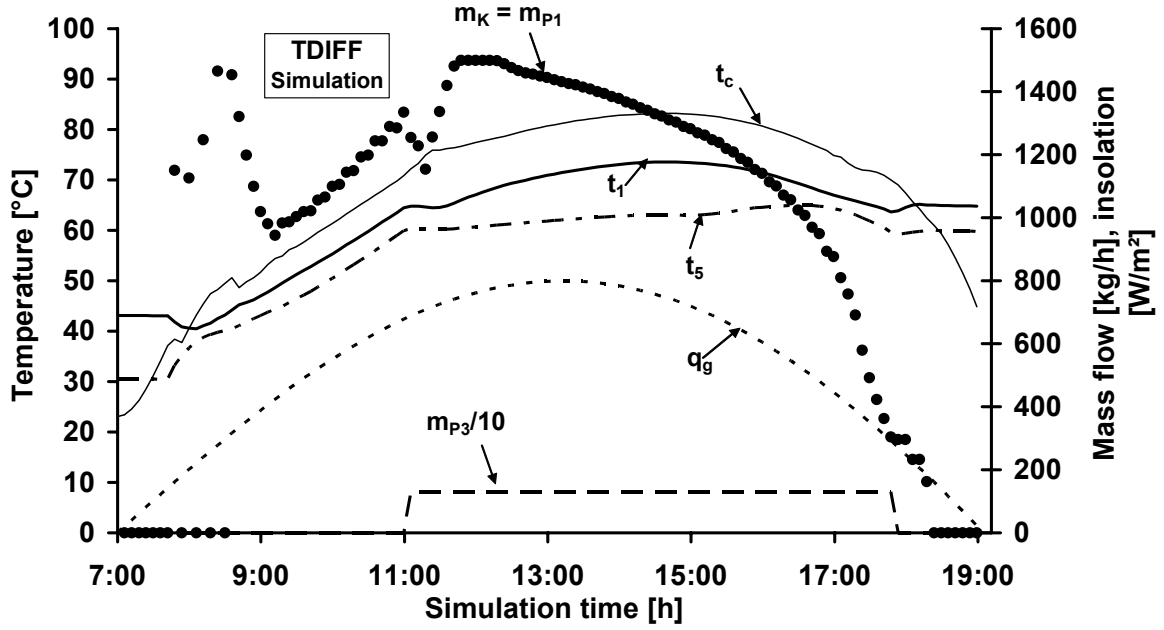

Figure 4.3.5. Simulation results for TDIFF at bell-curve insolation

4.3.2.2 Experimental results

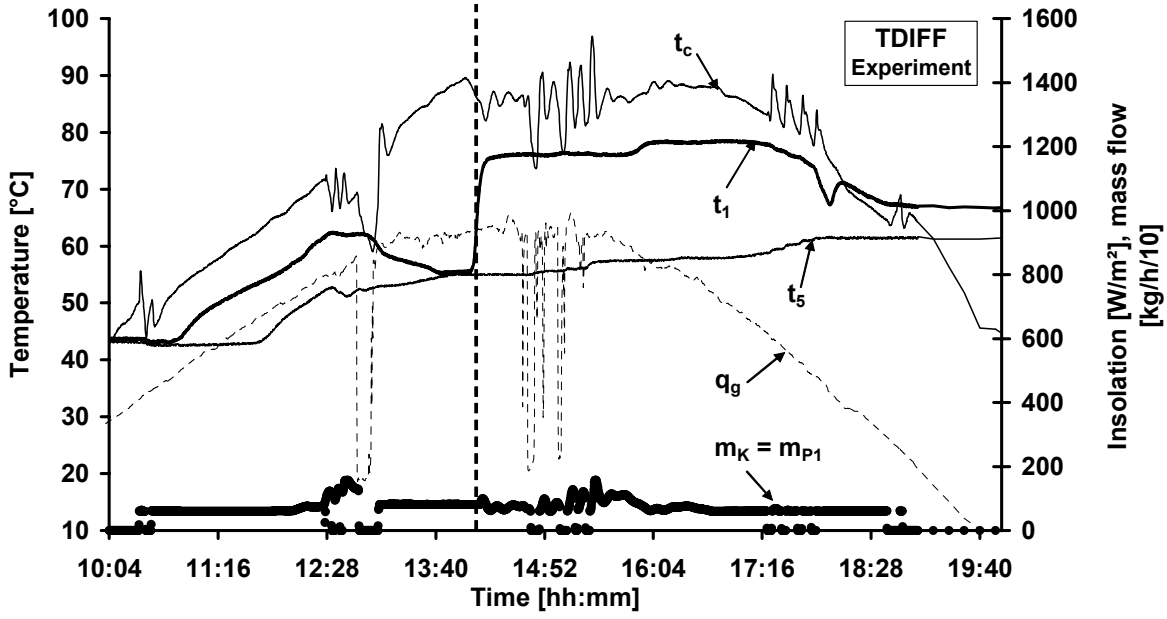

Figure 4.3.6. Experimental results for TDIFF with quasi-bell-curve insolation. Collector and storage tank temperatures are shown on the left ordinate, mass flow and insolation are shown on the right ordinate. The solar circuit mass flow is shown as one tenth of its value for better visibility. The dashed line marks the end of the time period without TDIFF control.

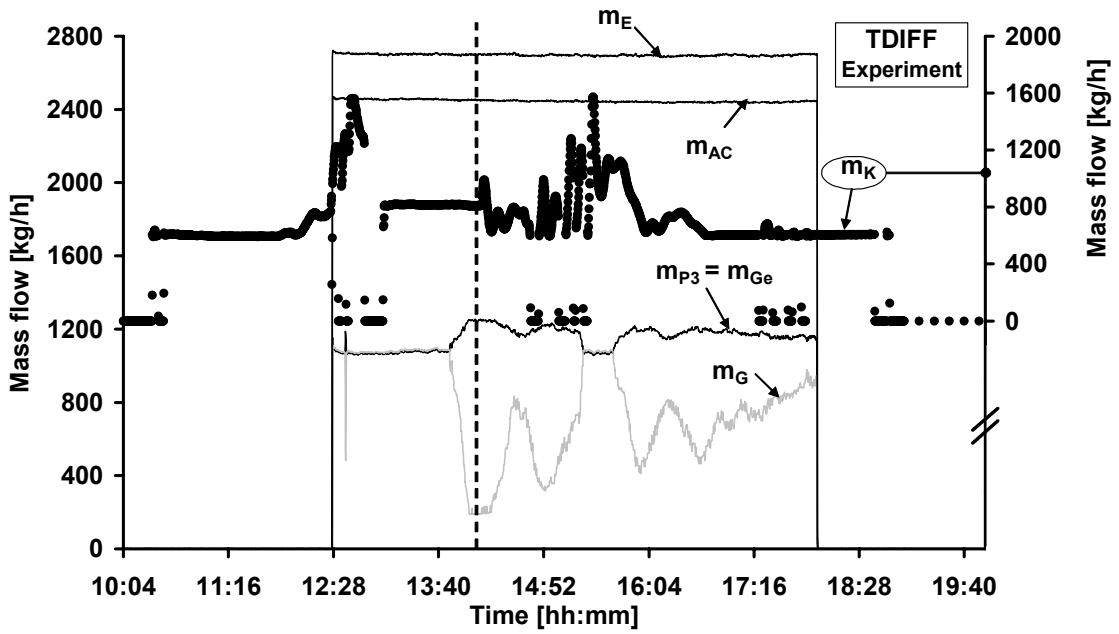

Figure 4.3.7. Experimental mass flows of TDIFF with quasi-bell-curve insolation. The dashed line marks the end of the time period without TDIFF control. The solar mass flow m_K is shown on the right ordinate, all other mass flows are shown on the left ordinate.

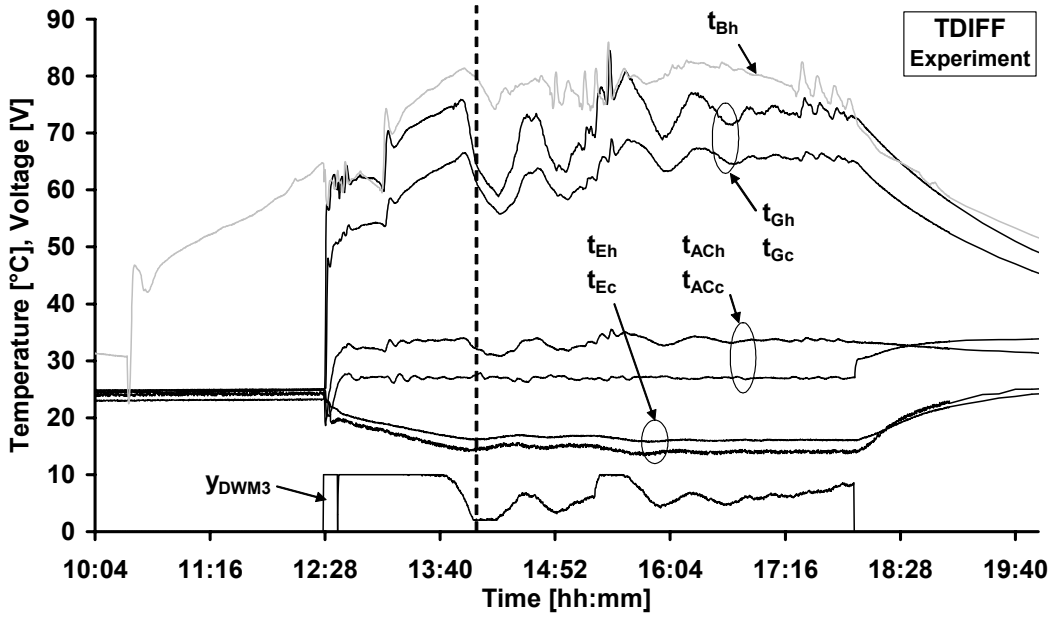

Figure 4.3.8. Experimental external temperatures of the chiller for TDIFF with quasi-bell-curve insolation. Also shown is the control voltage of the valve DWM 3. The dashed line marks the end of the time period without TDIFF control.

During this run, the TDIFF control was not in operation until 2:03 pm due to a malfunction of the software control code. The end of the time period with TDIFF not in operation is marked with a dashed line in the three experimental graphs. For the time period with TDIFF in operation, the

temperature difference between t_{coll} and t_{PS1} was set to 10K. Flat plate collectors were in use during this run, chilled and cooling water control were active.

The characteristic feature of TDIFF is the coupling of the solar mass flow to the temperature difference between collector and storage tank. Due to this variable mass flow, the pulsing of the solar pump is being reduced at lower insolation. This also yields less peaks in the collector outlet temperature, as visible in Figure 4.3.6. For the insolation range between 650-500 W/m², only four pulses can be seen. The insolation in Figure 4.3.6 is not perfectly bell-curve-shaped but has two "dents" at 12:37 pm and 2:50 pm where it decreases by approx. 700 W/m². The transient insolation around 2:50 pm results in several oscillations of the mass flow $\dot{m}_K$, as visible in Figure 4.3.7. During these oscillations the collector temperature cannot be maintained at 10K above the top layer temperature of the storage. From 3:21 pm onwards the set temperature difference can be maintained again until 4:43 pm. Then the mass flow $\dot{m}_K$ is at its minimum value of 600 kg/h and the 10K cannot be kept anymore due to decreasing insolation. The minimum mass flow of pumps P1 and P2 in the experiment is different from the simulation where the minimum mass flow was zero, as visible in Figure 4.3.5.

Cooling and chilled water mass flows are constant at 2400 and 2700 kg/h, respectively. The mass flow $\dot{m}_{Ge}$ through the generator of the chiller varies between 1080 and 1250 kg/h, again due to the unequal hydraulic balance. The setpoint of the cooling water inlet temperature is 27°C, the setpoint for the chilled water outlet temperature is 15 °C at the beginning and changed to 14 °C at 3:17 pm. The first setpoint is being reached at 1:42 pm and the second at 3:35 pm. The chilled water control starts at 1:47 pm. The chilled water outlet temperature t_{Ec} is then kept constant until 6:00 pm with maximum deviations around the set point of ±0.5 °C. The storage tank has an average temperature of 57.5 °C at chiller start-up, increases to a maximum of 68°C at 5:18 pm and decreases again to 65°C at chiller shutdown.

4.3.3 INSOL strategy

4.3.3.1 Simulation results

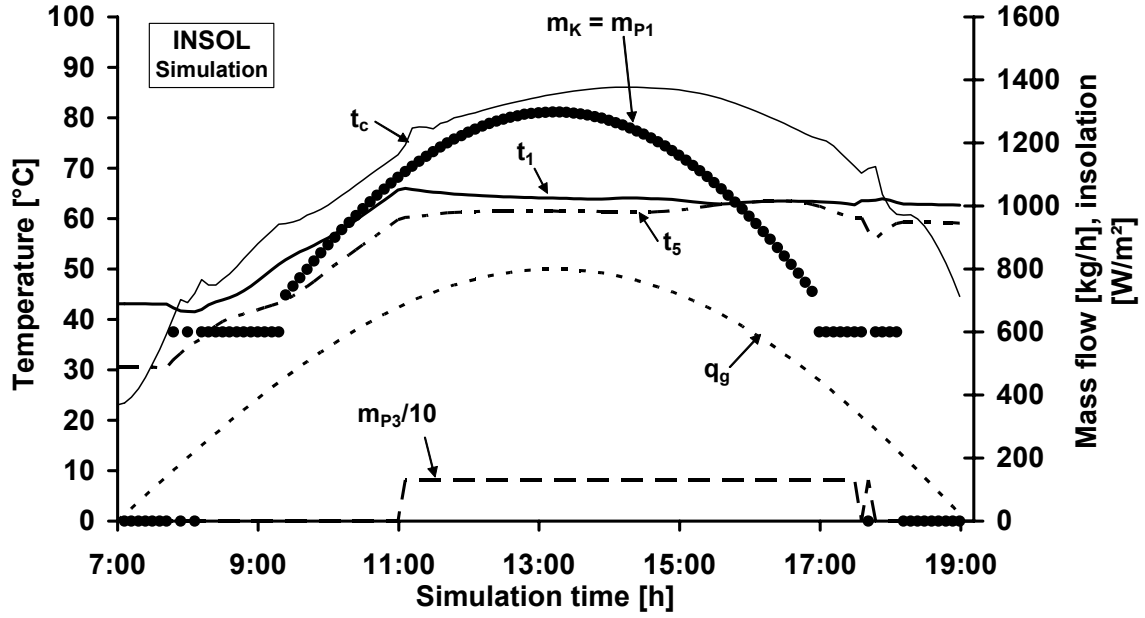

Figure 4.3.9. Simulation results for INSOL with bell-curve insolation.

4.3.3.2 Experimental results

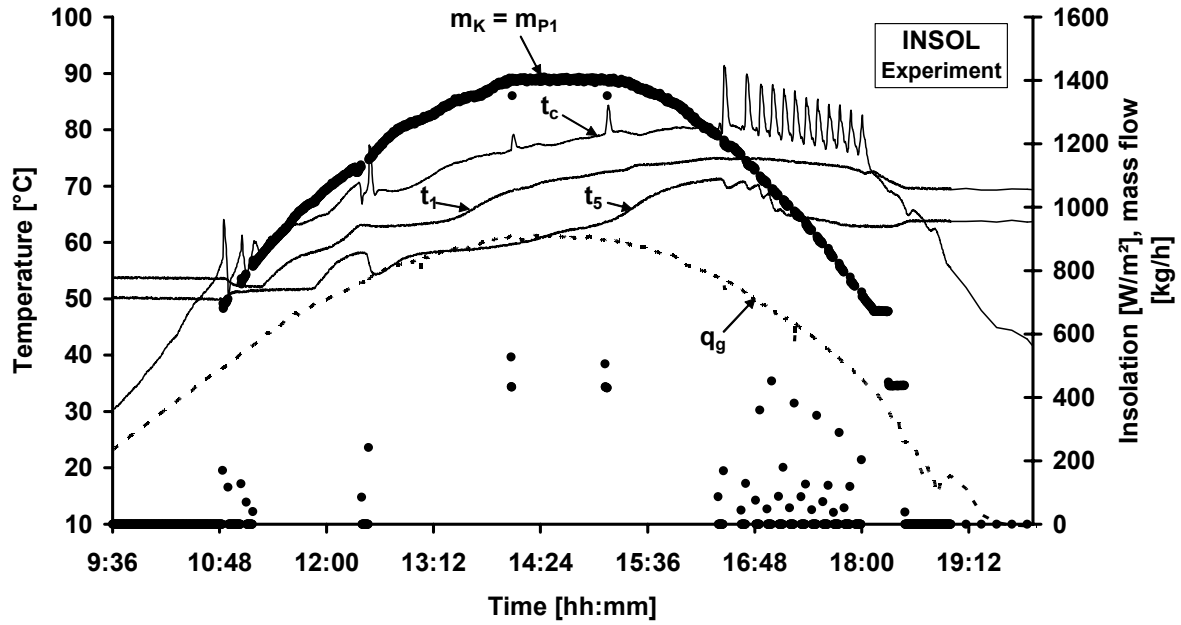

Figure 4.3.10. Experimental results for INSOL with bell-curve insolation. Collector and storage tank temperatures are shown on the left ordinate, mass flow and insolation are shown on the right ordinate.

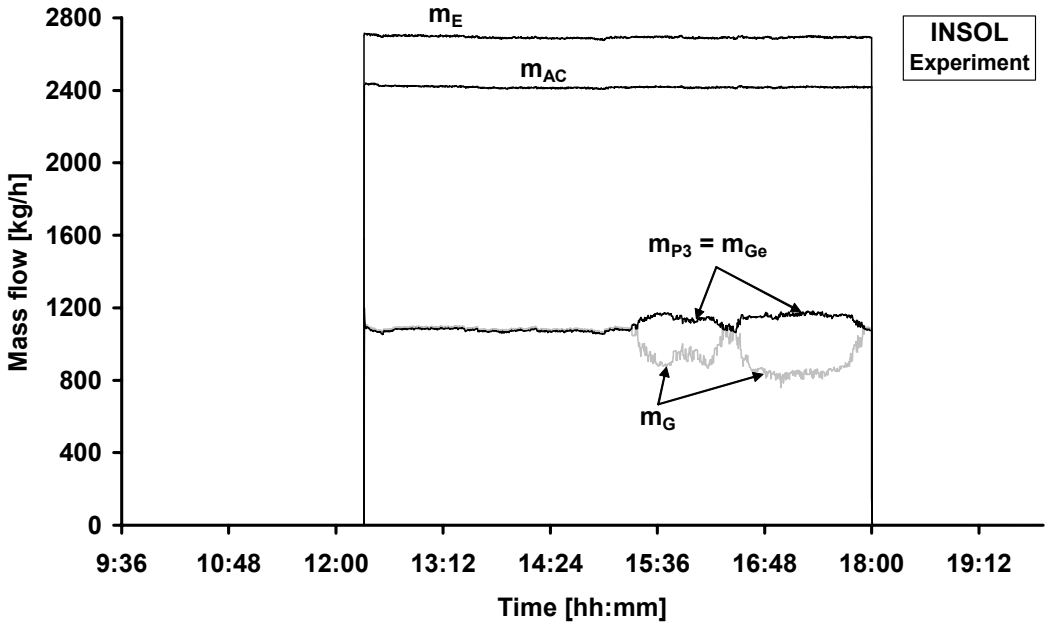

Figure 4.3.11. Experimental mass flows of INSOL with bell-curve insolation.

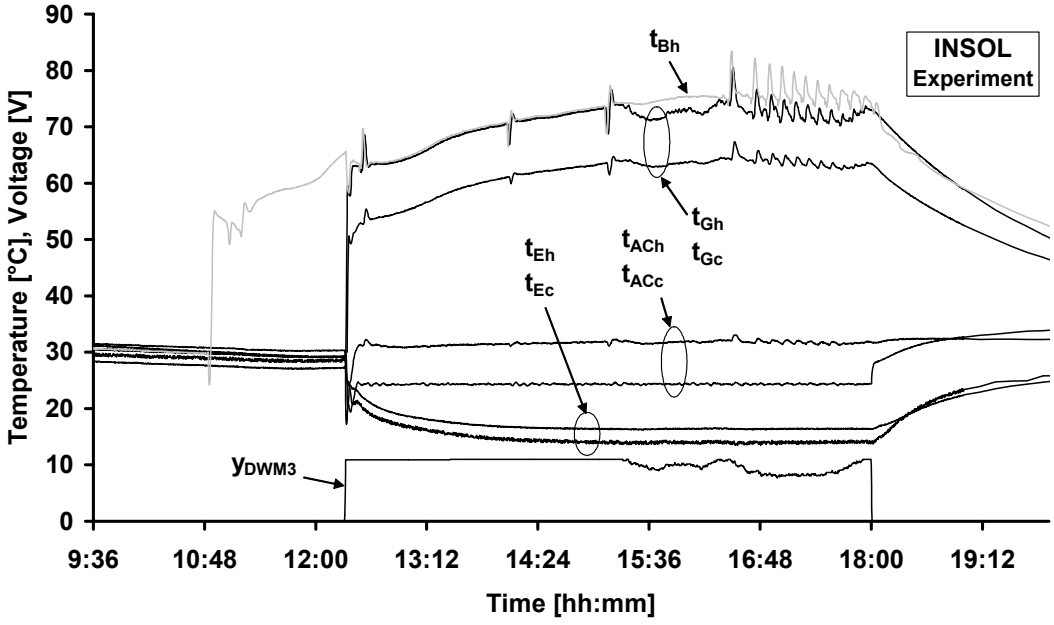

Figure 4.3.12. Experimental external temperatures of the chiller for INSOL with bell-curve insolation. Also shown is the control voltage of the valve DWM 3.

Figure 4.3.9 and Figure 4.3.10 show again good agreement between simulation and experiment. The variable solar circuit mass flow following a ten-minute average insolation value is clearly visible. The two negative mass flow peaks at 2:05 pm and 3:06 pm have been caused by a fault in the control software code and are not related to the insolation. Again, collector temperature peaks due to pump pulsations are visible at lower insolation. For the insolation range between 750 and 500 W/m², 12 pulses can be counted.

Cooling and chilled water mass flows are constant at 2390 and 2700 kg/h, respectively. The hot water mass flow through the chiller, $\dot{m}_{Ge}$, varies between 1080 and 1170 kg/h, depending on valve DWM 3. The chilled water control starts at 3:21 pm. The setpoint of 14 °C for the chilled water outlet temperature is being reached at 3:00 pm and kept constant until 6:00 pm. The deviations of t_{Ec} around the setpoint are +0.6 °C and -0.4 °C. Also shown is the hot water outlet temperature of the heat exchanger HX 12, i.e. the temperature t_{Bh} of the mass flow $\dot{m}_G$. There, the start of P1 and P2 is clearly visible at 10:48 am when t_{Bh} rises suddenly. The storage tank has an average temperature of 61 °C at chiller start-up which increases to maximum of 73 °C at 4:25 pm. At chiller shutdown the storage tank has an average temperature of 68 °C.

4.3.4 Discussion of simulation results

The integrated heat flow energy balance of the simulations is shown in Table 4.3.1, expressed in key figures for all three control strategies with bell-curve insolation.
The maximum values of Q_s, Q_E, t_{op} and a as well as the minimum values of Q_{el} and t_{start} are shown in bold numbers.

Table 4.3.1. Simulated key figures for bell-curve insolation

(units: Q_{el} [kWh_{el}], Q_S, Q_E [kWh_{th}], a [kWh_{th}/kWh_{el}], t_{start}, t_{op} [hours])

SIMULATION	Q_{el}	Q_S	Q_E	a	t_{op}	t_{start}
STAN	3.2	99.4	67.9	21.2	6.5	4.3
TDIFF	3.3	**104.5**	**69.9**	21.2	**6.8**	**4.1**
INSOL	**3.1**	104.2	69.7	**22.6**	6.6	**4.1**

For the bell-curve insolation pattern the TDIFF strategy delivers the biggest values for solar output, cooling capacity and operation time. The INSOL strategy has the lowest power consumption and the biggest yield factor. The start-up time is equal for TDIFF and INSOL. It is visible in Figure 4.3.1 and Figure 4.3.5 that TDIFF has less mass flow pulsations than STAN and –especially at decreasing insolation- a higher mass flow than INSOL (Figure 4.3.9). Therefore TDIFF yields a higher value of Q_s which also determines the longest operation time. With more energy in the storage tank due to a higher value of Q_s, the chiller can operate longer at decreasing radiation. The biggest value of t_{op} results in the highest cooling capacity for TDIFF. The INSOL strategy has the lowest time period of pulsating mass flow and although its average mass flow is lower than of TDIFF and STAN, its solar gain is not much lower than of TDIFF. It is still sufficient for the biggest yield factor due to the low power consumption of INSOL.

From the comparison of TDIFF and INSOL it can be deducted that a lower mass flow (INSOL) yields better results for bell-curve insolation. In consequence it can be stated that the mass flow of

TDIFF is too high and the correlation expressed in equation *(4.2.5)* is not the optimum one. If TDIFF had a lower mass flow course, better results for TDIFF could be expected.

For the STAN strategy it is clearly visible that full speed operation of the pumps at changing insolation does not yield best performance. Nevertheless, the yield factors of STAN and TDIFF are equal. Considering the bigger control effort made in TDIFF, this is quite surprising. The temperature-difference based variable mass flow control of TDIFF does not yield an advantage compared to the simple on/off control of STAN. Again, an adjustment of equation *(4.2.5)* will most likely improve the TDIFF performance and then result in a difference to STAN.

Comparing the lowest and highest yield factors of STAN/TDIFF and INSOL it can be seen that the use of the INSOL strategy can result in a reduction of the electrical power consumption per thermal kilowatt hour of approx. 6 %. Comparing TDIFF and INSOL with regard to electricity consumption, a time period of 100 operation days yields a reduction of electricity consumption of 20 kWh_{el} or operational cost savings of 3.4 € (at 0.17 €ct/kWh_{el}) if INSOL is being used. For a lifetime of 20 years at 100 operation days per year, a reduction of 68 € can be achieved if INSOL is being used. This comparison shows that the difference between the control strategies regarding electricity consumption is rather small.

Concluding from the simulations, STAN and TDIFF can be expected to perform with similar yield factors in the experiments. An advantage of INSOL compared to the other strategies can be expected in the experiments.

4.3.5 Discussion of experimental results

The key figures defined for the simulations can also be used for the experiments. Yet a sound comparison of key figures between experiments and simulations can only be made if the inputs and boundary conditions of the solar cooling system are equal for both. In the simulation, a perfect bell-curve insolation has been used. Consequently, experimental data consisting of cloud-free days with bell-curve insolation is required. Such days were recorded in full length for both the STAN and INSOL strategy, however for the TDIFF strategy no complete day with cloud-free insolation was recorded.
Subsequently, the external input parameters into the chiller should also be equal and constant during the experiment. In the simulations, a constant cooling water inlet temperature of 27°C as well as a constant setpoint for the chilled water outlet temperature of 14.5 °C were assumed. Such constant conditions were not recorded in the experiments. During the experimental run using the STAN strategy, the cooling water temperature was changed from 27°C to 25 °C. For the INSOL run, the cooling water inlet temperature was 25 °C. During the TDIFF run the chilled water temperature setpoint was changed from 15°C to 14°C.
Also, the storage temperature distribution at the beginning of each experimental day should be similar to the simulations. It influences the start-up time of the chiller and thus the cooling capacity. However, for all three days different storage temperatures at start-up were recorded.

The total electrical energy consumption in the simulation included pumps P1, P2 and P3. In the experiments, the electrical energy consumption of pumps P1 and P2 has been measured together. Pump P3 was also not measured individually but together with P4, P5a and P5b (see Figure 2.3.2). Thus measuring the total consumption of P1, P2 and P3 was not possible in the experiments.

Due to the experimental limitations above a direct comparison of absolute key figures between simulation and experiment is not possible. Yet even if absolute values are not comparable, the trends of simulation and experiment can be weighed against each other in a qualitative analysis. To do so, the experimental runs are being compared only to each other. Even so, some of the limitations above still have to be taken into account and correcting measures have to be applied for the comparison of the experimental runs to each other. In the following, the corrections applied to the experimental parameters used for the yield factor calculation are discussed one after the other.

a) Varying cooling water temperature

A linear relationship between cooling water temperature and heat flow into the evaporator can be derived from the characteristic equation for absorption chillers if all other input parameters are assumed constant [Ziegler 1997]. A correction of varying cooling water inlet temperatures can then be made. If the variations of the other input parameters are significant compared to the variation of the cooling water temperature, a linear relationship cannot be assumed anymore.

In the experimental runs both hot and chilled water temperature have bigger variations than the cooling water temperature, thus this method cannot be used. Instead, a correction of varying cooling water temperatures is being made by establishing the electrical energy consumption of the cooling tower fan as a measure for the cooling tower heat flow and thus the cooling water temperature level. Fan power and cooling tower heat flow are not linear dependent but influenced by ambient air conditions. While the influence of the dry bulb temperature of air can be neglected [Wiegand 2004], the dependency of the cooling tower heat flow on the wet bulb temperature of air has to be taken into account. For this, a wet bulb correction parameter can be formulated using the averaged measured wet bulb temperature per run compared to a maximum wet bulb temperature value. For Berlin, the latter is 21°C.

$$\tau_{wb} = \frac{t_{wb,av}}{t_{wb,\max}} \qquad (4.3.1)$$

The electrical energy consumption of the cooling tower can then be corrected using the quotient of the experimentally measured electrical energy consumption Q_{ct} by τ_{wb}.

$$Q_{ct,c} = \frac{Q_{ct}}{\tau_{wb}} \qquad (4.3.2)$$

Using Q_{el} and the corrected electrical energy consumption of the cooling tower $Q_{ct,c}$, a new experimental yield factor can be calculated as

$$a_e = \frac{Q_E}{Q_{el} + Q_{ct,c}} \qquad (4.3.3)$$

b) Different energy balances for electrical and thermal energy

The electrical energy consumption of the system components according to Figure 2.3.2 has been measured with analogue electricity meters whose values have been manually recorded before and after each experimental run. They were not recorded at the start-up and shutdown of the absorption chiller. Hence, Q_{el} includes the electrical energy consumption of P1 and P2 before, during and after chiller operation. In contrary, the cooling capacity Q_E was integrated only over the chiller runtime. A corrected value of Q_{el} can be calculated by estimating the electrical energy consumption of P1 and P2 before and after chiller operation and subtracting it from the total electrical energy consumption. Figure 4.3.2 and Figure 4.3.3 show that for the STAN strategy the total pump operation time equals the chiller operation time, thus no correction has to be made. Figure 4.3.6 and Figure 4.3.7 show for TDIFF that the pumps operate 50 minutes longer than the chiller at minimum mass flow. The minimum power consumption is 95W of P1 and 40W of P2. Thus a correction of 0.1 kWh is being made for TDIFF. The biggest overlap can be seen for INSOL in Figure 4.3.10 and Figure 4.3.11. The pumps P1 and P2 operate 80 minutes before and 30 minutes after chiller operation. As the mass flow changes during both time periods, an average value is being used for the power correction, resulting in a correction term of 0.3 kWh.

c) Varying storage temperatures at start-up

Different temperatures in the storage tank at the beginning of experimental days will result in different start-up times for each day. This influences the operation time of the chiller. It is however not a limitation for the experimental comparison using the yield factor, as the operation time influences both electrical power consumption and integrated cooling capacity in the same way.

Using the corrected yield factor calculation *(4.3.3)*, the experimental key figures can be calculated. Table 4.3.2 shows the results. The start-up and operation time have not been calculated as each experimental run has a different start-up condition.

Table 4.3.2. Experimental key figures for runs with bell-curve insolation

(units: $Q_{el,c}$, $Q_{ct,c}$ [kWh_{el}], Q_S, Q_E [kWh_{th}], a_e [kWh_{th}/kWh_{el}])

EXPERIMENT	$Q_{el,c}$	$Q_{ct,c}$	Q_S	Q_E	a_e
STAN	1.8 ±0.1	2.4 ±0.1	99.9 ±5.0	62.4 ±2.8	14.7 ±0.7
TDIFF	0.7 ±0.1	0.7 ±0.1	47.6 ±2.5	23.6 ±1.8	17.5 ±1.9
INSOL	1.1 ±0.1	1.5 ±0.1	74.1 ±3.7	39.5 ±1.9	15.4 ±1.0

The complete energy balance of all three runs can be found in Appendix 8.8.

The analysis of the dynamic behaviour shown in the experimental graphs of the different control strategies yields that the TDIFF strategy provides the best thermal performance for bell-curve insolation. It has the least pulses at low insolation which results in the lowest standstill time of the collector field. For this reason the lowest thermal loss and consequently the highest solar gain (in proportion to the insolation) can be expected. Due to the coupling of mass flow and temperature difference, a low power consumption can also be expected.

Combined in the experimental yield factor, the biggest value can indeed be seen for TDIFF in Table 4.3.2. Then again, the recorded TDIFF run was not a full day and the insolation was more transient than of STAN and INSOL, thus the results are not entirely sound. Also, the error on the experimental yield factor of TDIFF is quite significant due to the inaccuracy of the electricity meters in proportion to the small absolute electrical energy consumption. The magnitude of the error is also owed to the one-day experimental runs which have been recorded. If the experimental run time had included several days with similar operating conditions, the error would have been much smaller. Unfortunately this was not possible during the experiments. In consequence it can be seen that the error ranges of all three strategies overlap in a way that prohibits a serious comparison. It can nonetheless be stated that the differences in yield factor between the individual strategies are in the order of magnitude predicted by the simulation.

4.3.6 Chapter summary and conclusions

In this chapter, a comparison of three control strategies for the solar circuit mass flow in a solar cooling system is presented. It is described how the strategies have been applied to a solar cooling system and how simulations have been performed in TRNSYS. For this, different insolation patterns as input parameter have been used. Key figures have been defined for the comparison of the simulation results with a main regard to the integrated cooling capacity and electrical energy consumption of the pumps. The simulation performance has been analysed and verified using results achieved with constant insolation. Internal consistency and an agreement with estimated values has been found.

The control strategy performance has also been tested in experiments with the solar cooling system using an experimental yield factor as comparative key figure. It was found that the simulated results agree well with the experimental ones. This holds true for both the dynamic course of the variables as well as the integrated heat flow energy balance expressed in the yield factor.

From the simulations, an improvement of 6% in the yield factor for the INSOL strategy compared to the other strategies can be concluded.

From the experiments, the comparison of the dynamic behaviour yields the TDIFF strategy performing best. The comparison of the integrated experimental energy balances shows that there are only small differences between STAN, TDIFF and INSOL if the yield factor is being used as decisive value. A tendency towards one strategy as clear as in the simulations cannot be seen. For all three control strategies the differences between the strategies are in the magnitude of the error range of the yield factor. Thus, controlling the mass flow in the solar circuit of a solar cooling system does not influence the yield factor significantly if the methodology presented is being applied. This allows several conclusions on the methodology which will be presented and further discussed in chapter 6.

5 Transient absorption chiller performance

The previous chapter has presented investigations into the most complex system circuit with regard to thermal performance and power consumption, summarized in daily energy balances. By integrating the thermal performance into a daily value, information about the dynamic behaviour is not being taken into account. The influence of the dynamic behaviour is nevertheless important for the operation of the most complex system component, the absorption chiller. Its most important output, the chilled water temperature, is highly influenced by variations of the input conditions. Fluctuating hot water as well as cooling water temperatures and/or mass flows result in fluctuating chilled water temperatures. There, the dynamic behaviour of solar and storage circuit can induce considerable disturbances on the chilled water temperature. Of course, this is only important if there are close limits on this temperature, e.g. due to the chilled water distribution system. Then, a chilled water control of the variations described in chapter 3.4.1 has to be implemented.

In this chapter, the ground work for the development of such a control is being presented. Detailed knowledge about the thermal behaviour of the chiller is the basis for such a control development. Naturally, each absorption chiller model has its individual thermal behaviour and characteristic of the controlled system. The controlled system includes all components between measurement variable and control variable. The characteristic of the thermal behaviour of all these components in serial and/or parallel connection has to be found.

One way of determining the characteristic of the controlled system is to perform experiments with the system, analyse the received experimental data and identify a model. This model can then be used for simulations and forecasting of the system behaviour as well as controller development. The process of identifying such an experimental model is called system identification. However, this experimental procedure is complex and requires an effort of time, personnel and investment.

An easier and also quicker way can be the theoretical simulation of the transfer behaviour using a mathematical model of the chiller. Such a theoretical model incorporates physical data, e.g. energy and mass balances, as well as design data of the chiller and simulates transfer mechanisms based on mathematical correlations. An experimental procedure is not necessary for such a model, however the underlying theory has to reproduce the physical characteristics of the chiller with sufficient accuracy.

The methods of experimental identification and theoretical simulation have been investigated separately with regard to accuracy and applicability in this thesis. The methodology and a comparison of both methods is presented in the following two chapters with the focus on the development of a chilled water temperature control.

5.1 Experimental chiller identification

For the development of a chilled water temperature control the transfer behaviour of the absorption chiller has to be known. Yet simultaneous variations of hot, cooling and chilled water temperature make the identification of a transfer correlation rather difficult. Usually cooling water temperature and mass flow are therefore kept at constant values which reduces their transient influence on the chiller output, i.e. the chilled water temperature. Then the hot water and chilled water input temperatures are the dominating parameter for chilled water outlet temperature control. In the following work a chilled water temperature control using the hot water input temperature as the controlled variable is assumed.

For such a hot water based control according to Figure 4.1.1 the controlled system includes a three-way valve, the piping between valve and chiller and the piping between chiller and temperature sensor t_{Ec}. All these components can be assumed as subsystems, connected in series and with a subsystem transfer function.

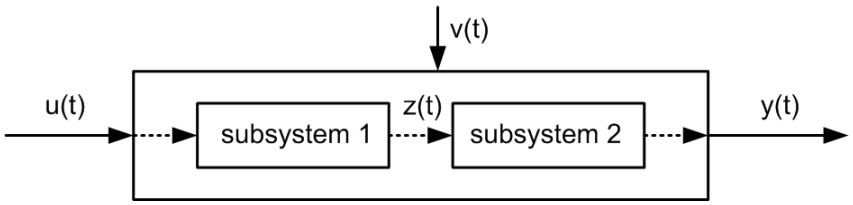

Figure 5.1.1. A general system

Figure 5.1.1 shows a general system with two subsystems. It has an input signal *u(t)*, a disturbance signal *v(t)* and an output signal *y(t)*. The system consists of two subsystems with an intermediate signal *z(t)*. It interacts with its environment through *u(t)*, *v(t)* and *y(t)*. The system character can be modelled by an appropriate mathematical function called transfer function *G*.

$$y(t) = G\big(u(t), v(t)\big) \qquad (5.1.1)$$

The transfer function is the mathematical formulation of a theoretical system model. Such a model has a black box character, characterising the system only by its inputs and outputs. Intermediate system parameters such as *z(t)* do not need to be known anymore.

The method of system identification used here is a practical and fast method described by Ljung. It is based on the analysis of experimental data of any kind and structure. Generally, the system identification process can be divided into two main parts, the model calculation and the model validation. Model calculation includes experimental data analysis, the choice of a model set and a criterion of fit. Model validation is the validation of the model using reference data of the system. The choice of a suitable model set and criterion of fit is an important decision for the quality of the resulting model. There are numerous possibilities of model sets, characterised by different

mathematical methods and designed for different applications. Same goes for criteria of fit, which influence the robustness and ease of computation of the model. Detailed information about model sets and criteria of fit shall not be presented and discussed here but can be found in [Ljung 1999].

During a system identification process, the use of more than one numeric model on a specific system is recommended. The quality of each model should then be determined by validating it against reference data. A range of models and fit criteria suitable for a wide range of engineering systems have been integrated into a commercial software tool included in the MATLAB software [MathWorks 2002]. The so called 'System Identification Toolbox' of MATLAB allows fast processing of experimental data and gives the user a choice of models and best fits. Several features such as data pre-processing or filtering are also included.

The System Identification Toolbox has been used for the work presented in order to develop the chilled water temperature control for the absorption chiller. The method of development of this control strategy requires the following:

- Identification of the controlled system and necessary subsystems, building of a theoretical model
- Development of a controller according to the theoretical model
- Testing of the controller in simulation and reality

The components involved in the controlled system for chilled water control include the three-way valve V3, a controller C3 and the chiller itself. This system is subdivided into the subsystems 'valve' and 'chiller' which are both being identified and modelled separately. Figure 5.1.2 shows the components and subsystems as well as the controller.

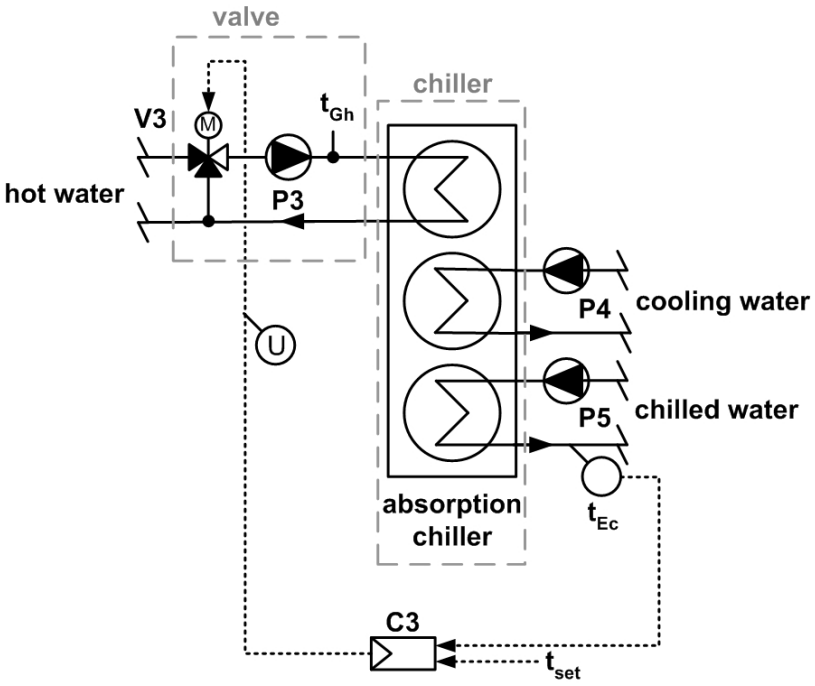

Figure 5.1.2. System definition with subsystems 'valve' and 'chiller' for the identification of models, controller type and control parameters

The chilled water outlet temperature of the absorption chiller t_{Ec} is being measured and compared to a set temperature t_{set}. The controller C3 adjusts the position of the three-way valve V3 according to the temperature difference between t_{Ec} and t_{set} by varying the control voltage U ($0<U<10V$) of the valve, thus controlling the return flow admixture. The resulting hot water inlet temperature t_{Gh} is the only controlling parameter for the chilled water outlet temperature, constant chilled and cooling water inlet temperatures assumed. Also all mass flows are assumed to be constant. The controller type (P, PI, PID etc.) and the control parameters have to be found by the system identification.

The goal of the system identification is to determine the transfer functions of the subsystems 'valve' and 'chiller' and combine both transfer functions to a single one with the input control voltage U [V] and the output chilled water temperature t_{Ec} [°C]. This process eliminates the hot water inlet temperature t_{Gh} [°C] which is an intermediate parameter and not necessary for the control. The structure of the transfer functions and the resulting model is shown in Figure 5.1.3.

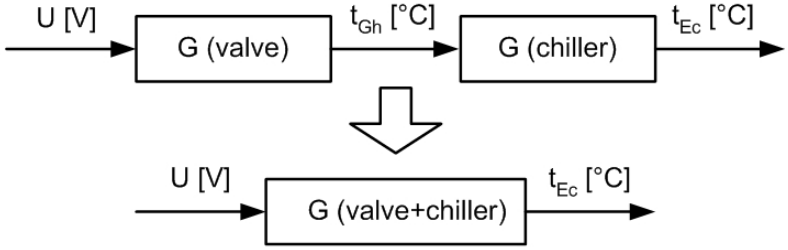

Figure 5.1.3. Structure of transfer functions (G) for system identification

The transfer functions G of each subsystem are being modelled separately and then combined to a single transfer function which can be used for simulation and determination of the control parameters.

5.1.1 Identification of subsystem 'valve'

In order to identify the transfer function between control voltage U and hot water inlet temperature t_{Gh}, measurement data of a forced control voltage step has been analysed. The chiller was put into operation and driven by hot water of 77 °C. The control voltage U of valve V3 was set to 2.5 V, equalling a valve position of 25% of the full lift and thus a recirculation of 75% of the return flow. See Appendix 8.6 for the characteristic diagram of valve V3. This recirculation yielded a hot water inlet temperature t_{Gh} of 58 °C for a hot water outlet temperature of 53.4 °C. Chilled and cooling water inlet temperatures were kept constant at 19.5 °C and 27 °C, respectively. All mass flows were also kept constant at 1.2 m³/h, 2.6 m³/h and 2.0 m³/h for hot, cooling and chilled water, respectively. After reaching steady-state operation of the chiller, a step of U from 2.5 to 10 V has been forced, resulting in a reaction temperature rise of t_{Gh} from 58 °C to 77 °C. Figure 5.1.4 shows a graph of the step.

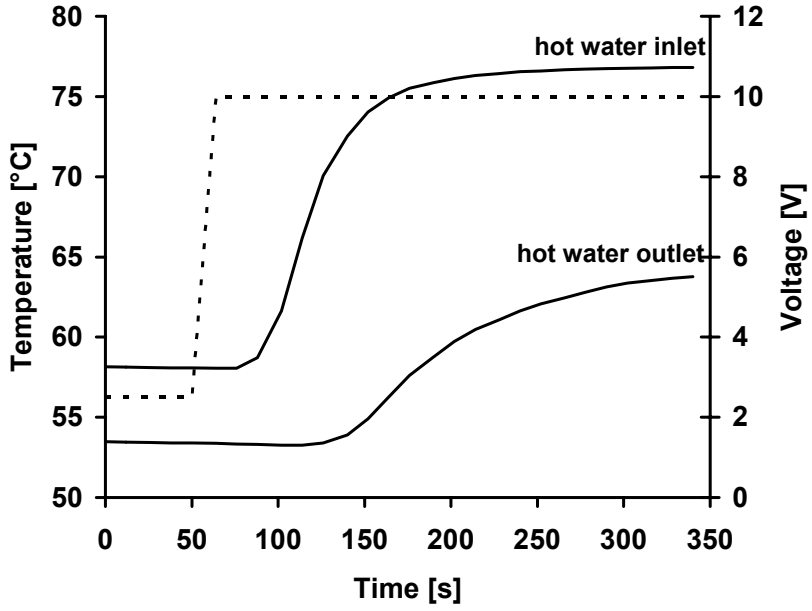

Figure 5.1.4. Forced step of control voltage U for valve V3 (dotted line) and resulting temperature change of hot water inlet temperature t_{Gh} (solid line). Also shown is the hot water outlet temperature of the chiller.

The course of the temperature change of t_{Gh} gives information about the behaviour of the controlled subsystem consisting of the valve V3, the piping between valve and temperature sensor t_{Gh} and the sensor itself. The information deducted from the measurements is thus only valid for the exact setup of these three components in combination with the chiller. The chiller can not be excluded from measurements as it determines the return temperature which is used for the recirculation.

The system identification method has been applied on the step data from Figure 5.1.4 using the software MATLAB and its System Identification Toolbox. For the Toolbox it is necessary to use data with a constant sampling rate, i.e. similar time intervals between measurement data. The data acquired from the measurements in the Phönix system however has a variable sampling rate between 12 and 14 seconds. It was therefore necessary to perform a linear interpolation between data points to achieve a data set with equal time intervals. A time interval of 10 s has been chosen for this. Also, the data needs to be standardised to zero origin. Instead of starting at 2.5 V and 58 °C and ending at 10 V and 77°C, the standardised step starts at 0 V and 0°C and ends at 7.5 V and 19 °C, i.e. the difference between both start and end values. Figure 5.1.5 shows the input voltage data and the output temperature data which was used for the system identification.

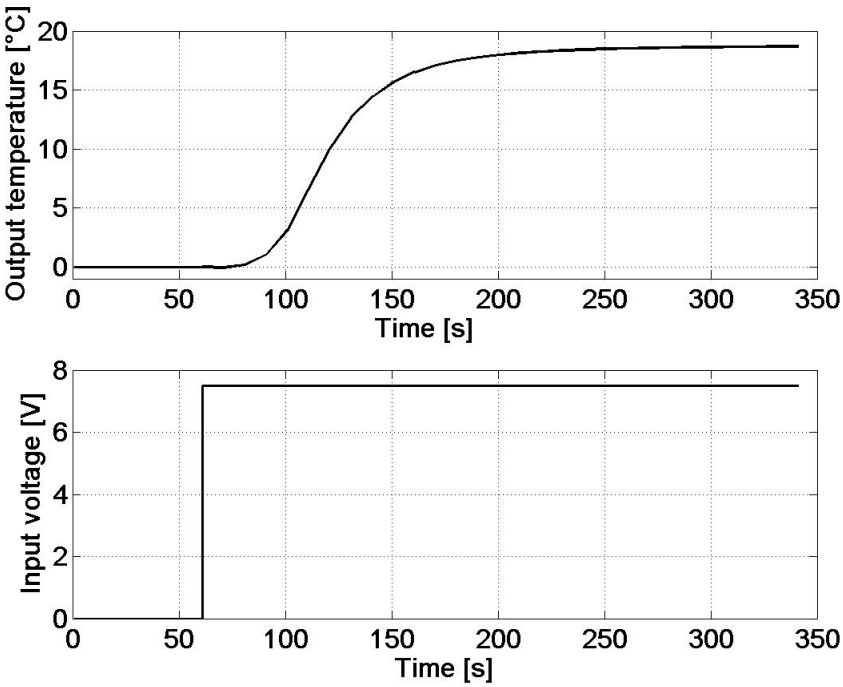

Figure 5.1.5. Standardised input and output values at equal time intervals for identification of subsystem 'valve'

Applied on the standardised set of data points with equal time intervals the System Identification Toolbox delivers an approximated model. Its dynamic characteristics are expressed via the model fit graph in Figure 5.1.6.

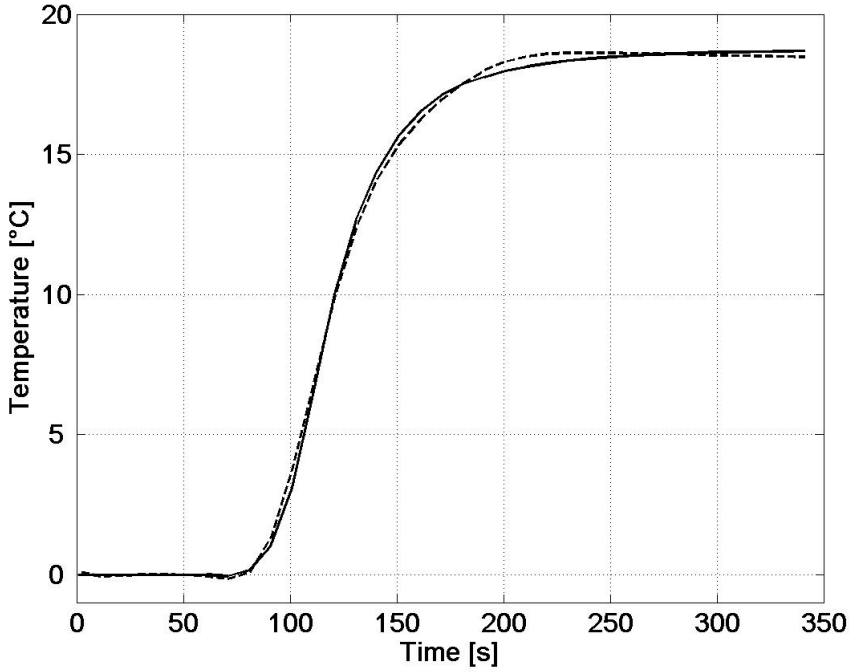

Figure 5.1.6. Measured (solid line) and simulated (dashed line) model output of subsystem 'valve'

Figure 5.1.6 shows the measured and simulated model output of the best fit. The transfer function G_v between control voltage U and hot water inlet temperature t_{Gh} for the simulated output reads

$$G_v = \frac{4.54e^{-4} \cdot s^3 - 2.61e^{-4} \cdot s^2 - 6.6e^{-5} \cdot s + 4.96e^{-4}}{s^4 + 0.11 \cdot s^3 + 0.013 \cdot s^2 + 5.1e^{-4} \cdot s + 8.5 \cdot e^{-6}} \qquad (5.1.2)$$

In equation (5.1.2), s is the Laplace-operator. This identification of the valve has been performed for a constant input temperature of 77 °C into the valve. The resulting gain of the controlled system K_v can be calculated from input and output start/end values as

$$K_v = \frac{\Delta y}{\Delta u} = \frac{y(0) - y(n)}{u(n) - u(0)} \qquad (5.1.3)$$

where y is the output, u is the input and n is the end time of the step. For the step of Figure 5.1.4 the gain of the controlled system can be calculated to K_v=2.48. Figure 5.1.7 shows the step response for unity step of G_v.

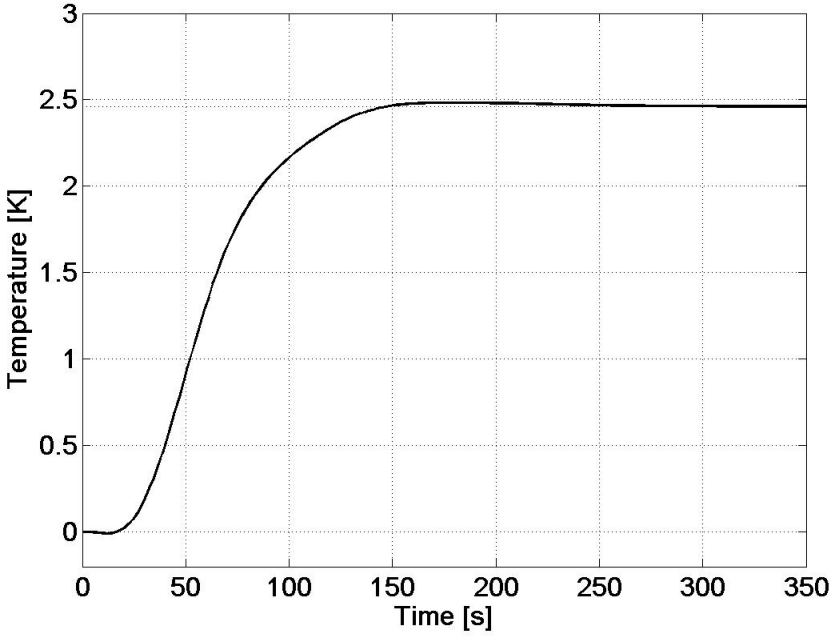

Figure 5.1.7. Step response of valve model G_v for unity step.

As visible in Figure 5.1.7, a voltage change of 1V results in an inlet temperature change of 2.48 K.

This value of K_v is valid only for the following conditions:

- an inlet temperature of 77°C into the valve
- a hot water mass flow through the chiller of 1.2 m³/h
- the specific heat transfer characteristic of the generator, i.e. the *UA* value resulting in a hot water outlet temperature of the chiller of 53.4 °C for an inlet temperature of 58 °C
- a constant LiBr solution mass flow in the generator of 146 l/h

For varying hot water inlet temperatures into the valve (t_{Gh1}, Figure 3.4.1) the value of K_v will also change. For a control loop, varying values of the gain of the controlled system can result in oscillating or unstable controller behaviour. It is therefore necessary to determine the range of K_v for the normal operation temperature range of the chiller and its consequences for the control.

The determination of the range of K_v is being done via a TRNSYS simulation using a steady-state simulation model of the absorption chiller based on the characteristic equation. The characteristic equation assumes a quasi-linear behaviour of the thermal performance of an absorption chiller, yet its underlying theory shall not be discussed in detail here. A comprehensive description can be found in [Hellmann *et al.* 1999]. Albers has applied the characteristic equation on the Phönix absorption chiller. He has developed a TRNSYS simulation type which simulates the 2nd generation model of the Phönix chiller from the year 2003 [Albers 2004b]. The description and documentation of this TRSNYS "Type 177" can be found on the CD-ROM in Appendix 8.9. It has been validated with experimental data as shown in Figure 5.1.8.

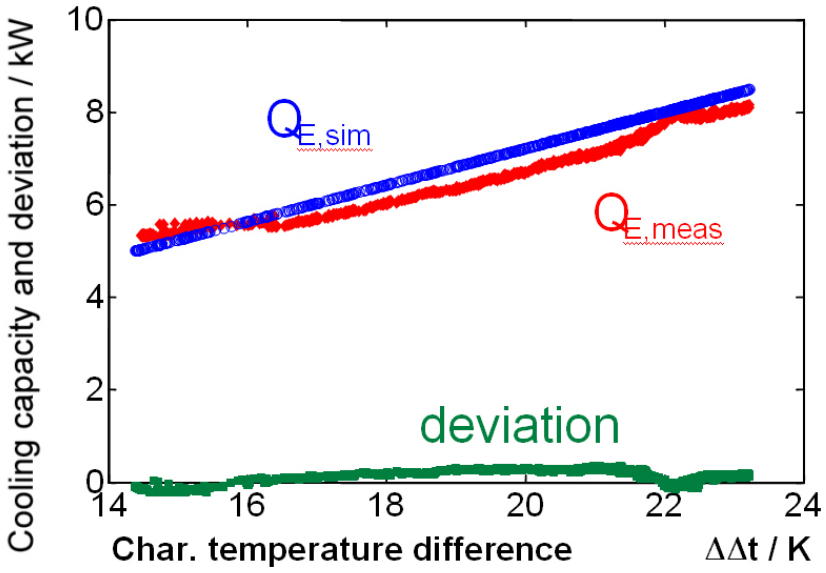

Figure 5.1.8. Validation of TRNSYS type 177. Figure modified from [Kohlenbach et.al. 2004b].

Figure 5.1.8 shows measured ($Q_{E,meas}$, red line) and simulated ($Q_{E,sim}$, blue line) values of the cooling capacity of the Phönix chiller versus the characteristic temperature difference. Also displayed is the difference between both capacities, i.e. the deviation between simulation and reality (green line). The maximum deviation between measured and simulated data in Figure 5.1.8 is 7.5%. Part of the deviation can be related to the fact that the Phönix system almost never operates at steady state conditions due to the transient insolation, whereas the simulation model is based on steady-state data and assumes all inputs as steady-state. Nevertheless, the accuracy of the model is sufficient and the type can be used for further simulations.

For a hot water inlet temperature into the valve t_{Gh1} of 90 °C, a K_v value of 3 has been simulated. For a temperature t_{Gh1} of 60 °C, a K_v value of 1.4 has been found. These two temperatures represent the normal operation range of the chiller. The measured value of K=2.5 lies in the middle of the simulated range. The characteristic diagram of the valve V3 is shown in Appendix 8.6. The TRNSYS project file and the simulation results can be found on the CD-ROM in Appendix 8.9.

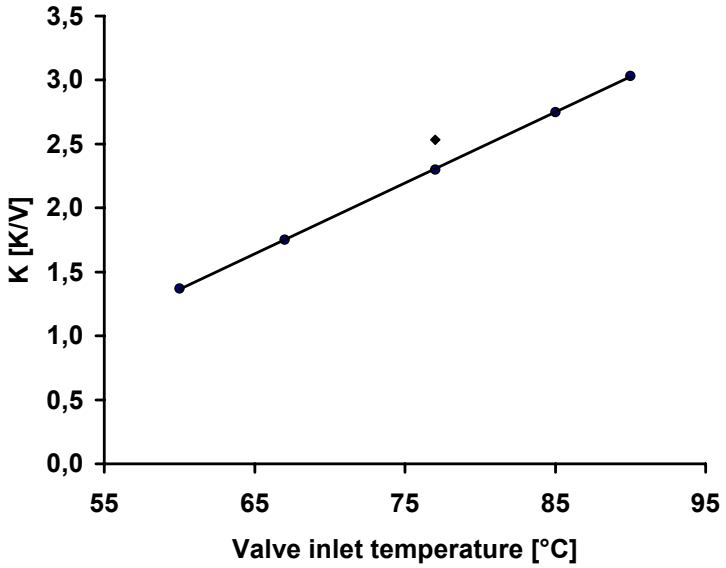

Figure 5.1.9. Gain of the controlled system K_v versus valve inlet temperature. Simulated values are displayed by line-connected circles, the measured value is displayed by a diamond.

Figure 5.1.9 shows the measured (diamond) and simulated (circle line) values of K_v versus the hot water inlet temperature t_{Gh1} of the valve. It can be seen that there is a linear dependency of the gain on the hot water inlet temperature into the valve. The consequences of varying values of K_v on the control accuracy are being described in Appendix 8.6.

5.1.2 Identification of subsystem 'chiller'

After identifying the transfer function between control voltage U and hot water inlet temperature t_{Gh} into the chiller it is now necessary to determine the transfer function between t_{Gh} and the chilled water outlet temperature t_{Ec}. It can also be found by analysis of the thermal performance of the chiller via system identification of the subsystem 'chiller'. For the subsystem identification, a step of t_{Gh} has to be forced from steady-state operating conditions and the resulting change of t_{Ec} has to be measured. In order to determine a possible temperature level dependency, steps have been performed at increasing starting temperature levels.

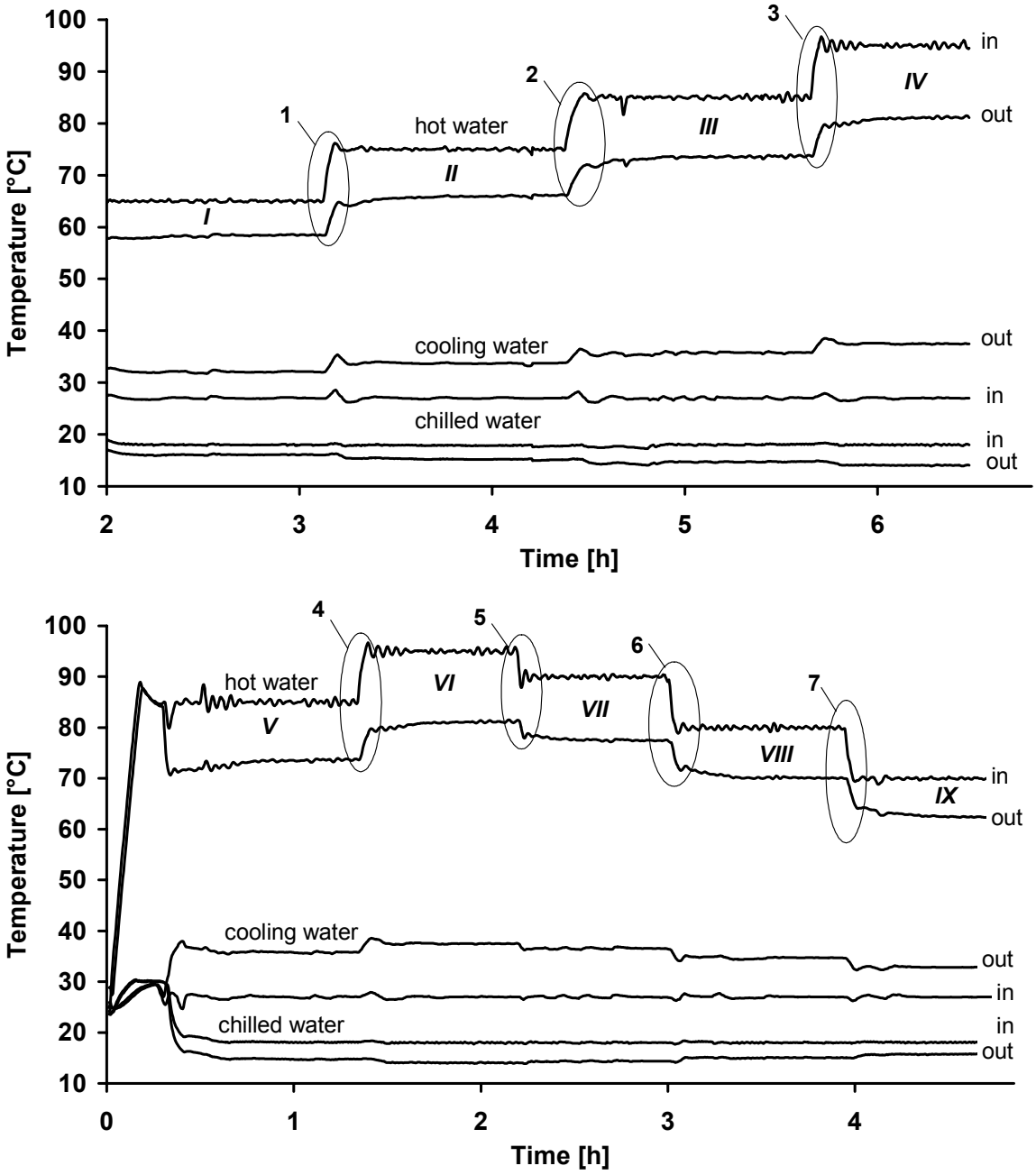

Figure 5.1.10. Graph of measured steady-state steps for subsystem 'chiller'

Figure 5.1.10 shows seven hot water temperature steps between 65°C and 95°C. Displayed are inlet/outlet temperatures of hot, cooling and chilled water. Each steady-state has been held at constant operation parameters until the difference of the solution concentrations between two averaged intervals of five minutes was smaller than 0.0005 kg/kg and the standard deviation of all external heat flows was smaller than 0.25 kW. Steps are marked in arabic numbers, steady-states are marked in roman numbers.

Table 5.1.1. Averaged measurement data of steady-state steps for subsystem 'chiller'

Step No.		Steady State No.	Temperatures						External Flows		
			Hot water inlet	Hot water outlet	Cooling water inlet	Cooling water outlet	Chilled water inlet	Chilled water outlet	Hot water	Cooling water	Chilled water
	-	-	°C	°C	°C	°C	°C	°C	m³/h	m³/h	m³/h
1		*I*	65.0 ± 0.4	58.5 ± 0.4		32.1 ± 0.1	18.0 ± 0.2	16.1 ± 0.1			
	2	*II*	75.0 ± 0.4	66.1 ± 0.4		33.7 ± 0.1	17.7 ± 0.2	15.1 ± 0.1			
3		*III*	85.0 ± 0.5	73.7 ± 0.5		35.8 ± 0.2	18.0 ± 0.2	14.7 ± 0.1			
		IV	95.0 ± 0.6	81.2 ± 0.5	27.0 ± 0.1	37.5 ± 0.2	18.0 ± 0.2	14.1 ± 0.1	1.2 ± 0.006	2.6 ± 0.013	2.9 ± 0.015
4		*V*	85.0 ± 0.6	73.7 ± 0.4		35.8 ± 0.2	18.1 ± 0.2	14.7 ± 0.1			
	5	*VI*	95.0 ± 0.6	81.2 ± 0.4		37.5 ± 0.2	18.0 ± 0.2	14.0 ± 0.1			
6		*VII*	90.0 ± 0.5	77.5 ± 0.4		36.5 ± 0.2	18.0 ± 0.2	14.4 ± 0.1			
	7	*VIII*	80.0 ± 0.4	70.1 ± 0.4		34.7 ± 0.1	18.0 ± 0.2	15.0 ± 0.1			
		IX	70.0 ± 0.4	62.4 ± 0.4		32.9 ± 0.1	18.1 ± 0.2	15.8 ± 0.1			

Table 5.1.1 shows the step measurement data averaged over a time period of 10 minutes before each step. Uncertainties given are systematic and statistical errors as described in Appendix 8.2. For the step measurements, hot and cooling water inlet temperatures, internal and external mass flows were kept constant. The mass flow of weak solution in the chiller was 0.13 m³/h, the mass flow of refrigerant was 0.22 m³/h for all steady-states. The chilled water inlet temperature was kept constant at 18 °C; although the average values of steady states *II*, *V* and *IX* differ from this set point due to control disturbances. These disturbances have to be taken into account as the chilled water outlet temperature is influenced by its corresponding inlet temperature. A comparison of the chilled water outlet temperature values of Table 5.1.1 would thus lead to wrong gains of the controlled system as the inlet temperatures vary. Therefore it was assumed that each inlet temperature deviation from the set point of 18 °C can be added to the outlet temperature. For example, the chilled water inlet/outlet temperatures of steady state *II* are 17.7 and 15.1 °C. Adding the deviation of 0.3 K (18.0 – 17.7 °C) to 15.1°C yields a corrected outlet temperature of 15.4°C.

Table 5.1.2 shows the temperature differences of hot and chilled water; the latter including corrected values for steady states *II*, *V* and *IX*.

Table 5.1.2. Chilled water temperature difference Δt_{Ec} and gain of the controlled system K_c for hot water steps at different temperature levels

Step No.	Step range hot water	Δt_{Gh}	Step range chilled water	Δt_{Ec}	K_c
1	65.0-75.0	10	16.1-15.4	0.7	0.07
2	75.0-85.0	10	15.4-14.7	0.7	0.07
3	85.0-95.0	10	14.7-14.1	0.6	0.06
4	85.0-95.0	10	14.6-14.0	0.6	0.06
5	95.0-90.0	5	14.0-14.4	0.4	0.08
6	90.0-80.0	10	14.4-15.0	0.6	0.06
7	80.0-70.0	10	15.0-15.7	0.7	0.07

The chilled water difference for a 10K step spans from 0.6 K to 0.7K, for a 5K step it is 0.4 K. No direct dependency of Δt_{Ec} on the hot water temperature level can be found. The gain of the controlled system 'chiller', K_c, is lower than of the subsystem 'valve', K_v.

Steps 1, 2 and 3 represent the total temperature range of all measured steps. They have therefore been used for model approximations and transfer function calculations with the System

Identification Toolbox using the same methodology as described in chapter 5.1.1. The step data has been equalized in its time intervals between data points and standardised to a zero origin. The input/output data used for the system identification is shown in Figure 5.1.11.

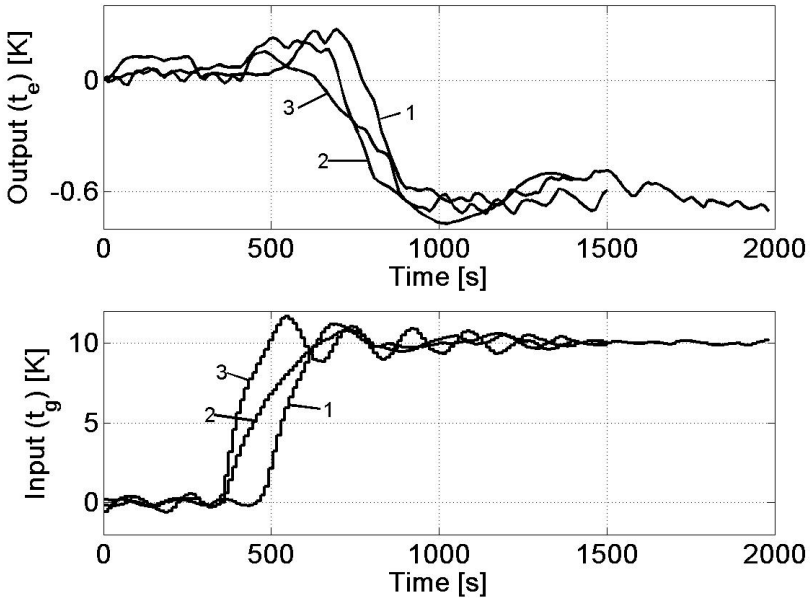

Figure 5.1.11. Standardised input and output values at equal time intervals for identification of subsystem 'chiller'. Line indices refer to step numbers of Table 5.1.1.

Compared to Figure 5.1.5 it can be seen that both input and output data of Figure 5.1.11 are stronger influenced by disturbance. The signals are less constant and oscillate around their average values. After using the data of Figure 5.1.11 for the System Identification Toolbox, a model has been chosen for each step. The model outputs are shown in Figure 5.1.12, Figure 5.1.13 and Figure 5.1.14.

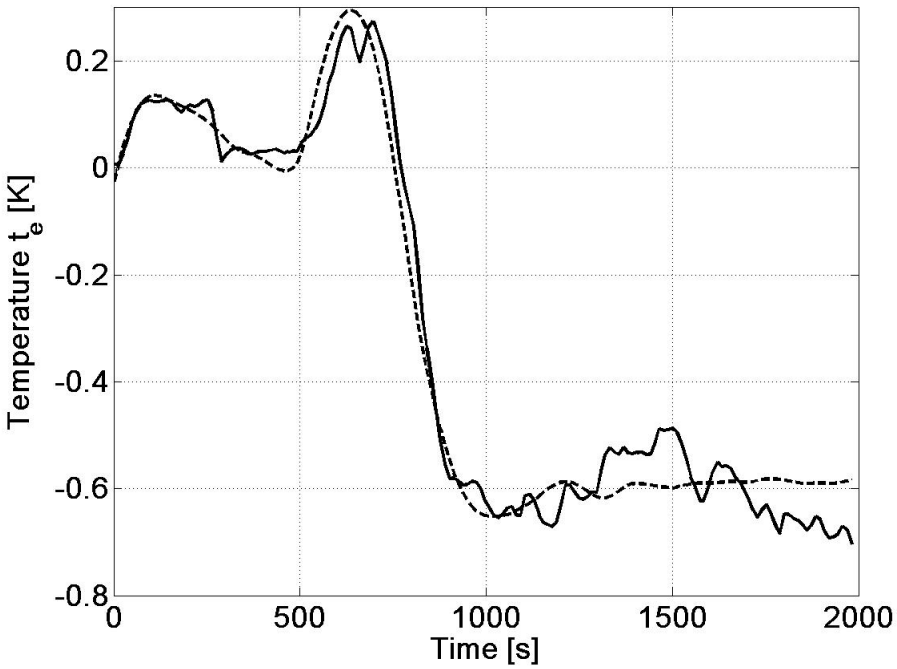

Figure 5.1.12. Measured (solid line) and simulated (dashed line) model output of subsystem 'chiller' for Step 1 (65-75 °C)

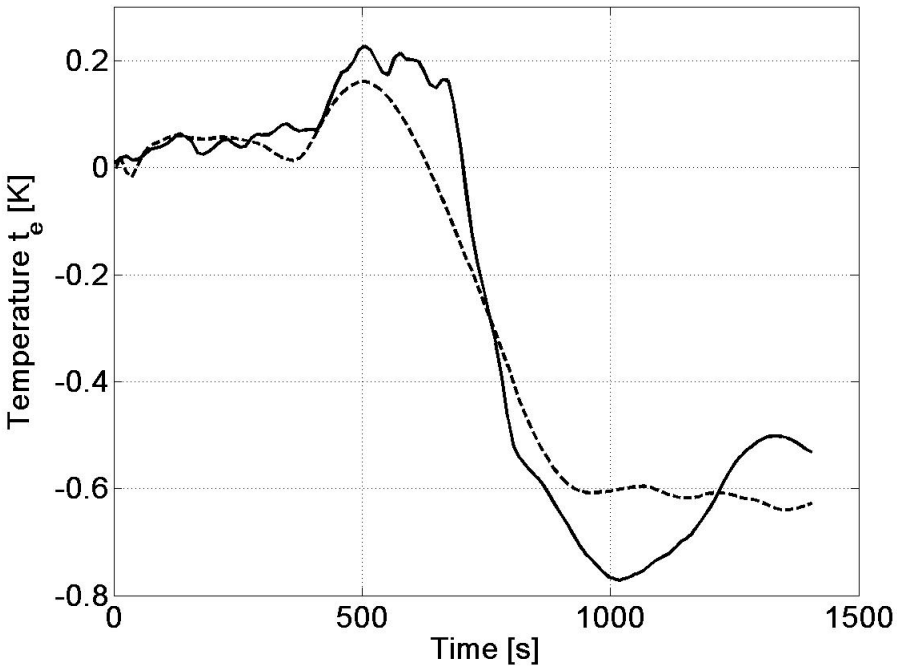

Figure 5.1.13. Measured (solid line) and simulated (dashed line) model output of subsystem 'chiller' for Step 2 (75-85 °C)

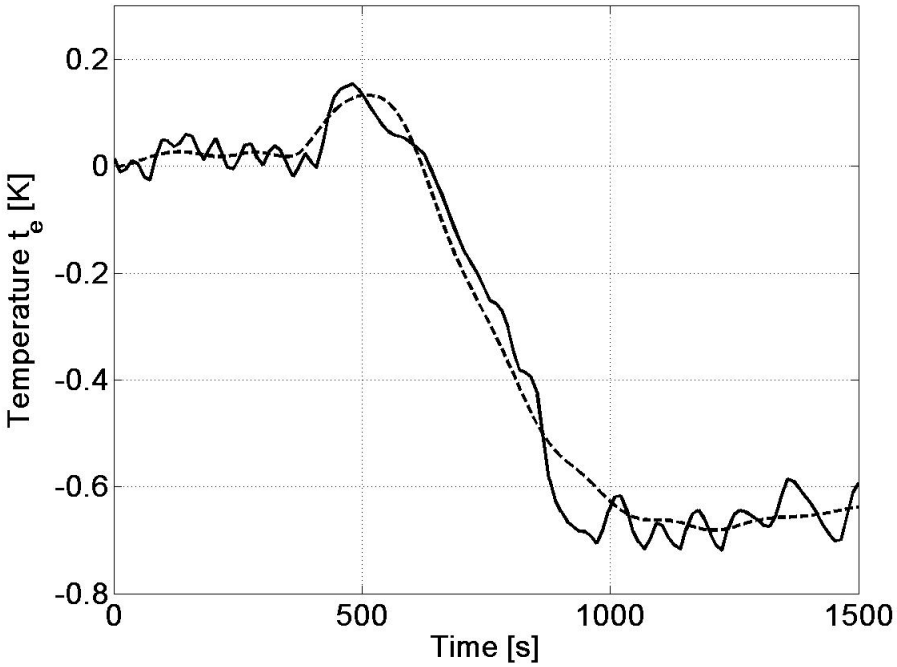

Figure 5.1.14. Measured (solid line) and simulated (dashed line) model output of subsystem 'chiller' for Step 3 (85-95 °C)

The quality of the input data influences the quality of the resulting model as well. A comparison of the R-squared values of the output plots shows that the fit quality of the chiller models is not as high as for the valve identification. The R-squared values for the three model fits are

- Step 1: $R^2 = 84$ %
- Step 2: $R^2 = 74$ %
- Step 3: $R^2 = 87$ %.

The highest deviation between measured and simulated data is approx. 0.25 K in the model of Step 2. The transfer functions of the models can be calculated as previously described and read as follows.

Step 1:
$$G_{c6575} = \frac{0.001132s - 5.298e^{-6}}{s^2 + 0.01273s + 9.046e^{-5}} \quad (5.1.4)$$

Step 2:
$$G_{c7585} = \frac{-3.895e^{-4}s^4 + 1.767e^{-4}s^3 + 8.203e^{-5}s^2 + 1.154e^{-5}s - 6.709e^{-8}}{s^4 + 0.09601s^3 + 0.01328s^2 + 1.945e^{-4}s + 1.096e^{-6}} \quad (5.1.5)$$

Step 3:
$$G_{c8595} = \frac{0.0003565s - 2.242e^{-6}}{s^2 + 0.007879s + 3.593e^{-5}} \quad (5.1.6)$$

Equations (5.1.4), (5.1.5) and (5.1.6) represent three models found for the subsystem 'chiller' by system identification. They are all based on a hot water temperature step of 10K, however at

different temperature levels between 65 and 95°C. For a control algorithm it could be possible to use each model for its original temperature range. This would require the identification of three parameter sets for the final system controller. However, the use of only one model for the whole temperature range is preferred due to reasons of simplicity. To determine which model of the three above to use, the step response of each model can be used. Figure 5.1.15 shows the step responses of the three models for a unity step.

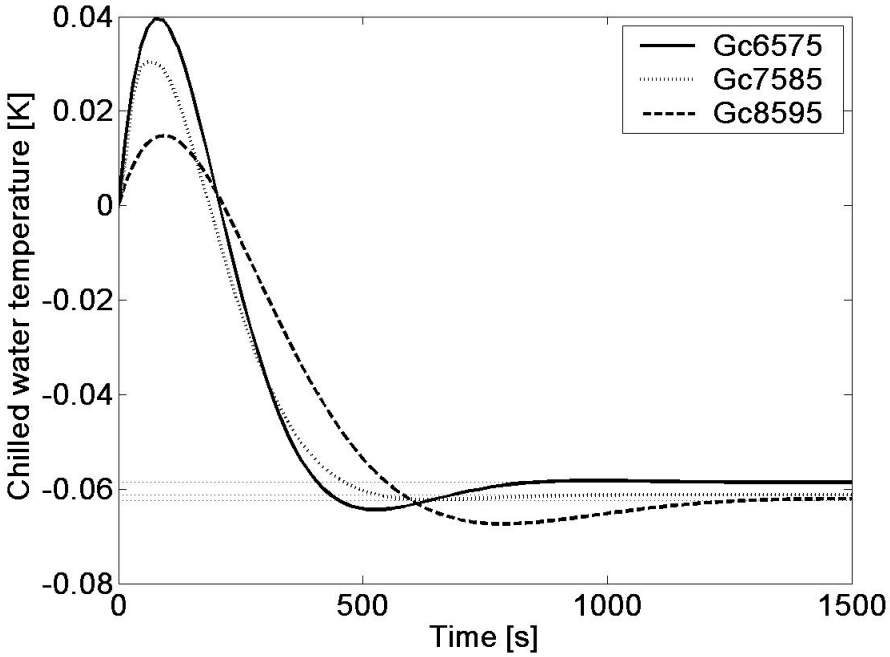

Figure 5.1.15. Step response of chiller models for unity step.

It can be seen in Figure 5.1.15 that the models have different transfer characteristics and end values. The latter do not differ much but there are small differences between each model. The positive overshoot of each transfer function can be related to small variations of the cooling water inlet temperature as visible in Figure 5.1.10. After the hot water step, the cooling water outlet temperature rises due to a bigger absorber heat flow and the control for the cooling water inlet temperature has to react in order to maintain a steady inlet temperature. Insufficient control behaviour during this reaction causes a small cooling water inlet temperature increase. This in turn results in lower absorber capacity and thus lower evaporator capacity. In consequence, the chilled water outlet temperature rises for a short time before it drops to the new steady state.

Together with information from the step responses, measurement data can be used to determine the quality of the models. For this, measurement data of each step (i.e. 1, 2 and 3) is fed into each model (i.e. G_{c6575}, G_{c7585} and G_{c8595}) and the R-squared value of the model fit is being calculated. Each model is therefore validated three times, once with its origin data and two times with data from the other two steps. Table 5.1.3 shows the resulting fits for the validation of each model with all input data sets.

Table 5.1.3. R-squared value of model fits for varying input data

Step No.	Input data	Model Fit R^2 [%] G_{c6575}	Model Fit R^2 [%] G_{c7585}	Model Fit R^2 [%] G_{c8595}
1	t_g (65°C→75°C)	84	81	73
2	t_g (75°C→85°C)	79	74	66
3	t_g (85°C→95°C)	64	70	87
	Average	76	75	75

It can be seen that the differences between the individual models are small. Step 1 has the highest average R-squared value and thus the highest accuracy when used with input data between 65 and 95 °C. It is therefore being chosen for the simulation of the subsystem 'chiller'.

The most important part of the system identification is the final validation of a model. This is being done by using measured data as model input and comparing the simulated with the corresponding measured output data. Figure 5.1.16 shows the results of the validation for the G_{c6575} model.

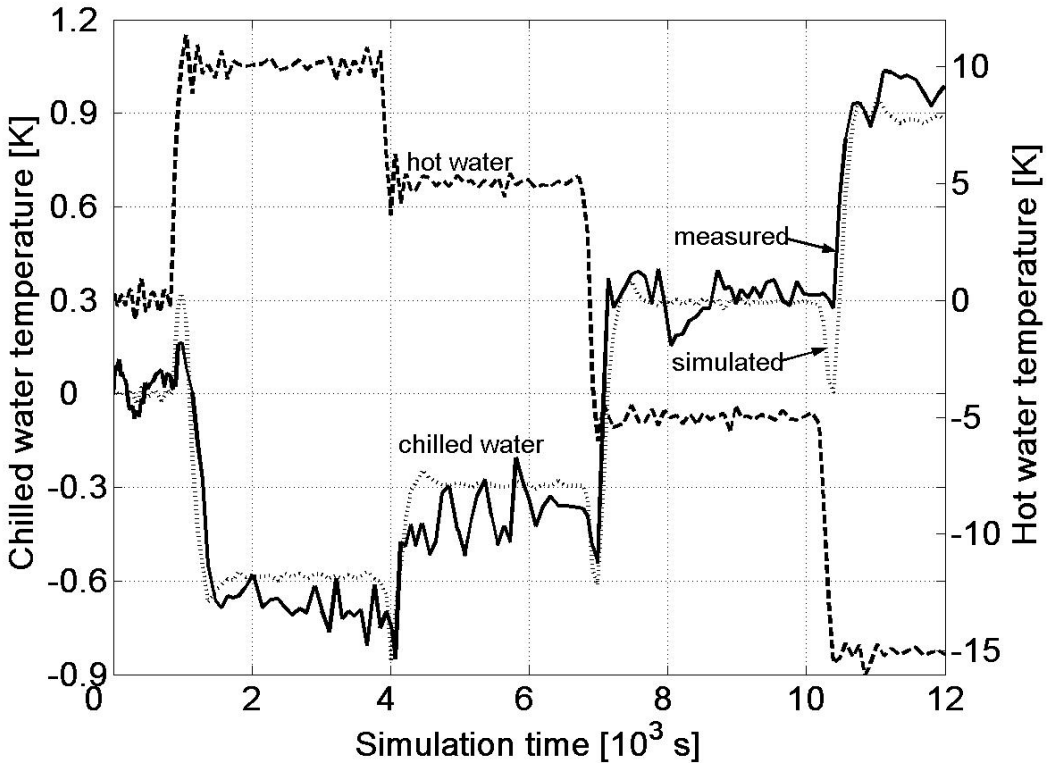

Figure 5.1.16. Validation of the G_{c6575} model with measured temperature data. Hot water temperature (dashed line) is displayed on the right y-axis, measured (solid line) and simulated (dotted line) chilled water temperature is displayed on the left y-axis.

In Figure 5.1.16, hot water input temperature data (dashed line) is displayed on the right y-axis. It is experimental measurement data from forced steps 4, 5, 6 and 7 of Figure 5.1.10. They have been used for validation purposes instead of measurement data from steps 1, 2 and 3 in order to see the model behaviour for different data. The resulting chilled water output temperature data is

shown on the left y-axis. Measured temperature is displayed in solid line, simulated temperature in dotted line. It can be seen that the simulation results agree with the measurement data with acceptable deviation. The maximum deviation between a measured and simulated data point in Figure 5.1.16 is 0.3 K. It is also visible that for the first two steps from 0 to 10 K and from 10 to 5K, the simulated temperature is approx. 0.1 K above the measured temperature. For the third step simulated and measured temperature agrees well.

5.1.3 Transfer function of the total system

The identification of the subsystems 'valve' and 'chiller' in the previous chapters has resulted in two subsystem transfer functions, G_v and G_{c6575}. These transfer functions can be multiplied to a single function which models the character of the whole system. This transfer function can then be used for designing a controller that controls the chilled water outlet temperature t_{Ec} by adjusting the voltage U of valve V3.

$$\mathrm{G_{vc}} = \mathrm{G_v} \cdot \mathrm{G_{c6575}}$$

$$G_{vc} = \frac{5.14e^{-7}s^4 - 2.97e^{-7}s^3 - 7.34e^{-8}s^2 + 2.41e^{-8}s - 1.11e^{-10}}{s^6 + 0.13s^5 + 0.014s^4 + 6.76e^{-4}s^{44} + 1.61e^{-5}s^2 + 1.54e^{-7}s + 7.71e^{-10}} \qquad (5.1.7)$$

The new transfer function G_{vc} combines the transfer characteristics of G_v and G_{c6575}. Figure 5.1.17 shows the unity step response of G_{vc}. The gain of the controlled system is negative, $K_{vc} \approx 0.14$K/V.

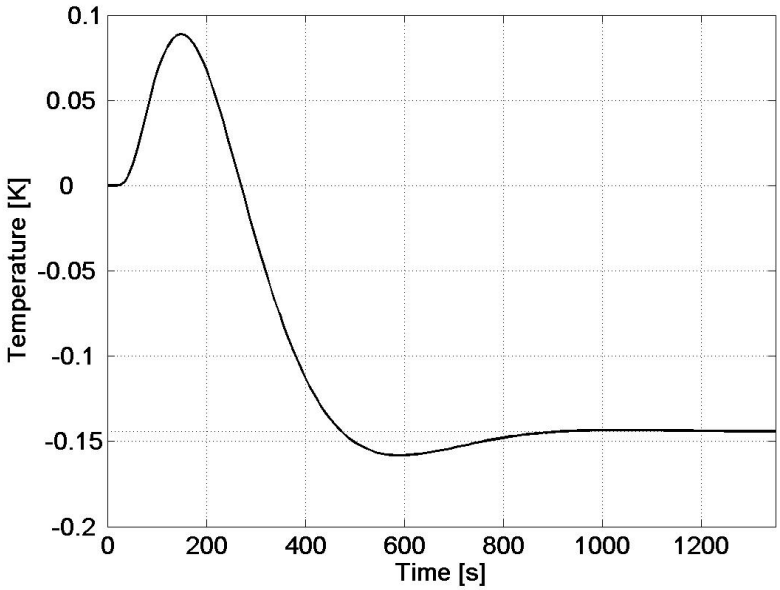

Figure 5.1.17. Step response for unity step of transfer function G_{vc}.

There is a dead time of approximately 20s before a reaction of the chilled water outlet temperature on a voltage step of 1V is visible. The outlet temperature has an overshoot of

approximately 0.09 K before it begins to drop below zero after approximately 270s. Then, there is a slight undershoot to approximately -0.16K. The steady-state of -0.14K is being reached at 1200s after the step. The overshoot is due to the cooling water variation after the step as visible in Figure 5.1.10. The dead time is related to the thermal inertia of the chiller. The transfer function determined experimentally (equation (5.1.7)) can only be used for the conditions at which it was identified. These are

- Inlet temperatures into three-way valve between 65 and 95 °C
- Internal/external mass flows as in Table 5.1.1
- Fixed length of piping between valve and chiller as used in identification process
- a valve with similar characteristic diagram as used in identification process
- Phönix 10 kW absorption chiller

The transfer function has been used for the design of a closed-loop controller. The development of such a controller is a standardized procedure and shall not be described here in detail. A summarized description of the controller testing procedure for the Phönix system can be found in Appendix 8.6. Instead, the transfer function G_{vc} found by experimental system identification shall be compared to a transfer function resulting from a dynamic chiller simulation.

5.1.4 Chapter summary and conclusion

In this chapter the identification process for the transfer function of an absorption chiller derived from experimental data has been presented. Such a transfer function can be used to model the dynamic chiller behaviour and to develop control parameters e.g. for a chilled water temperature control. It is a simple method where the chiller behaviour is being modelled with just one equation.

The three-way valve for hot water temperature control has been identified and a transfer function between control voltage and hot water outlet temperature of the valve has been found. Three different transfer functions of three different hot water temperature steps have been identified for the absorption chiller and validated with experimental data. A strong influence of the step conditions on the model behaviour has been found, expressed by differences in the step responses of the transfer functions. The temperature level of the hot water step has a small influence on the transfer functions compared to the influence of the external input parameters. In the steps presented, the cooling water temperature fluctuates slightly after the step. The amplitude of the fluctuations influences the identified transfer functions and results in an overshoot of the step responses during the first time period after the step.

The identification via experimental data yields a transfer function which can only be used within a limited operation range. For example, if constant volume flows during the identification process have been assumed, then a variation of such cannot be represented by the experimentally determined transfer function. The transfer function determined experimentally (equation (5.1.7)) can only be used for the conditions at which it was identified, which is a disadvantage of this method. An advantage is however the freedom to use any kind of parameter set that relates output to input. A step of ideal character is not necessary for the system identification.

5.2 Theoretical chiller simulation

The disadvantage of a limited application range of the system identification method presented in the previous chapter can be overcome by using a theoretical model for transfer behaviour simulations. Such a model reproduces the thermo-physical processes inside the chiller and takes all external input parameter simultaneously into account. Thus, all these parameters can be varied with a greater degree of freedom. Consequently, more than one mathematical equation is necessary to model the chiller with sufficient accuracy.

In general, two kinds of models are possible for the simulation of absorption chillers. Steady-state models simulate the chiller under constant operating conditions. They allow the determination of internal and external cycle parameters, such as heat exchanger sizes, pump flow rates, temperatures and heat flows. However, these simulations do not provide time-dependent information on the thermal behaviour of absorption chillers. The outputs of the chiller are calculated depending on the inputs, regardless of time-dependent chiller characteristics. A step change of input conditions results in an immediate step change of output conditions. These models are well suited for the simulation of different operating conditions. They are however also used in component-based transient system simulation software such as TRNSYS, Matlab/Simulink, INSEL etc., although they are not really appropriate for this purpose. They are not suitable for the identification of control parameters, as time constants and inertias are not included in these models.

In contrast, dynamic models allow the simulation of the transient behaviour of the chiller. Thermal inertias and time constants can be included in these models. A dynamic model can also provide steady-state results. However, after a step change of input conditions the output does not change immediately. According to the transfer characteristic of the chiller, the new steady state will be reached after a certain time. Such models are well suited for the simulation of the transfer behaviour if the characteristics of the chiller can be sufficiently reproduced in the underlying theory.

Research on dynamic system behaviour was carried out in many variations for both LiBr/water and Water/NH_3 heat pumps, chillers and components of such. Bian et. al. have performed a transient simulation of an absorption chiller. They present a chiller model that can be run using variable time steps for the simulation. It includes a temperature change term of each heat exchanger per time step as well as a mass storage term in the generator, i.e. a part of the strong solution is being stored in the generator in each time step. The model has been built in Matlab/Simulink using an ODE45 solver. It has been verified with experimental data and shows good agreement in the transiency of the thermal behaviour, even if absolute values do not exactly match [Bian *et al.* 2005].
Jeong et.al. present the dynamic simulation of a steam-driven LiBr/water absorption heat pump for the use of low-grad waste heat. Their model is based on the simultaneous solution of the differential equations of enthalpy and mass balances, pressure equations and property data.

Storage terms have been assumed with thermal capacities and solution mass storage in the vessels. Solution and vapour mass flow rates are calculated in proportion to pressure differences between vessels. The heat transfer coefficients as well as the simulation time step are assumed constant. The model has been verified using operational data of an absorption chiller with good agreement [Jeong *et al.* 1998].

The goal of the dynamic model presented here is to simulate the reaction of the chiller on a change of external conditions and to determine the most important parameters which dominate the transient behaviour. Of special interest is the response of the chilled water outlet temperature on a hot water step. Therefore, a very simple and transparent model was chosen in contrast to the approach in the cited references.
Figure 5.2.1 shows the single-effect LiBr/water absorption cycle with state points as assumed for the model.

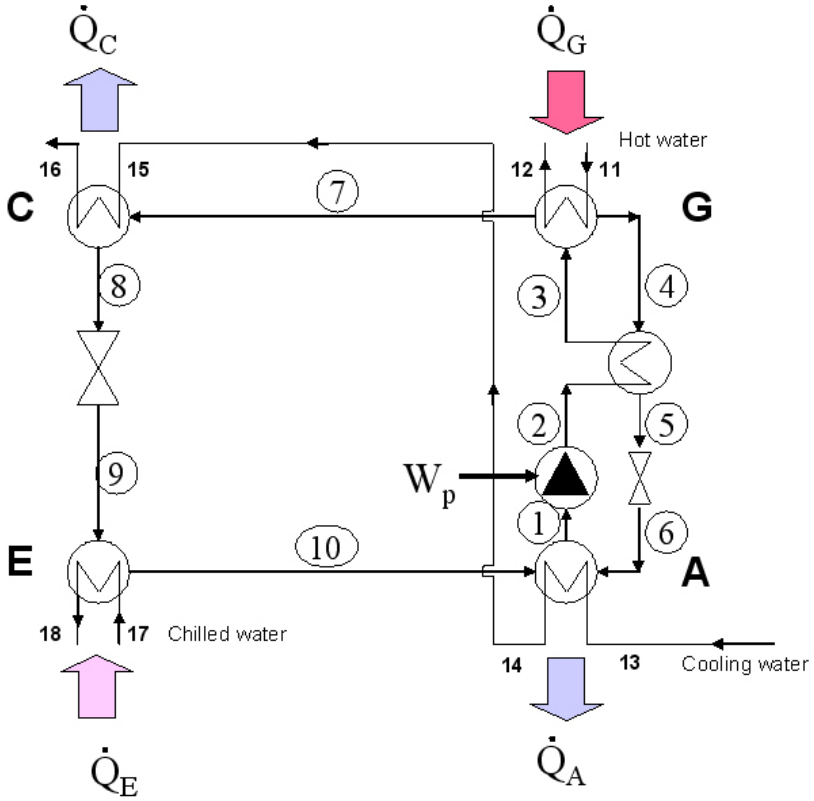

Figure 5.2.1. LiBr/water absorption cycle.

Visible are the four main components of an absorption chiller: generator (G), condenser (C), evaporator (E) and absorber (A). Also shown are solution heat exchanger, solution pump and the throttling valves between absorber/solution heat exchanger and condenser/evaporator. The internal state points characterize the thermodynamic properties of LiBr/water solution (points 1-6), water vapour (7, 10) and liquid water (8, 9). The external state points characterize the thermodynamic properties of hot water (11, 12), cooling water (13, 14, 15, 16) and chilled water (17, 18).

For simplicity reasons, not all internal temperatures in Figure 5.2.1 are being calculated in the model. Instead, each vessel is being modelled using internal mean temperatures of the heat carrier fluid as well as a mean vessel temperature. Figure 5.2.2 shows the temperature nomenclature as used for the model.

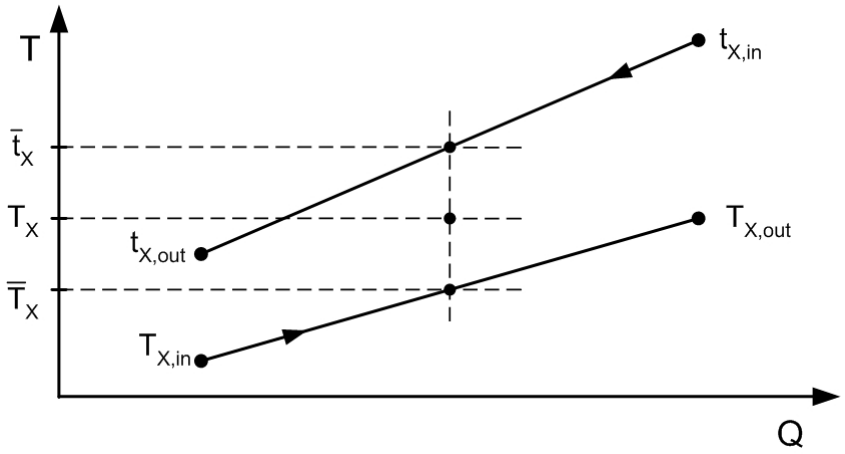

Figure 5.2.2. Temperature definition for dynamic model. External temperatures: t, internal temperatures: T. Subscript X symbolizes the four vessels, i.e. E (Evaporator), C (Condenser), G (Generator) and A (Absorber).

The external mean heat carrier temperatures $\bar{t}_X$ are being calculated using the arithmetic mean temperature of inlet and outlet temperature. The internal mean temperatures $\overline{T}_X$ are assumed to be the mean of the equilibrium temperatures of strong and weak solution and of the refrigerant. The mean vessel temperatures T_X are the arithmetic mean temperature of the external and internal mean temperatures.

5.2.1 Dynamic terms

The model is based on external and internal steady-state enthalpy balances for each main component but, in order to render it dynamic, mass storage terms in Absorber and Generator, thermal heat storage terms in all vessels and a time shift in the solution cycle have been included. These dynamic terms will be discussed shortly.

I. Mass storage

Both generator and absorber vessel have been modelled as a serial connection of a tube bundle heat exchanger and a solution sump. For this, two different concentrations and four different mass flows per vessel have been introduced in order to achieve more detailed information about the mass transfer inside the vessels. Introducing $\Delta\hat{t}$ as the time period between two simulation steps and *i* as index of each simulation interval, Figure 5.2.3 shows the concentration and mass flow definitions.

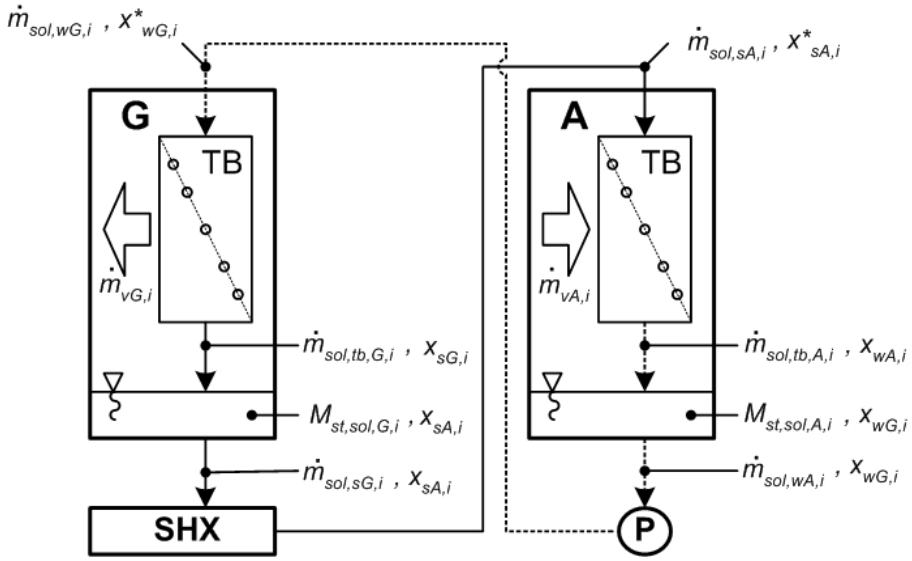

Figure 5.2.3. Definition of concentrations and mass flows in generator/absorber. Solid lines: strong solution, dotted lines: weak solution, white arrows: vapour, SHX: solution heat exchanger, P: pump, TB: tube bundle.

The vessel sump and the outlet solution of generator and absorber are assumed to have the same salt concentration, $x_{sA,i}$ and $x_{wG,i}$, respectively. The outlet of each tube bundle is assumed to exhibit the equilibrium concentration $x_{sG,i}$ and $x_{wA,i}$. The strong solution leaving the generator, $\dot{m}_{sol,sG,i}$, has to pass the solution heat exchanger and its adjacent piping before entering the absorber ($\dot{m}_{sol,sA,i}$, $x^*_{sA,i}$). In analogy, the weak solution leaving the absorber, $\dot{m}_{sol,wA,i}$, has to pass the solution pump and its piping before entering the generator ($\dot{m}_{sol,wG,i}$, $x^*_{wG,i}$). The total solution mass stored in generator and absorber sump is expressed by $M_{st,sol,G,i}$ and $M_{st,sol,A,i}$, respectively. There is no solution storage on the tube bundle, only in the sump below.

II. Thermal storage

After an external input temperature change, thermal heat storage applies to all external and internal components which are involved in heat transfer mechanisms. The temperature change of these components is a complex three-dimensional heat transfer problem. In a strong simplification, a mean temperature of a component can be assumed which follows the external temperature and thus dampens the heat transfer between external and internal media. Figure 5.2.4 shows an exemplary enthalpy balance for the generator tube bundle, assuming a mean vessel temperature T_x. The total heat capacity of the vessel is expressed by $\left(M \cdot c_p\right)_{tot}$.

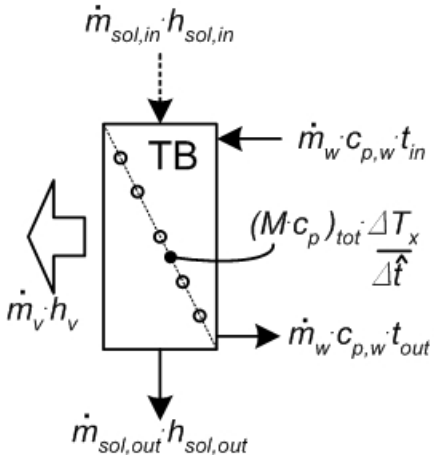

Figure 5.2.4. Simplified enthalpy balance for vessels. Refer to Figure 5.2.3 for line definitions.

The external heat flow is calculated using the external enthalpy difference of the water, the internal heat flow is the enthalpy difference of solution and vapour. The heat required for the temperature change of the thermal mass is calculated using the vessel temperature difference ΔT_x per time period $\Delta \hat{t}$. The total heat flow between internal and external media can also be calculated as

$$\dot{Q} = (UA)_{tot} \cdot (\bar{t}_x - \overline{T}_x) \qquad (5.2.1)$$

In equation (5.2.1), a mean heat transfer coefficient as well as a mean heat exchange area are assumed.

However, the assumption of mean values for vessel temperature, heat transfer coefficient and area of a vessel is not very precise. A closer approach to reality is the assumption that some components follow internal temperatures, e.g. the vessel walls which follow the sump temperature, and other components follow external temperatures. Then, time delays have also to be taken into account as external and internal components will most likely react differently. For the model presented, thermal time delays have not been included. However, to account for the different heat transfer rates in external and internal components, the total thermal mass has been divided into an external and an internal part. The external part follows the mean external temperature $\bar{t}_x$, the internal part follows the mean internal temperature $\overline{T}_x$. Also, different heat transfer coefficients and exchange areas have been assumed for the internal and external parts. Figure 5.2.5 shows the partition of the vessel into an external (right side) and internal (left side) part.

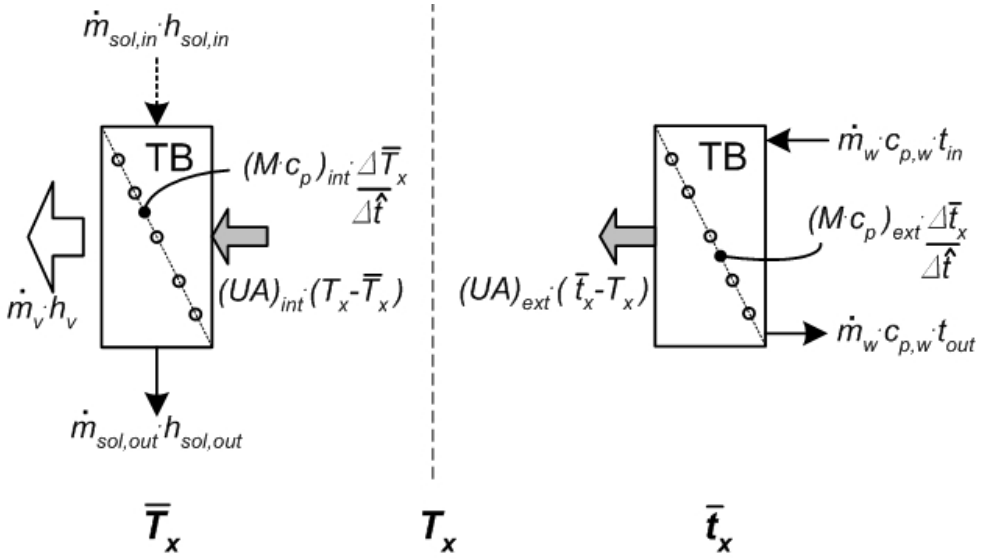

Figure 5.2.5. Advanced enthalpy balance for vessels. Grey arrows denote heat flow.

The heat capacities are now split in internal and external fractions. The heat flow between external and internal media has also been split into an internal heat flow with the driving temperature difference (T_x - $\bar{T}_x$) and an external heat flow with the driving temperature difference ($\bar{t}_x$ - T_x).

Note: Figure 5.2.5 shows the enthalpy balances for the generator. They are also valid for the absorber if the directions of vapour mass flow and heat flows are being reversed. They can also be applied to evaporator and condenser if the solution terms are being neglected and the direction of vapour mass flow is assumed correctly.

The components bearing thermal mass in the chiller are listed in Table 5.2.1 as assumed for the model.

Table 5.2.1. Heat capacities and mass of internal and external chiller components

Component	Material	Heat capacity [kJ/kgK]	Location	Mass in E [kg]	Mass in C [kg]	Mass in G [kg]	Mass in A [kg]
Vessel wall (10% of total weight)	St 37	0.48	external	2.0	2.0	1.9	1.9
External water header	St 37	0.48		7.6	7.3	9.8	10.6
Water in external parts	Water	4.19		8.5	7.4	12.6	11.9
Heat exchanger tube bundles (50%)	Copper	0.38		5.7	5.1	8.9	8.0
Heat exchanger tube bundles (50%)	Copper	0.38	internal	5.7	5.1	8.9	8.0
LiBr/water solution (50% each)	LiBr/water	3.70		-	-	19.0	19.0
Refrigerant water (50% each)	Water	4.19		7.5	7.5	-	-
Solution heat exchanger (50% each)	Copper	0.38		-	-	4.1	4.1
Solution pump (50% each)	St 37	0.48		-	-	5.0	5.0
Vessel walls (50% of total weight)	St 37	0.48		10.0	10.0	9.5	9.5

III. Solution time shift

A time shift is assumed in both solution circuit legs. The inlet values of solution mass flow $\dot{m}_{sol,sA,i}$ and concentration $x^*_{sA,i}$ at the absorber at time interval *i* are assumed the generator outlet values of time interval (*i*-c_1). In analogy, the inlet values of mass flow $\dot{m}_{sol,wG,i}$ and concentration $x^*_{wG,i}$ at the generator at time interval *i* are assumed the outlet values of the absorber at time step (*i*-c_2).

Absorber:

$$x^*_{sA,i} = x_{sA,i-c1} \quad (5.2.2)$$

$$\dot{m}_{sol,sA,i} = \dot{m}_{sol,s,i-c1} \quad (5.2.3)$$

Generator:

$$x^*_{wG,i} = x_{wG,i-c2} \quad (5.2.4)$$

$$\dot{m}_{sol,wG,i} = \dot{m}_{sol,w,i-c2} \quad (5.2.5)$$

Constants c_1 and c_2 account for dynamic effects due to the bidirectional solution transport time between generator and absorber. They depend on the momentary mass flow in both solution circuit legs but are assumed constant in the model. The error made by this assumption is negligible as long as the mass flows do not change too much.

5.2.2 Mass balances

According to Figure 5.2.3, the mass flow balances of generator and absorber sump yield

$$\dot{m}_{sol,tb,G,i} - \dot{m}_{sol,s,i} - \frac{m_{st,sol,Gi}}{\Delta\hat{t}} = 0 \quad (5.2.6)$$

$$\dot{m}_{sol,tb,A,i} - \dot{m}_{sol,w,i} - \frac{m_{st,sol,Ai}}{\Delta\hat{t}} = 0 \quad (5.2.7)$$

The mass storage term $\frac{m_{sol,st,X,i}}{\Delta\hat{t}}$ in equation (5.2.6) and (5.2.7) is the amount of solution which is added to the solution stored in either generator or absorber per simulation time interval *i*.

A salt flow balance in both sumps can be written as:

$$M_{st,sol,G,i} \cdot x_{s,A,i} = M_{st,sol,G,i-1} \cdot x_{s,A,i-1} + \dot{m}_{sol,tb,G,i} \cdot \Delta\hat{t} \cdot x_{s,G,i} - \dot{m}_{sol,s,i} \cdot \Delta\hat{t} \cdot x_{s,A,i} \quad (5.2.8)$$

$$M_{st,sol,A,i} \cdot x_{w,G,i} = M_{st,sol,A,i-1} \cdot x_{w,G,i-1} + \dot{m}_{sol,tb,A,i} \cdot \Delta\hat{t} \cdot x_{w,A,i} - \dot{m}_{sol,w,i} \cdot \Delta\hat{t} \cdot x_{w,G,i} \quad (5.2.9)$$

The term $M_{st,sol,X,i}$ in equations (5.2.8) and (5.2.9) is the total solution mass in the vessel sump. It is assumed that the salt mass in the sump at time interval *i* equals the salt mass at time interval *i-1* plus the difference of ingoing and outgoing salt flows at time interval *i*.

For the tube bundles, the mass flow balance yields

$$\dot{m}_{sol,w,i} - \dot{m}_{v,G,i} - \dot{m}_{sol,tb,G,i} = 0 \qquad (5.2.10)$$

$$\dot{m}_{sol,s,i-c1} + \dot{m}_{v,A,i} - \dot{m}_{sol,tb,A,i} = 0 \qquad (5.2.11)$$

The salt flow balance reads

$$\dot{m}_{sol,w,i} \cdot x_{w,G,i-c2} - \dot{m}_{sol,tb,G,i} \cdot x_{s,G,i} = 0 \qquad (5.2.12)$$

$$\dot{m}_{sol,s,i-c1} \cdot x_{s,A,i-c1} - \dot{m}_{sol,tb,A,i} \cdot x_{w,A,i} = 0 \qquad (5.2.13)$$

In equation (5.2.11) it is assumed that the mass flow entering the absorber tube bundle at time interval *i* equals the mass flow which has left the generator c_1 time intervals ago. Doing so, the physical incompressibility of the solution in the piping between generator and absorber is not modelled correctly. In reality, the mass flow entering the tube at time interval *i* should equal the mass flow leaving the tube at time interval *i*. The reason for which this incorrect assumption has been made is the time shift in the salt concentration. The salt concentration entering the absorber tube bundle per time interval *i* equals the salt concentration leaving the generator sump at time interval $i\text{-}c_1$. If the salt flow balance expressed in equation (5.2.13) was calculated using the solution mass flow of time interval *i*, the result would be a wrong salt mass entering the absorber at time interval *i*. While this would not have any effect during steady-state chiller operation it would affect the absorber concentration immediately after a step. This error would be severe, because it is linked directly to the interpretation of the transients. To avoid a rise of the absorber equilibrium concentration too early, i.e. before the time equivalent of c_1 has passed after an input step, equation (5.2.13) has been formulated this way, now yielding a correct salt balance for each time interval. In consequence, the mass flow in equation (5.2.11) had to be adjusted as well. The result is a hidden mass storage term in the solution tube. Per time interval *i*, the following solution mass is stored in the tube.

$$\Delta m_{sol,s} = \left(\dot{m}_{sol,s,i} - \left(\dot{m}_{tb,A,i} - \dot{m}_{v,A,i}\right)\right) \cdot \Delta\hat{t} \qquad (5.2.14)$$

The mistake which is made by doing so can be calculated and will be discussed in chapter 5.2.6. It is similar to assuming that no solution is stored on the tube bundles.

The strong solution flows from generator to absorber driven by gravity force and pressure gradient. The pressure loss of the solution heat exchanger and its adjacent piping is assumed

constant. This is valid as long as the flows do not vary strongly. Hence the mass flow of the strong solution depends only on the pressure difference between generator/absorber and the liquid solution column at heat exchanger inlet[1]. Figure 5.2.6 shows the arrangement of generator (G), absorber (A) and solution heat exchanger (SHX).

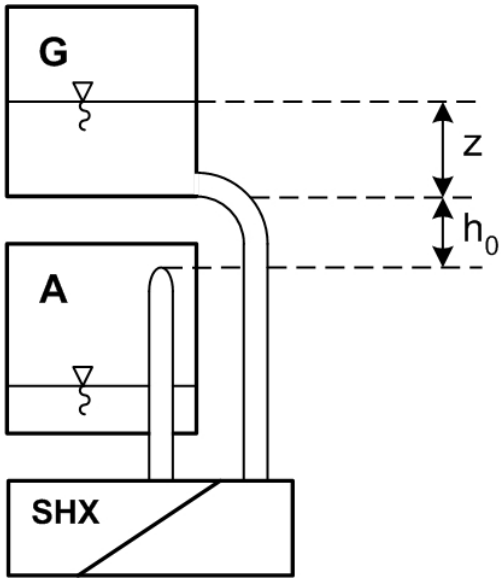

Figure 5.2.6. Hydraulic arrangement of generator, absorber and solution heat exchanger.

The static pressure difference between solution outlet at generator and inlet at absorber can be calculated according to

$$\Delta p_{stat,i} = \left(p_{G,i} - p_{A,i}\right) + \rho_{sol,s} \cdot g \cdot \left(h_0 + z_i\right) \qquad (5.2.15)$$

The level of strong solution in the generator sump, z_i, varies according to the momentary load of the chiller. It is calculated using the momentary amount of strong solution in the generator and equals zero if the solution level equals the sump bottom. A case differentiation is being made for the calculation of z_i. If the solution level is lower than the sump bottom (negative values of $M_{st,sol,G,i}$), the cross area used for the level calculation changes. Instead of using the cross area of the generator sump, A_G, the cross area of the solution pipe, A_t, is being used.

solution in generator sump:

$$z_i = \frac{M_{st,sol,G,i}}{\rho_{sol,s} \cdot A_G} \qquad (5.2.16)$$

no solution in generator sump:

$$z_i = \frac{M_{st,sol,G,i}}{\rho_{sol,s} \cdot A_t} \qquad (5.2.17)$$

[1] Other than shown in Figure 5.2.1 the pressure between Generator/Absorber is reduced only by the pressure loss of the solution heat exchanger. There is no additional expansion device assumed in the model.

The height between solution outlet at generator and inlet at absorber, h_0, is constant. The pressure loss of the flowing solution can be calculated as

$$\Delta p_{dyn,i} = \varsigma \cdot \frac{\rho_{sol,s}}{2} \cdot w_i^{\,2} \qquad (5.2.18)$$

The factor ς in equation (5.2.18) is the dimensionless resistance coefficient of the solution heat exchanger and the piping between generator and absorber. It expresses the pressure loss due to friction in the piping and the pressure loss due to single resistances in the flow. Both these terms cannot be individually determined for the chiller, so an estimate has to be made for the sum of both. However, the pressure loss of the solution heat exchanger is assumed to be dominant compared to the friction on the tube walls. Thus, the resistance coefficient has been calculated from manufacturer design data of the solution heat exchanger.
Now we have to link the mass flow to the velocity of the flowing solution, w_i.

$$\dot{m}_{sol,s,i} = w_i \cdot A_t \cdot \rho_{sol,s} \qquad (5.2.19)$$

During operation, the static pressure difference equals the pressure loss. Then, solving equation (5.2.18) for w and inserting equation (5.2.15) and (5.2.19) yields

$$\dot{m}_{sol,s,i} = A_t \cdot \sqrt{\frac{2 \cdot \rho_{sol,s} \cdot \left(p_{G,i} - p_{A,i} + \rho_{sol,s} \cdot g \cdot \left(h_0 + z_i\right)\right)}{\varsigma}} \qquad (5.2.20)$$

5.2.3 Enthalpy balances

According to Figure 5.2.5, the external enthalpy balance of the vessels can be written as follows.

$$\dot{m}_{X,w} \cdot c_{p,w} \cdot \left(t_{X,in} - t_{X,out}\right) = \left(UA\right)_{ext,X} \cdot \left(\bar{t}_{X,i} - T_{X,i}\right) + \left(M \cdot c_p\right)_{ext,X} \cdot \frac{t_{X,i} - t_{X,i-1}}{\Delta \hat{t}} \qquad (5.2.21)$$

Index X denotes the different vessels (E, C, G, A) with their respective external mass flows, temperatures, heat transfer coefficients and thermal mass.

According to Figure 5.2.1, the internal heat flows of the vessels read as follows.

Evaporator: $$\dot{Q}_{E,\mathrm{int},i} = \dot{m}_{v,i} \cdot (h_{10,i} - h_{8,i}) \qquad (5.2.22)$$

Condenser: $$\dot{Q}_{C,\mathrm{int},i} = \dot{m}_{v,i} \cdot (h_{7,i} - h_{8,i}) \qquad (5.2.23)$$

Absorber: $$\dot{Q}_{A,\mathrm{int},i} = \dot{m}_{v,i} \cdot h_{10,i} - \dot{m}_{sol,w} \cdot h_{1,i} + (\dot{m}_{sol,w} - \dot{m}_{v,i}) \cdot h_{5,i} \quad (5.2.24)$$

Generator: $$\dot{Q}_{G,\mathrm{int},i} = \dot{m}_{v,i} \cdot h_{7,i} + (\dot{m}_{sol,w} - \dot{m}_{v,i}) \cdot h_{4,i} - \dot{m}_{sol,w} \cdot h_{3,i} \quad (5.2.25)$$

where $\dot{m}_{sol,w}$ is the constant mass flow of the diluted solution and $\dot{m}_{v,i}$ is the mass flow of the water vapour. Assuming an ideal gas and a liquid with constant density, equations (5.2.22) to (5.2.25) can be transformed using the latent heat of evaporation and sorption, *r* and *l* [Ziegler 1997]. Different vapour mass flows from generator to condenser and evaporator to absorber are being introduced to account for dynamic effects in the chiller. This yields the following internal heat flow calculations.

E: $$\dot{Q}_{E,\mathrm{int},i} = \dot{m}_{v,A,i} \cdot \left(r_{(pc)} - c_{p,v} \cdot \left(\overline{T}_{C,i} - \overline{T}_{E,i} \right) \right) \quad (5.2.26)$$

C: $$\dot{Q}_{C,\mathrm{int},i} = \dot{m}_{v,G,i} \cdot \left(r_{(pc)} + c_{p,v} \cdot \left(\overline{T}_{G,i} - \overline{T}_{C,i} \right) \right) \quad (5.2.27)$$

G: $$\dot{Q}_{G,\mathrm{int},i} = \dot{m}_{v,G,i} \cdot \left(r_{(pc)} + l_{(pc)} + c_{p,w} \cdot \left(\overline{T}_{G,i} - \overline{T}_{A,i} \right) \right) + \dot{Q}_{SHX,i} \quad (5.2.28)$$

A: $$\dot{Q}_{A,\mathrm{int},i} = \dot{m}_{v,A,i} \cdot \left(r_{(pc)} + l_{(pc)} - c_{p,v} \cdot \left(\overline{T}_{G,i} - \overline{T}_{E,i} \right) + c_{p,w} \cdot \left(\overline{T}_{G,i} - \overline{T}_{A,i} \right) \right) + \dot{Q}_{SHX,i} \quad (5.2.29)$$

The solution heat exchanger is assumed perfectly insulated with no heat loss to ambient. It does however not exchange the maximum possible heat between its two flows. The difference between actual and ideal heat transfer can be assumed as a parasitic heat flow which has to be added to the generator and leaves at the absorber. It can be calculated as

$$\dot{Q}_{SHX,i} = (1 - \eta_{SHX}) \cdot \dot{m}_{sol,s,i} \cdot c_{p,sol,s} \cdot \left(\overline{T}_{G,i} - \overline{T}_{A,i} \right), \quad (5.2.30)$$

if the effectiveness η_{SHX} is assumed to be constant.

According to Figure 5.2.5, the internal enthalpy balances can then be written as

E: $$\dot{m}_{v,A,i} \cdot \left(r_{(pc)} - c_{p,v} \cdot \left(\overline{T}_{C,i} - \overline{T}_{E,i} \right) \right) + \left(M \cdot c_p \right)_{E,\mathrm{int}} \cdot \frac{\overline{T}_{E,i} - \overline{T}_{E,i-1}}{\Delta \hat{t}} = (UA)_{E,\mathrm{int}} \cdot \left(T_{E,i} - \overline{T}_{E,i} \right) \quad (5.2.31)$$

C: $$\dot{m}_{v,G,i} \cdot \left(r_{(pc)} + c_{p,v} \cdot \left(\overline{T}_{G,i} - \overline{T}_{C,i} \right) \right) + \left(M \cdot c_p \right)_{C,\mathrm{int}} \cdot \frac{\overline{T}_{C,i} - \overline{T}_{C,i-1}}{\Delta \hat{t}} = (UA)_{C,\mathrm{int}} \cdot \left(T_{C,i} - \overline{T}_{C,i} \right) \quad (5.2.32)$$

G:
$$\dot{m}_{v,G,i}\cdot\left(r_{(pc)}+l_{(pc)}+c_{p,w,i}\cdot\left(\overline{T}_{G,i}-\overline{T}_{A,i}\right)\right)+\dot{Q}_{SHX,i}+\left(M\cdot c_p\right)_{G,\mathrm{int}}\cdot\frac{\overline{T}_{G,i}-\overline{T}_{G,i-1}}{\Delta\hat{t}}=\left(UA\right)_{G,\mathrm{int}}\cdot\left(T_{G,i}-\overline{T}_{G,i}\right) \quad (5.2.33)$$

A:
$$\dot{m}_{v,A,i}\cdot\left(r_{(pc)}+l_{(pc)}-c_{p,v}\cdot\left(\overline{T}_{G,i}-\overline{T}_{E,i}\right)+c_{p,w}\cdot\left(\overline{T}_{G,i}-\overline{T}_{A,i}\right)\right)+\dot{Q}_{SHX,i}+\left(M\cdot c_p\right)_{A,\mathrm{int}}\cdot\frac{\overline{T}_{A,i}-\overline{T}_{A,i-1}}{\Delta\hat{t}}=\left(UA\right)_{A,\mathrm{int}}\cdot\left(T_{A,i}-\overline{T}_{A,i}\right) \quad (5.2.34)$$

5.2.4 Pressure and saturation temperature

Generator/condenser and evaporator/absorber pressure in equation (5.2.20) can be calculated using the equation of Clausius-Clapeyron.

$$\ln\left(\frac{p}{p_0}\right)=\frac{r_0}{R}\cdot\left(\frac{1}{T_0}-\frac{1}{T}\right) \quad (5.2.35)$$

Assuming small changes between two simulation time intervals, known values of time interval (*i-1*) can be used for p_0 and T_0 . The pressures of time interval *i* can thus be calculated as

$$\ln\left(\frac{p_{C,i}}{p_{C,i-1}}\right)=\frac{r_0}{R}\cdot\left(\frac{1}{\overline{T}_{C,i-1}}-\frac{1}{\overline{T}_{C,i}}\right)\ \text{and}\ \ln\left(\frac{p_{E,i}}{p_{E,i-1}}\right)=\frac{r_0}{R}\cdot\left(\frac{1}{\overline{T}_{E,i-1}}-\frac{1}{\overline{T}_{E,i}}\right) \quad (5.2.36)$$

where $p_{C,i}$ equals $p_{G,i}$ and $p_{E,i}$ equals $p_{A,i}$. The evaporation enthalpy r_0 is assumed constant for each state.

The boiling temperature of saturated LiBr/water solution can be calculated using the Duehring relation. In the model, this temperature is per definition the mean of the equilibrium temperatures of strong (or weak) solution, $\overline{T}_x$.

$$\overline{T}_x=A_d(X)+B_d(X)\cdot D \quad (5.2.37)$$

with *X* being the mole ratio, D being the dew point temperature of the water vapour and *M* being the molar mass of water or salt, respectively. The mole ratio is defined as

$$X=\frac{M_w}{M_{salt}}\cdot\frac{x}{1-x} \quad (5.2.38)$$

The coefficients in equation (5.2.37) can be calculated according to Feuerecker [Feuerecker 1994].

$$A_d = \sum_{i=0}^{4} A_i X^{i/2} \,,\; B_d = \sum_{i=0}^{4} B_i X^{i/2}$$

i	A_i	B_i
0	340.897	-0.01050
1	-2638.978	6.70042
2	7262.473	-15.42090
3	-8119.078	16.42477
4	3302.087	-6.34249

For the dynamic model, the mole ratio is being calculated using the internal equilibrium concentrations as in Figure 5.2.3. With the equilibrium temperature of evaporator and condenser being the respective vapour dew point temperature, equation (5.2.37) reads

Generator:
$$\overline{T}_{G,i} = A_d \cdot \left(\frac{M_w}{M_{salt}} \cdot \frac{x_{s,G,i}}{1 - x_{s,G,i}} \right) + B_d \cdot \left(\frac{M_w}{M_{salt}} \cdot \frac{x_{s,G,i}}{1 - x_{s,G},i} \right) \cdot \overline{T}_{C,i} \qquad (5.2.39)$$

Absorber:
$$\overline{T}_{A,i} = A_d \cdot \left(\frac{M_w}{M_{salt}} \cdot \frac{x_{w,A,i}}{1 - x_{w,A,i}} \right) + B_d \cdot \left(\frac{M_w}{M_{salt}} \cdot \frac{x_{w,A,i}}{1 - x_{w,A,i}} \right) \cdot \overline{T}_{E,i} \qquad (5.2.40)$$

5.2.5 Model assumptions

After eliminating a number of variables the system exhibits a total of 23 equations and 23 unknowns. The equation system can now be solved for each time step using MATLAB. A Newton-Raphson procedure with finite-difference Jacobian approximation is being used for the simultaneous solving of the nonlinear equations [Urroz 2004]. The inputs, outputs and constants of the model needed for each time interval are shown in Appendix 8.7.

Further assumptions have been made for the model. A differentiation into standard and critical assumptions can be made by considering their effects on the model dynamic and accuracy. Standard assumptions are simplifications of physical effects which have only small influences on the dynamic chiller behaviour. Applied to the model development these assumptions simplify the underlying mathematical theory significantly but do not adulterate the dynamic response. These assumptions apply to most absorption heat pumps and are typically being made for the majority of dynamic simulations on such. For the model presented, standard assumptions are:

(a) no thermal heat loss to ambient, all components are adiabatic
(b) the pump work is neglected
(c) the solution leaving generator and absorber tube bundle is saturated
(d) the external inlet temperatures t_{11}, t_{13}, t_{17} are constant, if not specified differently
(e) absorber cooling water outlet temperature equals condenser inlet temperature (t_{14}=t_{15})
(f) constant solution heat exchanger effectiveness η_{SHX}

(g) constant property data of water and LiBr/water solution
(h) constant external and internal heat transfer coefficients (UA-values)
(i) constant evaporation and solution enthalpy

Critical assumptions simplify the model but influence the dynamic behaviour in a direct way. They read:

(j) the mass flow of diluted solution $\dot{m}_{sol,w,i}$ from absorber to generator is constant
(k) generator pressure equals condenser pressure, absorber pressure equals evaporator pressure
(l) the pressure loss due to friction in the strong solution tube is neglected

In other chillers, these assumptions might not be of significance but for this chiller design they influence the dynamics. Assumption (j) affects the time shift of the weak solution between absorber and generator and is thus a direct dynamic term. Assumption (k) neglects the small steam pressure loss induced by the steam louvers which separate both upper and lower vessels. It allows the model calculation with only two pressure levels but ignores the dynamic effect of pressure difference in reality. This is however quite small as long as the pressure loss is small, too. Assumption (l) affects the free flow of the strong solution between generator and absorber. However, the pressure loss of the solution heat exchanger can be expected to dominate the total pressure loss, thus this assumption has also no significant influence on the dynamic behaviour.

5.2.6 Performance analysis

The following simulation results have been achieved using the input values and constants shown in Appendix 8.7, unless otherwise stated. Most of the constant values are design-related and have been deducted from real chiller data as good as possible. However, some of them could not be determined exactly and had to be estimated. These include:

– external and internal UA-values
– external and internal thermal heat capacities

The values of these constants do not represent the closest possible approximation of the model to reality, they still have to be calibrated to real values. This has not been done in this thesis since the primary intent was to develop a sound model which is internally consistent. However, the estimations made for the constant values have to be plausible which shall be discussed shortly.

The heat transfer coefficients (UA-values) assumed for the model are higher than in reality. The enlargement ranges between a factor of 1.6 for evaporator/condenser and a factor of 2.4 for generator/absorber. The bigger values were chosen for convergence reasons of the equation solver used in the model. This affects the heat transfer to and from the heat exchangers and consequently the steady-state results of the simulation. A difference between measured and

simulated steady-state values can be expected. As long as both internal and external UA-values are equal (as assumed in the model), no influence on the dynamic behaviour will occur. The UA-values as in Appendix 8.7 are however an educated guess and can be further reduced towards the convergence threshold.

The thermal heat capacities are being calculated as the product of mass and specific heat capacity. While the latter can be determined relatively exact from literature, the mass involved in the heat transfer can only be estimated. However, design data of the chiller is available and a plausible calculation of the mass can be made. A wrong assumption of the thermal mass will influence the dynamic behaviour, not the steady-state results.

Even without an exact calibration, a sound physical model can already yield quite satisfactory results but a model that is not internally consistent can be calibrated and yet violate basic principles. The internal consistency shall be analysed now by applying an ideal input step to the model.

A step from 75°C to 85°C in the hot water inlet temperature has been used. Cooling and chilled water temperatures have been kept constant at 27°C and 18°C, respectively. The time period $\Delta\hat{t}$ between two simulation intervals was 1s. The temperature step was set at 200s after simulation start. This time period was chosen in order to equalize the differences between initial and steady-state values.

In order to start with the most simple deviation from conventional steady-state simulation, only solution storage and time shift were assumed. No thermal storage terms were introduced. The time shift in the solution circuit was 2s between generator and absorber and 1s the other way round. Figure 5.2.7 shows all results for the total simulation time, Figure 5.2.8 shows all results for the time period before and after the temperature step and Figure 5.2.9 shows the external heat flows before and after the temperature step.

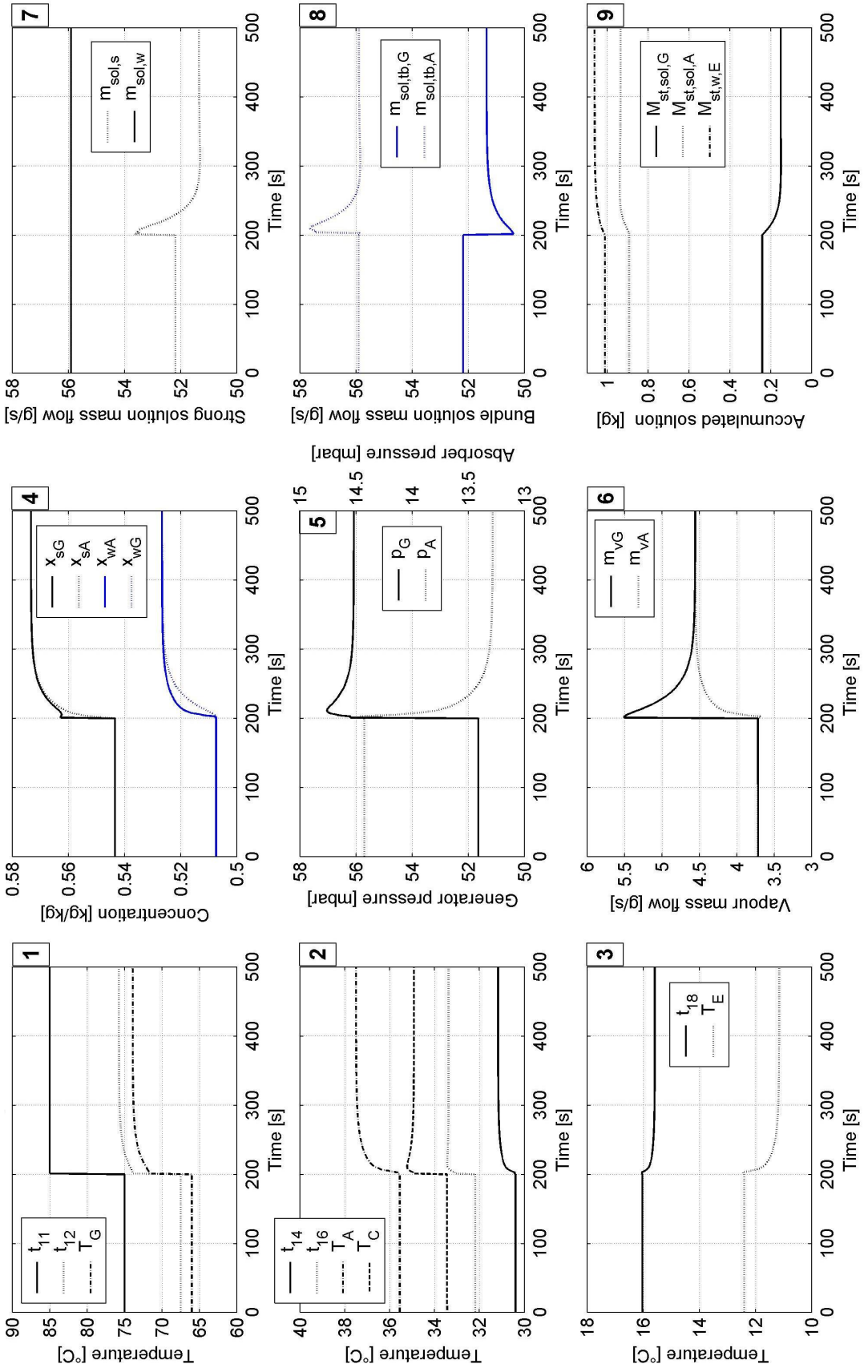

Figure 5.2.7. All parameters of simulated chiller response on 10K step in generator inlet temperature without thermal mass.

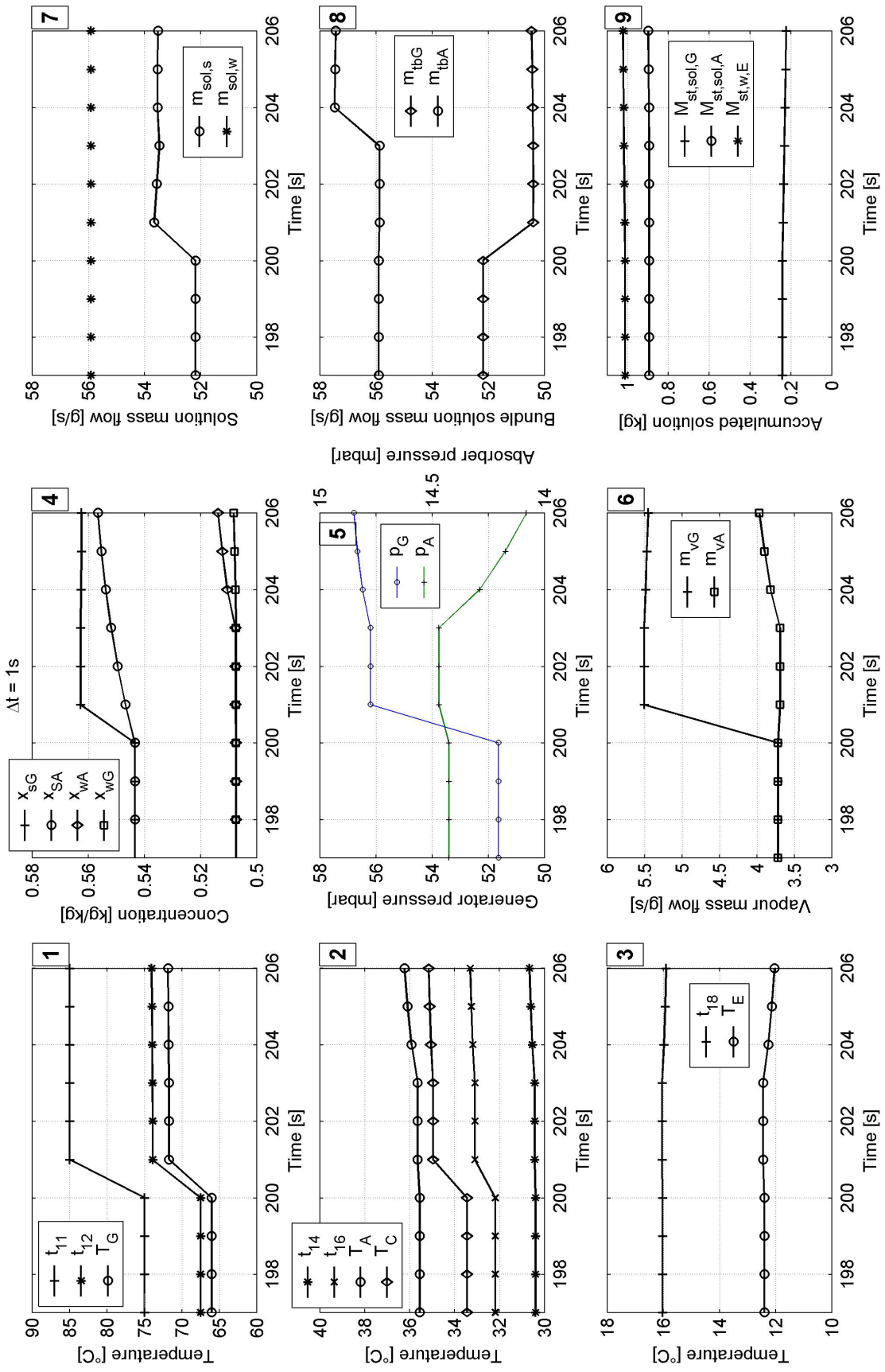

Figure 5.2.8. Simulated chiller response on 10K step in generator inlet temperature without thermal mass. Time period around step only.

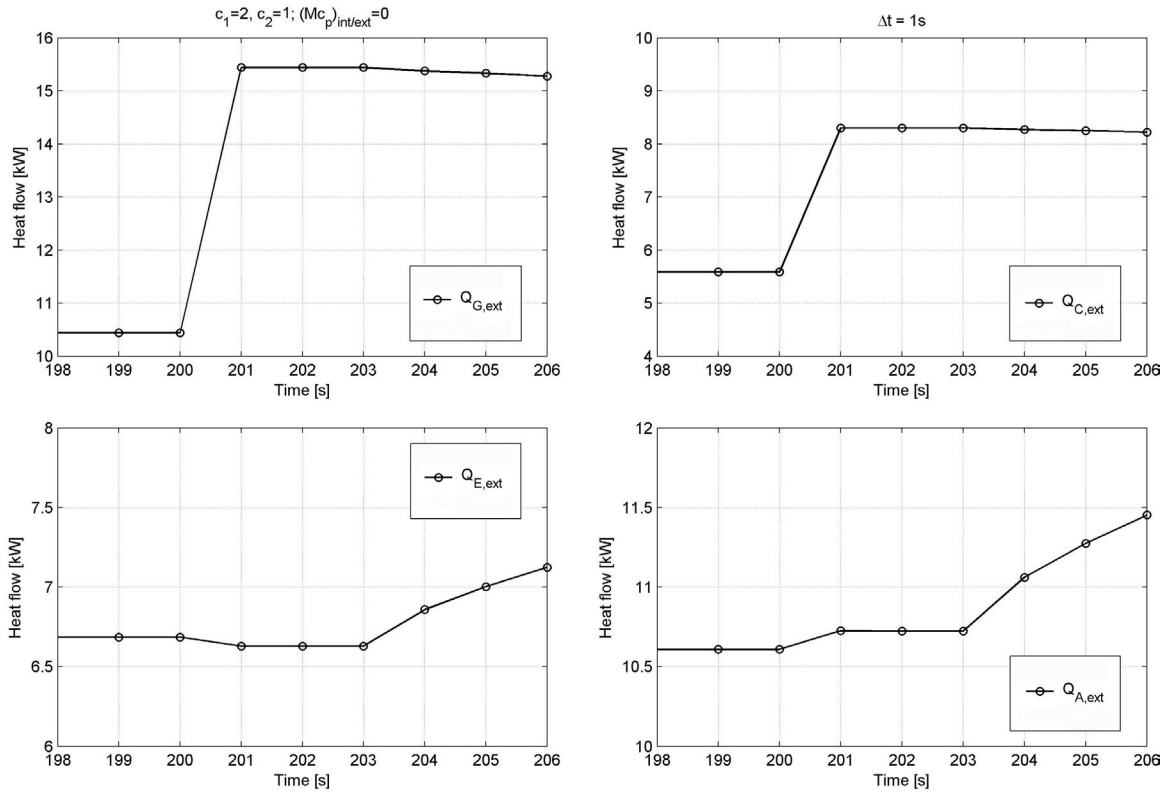

Figure 5.2.9. External heat flows of simulated chiller response on 10K step in generator inlet temperature without thermal mass. Time period around step only.

The steady-state end values shall not be subject of discussion here. Instead, the absorption cycle behaviour per each simulation interval shall be discussed using Figure 5.2.8 and Figure 5.2.9.

At time interval 200 all values are at steady-state level and constant. At time interval 201 the effects of the temperature step occur. Graph 1 in Figure 5.2.8 shows the temperature rise of external inlet and outlet temperature as well as the equilibrium temperature in the generator. Both equilibrium and hot water outlet temperature rise immediately after the step as no thermal mass is assumed. In consequence, the heat flow into the generator increases (Figure 5.2.9, top left graph), yielding a bigger vapour mass flow from generator to condenser as shown in Figure 5.2.8, graph 6. Due to this, both equilibrium and sump concentration of the strong solution in the generator also rise, as visible in graph 4. The sump concentration however rises slower due to the mixing of the solution in the sump. The solution mass flow leaving the generator tube bundle is decreased by the value of the increase of vapour mass flow to the condenser as shown in graph 8. Furthermore the equilibrium temperature in the condenser (graph 2) and thus the generator pressure (graph 5) increase. The condenser outlet temperature of the cooling water increases due to the higher condensation heat flow (Figure 5.2.9, top right graph) as visible in graph 2.
The strong solution mass flow increase in graph 7 is for the most part the result of a bigger pressure difference between generator and absorber. The simultaneous reduction of static head due to a decreasing solution level in the generator sump (graph 9) is small compared to the pressure difference increase.

Due to the assumed time shift in the solution circuit, no changes of absorber and evaporator parameters should occur during the first 2s after the temperature step. The solution entering the absorber has per definition the same concentration as before the temperature step. There is however a very small change in the equilibrium concentration of the absorber, barely visible in graph 4. This also results in small changes of the vapour mass flow from evaporator to absorber (graph 6), the evaporator equilibrium temperature (graph 3) and the absorber pressure (graph 5). The concentration changes by a value of 0.0002 kg/kg, the equilibrium temperature in the evaporator changes by 0.017K. This results in a vapour mass flow change of $2e^{-5}$ kg/s. These changes are the consequence of the way the solution heat exchanger is being modelled. It is not assumed as an individual component with a capacity and volume, instead its parasitic heat loss as in equation (5.2.30) is included in the enthalpy balances of generator and absorber. In time interval 201, the increase of strong solution mass flow and equilibrium temperature in the generator results in an increase of the solution heat exchanger heat flow as well. Therefore, more heat has to be dissipated to the cooling water in the absorber, as visible in Figure 5.2.9 (bottom left graph). In consequence, the absorber pressure rises and less vapour can be absorbed, resulting in an equilibrium concentration change in the absorber and a temperature rise in the evaporator. However, the order of magnitude of these changes is very small and can be neglected for the overall model performance.

At time interval 202 and 203, the solution in the generator sump keeps mixing with the solution leaving the tube bundle which has a bigger concentration, therefore the sump concentration increases (graph 4). Also, the sump level decreases due to the bigger pressure difference between generator and absorber (graph 9). This in turn influences the strong solution mass flow leaving the generator which also decreases (graph 7). All other parameters have the same value as in time interval 201.

At time interval 204, the solution which has left the generator after time interval 201 now enters the absorber. The equilibrium concentration in the absorber (graph 4) and thus the vapour mass flow from the evaporator increase (graph 6). Both evaporator temperatures (graph 3) and the absorber pressure (graph 5) decrease. The outlet temperature of the cooling water after condenser and absorber rises as well as the equilibrium temperatures of both vessels (graph 2). Due to the smaller concentration of the weak solution, the vapour mass flow from the generator decreases (graph 6) and the equilibrium and outlet temperatures rise (graph 1). The strong solution mass flow increases again (graph 7) as the pressure difference between absorber and generator has also increased. The amount of solution stored in the absorber rises due to the increased strong solution mass flow of time interval 201 which per definition enters the absorber in this interval (graph 8).
The difference between solution entering and leaving the absorber tube bundle can now be calculated according to equation (5.2.14). The result for the time period around the temperature step is being displayed in Figure 5.2.10.

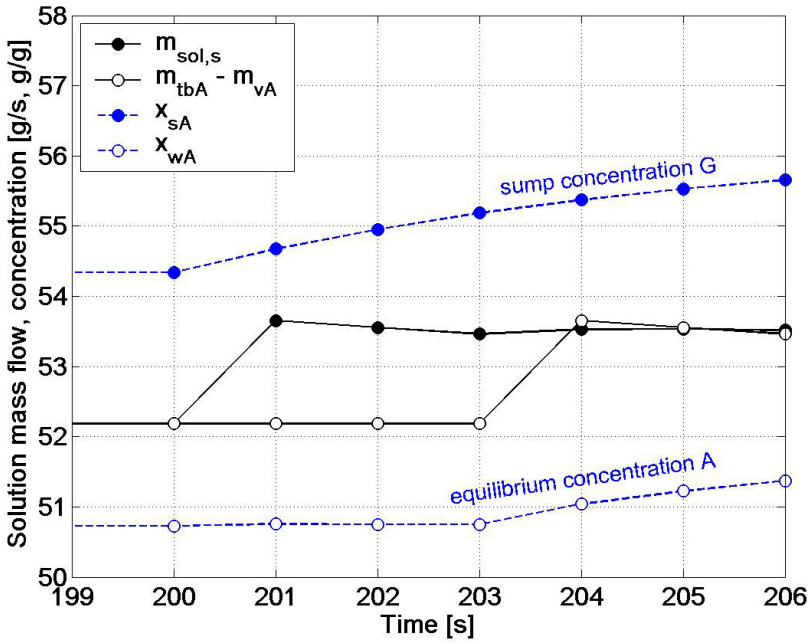

Figure 5.2.10. Solution mass flow balance at absorber tube bundle.

Calculating the mass balance around the absorber tube bundle, the difference between ingoing solution, $\dot{m}_{sol,s}$, and outgoing solution $\dot{m}_{tb,A} - \dot{m}_{v,A}$ can be seen clearly. Before the step, the difference is zero. During the time shift period 201 to 203, the difference is approximately 1.4 g/s. After the time equivalent of c_1, the difference again approaches zero. It can clearly be seen that the values of interval *i* and interval *i-c*$_1$ are identical, thus the solution mass balance is correct. Also shown are the concentrations of generator sump and equilibrium in the absorber. The salt mass flows leaving the generator and entering the absorber tube bundle are displayed in Figure 5.2.11.

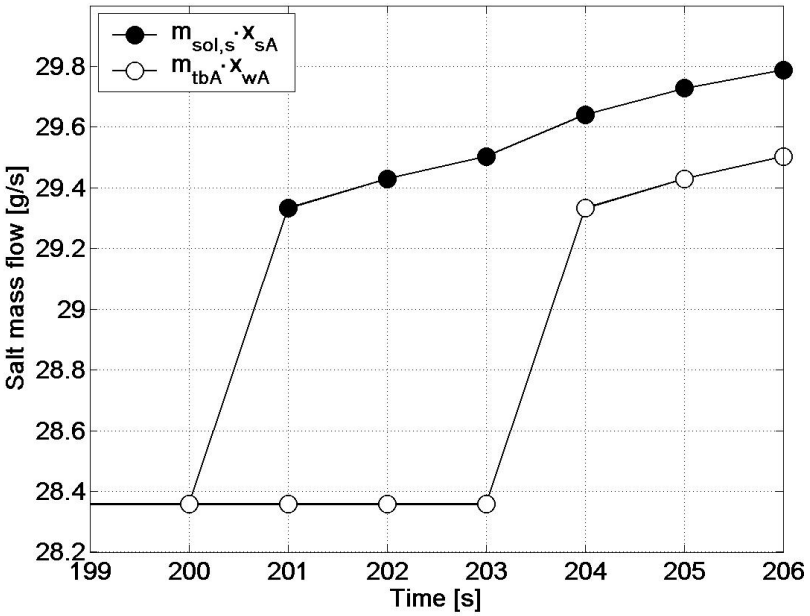

Figure 5.2.11. Salt mass flow balance at absorber tube bundle.

The calculation of the salt mass flow balance around the absorber tube bundle shows that the salt flows of step *i* and step *i-c*$_1$ are identical, thus the salt balance is also correct. The difference in salt during the time shift period can also be seen. It amounts to approximately 1g/s.

The amount of solution which is stored in the tube between generator and absorber due to the calculation procedure is small compared to the amount of solution stored in the generator per time interval *i*. The stored solution mass in the generator at time interval 201 equals 238 g, the stored solution mass in the tube amounts to 1.4 g. In proportion, the stored solution mass in the tube is approximately 0.59 % of the generator sump mass. For the model simulations presented this inaccuracy is being negligible. It can be further reduced if a bigger solution mass in the generator sump is used as an initial value for the simulation.

5.2.7 Parameter analysis

In the following, the influence of the thermal storage will be investigated. The dynamic parameters characterising the thermal storage are the values of $\left(Mc_p\right)_{X,ext}$ and $\left(Mc_p\right)_{X,\mathrm{int}}$. To investigate the influence, minimum and maximum values have been simulated.

a) $\left(Mc_p\right)_{X,ext} = \left(Mc_p\right)_{X,\mathrm{int}} = 0$ (c_1=67s, c_2=61s)

b) $\left(Mc_p\right)_{X,ext} = \left(Mc_p\right)_{X,\mathrm{int}} = \max.$ (c_1=67s, c_2=61s)

Maximum values of $\left(Mc_p\right)_{X,ext}$ and $\left(Mc_p\right)_{X,\mathrm{int}}$ are given in Table 5.2.1 as calculated for the Phoenix absorption chiller. Input values as in Appendix 8.7 for all combinations. Again a hot water temperature step from 75°C to 85°C at 200s after simulation start has been used as the model input for a) and b). In contrast to the simulation results presented so far, real values for the time shift in the solution circuit have been used.

The heat flows in the vessels for combination a) are shown in Figure 5.2.12, Figure 5.2.13 shows all simulation parameters.

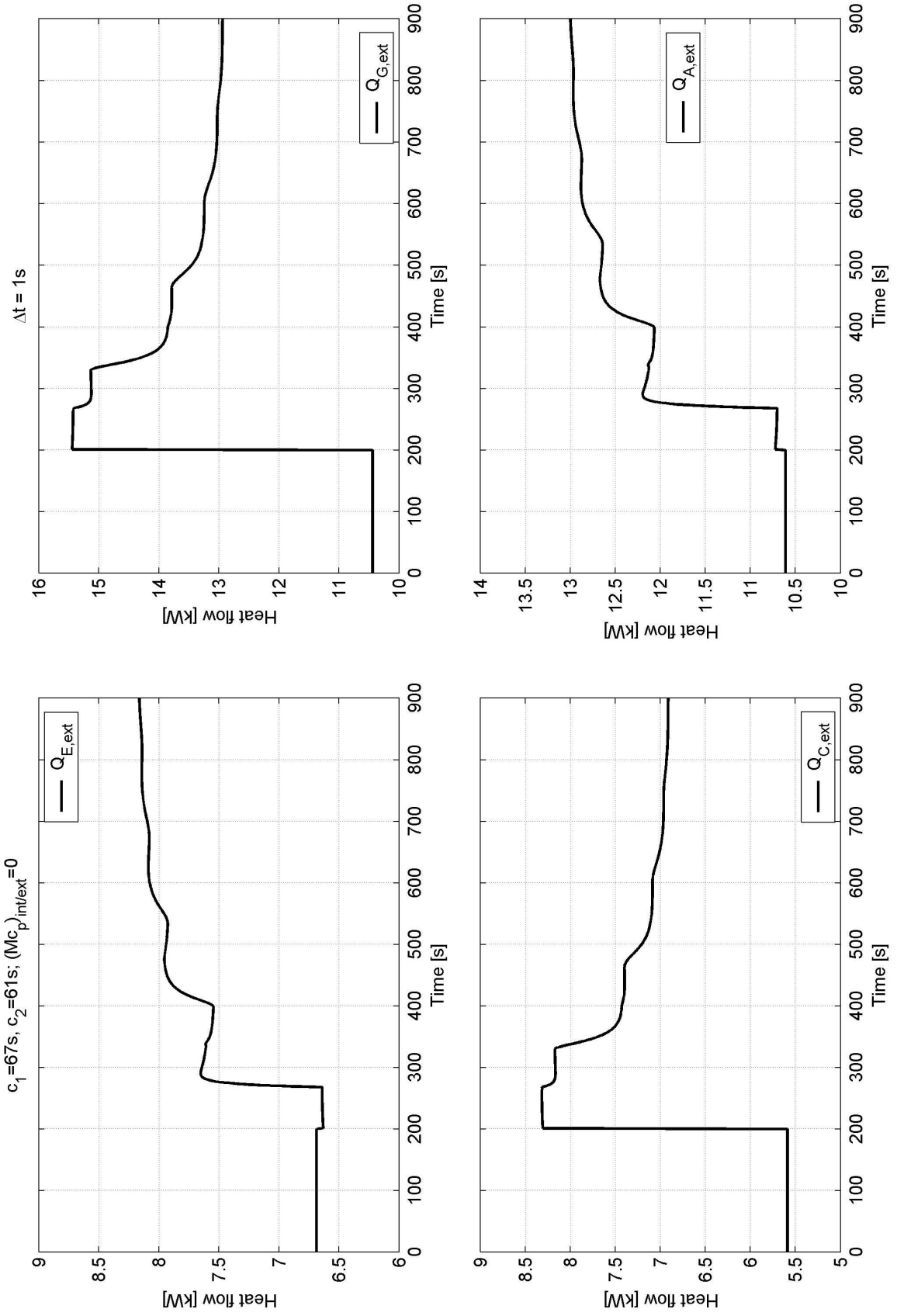

Figure 5.2.12. External heat flows of simulated chiller response on 10K generator inlet temperature step without thermal mass. Real values assumed for the solution time shift.

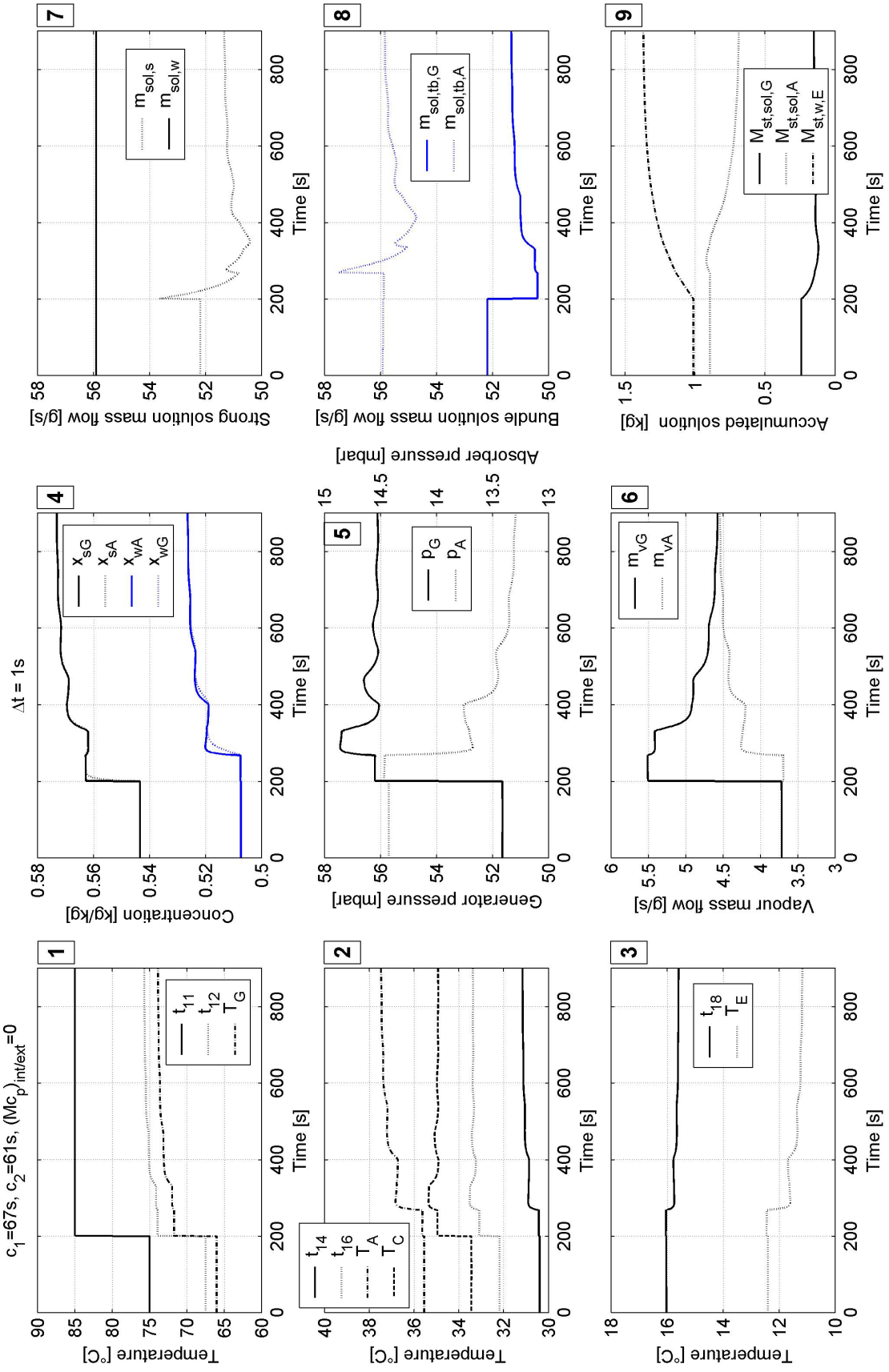

Figure 5.2.13. All parameters of simulated chiller response on 10K generator inlet temperature step without thermal mass. Real values assumed for the solution time shift.

In Figure 5.2.12, the external heat flows in generator and condenser change immediately after the temperature step as already discussed in Figure 5.2.9. Also, the heat flow of the absorber increases and the evaporator heat flow decreases by approximately 0.1 kW as the result of the increased solution heat exchanger loss. From time interval 201 to 267 generator and condenser heat flow are constant, absorber and evaporator heat flow decrease slightly due to the decrease of the strong solution mass flow as visible in Figure 5.2.13, graph 7. At time interval 268, the heat flows of absorber and evaporator increase suddenly due to the effect of the solution shift. Simultaneously, condenser and generator heat flow decrease due to the effect of the weak solution entering the latter. At time interval 330, the next reactions in generator and condenser heat flow can be seen. There, the solution has completed one loop in the solution circuit. For absorber and evaporator, this effect takes place with a delay of time constant c_1, around time interval 400. After time interval 400, the effects of the solution circling between generator and absorber can be seen with decreasing extent for the rest of the simulation time. Approximately 700s after the temperature step a new steady-state is being reached.

Figure 5.2.13 shows mainly the same parameter reactions as Figure 5.2.7, although the influence of a bigger solution time shift is clearly visible.

For combination b), the results are shown in Figure 5.2.14 and Figure 5.2.15.

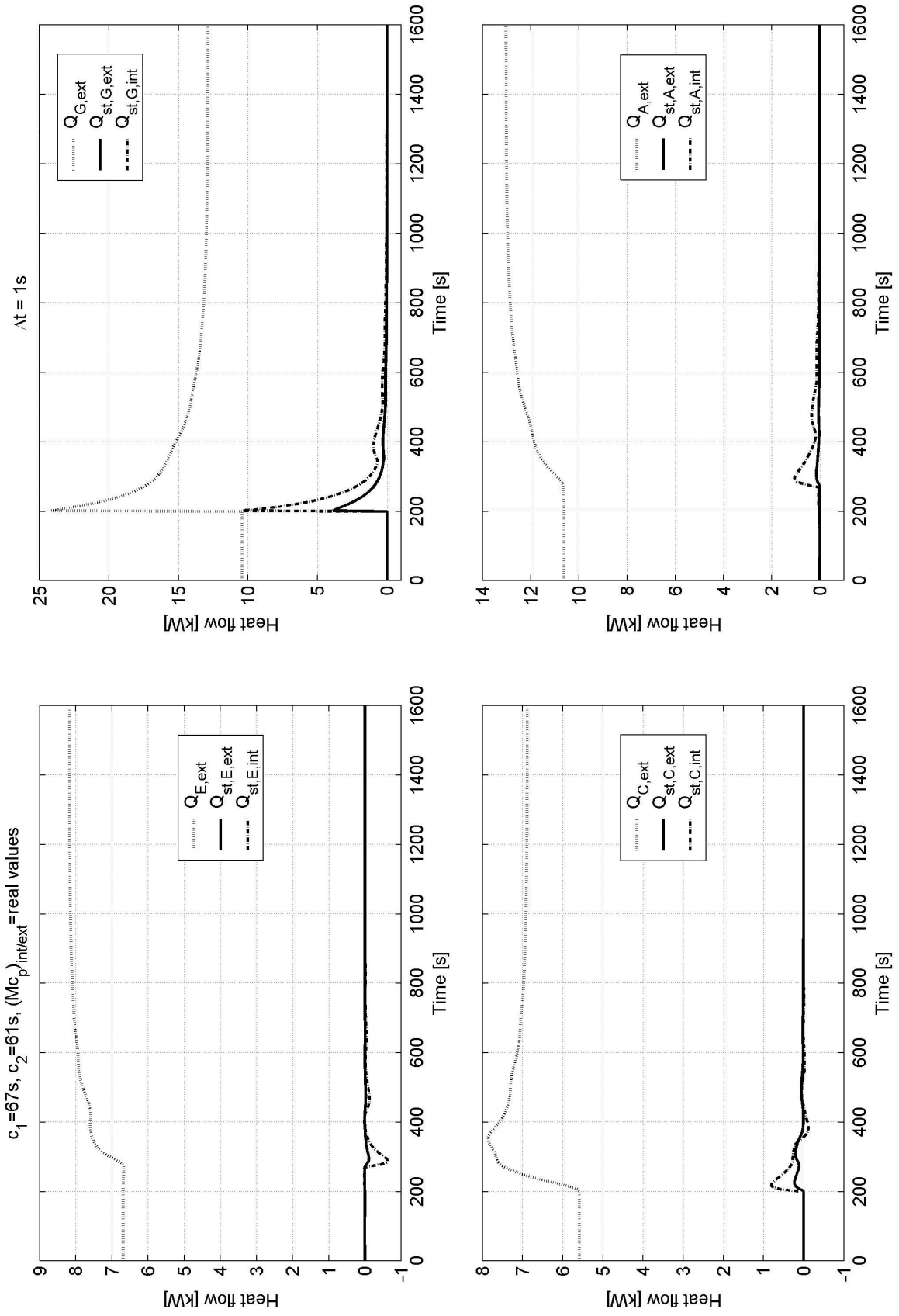

Figure 5.2.14. External and internal heat flows of simulated chiller response on 10K generator inlet temperature step. Real values assumed for solution time shift and thermal mass.

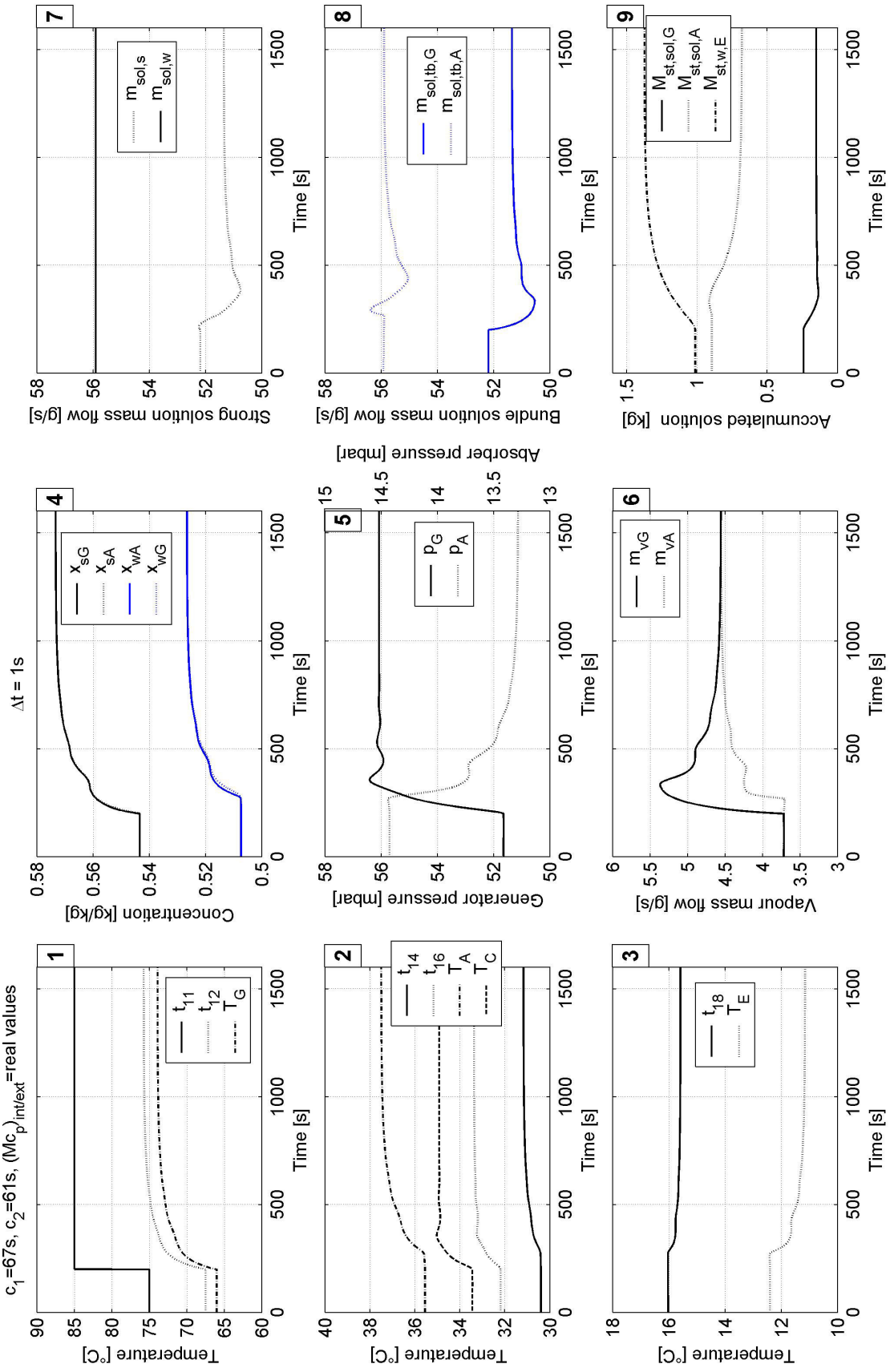

Figure 5.2.15. All parameters of simulated chiller response on 10K generator inlet temperature step. Real values assumed for solution time shift and thermal mass.

Figure 5.2.14 shows three heat flows per vessel. $\dot{Q}_{X,ext}$ is the external heat flow into or out of the vessel. The other two heat flows are associated to the components which have been included in the thermal storage terms. $\dot{Q}_{st,X,ext}$ is the heat flow going into the external thermal mass, $\dot{Q}_{st,X,\mathrm{int}}$ is the heat flow going into the internal thermal mass.

Of all vessels, the biggest heat flow related to the thermal storage effect goes into warming-up the external and internal parts of the generator. Evaporator, absorber and condenser show only small heat flow changes. Again, generator and condenser react immediately after the temperature step, absorber and evaporator react delayed according to c_1. It can also be seen that the amplitude of the heat flow going into or out of internal components is always bigger than into or out of external ones. This is due to the assumptions being made there which resulted in generally bigger values for the internal heat storage capacity.

The sudden heat flow changes which occurred without thermal mass have been dampened, however the influence of the solution time shift is still visible. This effect can be seen even better in Figure 5.2.15, e.g. in graphs 6, 7 and 8. The spikes and peaks in the mass flows which occur without thermal mass are softened and the changes take place less rapidly. The thermal mass dampens each effect in amplitude. It also increases the simulation time to achieve a new steady state. Without thermal mass, approximately 10 minutes were necessary, with thermal mass more than 20 minutes, i.e. the double time.

5.2.8 Comparison of simulated to experimental data

The agreement between simulated and experimental data has been tested using the measured step nr. 2 from 75 to 85 °C shown in Figure 5.1.10, chapter 5.1. The results of the simulation using this input data are shown in Figure 5.2.16. There, index ‘meas’ refers to measured data, index ‘sim’ to simulated data.

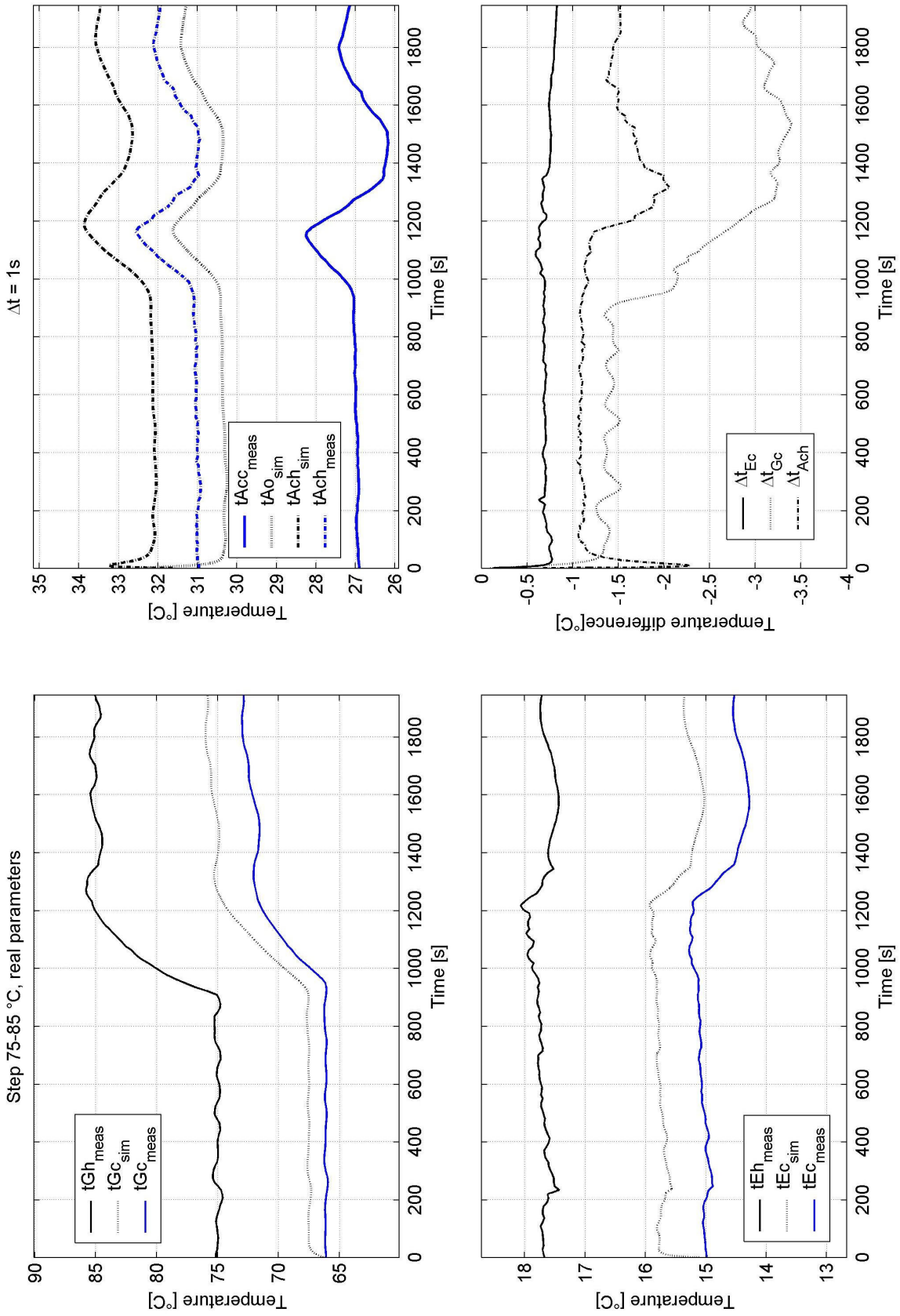

Figure 5.2.16. Simulated external temperatures using experimentally measured input data. All measured outlet temperatures are shown in blue colour. Refer to Figure 2.3.2 for parameter names.

It can be seen in Figure 5.2.16 that the dynamic agreement between measured and simulated output data is very good. The top left graph shows that the fluctuations of simulated and measured hot water outlet temperature are fairly synchronized, although there is a slight delay of approximately 10s of measured to simulated values. The top right graph shows the Absorber and Condenser inlet and outlet temperatures. There, simulated values are approximately 25s ahead of the measured values. Unfortunately, measurement data of the Absorber outlet temperature was not available for this step. The dynamic agreement between measured and simulated chilled water outlet temperature was a 10s shift with simulated values ahead of measured ones.

The dynamic time shift between simulation and experiments can to some extent be explained with the assumptions of thermal mass for the individual vessels. These assumptions have been made as an educated guess but have not been calibrated yet. In Condenser and Evaporator, an increase of thermal mass should result in the synchronization of the graphs. In the Generator, thermal mass should be reduced to achieve the same. Another reason for the time shifts between simulation and experiment is most likely the fact that some time delays existing in reality have not been incorporated into the model. Amongst others, these include the forced circulation of refrigerant in the evaporator by means of a second internal pump. Also, the condensed refrigerant flowing from condenser to evaporator has a time delay which has been neglected. There is no vapour storage in the vessels assumed. The time constant c_1 has been assumed constant although it changes in proportion to the strong solution mass flow. The time shift in the cooling water between absorber outlet and condenser inlet due to piping length has also been neglected. Solution storage on the tube bundles has been neglected.

The steady-state agreement between measured and simulated values is reasonably well despite the fact that the model has not been calibrated so far. However, at simulation start the simulated temperatures diverge from the initial measured state towards a different steady-state. The graph on the bottom right side shows the deviation between measured and simulated outlet temperatures for the vessels. For the hot water, the maximum temperature difference amounts to approximately -1.5K before and -3.5K after the step. The cooling water difference is approximately -1K before and -1.5K after the step. The best agreement can be found for the chilled water temperature where the difference is approximately 0.7 K during the whole simulation. A reason for the deviation in steady-state values can be the estimates made for the UA-values of external and internal heat exchange, as discussed in chapter 5.2.6. In general, the difference is larger after the step. This shows that there is a dependency of the model output on the level of the temperature step. This can be related to temperature-dependent parameters which have been assumed constant for the simulation, such as evaporation and solution enthalpy, density and specific heat capacity.

5.2.9 Transfer function identification

The system identification procedure described in chapter 5.1 can now be applied to determine the transfer function between hot and chilled water temperature of the chiller via simulated output

values. For this, two different identifications have been made. First, the ideal hot water temperature step as shown in the top left graph of Figure 5.2.15 is used as input with cooling and chilled water input temperature assumed constant at 27°C and 18°C, respectively. Second, the measured hot water temperature step shown in the top left graph of Figure 5.2.16 is used as input with also cooling and chilled water input temperature assumed constant at 27°C and 18°C, respectively. The transfer functions of both identifications read

ideal step: $$G_{csim} = \frac{1.32e^{-8}\,s^4 + 2.18e^{-8}\,s^3 + 4.19e^{-8}\,s^2 + 6.10e^{-8}\,s - 5.96e^{-8}}{s^4 + 0.054\,s^3 + 0.014\,s^2 + 2.1e^{-4}\,s + 1.44e^{-6}} \qquad (5.2.41)$$

measured step: $$G_{cmeas} = \frac{9.99e^{-6}\,s^4 + 2.19e^{-5}\,s^3 + 2.47e^{-5}\,s^2 + 2.57e^{-6}\,s - 1.16e^{-7}}{s^4 + 0.042\,s^3 + 0.024\,s^2 + 4.16e^{-4}\,s + 2.8e^{-6}} \qquad (5.2.42)$$

Both transfer functions found via simulation (equations (5.2.41) and (5.2.42) can now be compared to the experimentally found transfer function (equation 5.1.7) using the step response on a unity step as displayed in Figure 5.2.17.

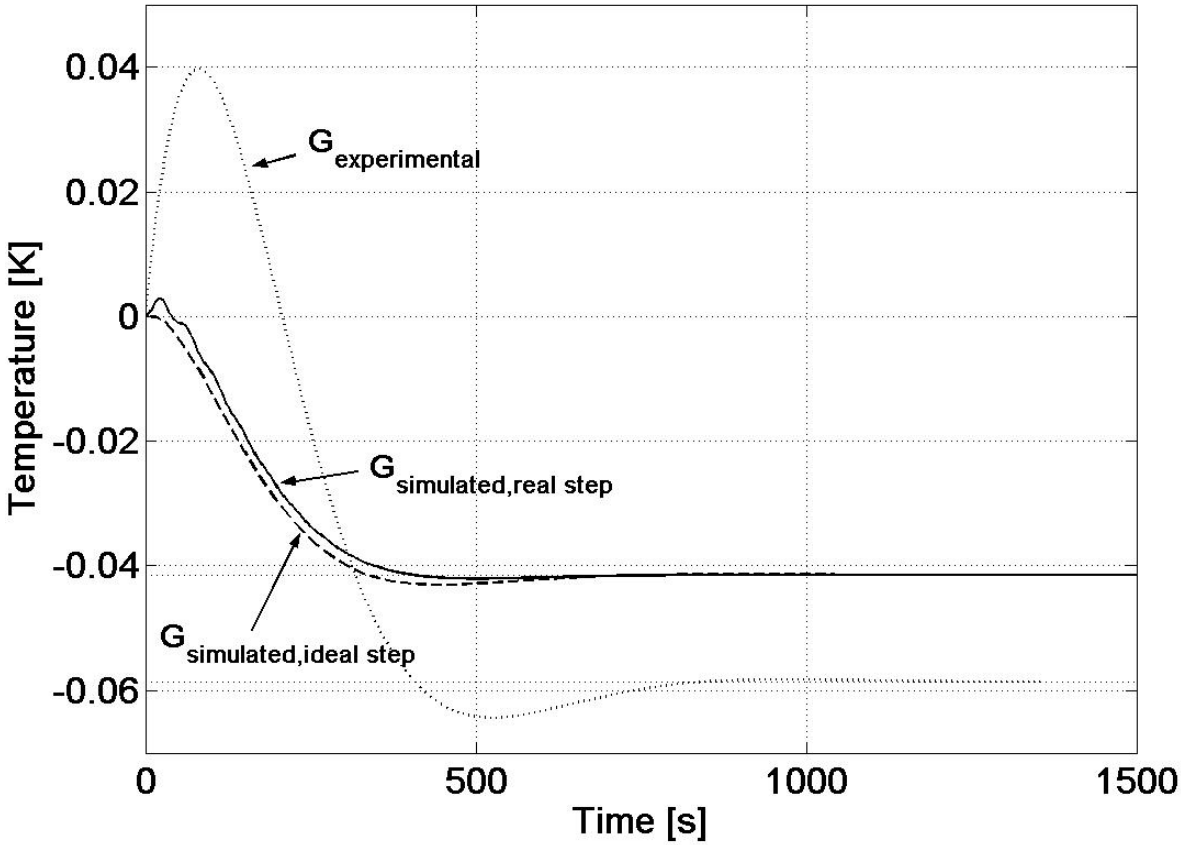

Figure 5.2.17. Step responses of experimental and simulated transfer functions for unity step.

There is an obvious difference between the transfer function derived from experimental measurements, $G_{experimental}$, and the transfer functions derived from dynamic simulations. $G_{simulated,\ real\ step}$

is the transfer function derived from a measured step, $G_{simulated,\ ideal\ step}$ is the transfer function from an ideal step. First, it can be seen that the end values of the two simulated transfer functions converge to a value bigger than the end value of the experimental one. The steady-state time of simulated and measured transfer functions is also different. The simulated transfer functions converge after approximately 13 minutes while it takes approximately 15 minutes for the measured transfer function to converge. This agrees with the dynamic behaviour of the evaporator where the simulation is also faster than reality.

The experimental transfer function has a temperature overshoot of 0.04K before it decreases below zero. The reason for this was a variation of cooling water temperature during the step as explained in chapter 5.1.2. The simulated transfer function with an ideal step has no overshoot, however the simulated transfer function with a measured step has a small overshoot of approximately 0.05K. The reason for this is the underlying numeric model from the system identification which exhibits such an overshoot. It was chosen because the accuracy of its model fit was higher compared to a second model which was also identified for the same temperature output. Figure 5.2.18 shows the comparison of the measured temperature data and two model fits achieved by the system identification process. The blue arrow marks the overshoot.

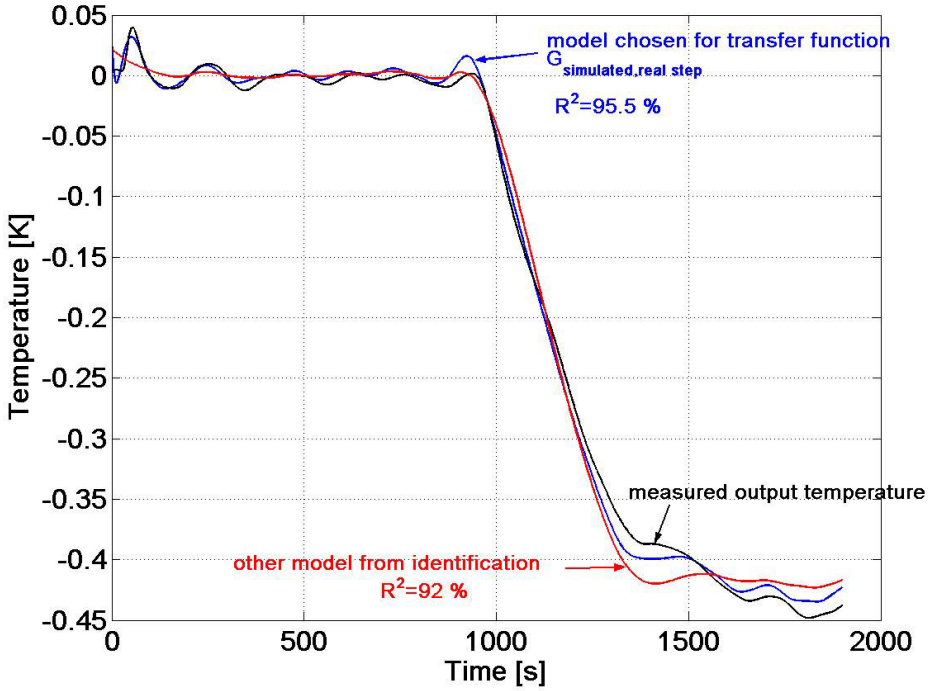

Figure 5.2.18. Comparison of two model fits with measured data.

The two simulated transfer functions, $G_{simulated,\ ideal\ step}$ and $G_{simulated,\ real\ step}$ in Figure 5.2.17 have almost the same course and converge into the same end value. Neglecting the small difference, both transfer functions can be assumed similar and it can be stated that the quality of the input temperature step does not influence the transfer function. The dynamic model behaviour does not depend on the input conditions which is again a proof of the model quality and internal

consistency. It can be stated that the dynamic simulation methodology presented above is an appropriate way of representing the transient behaviour of an absorption chiller.

5.2.10 Chapter summary and conclusion

In this chapter, the development of a dynamic model for absorption chillers has been presented. It is based on external and internal energy balances as well as mass balances. Dynamic behaviour is implemented via eight thermal and two mass storage terms as well as two delay times. The model can use variable forms of input, such as ideal temperature or mass flow steps, ramps and measurement data. General functionality of the model has been demonstrated and a parameter analysis has been performed regarding the thermal storage terms. The thermodynamics of the model have been found to be consistent with reality, although a slight inaccuracy in the mass balance of the solution tube between generator and absorber has been incorporated.

As expected, the thermal mass of external and internal heat exchanger components has been found to dampen the parameter fluctuations caused by the solution time shift in their amplitude. It also increases the time which is required to achieve a new steady state.

A thorough model calibration was not the goal of this thesis, nevertheless the model has been tested with experimental data. The dynamic agreement between experiment and simulation is very good with dynamic temperature deviations between 10 and 25 s. The total time to achieve a new steady-state after an input temperature step amounts to approximately 20 minutes. Compared to this, the present dynamic deviations are in the magnitude of approximately 2 % and therefore of sufficient exactness. Steady-state results are being reproduced with temperature deviations between 0.7 and 3.5 K in the model. However, a high steady-state accuracy of the model was not the main task. A calibration still needs to be performed.

Two transfer functions have been identified from simulated data using an ideal and a measured input step. Internal consistency is demonstrated by the fact that both transfer functions are very similar. Differences are only caused by the chosen model fit of the identification process.

The advantages of a dynamic simulation compared to experimental measurements are a less time-consuming identification process and the ability to reproduce the whole operation range of the chiller. The development of the model itself is more complex than the experimental identification, however once finished, multiple simulations can be performed with it and later modifications can easily be incorporated.

The dynamic simulation model developed in this thesis allows the identification of transfer functions and in consequence control parameters of absorption chillers without the need to perform experiments. The model has been designed for the Phönix 10kW chiller but can easily be adapted to other LiBr/water absorption chillers if the required design data of these chillers is available. Furthermore, it can be a useful tool in the overall design process of absorption chillers. Technical changes in the construction of an existing absorption chiller model can be tested quick and easy by incorporating the design changes in the model. Also, new chiller designs can be tested on their performance without the need to build a prototype.

6 Conclusions and prospect

Summary and conclusions

The aim of the research conducted throughout this thesis work is to improve the state of the art in controlling solar cooling systems using absorption chillers. The motivation for this kind of research is derived from an analysis of present solar cooling systems which has shown that a malfunctioning or incorrect control is one of the main causes for system failure or faulty operation. Although the full potential of solar cooling technology is far from being realised, a growing number of such systems can be seen, based on the recent development and commercial availability of small-scale absorption chillers suitable for solar cooling. The desirable further propagation of this new technology can only be accelerated if the strict market demands set by present cooling or comfort air-conditioning technology are being met. Apart from investment cost and other economic factors this implies as a matter of course a trouble-free system operation. The proper design and operation of both system hardware and control is essential for this.

In this thesis, the control issue has been investigated deeper in two main approaches. In the first approach, system circuit control strategies have been presented and discussed in the context of total system operation. Various possibilities of temperature and mass flow control for the external circuits of hot, cooling and chilled water have been described in this thesis in a state of the art overview. Guidelines for the incorporation of the storage tank in the system control are being given with regard to reference layer and hysteresis temperature.

The solar circuit as the most complex circuit has been subject of more profound research. A differential, a temperature-based and an insolation-based mass flow control strategy for the heat carrier fluid in this circuit have been tested in simulations and experiments. Using these strategies, the focus of attention was the overall system performance, expressed by the key figures of cooling capacity and power consumption. These parameters have been integrated and combined in a daily yield factor which has been used for the comparison of the individual strategies in simulation and experiment. The ambition was to find the strategy with the lowest power consumption and simultaneously biggest cooling effect. The absolute results of the key figures in simulations and experiments could not be compared directly to each other due to different boundary conditions. In a relative comparison, good agreement between simulations and experiments has been found. This holds true for both the dynamic course of the variables as well as the integrated energy balance expressed in the yield factor.

From the simulations, the insolation-based strategy (INSOL) has been found to perform best at cloudless conditions regarding the yield factor. An improvement of 6% in the yield factor for the insolation-based strategy compared to the other strategies has been found.

From the experimental comparison of the dynamic behaviour, the temperature-difference based control strategy (TDIFF) has been found to yield the best performance. It has the least standstill time and thus lowest thermal loss. However, the experimental comparison of the integrated energy balances for all three control strategies shows that the differences between the strategies are in the magnitude of the error range of the yield factor. A clear tendency towards one strategy cannot be seen. From the experiments it can therefore be concluded that mass flow control in the solar circuit of a solar cooling system does not influence the yield factor significantly if the methodology presented is being applied. This allows several conclusions on the methodology which shall be discussed now one after the other.

Firstly, the experimental time period of one day is too short to yield significant differences between the strategies, especially if a large measurement error occurs. A solution to this would be the evaluation of a longer experimental time period per control strategy. Although this is not simple due to the daily weather variations it should be possible to achieve at least a similar insolation course for several days per year.

Secondly, the yield factor as decisive value is not suitable for a comparison. A combination of different key figures and other measures could be used which then might result in differences between the strategies. Different key figures can be the level and the steadiness of the driving temperature for the chiller, the solar gain or the efficiency solar-to-cold. Other measures can be the number of controlled components or the investment cost.

Thirdly, the bell-curve insolation chosen for comparison is not suitable for a control strategy test. A cloudless day requires the least control effort due to its low insolation gradient. It could be useful to introduce a measure for the gradient of insolation and to perform experiments on days with various degrees of insolation fluctuations. Such a measure could be the deviation of the insolation to an ideal bell-curve. The difference in control behaviour could become more clearly if the demand on the control gets bigger with increased transient fluctuations.

Fourthly, the empirically determined control parameters for TDIFF and INSOL are not the optimum ones. It could be possible that each strategy performs better if the mass flow correlations are being optimized in a separate parameter study. This could emphasize the differences between TDIFF and INSOL.

Lastly, the steady-state model of the absorption chiller chosen for the TRNSYS simulations does not provide results close enough to reality. The transient chiller behaviour is not modelled with sufficient accuracy and the influence of a delayed chiller response does not have a feedback to the system. The use of a dynamic model, e.g. the one developed in this thesis, could provide simulation results with bigger performance differences.

These five conclusions on the methodology could not be put into practice in this thesis for reasons of time. Nonetheless, a foundation has been laid by the work presented. The energy balance results from the methodology applied in this thesis do not prove the results expected from the dynamic behaviour, however five solutions and alternative research paths have been identified to achieve clearer results. If applied in future work, these will most likely increase the differences between the individual strategies and reduce the ambiguousness.

The second approach shifts from the system and its circuits to its main component, the absorption chiller. Its transient performance is crucial to know if the chiller is to be included in a control strategy. Two different methods of determining the transfer behaviour have been used, an experimental identification and a theoretical simulation method. For both methods presented, the transfer function between hot water input and chilled water output has been determined as necessary for a chilled water temperature control.

In the experimental method, individual transfer functions have been determined for the three-way valve in the hot water circuit and the absorption chiller using the system identification method of Ljung. For this, measurement data of hot water temperature steps into valve and chiller have been used for the identification of each transfer function. Both transfer functions have then been combined into a single transfer function. The identification of the valve was necessary because the hot water temperature -as a result of the valve recirculation- is the control variable for the chilled water temperature control. With the combined transfer function of valve and chiller a controller has been designed. The functionality of the method has been verified by the successful application of the controller to the Phönix solar cooling system. The method of experimental system identification has the advantage that any kind of available measurement data describing the system can be used. However, the transfer function determined by this method can only be used for the conditions and operation range at which it was identified, which is a disadvantage of this method.

The theoretical simulation method is based on the mathematical reproduction of the transient internal heat and mass transfer of the chiller. In the dynamic simulation model developed in this thesis, transient behaviour is implemented via eight thermal and two mass storage terms as well as two delay times. General functionality and internal consistency of the model have been demonstrated. The thermodynamic calculations of the model have been found to reproduce the real chiller with sufficient accuracy. The model calibration on steady-state values of the absorption chiller was not the goal of this thesis, instead the focus of attention has been laid on the dynamic model performance. Using experimental data for verification, it has been proven that dynamic effects are being accounted for in a very satisfying way. Maximum dynamic deviations between vessel temperatures in simulation and reality of 25 seconds have been achieved. Compared to the total time to achieve a new steady-state after a step, the present deviations are in the magnitude of approximately 2% and thus insignificant. The model provides the ability to reproduce the whole operation range of the chiller using variable forms of input, such as ideal temperature or mass flow steps, ramps and measurement data. The advantage of a theoretical simulation compared to the experimental method is a less time-consuming identification process for the transfer behaviour of the chiller and the ability to simulate the transfer behaviour for changes of more than one input parameter.

The model developed in this thesis has been designed for the Phönix 10 kW absorption chiller but can easily be adapted to other LiBr/water absorption chillers if the required design data of these chillers is available. It can be used for the development of a temperature control strategy in chilled or cooling water circuit with regard to the transfer performance between measured and controlled variable. Furthermore, it can be a useful tool in the overall design process of absorption chillers. Technical changes in the construction of an existing absorption chiller model can be tested quick and easy by incorporating the design changes in the model. Also, new chiller designs can be tested

on their performance without the need to build a prototype. Finally, the dynamic model contributes significantly to the field of transient system simulations. It provides an upgrade compared to present steady-state models if applied in a modular simulation software. The transient characteristics of solar cooling systems can now be reproduced in a more accurate way.

This thesis work has further developed the knowledge-base on control strategies of solar cooling systems using absorption chillers. A foundation for energy-saving operation of solar and storage circuit has been laid and further research paths towards this goal have been identified. A helpful tool for controller design and general performance analysis of absorption chillers has been made available with the dynamic model presented.

Prospect

The comparison of different mass flow control strategies for the solar circuit described in chapter 3.2 and chapter 4 has shown that a sound statement about the best energy-saving strategy is not possible if the yield factor is being used. However, the methodology being used for the comparison can still be improved as described. If the five conclusions are being put into practice, a bigger difference between the individual control strategies can be expected. A sound statement about the strategy with the best performance should then be possible. If applied in future solar cooling systems, a significant reduction of the parasitic power consumption can then be achieved.

In chapter 5.2 it was shown that the dynamic model for absorption chillers developed in this thesis provides very good dynamic results but still has deviations in the steady-state values. Several influences on the dynamic behaviour of such a chiller have been neglected in the present model. In future research, these could be integrated in the model to improve the model results. They include:

- The time shift in the strong solution flowing from generator to absorber has been assumed constant, although it depends on the momentary strong solution mass flow. It could be calculated dynamically in future versions.
- No time delay has been assumed for the cooling water temperature between absorber and condenser. If both vessels are connected in series, a delay occurs due to the flow time of the cooling water.
- No time delay and mass storage terms have been included for the solution on the tube bundles of the heat exchangers. In reality, some solution will be stored there and it takes a certain time for the solution to flow from top to bottom of the bundle.
- No mass storage term has been assumed for the water vapour. In the model it is assumed that the total vapour mass flow is being absorbed or condenses at once. In reality, this is not the case, a certain amount of vapour will always be stored in the vessel.
- A solution mass storage term has been incorporated in the model which does not occur in reality. The solution stored in the tube between generator and absorber can be avoided in future version by including an advanced mass balance calculation.
- No thermal storage terms have been assumed for the solution in the vessel sumps. In reality, there is heat transfer to or from the vessel walls which influences the temperature of the solution in the sump.
- The solution heat exchanger has not been modelled as an individual component with time delay and storage terms. If the present calculation of the solution heat exchanger loss is being replaced with the assumption of a full component, the early reactions in the absorber observed at the moment can be avoided.

The accuracy of the steady-state results can be expected to improve significantly if correct values for the heat transfer coefficients will be assumed. Also, all properties should be calculated temperature-dependent instead of being assumed constant as in the present model. Nonetheless, the present model is quite simple and easy to understand. The accuracy advantage of each improvement stated above should be weighed against the additional complexity caused by its application.

If improved with the above suggestions, the model could be used for investigations on the influence of hot water input fluctuations on the chilled water outlet temperature. Both frequency and amplitude of hot water fluctuations determine whether an influence on the chilled water is being transmitted through the chiller. The thermal mass and the buffer function of solution and refrigerant delay the response on such input fluctuations. Too low amplitudes and too high frequencies will not be transmitted. The chiller performs like a low-pass filter regarding the latter. Using the model, a threshold matrix can be determined containing those frequency and amplitude combinations below or above which an influence on the chilled water temperature can not be detected anymore. This information can then be used to improve the solar circuit control strategy regarding hot water fluctuations.

The dynamic model developed in this thesis should be incorporated into transient simulation platforms, such as TRNSYS, Insel, Smile etc.. So far, only steady-state chiller models are available for this. Then, the simulations presented in chapter 4 should be repeated with dynamic instead of steady-state behaviour of the chiller. Also, the adaptive control of absorption chiller parameters could be possible if the dynamic model is being included in the system controller. The output reaction of the chiller on external input changes can then be forecast and respective control measures can be initiated previous to the reaction instead of afterwards, as in present controllers. This way, the overall controllability of solar cooling systems could be improved.

7 References

Albers, J. (2003). "Solar gestützte Sorptionskältesysteme bei den umzugsbedingten Bundesbaumassnahmen. Teil 1:Systemdarstellung." *KI Luft- und Kältetechnik*, 8, 339-343.

Albers, J. (2004a) "Planungs- und Betriebserfahrungen bei solaren Kühlsystemen mit geschlosssenen Sorptionskälteanlagen." *AAE-Tagungsband: Solares Kühlen, Ergebnisse aus dem IEA-Forschungsprogramm, SHC TASK25, Arbeitsgemeinschaft Erneuerbare Energie, Wien 07.05.2004, p. 5/1-5/10*.

Albers, J. (2004b). "TYPE 177: Phönix-Absorption Chiller - TRNSYS user's manual." Institute for Rehabilitation and Modernization of Buildings (IEMB), Berlin, Germany. Downloadable from www.sonnenwaermeag.de.

Bian, J., Radermacher, R., and Moran, D. (2005) "Transient simulation of an absorption chiller in a CHP system." *International Sorption Heat Pump Conference, June 22-24, 2005*, Denver, CO, USA.

Bong, T. Y., Ng, K. C., and Tay, O. A. (1987). "Performance study of a solar-powered air-conditioning system." *Solar Energy*, 39(3), 173-182.

BP (2004). "Statistical Review of World Energy June 2004." BP p.l.c., www.bp.com/statisticalreview2004.

BSRIA (2002). "World market for Air-conditioning. Comparative study." BSRIA, Bracknell, UK.

Clauss, V. (2003). "Theoretische Entwicklung und experimenteller Aufbau einer Regelung für eine solarbetriebene Kälteanlage," Diploma thesis, Fachhochschule für Technik und Wirtschaft Berlin, Studiengang Umwelttechnik/Regenerative Energie.

Clauss, V., and Kohlenbach, P. (2004). "Entwicklung einer Kaltwasserregelung für die Phönix Absorptionskältemaschine FA1." Technical report, Phönix SonnenWärme AG, Berlin.

Cube, H. L. v., Steimle, F., Lotz, H., and Kunis, J. (1997). *Lehrbuch der Kältetechnik*, C.F. Müller Verlag, Heidelberg, Germany.

DIN (1995). "DIN EN 60751, Industrielle Platin-Widerstandsthermometer und Platin-Messwiderstände. German Industry Norm."

EIA (2005). "U.S. Household Electricity Report." Energy Information Administration, Department of Energy, U.S.A.

Feuerecker, G. (1994). "Entropieanalyse für Wärmepumpensysteme: Methoden und Stoffdaten," PhD thesis, Faculty of Physics, Technical University of Munich, Germany.

Feuermann, D., Gordon, J. F., and Huleihil, M. (2002). "Solar Fiber-Optic Mini-Dish Concentrators: First Experimental Results and Field Experience." *Solar Energy*, 72(6), 459-472.

Fisenko, S. P., Brin, A. A., and Petruchik, A. I. (2004). "Evaporative cooling of water in a mechanical draft cooling tower." *International Journal of Heat and Mass Transfer*, 47, 165-177.

Fisenko, S. P., and Petruchik, A. I. (2004). "Toward to the control system of mechanical draft cooling tower of film type." *International Journal of Heat and Mass Transfer*, 48, 31-35.

Florides, G. A., Tassou, S. A., Kalogirou, S. A., and Wrobel, L. C. (2002). "Review of solar and low energy cooling technologies for buildings." *Renewable & Sustainable Energy Reviews*, 6, 557-572.

Glaser, H. (2005). "Beiträge zur Betriebsoptimierung solarthermisch betriebener Adsorptionskälteanlagen," PhD-Thesis, Faculty III - Process Engineering, Technical University of Berlin.

Grassie, S. L., and Sheridan, N. R. (1977). "Modelling of a solar-operated absorption air conditioner system with refrigerant storage." *Solar Energy*, 19, 691-700.

Harrington, P. (2003) "Cooling a warming world: the role of policy." *International Energy Agency (IEA), BCG Workshop*, Paris, December 2nd 2003. (www.iea.org/textbase/work/2003/bria/harrington.pdf).

Hellmann, H.-M., Schweigler, C., and Ziegler, F. (1999) "The Characteristic Equations of Absorption Chillers." *International Sorption Heat Pump Conference 1999*, München, 169-172.

Henning, H.-M. (2004). *Solar-Assisted Air-Conditioning in Buildings*, Springer-Verlag Wien New York, Wien.

Hindenburg, C., and Henning, H.-M. (1999). "Solare Gebäudeklimatisierung mit thermischer Solarenergie." *Erneuerbare Energie*, 1/1999.

IEA (2002). "Ongoing Research Relevant for Solar Assisted Air Conditioning Systems." International Energy Agency, Technical report Task 25: Solar-assisted air-conditioning of buildings.

Isakson, P., and Eriksson, L. O. (1993). "Matched Flow Collector Model for simulation and testing - TRNSYS user's manual." Royal Institute of Technology, Stockholm, Sweden.

Jeong, S., Kang, B. H., and Karng, S. W. (1998). "Dynamic simulation of an absorption heat pump for recovering low grade waste heat." *Applied Thermal Engineering*, 18(1-2), 1-12.

Kaelke, M., Keil, C., Kren, C., and Schweigler, C. (2003). "Querschnittsauswertung Solarunterstützte Klimatisierungsanlagen in Deutschland (QASUK)." FIA-Projekt Nr. 88, Fachinstitut Gebäude-Klima e.V., Bietigheim-Bissingen.

Klein, S. A., Beckman W.A., Mitchell J.W., Duffie, J. A., and others (1996). "TRNSYS - A transient system simulation program." Solar Energy Laboratory, Univ. of Wisconsin, Madison, USA.

Klingenberger, U. M. (2000). "Regelung und Steuerung von solarthermischen Großanlagen zur Brauchwassererwärmung," Diploma thesis, Fachhochschule Offenburg, Fachbereich Maschinenbau.

Kohlenbach, P., Harm, M., and Kühn, A. (2004a) "Solar Cooling System with Low Driving Temperature." *Int. Conference on Improving Energy Efficiency in Commercial Buildings (IEECB 2004)*, Frankfurt/Main, Germany.

Kohlenbach, P., Tamm, O., Schweigler, C., Harm, M., Albers, J., Kühn, A., and Petersen, S. (2004b) "Entwicklung eines Systems zur solaren Kühlung im kleinen Leistungsbereich." *14. OTTI-Symposium Thermische Solarenergie, 2004*, Staffelstein, 546-551.

Krause, M., Vajen, K., Wiese, F., and Ackermann, H. (2002). "Investigations on optimizing large solar thermal systems." *Solar Energy*, 73(4), 217-225.

Kreetz, H. (2001). "Heat Recovery in a Solar Thermochemical Power System," PhD Thesis, Australian National University, Canberra, Australia.

Lebert, S. (2005). "Ein Mann läuft Sturm." Die ZEIT, Nr. 37, Sept. 8th 2005.

Li, Z. F., and Sumathy, K. (2001). "Experimental Studies on a Solar Powered Air Conditioning System with Partitioned Hot Water Storage Tank." *Solar Energy*, 71(5), 285-297.

Ljung, L. (1999). *System identification. Theory for the user.*, Prentice Hall PTR, Upper Saddle River, New Jersey.

MathWorks (2002). "MATLAB - The language of technical computing." Version 6.5, Math Works Inc.

Michel, E., Bonnefoi, F., Deves, A., Schweigler, C., Costa, A., Balaras, C. A., Villier, D., Olesen, B., and Argiriou, A. (2001). "Study and development of heating/cooling systems using renewable energy." Publishable Final Report, EU-Commission, JOULE III Program, Contract JOR3 – CT97 – 0181.

Paar, A., and Heunemann, F. (2004). "Solare Klimatisierung - Arbeitsplatzkomfort und Klimaschutz." Broschüre der Berliner Energieagentur GmbH, Berlin.

Streicher, E., Heidemann, W., and Müller-Steinhagen, H. (2003) "Einfluss von Systemertrag und Pumpenlaufzeit auf die energetische Amortisationszeit von thermischen Solaranlagen." *13. OTTI-Symposium Thermische Solarenergie, 2003*, Staffelstein, 307-312.

Tamm, O. (2004). "Fehlerbetrachtung der Messdatenerfassung eines Teststandes," Diploma thesis, Fachhochschule für Technik und Wirtschaft (FHTW) Berlin, Studiengang Umwelttechnik/Erneuerbare Energien.

Urroz, G. E. (2004). "Solution of non-linear equations." Lecture handout, Utah State University, U.S.A.

VDI (1997). "VDI-Wärmeatlas." Verein Deutscher Ingenieure. Springer Verlag Berlin Heidelberg.

Wiegand, E. (2004). "Vermessung des Betriebsverhaltens und Entwicklung einer Leistungssteuerung eines Nasskühlturms," Diploma thesis, Fachhochschule Wiesbaden, Fachbereich Maschinenbau.

Wiegand, E., Kohlenbach, P., Kühn, A., Petersen, S., and Ziegler, F. (2005). "Entwicklung eines offenen Nasskühlturms kleiner Leistungsklasse." *KI Luft- und Kältetechnik*, 10/2005.

Wittwer, C., Rommel, M., and Lustig, K. (2002) "ConCheck-Der simulationsgestützte Regelungsentwurf von Solarthermie 2000 Anlagen." *12. OTTI-Symposium Thermische Solarenergie*, Staffelstein, 2002, 399-403.

Wolkenhauer, H., and Albers, J. (2001). "Systemlösungen und Regelungskonzepte von solarunterstützten Klimatisierungssystemen." *HLH-Lüftung/Klima-Heizung/Sanitär-Gebäudetechnik*, 52(12), 41-49.

WTRG (2005). "WTRG Economics, www.wtrg.com."

Yeung, M. R., Yuen, P. K., Dunn, A., and Cornish, L. S. (1992). "Performance of a solar-powered air conditioning system in Hong Kong." *Solar Energy*, 48(5), 309-319.

Ziegler, F. (1997). "Sorptionswärmepumpen," Habilitation Thesis, Forschungsberichte des Deutschen Kälte- und Klimatechnischen Vereins, Nr. 57, Erding.

Ziegler, F., and Lamp, P. (1998). "European Research for Solar Assisted Air-Conditioning." *International Journal of Refrigeration*, 21(2), 89-99.

8 Appendix

8.1 Technical data of solar cooling system

Table 8.1. Technical data of system components

Circuit	Component	Model
Solar circuit	Flat plate collectors	Eurostar SI 24
	Evacuated tube collectors	Seido 2-16, VRSK-5
	Pump P1	WILO Stratos 30/1-12
	Heat exchanger HX 12	Alfa-Laval CB 51-20H
	Heat transfer fluid	Tyfocor LS
	Pyranometer	Kipp&Zonen CM11 and CM 3
	MID	Krohne ECOFLUX DN 15
Storage circuit	Pump P2	Grundfos UPE 25/80
	MID	Krohne ECOFLUX DN 15
	Heat transfer fluid	Water
	Backup heater	MAN Duomat, LNG version
Hot water circuit	Pump P3	Grundfos UPE 25/60
	Three-way valve	Siemens VXG 44.15-6.3
	MID	Krohne ECOFLUX DN 15
	Heat transfer fluid	Water
Cooling water circuit	Pump P4	Grundfos CR 1-3
	Three-way valve	Siemens VXG 44.15-6.3
	Heat transfer fluid	Water
	MID	Krohne ECOFLUX DN 25
	Cooling tower	Balcke-Dürr, MITA PMS 4/65
Chilled and ceiling water circuit	Pump P5a	WILO Top S30/10
	Pump P5b	Grundfos UPE 32/120 F(B)
	Heat exchanger HX 45	Alfa-Laval CB 51-20H
	Heat transfer fluid	Water
	MID	Krohne ECOFLUX DN 25

The hydraulic design of the collector field can be seen in Figure 8.1.1, technical data of the two collector types is given in Table 8.2.

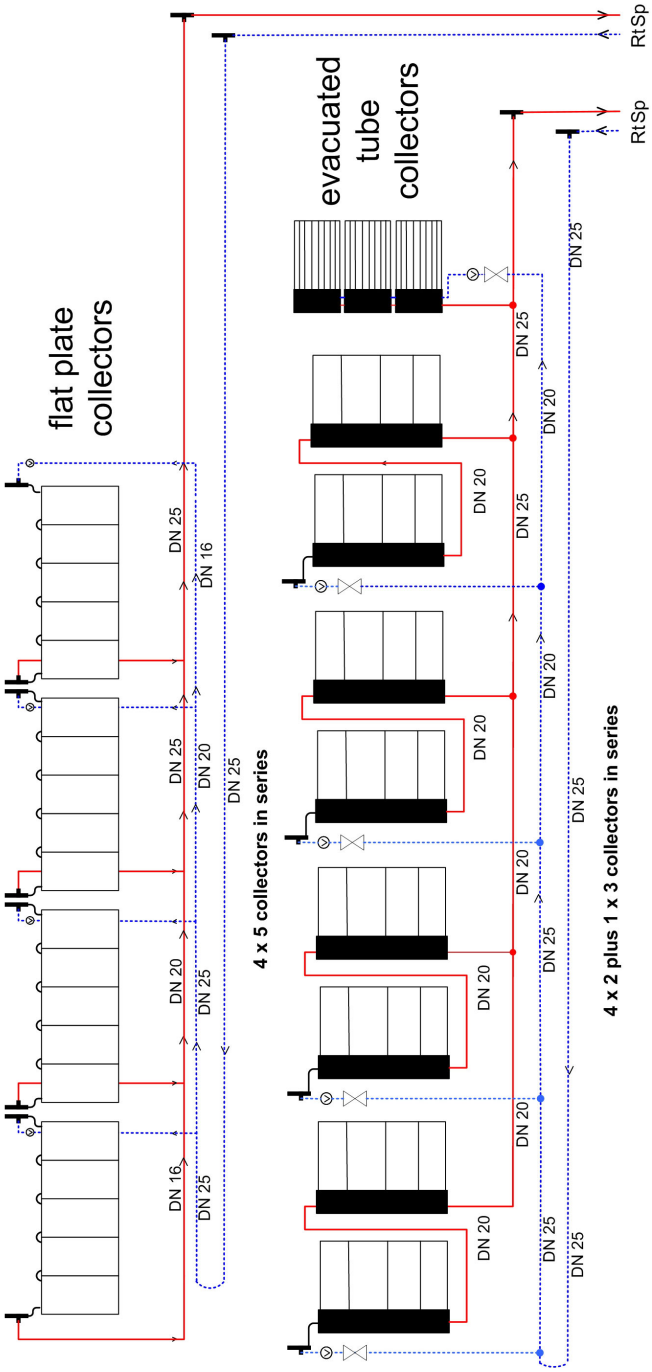

Figure 8.1.1 Design and piping of flat plate and evacuated tube collector fields. (Rt: return flow, Sp: supply flow)

Table 8.2. Technical data of collectors.

Parameter	Eurostar SI 24	Seido 2-16
Net absorber area	2.1 m²	2.78 m² (16 tubes)
Optical efficiency	0.78	n.A.
k1	3.54 W/m²K	n.A.
k2	0.0133 W/m²K²	n.A.
Dimensions (LxWxH)	2.0x1.18x0.11 m	2.11x1.92x0.125 m
Weight	46 kg	100 kg

8.2 Error analysis of system measurements

A detailed error analysis of the Phönix solar cooling system has been provided by Tamm in the course of a diploma thesis in parallel but separate to this thesis, co-supervised by the author [Tamm 2004]. All sensors used for energy balances and system control have been investigated with regard to systematic and statistical errors. This includes all PT100/PT1000 temperature sensors, all MID mass flow sensors and the pyranometer insolation sensor. All PT100 temperature sensors are 1/3 class B sensors according to German Industry Norm DIN IEC 751 and have been calibrated using an Isotech Venus 2140S Plus calibration device. Calibration temperatures of 0, 20, 65 and 120 °C were recorded for each sensor and compared to the respective reference temperature. The measured temperatures (degree Celsius) were then transformed into a resistance value (Ohms) according to German/European Industry Norm DIN EN 60751 using the following equation:

$$R = 100 \cdot \left(1 + 3.9083 \cdot 10^{-4} \cdot t_{cal} - 5.775 \cdot 10^{-8} \cdot t_{cal}^2\right) \qquad (8.2.1)$$

with R being the resistance value of the sensor $[\Omega]$ and t_{cal} being the recorded calibration temperature [°C] [DIN 1995]. The resistance values were then interpolated into a calibration curve of the form $T = f(R)$. This was necessary because the data acquisition unit measures the resistance of the temperature sensors in Ohms. The MID mass flow sensors and the pyranometer have not been individually calibrated; manufacturer data has been used instead. The pressure transducers are only being used for monitoring purposes and have also not been calibrated.

8.2.1 Systematic error

The determination of the systematic error of the energy balances has been made as follows. A number of measured values with an individual uncertainty

$$x_i = \bar{x}_i \pm \Delta x_i \quad (i=1\ldots n) \qquad (8.2.2)$$

is being used for the calculation of a parameter y.

$$\bar{y} = f(\bar{x}_1, \bar{x}_2, ..., \bar{x}_n) \qquad (8.2.3)$$

If $\Delta x_i \ll x_i$, a maximum uncertainty Δy of $\bar{y}$ can be calculated as

$$\Delta y = \left|\left(\frac{dy}{dx_1}\right)\right| \cdot \Delta x_1 + \left|\left(\frac{dy}{dx_2}\right)\right| \cdot \Delta x_2 + \ldots + \left|\left(\frac{dy}{dx_n}\right)\right| \cdot \Delta x_n \qquad (8.2.4)$$

Equation (8.2.4) does not consider possible compensation between single uncertainties which can be positive or negative.
For the calculation of an absolute mean uncertainty consisting of various single uncertainties it is thus reasonable to use instead of equation (8.2.4) the propagation theorem according to Gauß:

$$\Delta y = \sqrt{\left(\frac{dy}{dx_1}\cdot\Delta x_1\right)^2 + \left(\frac{dy}{dx_2}\cdot\Delta x_2\right)^2 + \ldots + \left(\frac{dy}{dx_n}\cdot\Delta x_n\right)^2} \qquad (8.2.5)$$

The maximum absolute uncertainty of $y = f(\bar{x}_i) = \bar{y} \pm \Delta y$ can now be calculated.

Equation (8.2.5) can be applied to the energy balance calculations. All calculations of energy amounts transferred through the system by a heat transfer medium follow the main equation

$$Q_{x,i} = \dot{V}_{x,i}\cdot\rho_{x,i}\cdot c_{p,x,i}\cdot\left(t_{x,in,i} - t_{x,out,i}\right)\cdot\hat{t}_{ts,i} \qquad (8.2.6)$$

where subscript *x* symbolizes a system circuit according to Figure 2.3.2 (K, B, AC…etc.). $Q_{x,i}$ is the energy amount transferred per time step $\hat{t}_{ts,i}$ at a heat exchanger in the system.

The energy transfer to the collectors via solar radiation is calculated according to

$$Q_{gt,i} = \dot{q}_{gt,i}\cdot A_{abs}\cdot\hat{t}_{ts,i} \qquad (8.2.7)$$

The calculation of the absolute mean uncertainty of equation (8.2.6) according to equation (8.2.5) reads as

$$\Delta Q_{x,i} = \sqrt{\begin{aligned}&\left(\frac{dQ_{x,i}}{d\dot{V}_{x,i}}\cdot\Delta\dot{V}_x\right)^2 + \left(\frac{dQ_{x,i}}{d\rho_{x,i}}\cdot\Delta\rho_x\right)^2 + \left(\frac{dQ_{x,i}}{dc_{px,i}}\cdot\Delta c_p\right)^2 \\ &+\left(\frac{dQ_{x,i}}{dt_{x,in,i}}\cdot\Delta t_{x,in}\right)^2 + \left(\frac{dQ_{x,i}}{dt_{x,out,i}}\cdot\Delta t_{x,out}\right)^2 + \left(\frac{dQ_{x,i}}{d\hat{t}_{ts,i}}\cdot\Delta\hat{t}_{ts}\right)^2\end{aligned}} \qquad (8.2.8)$$

Density and specific heat capacity are temperature-dependent parameters. They are being calculated as described in chapter 2.4. The error on a calculated value of ρ and c_p is very small compared to the error of the temperature measurements and can therefore be neglected [Tamm 2004]. The time interval of recorded data $\hat{t}_{ts,i}$ is determined by the data acquisition unit. It is also assumed to have no error. This reduces equation (8.2.8) to

$$\Delta Q_{x,i} = \sqrt{\left(\frac{dQ_{x,i}}{d\dot{V}_{x,i}} \cdot \Delta \dot{V}_x\right)^2 + \left(\frac{dQ_{x,i}}{dt_{x,in,i}} \cdot \Delta t_{x,in}\right)^2 + \left(\frac{dQ_{x,i}}{dt_{x,out,i}} \cdot \Delta t_{x,out}\right)^2} \qquad (8.2.9)$$

The partial differentials read

$$\frac{dQ_{x,i}}{d\dot{V}_{x,i}} = \rho_{x,i} \cdot c_{p,x,i} \cdot (t_{x,in,i} - t_{x,out,i}) \cdot \hat{t}_{ts,i} \qquad (8.2.10)$$

$$\frac{dQ_{x,i}}{dt_{x,in,i}} = \dot{V}_{x,i} \cdot \rho_{x,i} \cdot c_{p,x,i} \cdot \hat{t}_{ts,i} \qquad (8.2.11)$$

$$\frac{dQ_{x,i}}{dt_{x,out,i}} = -\dot{V}_{x,i} \cdot \rho_{x,i} \cdot c_{p,x,i} \cdot \hat{t}_{ts,i} \qquad (8.2.12)$$

Equation (8.2.9) can now be rewritten as

$$\Delta Q_{x,i} = \rho_{x,i} \cdot c_{p,x,i} \cdot \hat{t}_{ts,i} \cdot \sqrt{\left((t_{x,in,i} - t_{x,out,i}) \cdot \Delta \dot{V}_x\right)^2 + \left(\dot{V}_{x,i} \cdot \Delta t_{x,in}\right)^2 + \left(-\dot{V}_{x,i} \cdot \Delta t_{x,out}\right)^2} \qquad (8.2.13)$$

The error deviations $\Delta \dot{V}_x$, $\Delta t_{x,in}$ and $\Delta t_{x,out}$ can be found for each circuit in Appendix 8.3.

Equation (8.2.13) is the absolute uncertainty of $Q_{x,i}$. However, usually the relative uncertainty is being used. It is defined as

$$\frac{\Delta Q_{x,i}}{Q_{x,i}} = \sqrt{\left(\frac{\Delta \dot{V}_x}{\dot{V}_x}\right)^2 + \left(\frac{\Delta t_{x,in}}{t_{x,h,i} - t_{x,c,i}}\right)^2 + \left(\frac{-\Delta t_{x,out}}{t_{x,h,i} - t_{x,c,i}}\right)^2} \qquad (8.2.14)$$

It is visible in equation (8.2.14) that the error is indirect proportional to the temperature spread, not the absolute temperature. This is especially important in circuits where a small temperature spread occurs, such as the chilled water and the ceiling panel circuit. There, the uncertainties of sensors have a larger influence than in circuits with a bigger temperature spread.

Similarly to equation (8.2.13), the calculation of the mean uncertainty of equation (8.2.7) can be done.

$$\Delta Q_{gt,i} = \sqrt{\left(\frac{dQ_{gt,i}}{d\dot{q}_{gt,i}} \cdot \Delta \dot{q}_{gt}\right)^2 + \left(\frac{dQ_{gt,i}}{dA_{abs}} \cdot \Delta A_{abs}\right)^2} \qquad (8.2.15)$$

Again, the error on the time interval has been neglected here. The partial differentials read

$$\frac{dQ_{gt,i}}{d\dot{q}_{gt,i}} = A_{abs} \cdot \hat{t}_{ts,i} \qquad (8.2.16)$$

$$\frac{dQ_{gt,i}}{dA_{abs}} = \dot{q}_{gt,i} \cdot \hat{t}_{ts,i} \qquad (8.2.17)$$

The absolute error on radiation measurements can now be calculated as follows.

$$\Delta Q_{gt,i} = \hat{t}_{ts,i} \cdot \sqrt{\left(A_{abs} \cdot \Delta\dot{q}_{gt}\right)^2 + \left(\dot{q}_{gt,i} \cdot \Delta A_{abs}\right)^2} \qquad (8.2.18)$$

The uncertainty on the value of the absorber area ΔA_{abs} is estimated to be 0.1 m². The uncertainty on the radiation measurement can be found in Appendix 8.3.

The mean errors calculated in equations (8.2.13) and (8.2.18) are the errors on the energy amounts of each time step *i*. For the energy balances, integrated daily sums of transferred energy amounts are being calculated. In order to get an error deviation for the integrated sum, the individual errors of each time step *i* have to be integrated as well. This is being done using the arithmetic mean value of all individual errors according to equation (8.2.5).

$$\Delta Q_x = \frac{\Delta Q_{x,1} + \Delta Q_{x,2} + \ldots + \Delta Q_{x,n}}{n} \qquad (8.2.19)$$

where *n* is the number of time steps over which the sum is being integrated. For a daily energy balance ΔQ_x is the mean error.

For the comparison of different control strategies the yield factor has been introduced in chapter 4. It is calculated as

$$a = \frac{Q_E}{Q_{el}} \text{ [kWh}_{th}\text{ /kWh}_{el}\text{]}. \qquad (8.2.20)$$

where Q_{el} is the integrated power consumption of the system pumps and Q_E is the integrated cooling capacity over a defined time period. In analogy to the methodology described above the error on the yield factor can be calculated as

$$\Delta a = \sqrt{\left(\frac{1}{Q_{el}} \cdot \Delta Q_E\right)^2 + \left(\frac{-Q_E}{Q_{el}^2} \cdot \Delta Q_{el}\right)^2} \qquad (8.2.21)$$

The error ΔQ_E on the integrated cooling capacity Q_e is being calculated according to equation (8.2.13). The error ΔQ_{el} is 0.1 kWh. It is determined by the inaccuracy of the electricity meters used for power consumption measurements.

The COP is being calculated as

$$COP = \frac{Q_E}{Q_G} \qquad (8.2.22)$$

The error on the COP can be calculated in analogy and reads

$$\Delta COP = \sqrt{\begin{aligned} &\left(\frac{t_{Eh}-t_{Ec}}{\dot{V}_G\cdot(t_{Gh}-t_{Gc})}\cdot\Delta\dot{V}_E\right)^2+\left(\frac{\dot{V}_E}{\dot{V}_G\cdot(t_{Gh}-t_{Gc})}\cdot\Delta t_{Eh}\right)^2 \\ &+\left(\frac{-\dot{V}_E}{\dot{V}_G\cdot(t_{Gh}-t_{Gc})}\cdot\Delta t_{Ec}\right)^2+\left(\frac{\dot{V}_E\cdot(t_{Eh}-t_{Ec})}{\dot{V}_G^2\cdot(t_{Gh}-t_{Gc})}\cdot\Delta\dot{V}_G\right)^2 \\ &+\left(\frac{\dot{V}_E\cdot(t_{Eh}-t_{Ec})}{\dot{V}_G\cdot t_{Gh}^2}\cdot\Delta t_{Gh}\right)^2+\left(\frac{-\dot{V}_E\cdot(t_{Eh}-t_{Ec})}{\dot{V}_G\cdot t_{Gc}^2}\cdot\Delta t_{Gc}\right)^2 \end{aligned}} \qquad (8.2.23)$$

The error on the wet bulb temperature measurements has been experimentally determined by Wiegand. The measured values have been compared to those of a handheld humidity sensor (Model GFTH 200 of Greisinger Electronic GmbH) with an absolute uncertainty of ± 1%. A mean relative error of ± 2.4% was calculated for the wet bulb temperature measurements [Wiegand 2004].

The systematic uncertainties of each sensor used for energy balances and system control are displayed in summary in Appendix 8.3.

8.2.2 Statistical error

The statistical error is a random and unpredictable deviation of measurement values caused by fluctuation in the measurement apparatus. It can be calculated using the mean and the standard deviation. The mean $\bar{x}$ of n measurements with individual values x_i reads

$$\bar{x} = \frac{1}{n}\sum_{i=1}^{n} x_i \qquad (8.2.24)$$

Using the standard deviation, the mean error of the individual measurements s_x can be calculated as

$$s_x = \sqrt{\frac{1}{n-1}\sum_{i=1}^{n}(x_i - \bar{x})^2} \qquad (8.2.25)$$

The mean statistical error of the mean $\bar{x}$ then reads

$$\bar{s}_x = \frac{s_x}{\sqrt{n}} \qquad (8.2.26)$$

A case differentiation has to be made for the parameters of interest deducted from the experiments presented in this thesis. For the steady-state temperature step measurements presented in chapter 5.1.2, a statistical error can be calculated according to the method above. Each steady-state contains a sufficient number of measurement values which allows the determination of statistical fluctuations. For the temperature step measurements of the chiller, the total error presented is the quadratic sum of systematic and statistical error.

$$\Delta x_{tot} = \sqrt{(\Delta x)^2 + (\bar{s}_x)^2} \qquad (8.2.27)$$

However, this does not apply to the experimental energy balances presented in chapter 4.3.5. The integration of the thermal and electrical heat flows yields just one value per day. Each day has been recorded only one time and cannot be reproduced due to the individual character of the insolation. Furthermore, the measurements per day are highly transient. Stationary measurements with the solar cooling system at Phönix have not been performed during the course of this thesis. Therefore the magnitude of the statistical error cannot be determined for the energy balances presented. Even the statistical error determined for the chiller temperature measurements in chapter 3.2.2.3 cannot be used, as the apparatus of the chiller temperature measurements was a different one.

The order of magnitude of the statistical error can however be estimated from the transient measurements. Figure 8.2.1 shows part of the INSOL temperature measurements (visible in total in Figure 4.3.12). Figure 8.2.2 shows part of the corresponding heat flows of this experimental run as well as the global insolation. It is visible that the fluctuations which occur are in the order of magnitude of the graph symbols. It cannot be stated whether the origin of these fluctuations is related to statistical or systematic effects. However, the fluctuations are in an order of magnitude that makes the systematic error determined in chapter 8.2.1 the dominant one. For the energy balances, the total error presented is the systematic error. The statistical error has been neglected.

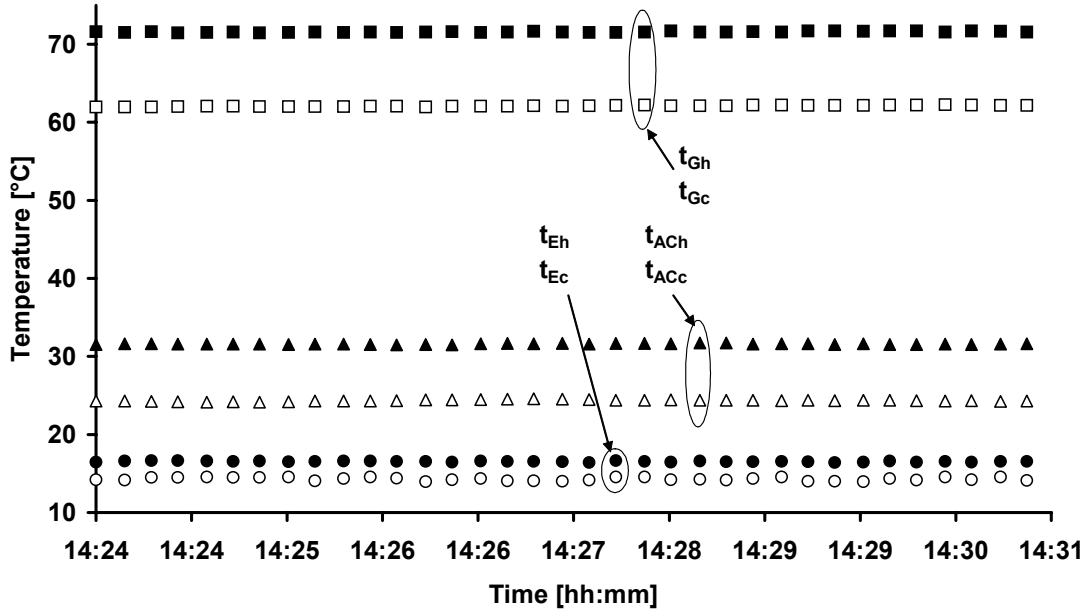

Figure 8.2.1. External chiller temperatures of INSOL. Refer to Figure 2.3.2 for parameter names. The figure is not a steady-state measurement.

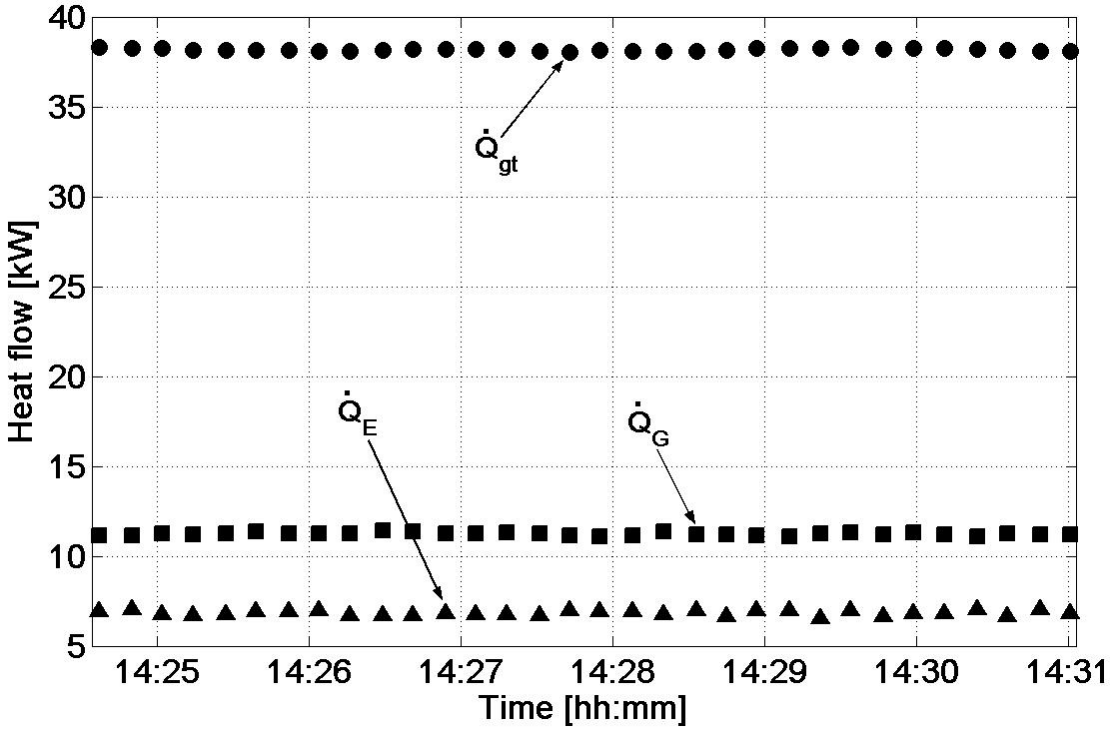

Figure 8.2.2. External heat flows corresponding to Figure 8.2.1. Refer to Figure 2.3.2 for parameter names. The figure is not a steady-state measurement.

8.3 List of system parameters

Circuit	Nr	Name Sensor	Name Actuator	Description	Output Sensor	Output Actuator
Solar	1	q_gt		Global insolation on absorber plane of collectors 35°	0-10 VDC	
	2	q_gh		Global insolation on horizontal plane 0°	0-10 VDC	
	3	p_MAGFK		Membrane expansion tank pressure flat plate collectors	0-10 VDC	
	4	p_MAGVK		Membrane expansion tank pressure evacuated tube collectors	0-10 VDC	
	5	t_MAGFK		Membrane expansion tank inlet temperature flat plate collectors	PT 1000	
	6	t_MAGVK		Membrane expansion tank inlet temperature evacuated tube collectors	PT 1000	
	7	t_FK1o		Outlet temperature flat plate collectors subfield 1	PT 1000	
	8	t_FK2o		Outlet temperature flat plate collectors subfield 2	PT 1000	
	9	t_FK3o		Outlet temperature flat plate collectors subfield 3	PT 1000	
	10	t_FK4o		Outlet temperature flat plate collectors subfield 4	PT 1000	
	11	t_VK1o		Outlet temperature evacuated tube collectors subfield 1	PT 1000	
	12	t_VK2o		Outlet temperature evacuated tube collectors subfield 2	PT 1000	
	13	t_VK3o		Outlet temperature evacuated tube collectors subfield 3	PT 1000	
	14	t_VK4o		Outlet temperature evacuated tube collectors subfield 4	PT 1000	
	15	t_VK5o		Outlet temperature evacuated tube collectors subfield 5	PT 1000	
	16	t_aussen		Ambient temperature measured on roof	PT 1000	
	17	t_Kh		Outlet (feed) temperature of collector field	PT 100	
	18	t_Kc		Inlet (return) temperature of collector field	PT 100	
	19	V_K		Volume flow of solar circuit	4...20 mA	
	20		Y_KP1	On/off signal for collector field pump P1		Relay
	21		N_KP1	Pump speed of collector field pump P1		0-10 VDC
Storage	22	t_Bh		Outlet temperature of heat exchanger	PT 100	
	23	t_Bc		Inlet temperature of heat exchanger	PT 100	
	24	V_B		Volume flow of storage circuit	4...20 mA	
	25		Y_BP2	On/off signal for storage pump P2		Relay
	26		N_BP2	Pump speed of storage pump P2		0-10 VDC
	27	t_PS1		Temperature storage tank Layer 1	PT 1000	
	28	t_PS2		Temperature storage tank Layer 2	PT 1000	
	29	t_PS3		Temperature storage tank Layer 3	PT 1000	
	30	t_PS4		Temperature storage tank Layer 4	PT 1000	
	31	t_PS5		Temperature storage tank Layer 5	PT 1000	
	32	t_Stc		Inlet temperature of storage tank	PT 1000	
	33	t_Sth		Outlet temperature of storage tank	PT 1000	
Hot water	34	V_G		Volume flow of hot water circuit before valve DWM 3	4...20 mA	
	35	V_Ge		Volume flow of hot water circuit after valve DWM 3 (through chiller)	4...20 mA	
	36	t_Gh		Hot water inlet (feed) temperature of chiller	PT 100	
	37	t_Gc		Hot water outlet (return) temperature of chiller	PT 100	
	38		VE_G	Position of three-way valve DWM 3 (0-100% admixture)		0-10 VDC
	39	Y_VEG		Feedback signal of position three-way valve DWM 3	0-10 VDC	
	40		Y_GP3	On/off signal for hot water pump P3		Relay
	41		N_GP3	Pump speed of hot water pump P3		0-10 VDC
Cooling water	42	V_ACe		Cooling water flow after valve DWM 4 (through chiller)	4...20 mA	
	43	V_AC		Cooling water flow before valve DWM 4	4...20 mA	
	44	t_ACc		Inlet (feed) temperature of cooling water in chiller	PT 100	
	45	t_ACh		Outlet (return) temperature of cooling water from chiller	PT 100	
	46		VE_AC	Position of three-way valve DWM 4 (0-100% admixture)		0-10 VDC
	47	Y_VEAC		Feedback signal of position three-way valve DWM 4	0-10 VDC	
	48		Y_ACP4	On/off signal for cooling water pump P4		Relay
	49		N_BP4	Pump speed of cooling water pump P4		0-10 VDC
	50		N_KT	Fan speed of cooling tower		0-10 VDC
Chilled water and ceiling panels	51	t_Ec		Outlet temperature of chilled water from chiller	PT 100	
	52	t_Eh		Inlet temperature of chilled water in chiller	PT 100	
	53	V_E		Volume flow of chilled water through chiller		
	54	t_Ch		Inlet (feed) temperature of chilled water in ceiling panels	PT 100	
	55	t_Cc		Outlet (return) temperature of chilled water in ceiling panels	PT 100	
	56	V_C		Volume flow of chilled water through ceiling panels	4...20 mA	
	57		Y_EP5ab	On/off signal for chilled water pumps P5a and P5b		Relay
Power & water	58	V_KT		Water consumption of cooling tower	Liter	
	59	P_S		Power consumption of P1 and P2	kWh	
	60	P_AKA		Power consumption of chiller	kWh	
	61	P_KT		Power consumption of cooling tower fan	kWh	
	62	P_EXT		Power consumption of P3, P4, P5a and P5b	kWh	
Building and ambient conditions	63	t_VB		Room temperature 1	PT 100	
	64	t_TK		Room temperature 2	PT 100	
	65	t_FE		Room temperature 3	PT 100	
	66	t_BZ		Room temperature 4	PT 100	
	67	y_VB		Feedback of position shut-off valve Room 1	0-30 VAC	
	68	y_TK		Feedback of position shut-off valve Room 2	0-30 VAC	
	69	y_FE		Feedback of position shut-off valve Room 3	0-30 VAC	
	70	y_BZ		Feedback of position shut-off valve Room 4	0-30 VAC	
	71	t_wetbulb		Wet bulb temperature measured on roof	PT 100	
	72	t_Amb		Room temperature Laboratory (Chiller location)	PT 100	

Uncertainties of system parameters (M: manufacturers data, C: calibrated data)

Circuit	Nr	Name Sensor	Type	Error deviation	Source
Solar	1	q_gt	Kipp & Zonen CM11	± 3 %	M
	2	q_gh	Kipp & Zonen CM3	± 10 %	M
	3	p_MAGFK	Schmidt	± 0.5 %	M
	4	p_MAGVK	Schmidt	± 0.5 %	M
	5	t_MAGFK	Class B PT 1000	0.3 + 0.005 |t| °C	M
	6	t_MAGVK	Class B PT 1000	0.3 + 0.005 |t| °C	M
	7	t_FK1o	Class B PT 1000	0.3 + 0.005 |t| °C	M
	8	t_FK2o	Class B PT 1000	0.3 + 0.005 |t| °C	M
	9	t_FK3o	Class B PT 1000	0.3 + 0.005 |t| °C	M
	10	t_FK4o	Class B PT 1000	0.3 + 0.005 |t| °C	M
	11	t_VK1o	Class B PT 1000	0.3 + 0.005 |t| °C	M
	12	t_VK2o	Class B PT 1000	0.3 + 0.005 |t| °C	M
	13	t_VK3o	Class B PT 1000	0.3 + 0.005 |t| °C	M
	14	t_VK4o	Class B PT 1000	0.3 + 0.005 |t| °C	M
	15	t_VK5o	Class B PT 1000	0.3 + 0.005 |t| °C	M
	16	t_aussen	1/3 Class B PT 100	± 0.4 %	C
	17	t_Kh	1/3 Class B PT 100	± 0.71 %	C
	18	t_Kc	1/3 Class B PT 100	± 1.35 %	C
	19	V_K	Ecoflux DN 15	V_K < 0.19 m³/h : (0.1272/V_K) %; V_K > 0.19 m³/h : 0.5 %	M
	20	-	-	-	-
	21	-	-	-	-
Storage	22	t_Bh	1/3 Class B PT 100	± 0.56 %	C
	23	t_Bc	1/3 Class B PT 100	± 0.55 %	C
	24	V_B	Ecoflux DN 15	V_B < 0.19 m³/h : (0.1272/V_B) %; V_B > 0.19 m³/h : 0.5 %	M
	25	-	-	-	-
	26	-	-	-	-
	27	t_PS1	Class B PT 1000	0.3 + 0.005 |t| °C	M
	28	t_PS2	Class B PT 1000	0.3 + 0.005 |t| °C	M
	29	t_PS3	Class B PT 1000	0.3 + 0.005 |t| °C	M
	30	t_PS4	Class B PT 1000	0.3 + 0.005 |t| °C	M
	31	t_PS5	Class B PT 1000	0.3 + 0.005 |t| °C	M
	32	t_Stc	Class B PT 1000	0.3 + 0.005 |t| °C	M
	33	t_Sth	Class B PT 1000	0.3 + 0.005 |t| °C	M
Hot water	34	V_G	Ecoflux DN 15	V_G < 0.19 m³/h : (0.1272/V_G) %; V_G > 0.19 m³/h : 0.5 %	M
	35	V_Ge	Ecoflux DN 15	V_Ge < 0.19 m³/h : (0.1272/V_Ge) %; V_Ge > 0.19 m³/h : 0.5 %	M
	36	t_Gh	1/3 Class B PT 100	± 0.58 %	C
	37	t_Gc	1/3 Class B PT 100	± 0.63 %	C
	38	-	-	-	-
	39	Y_VEG	-	-	-
	40	-	-	-	-
	41	-	-	-	-
Cooling water	42	V_ACe	Ecoflux DN 25	V_ACe < 0.53 m³/h : (0.1272/V_ACe) %; V_ACe > 0.53 m³/h : 0.5 %	M
	43	V_AC	Ecoflux DN 25	V_AC < 0.53 m³/h : (0.1272/V_AC) %; V_AC > 0.53 m³/h : 0.5 %	M
	44	t_ACc	1/3 Class B PT 100	± 0.50 %	C
	45	t_ACh	1/3 Class B PT 100	± 0.44 %	C
	46	-	-	-	-
	47	Y_VEAC	-	-	-
	48	-	-	-	-
	49	-	-	-	-
	50	-	-	-	-
Chilled water and ceiling panels	51	t_Ec	1/3 Class B PT 100	± 0.54 %	C
	52	t_Eh	1/3 Class B PT 100	± 0.86 %	C
	53	V_E	Ecoflux DN 25	V_E < 0.53 m³/h : (0.1272/V_E) %; V_E > 0.53 m³/h : 0.5 %	M
	54	t_Ch	1/3 Class B PT 100	± 0.52 %	C
	55	t_Cc	1/3 Class B PT 100	± 0.59 %	C
	56	V_C	Ecoflux DN 25	V_C < 0.53 m³/h : (0.1272/V_C) %; V_C > 0.53 m³/h : 0.5 %	M
	57	-	-	-	-
Power & water	58	V_KT	Techem aquapuls 10		
	59	P_S	Class 1		
	60	P_AKA	Class 1		
	61	P_KT	Class 1		
	62	P_EXT	Class 1		
Building and ambient conditions	63	t_VB	1/3 Class B PT 100	± 0.42 %	C
	64	t_TK	1/3 Class B PT 100	± 0.06 %	
	65	t_FE	1/3 Class B PT 100	± 0.48 %	
	66	t_BZ	1/3 Class B PT 100	± 2.44 %	
	67	y_VB	-	-	-
	68	y_TK	-	-	-
	69	y_FE	-	-	-
	70	y_BZ	-	-	-
	71	t_wetbulb	1/3 Class B PT 100	± 0.17 %	C
	72	t_Amb	1/3 Class B PT 100	± 0.64 %	C

8.4 List of internal chiller parameters

Circuit	Nr	Name Sensor	Name Actuator	Description	Output Sensor	Output Actuator
Chiller internal	73	t_AoCi		Temperature of cooling water between absorber and condenser	PT 100	
	74	m_Sr		Mass flow of solution	4-20mA	
	75	V_Sr		Volume flow of solution	4-20mA	
	76	V_R		Volume flow refrigerant	4-20mA	
	77	D_Sr		Density of solution	4-20mA	
	78	T_AoSr		Temperature of weak solution leaving absorber	PT 100	
	79	T_GiSr		Temperature of weak solution entering generator	PT 100	
	80	T_GoSw		Temperature of strong solution leaving generator	PT 100	
	81	T_AiSw		Temperature of strong solution entering absorber	PT 100	
	82	T_As		Temperature absorber sump	PT 100	
	83	T_USGo		Temperature of U-tube solution generator outlet	PT 100	
	84	T_USAi		Temperature of U-tube solution absorber inlet	PT 100	
	85	T_Ks		Temperature of condenser sump	PT 100	
	86	T_UREi		Temperature of U-tube refrigerant evaporator inlet	PT 100	
	87	T_Ei		Temperature of refrigerant distribution vessel	PT 100	
	88	T_Es		Temperature of evaporator sump	PT 100	
	89	T_Gs		Temperature of generator sump	PT 100	
	90	p_E		Pressure Absorber-Evaporator	4-20mA	
	91	p_C		Pressure Generator-Condenser	4-20mA	
	92	p_spi		Pressure of liquid column on solution pump inlet	4-20mA	
	93	p_spo		Head of solution pump	4-20mA	
	94	p_rpi		Pressure of liquid column on refrigerant pump inlet	4-20mA	
	95		Y_SP	On/off signal for solution pump P6		Relay
	96		N_SP	Pump speed of solution pump P6		0-10 VDC
	97		Y_RP	On/off signal for refrigerant pump P7		Relay
	98		Y_MV1	Open/close signal for magnetic shut-off valve MV1		Relay

Uncertainties of chiller parameters

(M: manufacturers data, C: calibrated data)

Circuit	Nr	Name Sensor	Type	Error deviation	Source
Chiller internal	73	t_AoCi	1/3 Class B PT 100	1/3 (0.3 + 0.005 |t|) °C	M
	74	m_Sr	Danfoss DN 15	$m\_Sr < 78g/s : 0.1\%$ $m\_Sr > 78g/s : \sqrt{0.1^2 + \frac{66}{m\_Sr}}\%$	M
	75	V_Sr	Danfoss DN 15	$V\_Sr < 184l/h : 0.1\%$ $V\_Sr > 184l/h : \sqrt{0.1^2 + \frac{66}{V\_Sr}}\%$	M
	76	V_R	Ecoflux DN 10	V_R < 80 l/h : (56.48/V_R) %; V_R > 80 l/h : 0.5 %	M
	77	D_Sr	Danfoss DN 15	± 0.0005 g/cm³	M
	78	T_AoSr	1/3 Class B PT 100	1/3 (0.3 + 0.005 |t|) °C	M
	79	T_GiSr	1/3 Class B PT 100	1/3 (0.3 + 0.005 |t|) °C	M
	80	T_GoSw	1/3 Class B PT 100	1/3 (0.3 + 0.005 |t|) °C	M
	81	T_AiSw	1/3 Class B PT 100	1/3 (0.3 + 0.005 |t|) °C	M
	82	T_As	1/3 Class B PT 100	1/3 (0.3 + 0.005 |t|) °C	M
	83	T_USGo	1/3 Class B PT 100	1/3 (0.3 + 0.005 |t|) °C	M
	84	T_USAi	1/3 Class B PT 100	1/3 (0.3 + 0.005 |t|) °C	M
	85	T_Ks	1/3 Class B PT 100	1/3 (0.3 + 0.005 |t|) °C	M
	86	T_UREi	1/3 Class B PT 100	1/3 (0.3 + 0.005 |t|) °C	M
	87	T_Ei	1/3 Class B PT 100	1/3 (0.3 + 0.005 |t|) °C	M
	88	T_Es	1/3 Class B PT 100	1/3 (0.3 + 0.005 |t|) °C	M
	89	T_Gs	1/3 Class B PT 100	1/3 (0.3 + 0.005 |t|) °C	M
	90	p_E	E&H PMC 131	± 0.5 %	M
	91	p_C	E&H PMC 131	± 0.5 %	M
	92	p_spi	E&H PMC 131	± 0.5 %	M
	93	p_spo	E&H PMC 131	± 0.5 %	M
	94	p_rpi	E&H PMC 131	± 0.5 %	M
	95	-	-	-	-
	96	-	-	-	-
	97	-	-	-	-
	98	-	-	-	-

8.5 Manufacturer data of Tyfocor LS

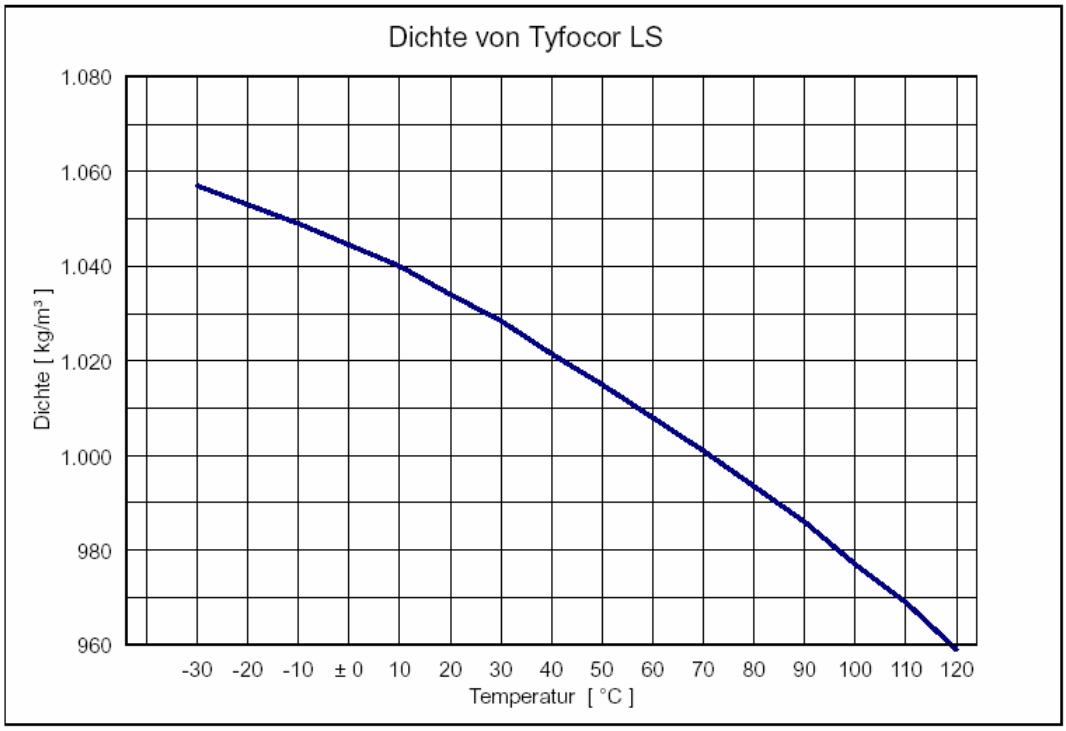

Figure 8.5.1. Density [kg/m³, ordinate] of Tyfocor LS displayed versus temperature [°C, abscissa].

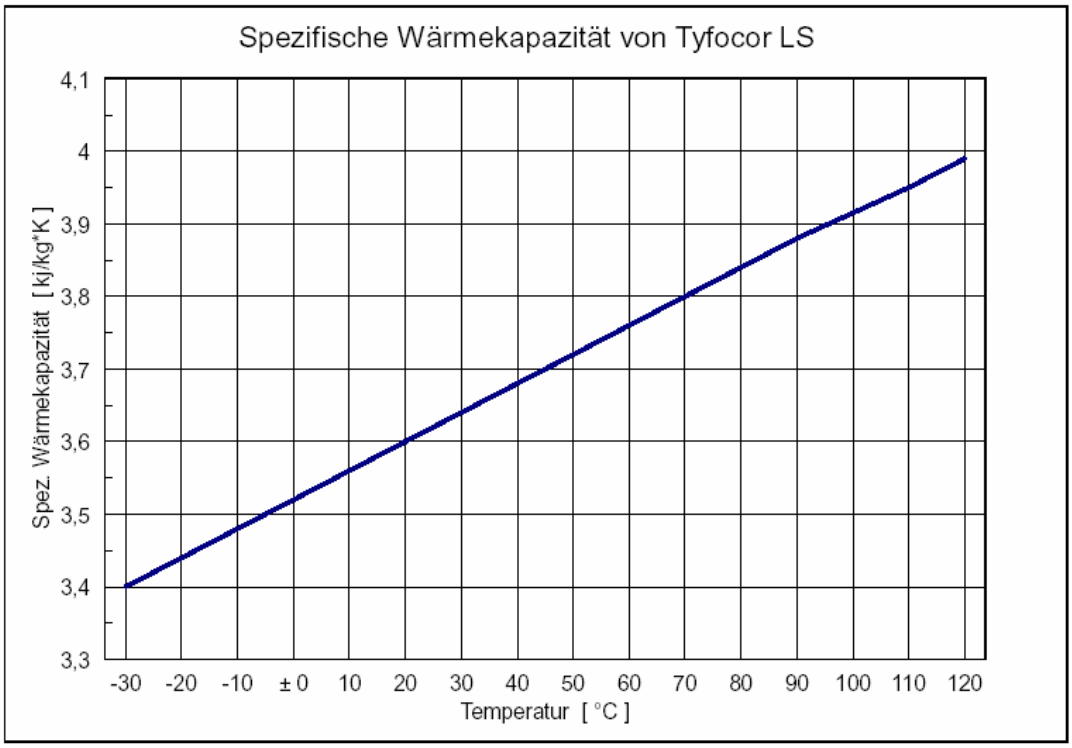

Figure 8.5.2. Specific heat capacity [kJ/kgK, ordinate] of Tyfocor LS displayed versus temperature [°C, abscissa].

8.6 Determination of limits for chilled water control

Using the experimentally determined transfer function G_{vc}, a PI-controller has been designed. The methodology of the controller development has been performed for the solar cooling system but shall not be described in detail here. It can be found in detailed description in a technical report of Phönix SonnenWärme AG [Clauss and Kohlenbach 2004].

The general equation for a PI-controller reads

$$F = K \cdot \left(1 + \frac{1}{T_i \cdot s}\right), \qquad (8.6.1)$$

with K being the proportional coefficient and T_i the integral coefficient. Getting to know the behaviour of the control loop is important before using it in a practical application. The quality of control can be evaluated by applying sudden changes or steps on the input and output values of the controller in a closed loop. The reaction of the controller on these input/output changes needs to be tested before using the controller. In order to test the quality of the PI-controller, closed simulation loops have been built in MATLAB/Simulink. The forced response as well as the disturbance response to a unity step can be simulated using the Simulink loops shown in Figure 8.6.1.

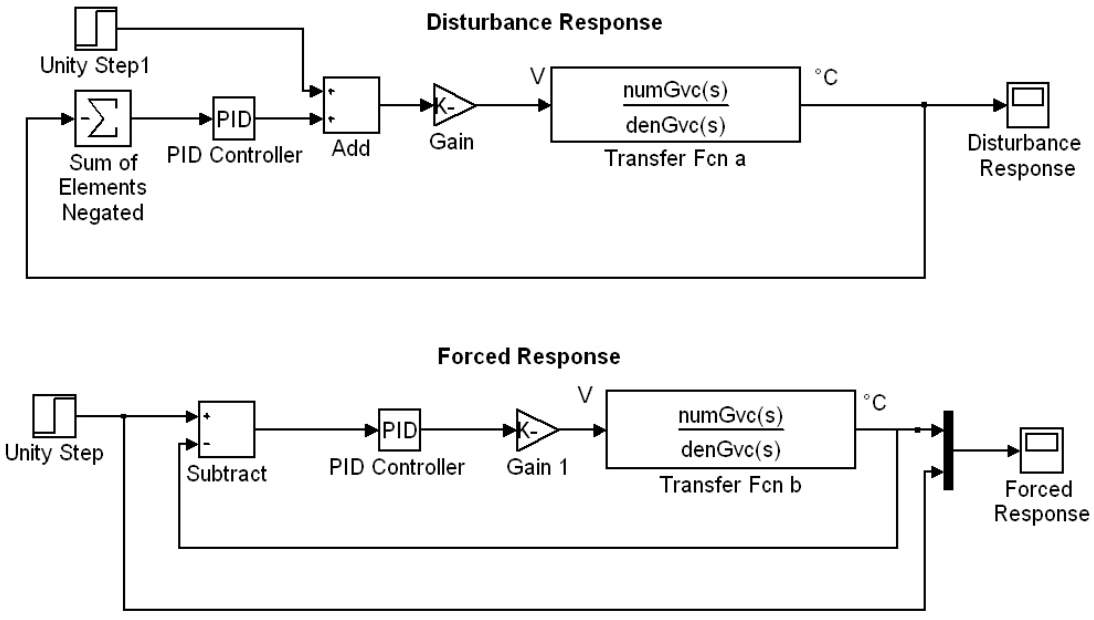

Figure 8.6.1. Closed simulation loops for forced and disturbance response simulation.

The upper loop simulates the disturbance response; the lower loop simulates the forced response for a unity step. Both loops use a PID controller block with the following parameters:

$$\begin{aligned} \textit{Proportional:} &\quad \textit{1.47} \\ \textit{Integral:} &\quad \textit{1/89} \\ \textit{Differential:} &\quad \textit{0.0} \end{aligned} \qquad (8.6.2)$$

These parameters are the result of the controller design. Both loops also use the transfer function G_{vc} as the model for the controlled system, expressed by the coefficients of numerator and denumerator in equation (3.2.2). A gain block with a negative gain of -1 had to be implemented before the transfer function block to prevent positive feedback due to the negative value of K_{vc}. Using a unity step as input yields the following plots of the disturbance response and the forced response.

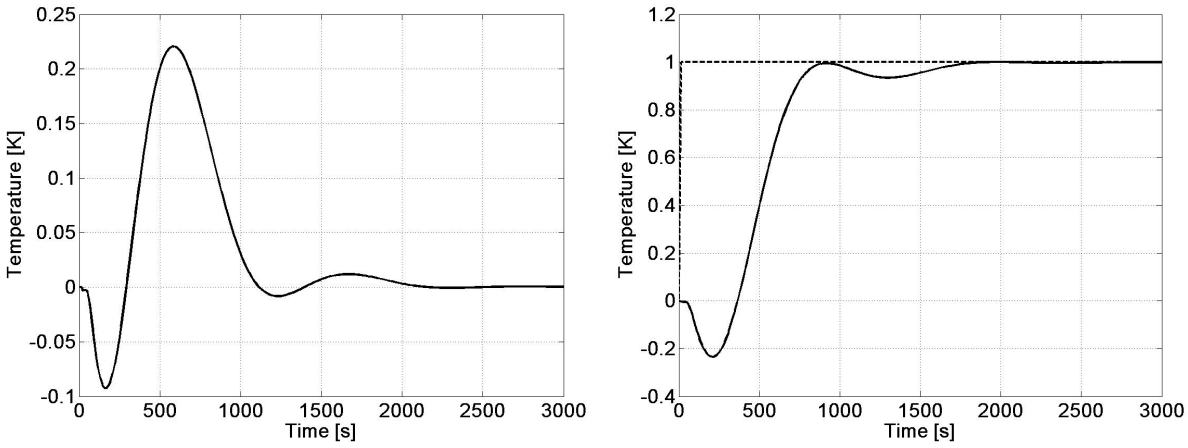

Figure 8.6.2. Disturbance response (left) and forced response (right) plots for testing closed-loop controller behaviour.

Figure 8.6.2 shows the results of closed-loop controller tests. The left plot shows the disturbance response for a unity step added to the controller output. The controller has to equalize the disturbance and restore original stable operation. It can be seen in the left plot that a disturbance of 1V on the controller output results first in an undershoot of approx. 0.09K and then in an overshoot of approx. 0.22 K in the chilled water temperature. After approx. 2000 s the original operation state has been restored by the controller. The right plot of Figure 8.6.2 shows the forced response of the controller after adding a unity step on the controller set point. The controller has to follow the new set point and adjust its output value accordingly. It is visible that it takes approx.

1800 s for the controller to achieve stable operation at the new set point. There is no overshoot but a slight undershoot of approx. 0.2K.

8.6.1 Experimental testing of controller

The control behaviour displayed in Figure 8.6.2 shows that stable operation in theory should be possible. However, a practical test has to be performed as well to make sure that theory and practice agree. The control parameters of equation (8.6.2) were implemented into the LabView-based control algorithm of the Phönix solar cooling system and experimental tests have been performed during 2004. Figure 8.6.3 shows the experimental data.

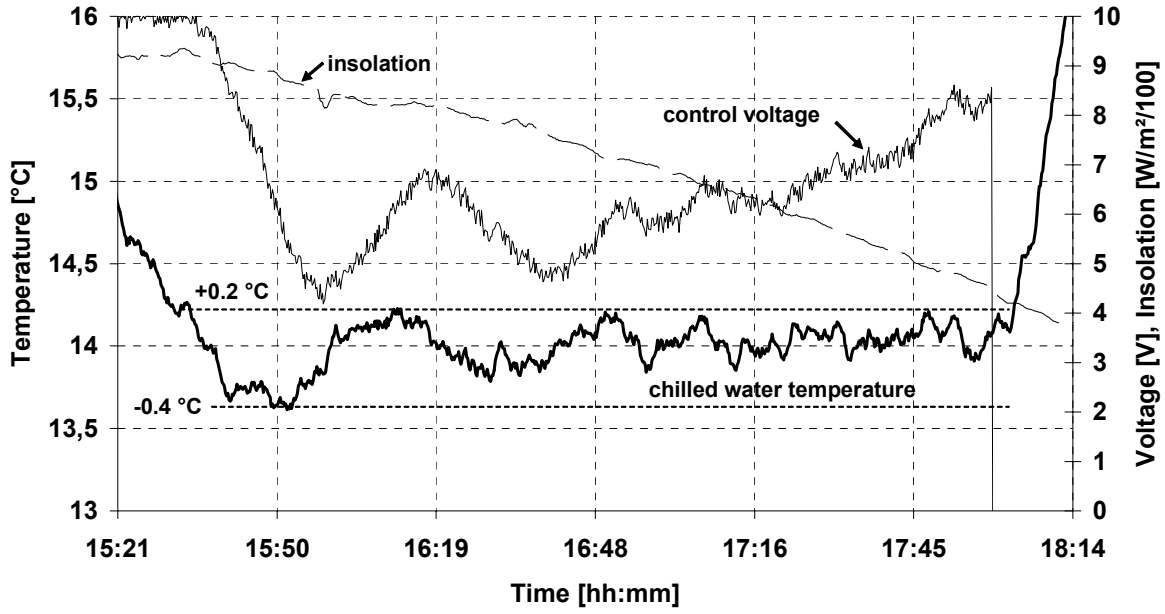

Figure 8.6.3. External chilled water outlet temperature (left ordinate), control voltage of valve DWM3 and global insolation divided by 100 (right ordinate).

The quality of the control can be seen in Figure 8.6.3. Displayed is the chilled water outlet temperature. Also shown is the control output voltage for the valve DWM3 and the global insolation which has been divided by 100 for display reasons. The figure shows the chilled water outlet temperature just after a setpoint change from 15 °C to 14 °C. After an initial equalisation period with an undershoot of –0.4 °C a stable chilled water outlet temperature can be seen. Fluctuations between 4:00 pm and 6:00 pm are in the range of ± 0.2 °C. The decreasing insolation results in increasing values of the valve control voltage and thus a decreasing recirculation rate. The control voltage of valve DWM3 varies between 4.5 and 8.5 V in order to maintain the temperature setpoint.

The undershoot and the decreasing amplitude of fluctuations after the setpoint change in Figure 8.6.3 is similar to the simulation in Figure 8.6.2, right plot. In the simulated forced response on a 1K setpoint change an undershoot as well as decreasing fluctuations can be seen. A new steady-state is being reached approximately 30 minutes after the step. In the experiment, a steady-state is not being reached due to the transient insolation. However, temperature fluctuations stay within a range of ±0.2 °C from approximately 4:00 pm onwards which can roughly be assumed as steady-state. The setpoint change was at 3:20 pm, therefore a time constant of 40 minutes applies in the experiment. This agrees quite well with the simulations and shows that the methodology of controller development is applicable.

8.6.2 Control limitations

The control development as described above resulted in finding a PI-controller for maintaining constant chilled water temperatures. The control has been tested in theory and practice with maximum deviations of 0.4 K around the setpoint observed. However, certain restrictions apply to the control use. The identification of the valve as described in chapter 5.1.1 is only valid for the temperatures and mass flows used in the identification process. Therefore the transfer function G_v can only be valid for this specific input data. The identification of the chiller has been performed for a temperature range from 65 to 95 °C and constant mass flows as well. For chiller operation outside this range the control behaviour has not been evaluated.

Nevertheless, estimations about the control behaviour at other than tested conditions can be made using the gain of the controlled systems 'valve' and 'chiller', K_v and K_c. While K_c has been experimentally determined over a reasonable temperature range, K_v has only been measured for one temperature level. Simulations with TRNSYS delivered maximum and minimum values for K_v of 3 and 1.4, respectively. Table 8.3 shows the simulation results.

Table 8.3. Simulated values of steady-states using various recirculation rates for V3.

Data point	$t_{G,source}$	t_{Gc}	t_{Gh}	U_{V3}	$\dot{V}_A$	$\dot{V}_B$	$\dot{V}_{AB}$	ΔU	K	Origin
Unit	°C	°C	°C	V	m³/h	m³/h	m³/h	V	K/V	-
1	77	54	59.8	2.5	0.3	0.9	1.2	7.5	2.3	simulated
2	90	59.7	67.3	2.5	0.3	0.9	1.2	7.5	3.0	simulated
3	60	46.3	49.7	2.5	0.3	0.9	1.2	7.5	1.4	simulated
4	85	57.5	64.4	2.5	0.3	0.9	1.2	7.5	2.8	simulated
5	67	49.5	53.9	2.5	0.3	0.9	1.2	7.5	1.8	simulated
6	77	53.4	58	2.5	0.25	0.95	1.2	7.5	2.5	measured

The volume flows $\dot{V}_A$, $\dot{V}_B$ and $\dot{V}_{AB}$ in Table 8.3 refer to the in- and outputs of the three-way valve V3. Figure 8.6.4 shows the characteristic diagram of V3.

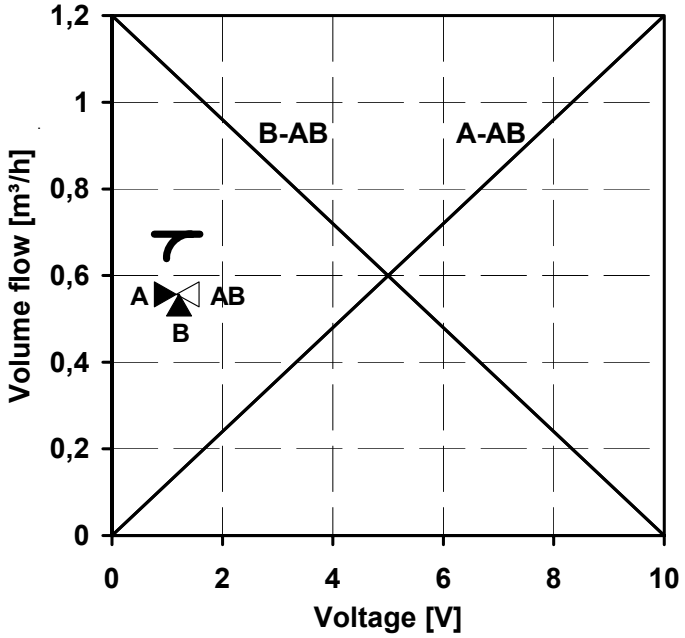

Figure 8.6.4. Characteristic diagram of valve V3/DWM 3.

In order to test the control behaviour of the whole system at these maximum and minimum values, closed-loop simulations were performed. The experimentally measured value of K_v was 2.5 K/V. A new transfer function of the valve with maximum gain $K_{v,max}$ = 3.0 K/V can be calculated as

$$G_{v,\max} = G_v \cdot \frac{K_{v,\max}}{K_v} = G_v \cdot 1.2 \qquad (8.6.3)$$

The gain of the controlled system of $G_{v,max}$ increases by 20% compared with G_v. In analogy the transfer function with minimum gain $K_{v,min}$ =1.4 K/V can be calculated as

$$G_{v,\min} = G_v \cdot \frac{K_{v,\min}}{K_v} = G_v \cdot 0.56 \qquad (8.6.4)$$

The gain of the controlled system of $G_{v,min}$ decreases by 44% compared with G_v. The new transfer functions of the whole system can now be calculated. The step response for a unity step of all three transfer functions of the whole system is shown in Figure 8.6.5.

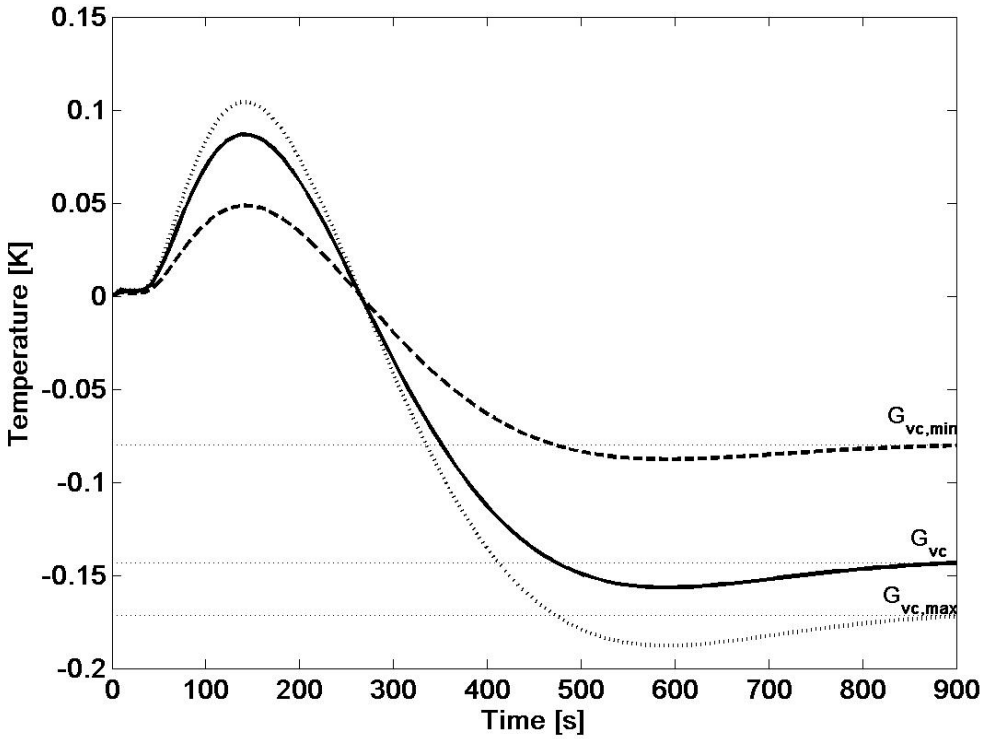

Figure 8.6.5. Step responses of minimum (dashed line), normal (solid line) and maximum (dotted line) transfer functions of the whole system.

It can be seen in Figure 8.6.5 that temperature end values and overshoot of $G_{vc,max}$ and $G_{vc,min}$ differ from the end value of G_{vc}. The influence of this on the control behaviour of the closed-loop can again be simulated in MATLAB/Simulink using the same setup as shown in Figure 8.6.1. Instead of the transfer function G_{vc} now $G_{vc,max}$ and $G_{vc,min}$ are being used. Figure 8.6.6 shows an overview of all three transfer function models of the whole system with disturbance and forced response on unity step displayed.

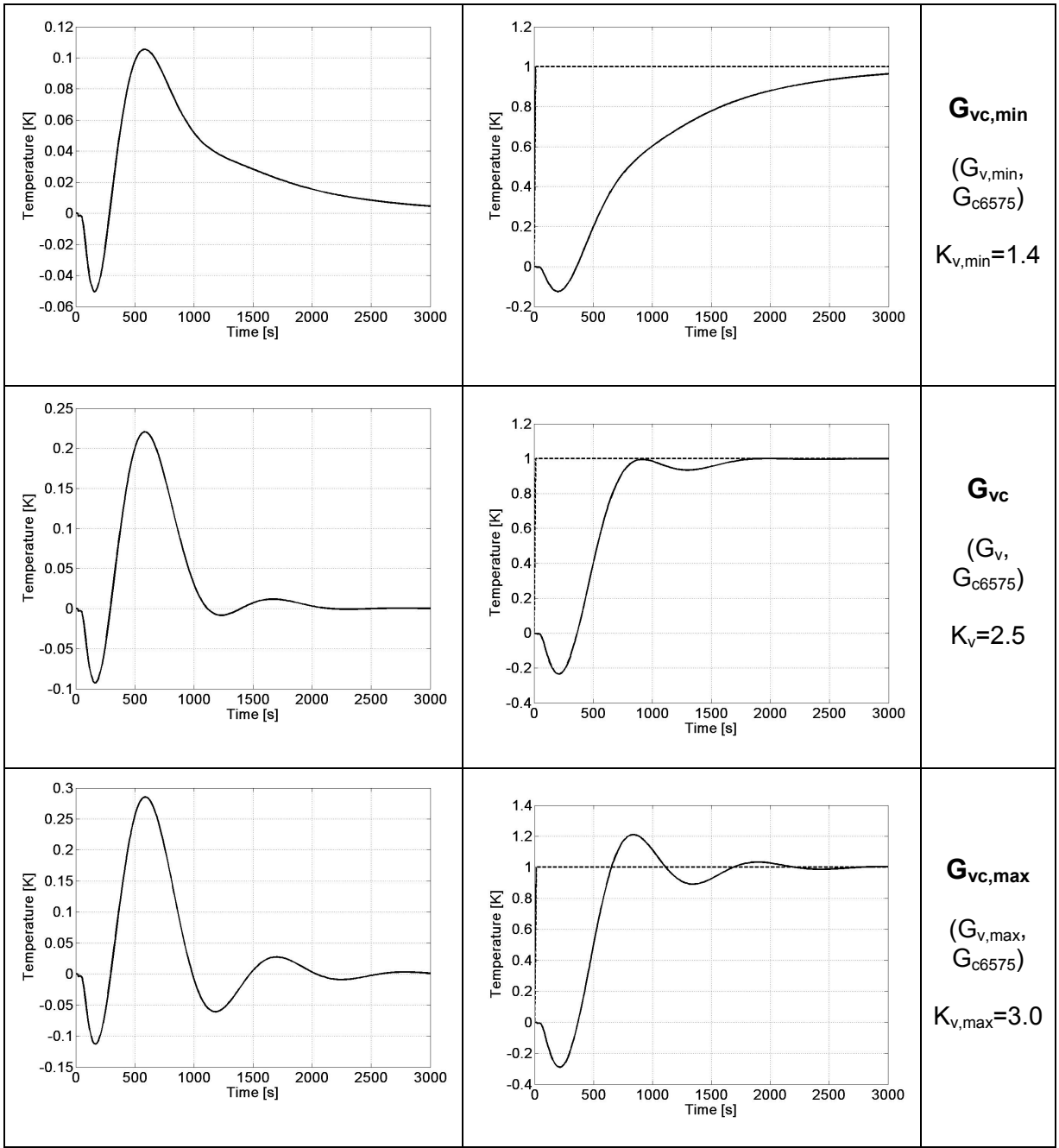

Figure 8.6.6. Disturbance (left) and forced (right) responses for models G_{vc}, $G_{vc,min}$ and $G_{vc,max}$.

The closed-loop control behaviour for varying gain of the controlled system is shown in Figure 8.6.6. The influence of the gain of the controlled system is clearly visible in the plots of disturbance and forced response. The smallest gain of 1.4 results in slow but stable control behaviour with long time constants. A disturbance of unity on the controller output needs over 3000s until it is

equalized. A setpoint change of unity also results in a time period over 3000s until the new output value is being reached.
The maximum gain of the controlled system of 3.0 results in larger overshooting of the output temperature. Compared to the G_{vc} model with no overshoot, $G_{vc,max}$ results in an overshoot of approx. 0.2K and more subsequent oscillations. The time until a disturbance of unity has been equalized is approx. 3000s. A forced setpoint change takes about 2500s until the new output has been reached stable.

In conclusion it can be stated that a variable gain of the controlled system 'valve' between 1.4 and 3.0 does not produce instabilities in the control behaviour. The quality of control however decreases and there are larger overshoots at gains other than 2.5. The control is nevertheless still applicable and will result in a stable behaviour. It can only be used on the Phönix solar cooling system as described in chapter 2.3.

8.7 Inputs, outputs and constant variables of the dynamic model

The MATLAB program requires the time period between two intervals, $\Delta\hat{t}$, as well as the number of simulation intervals, *n*, as inputs. Also required is an input matrix which contains the input temperatures t_{11}, t_{13} and t_{17}. In this matrix, all external variations (e.g. steps, ramps etc.) have to be set for the model. The program yields four output matrices containing temperature values (matrix T), concentration and pressure values (matrix Y), mass flows/mass storage terms (matrix MST) and external/internal heat flows (matrix Q).

Table 8.4. Input parameter of the dynamic model.

No.	Inputs	Unit	Description
1	$t_{11,i}$	°C	Generator hot water inlet temperature at time interval i
2	$t_{17,i}$	°C	Evaporator chilled water inlet temperature at time interval i
3	$t_{13,i}$	°C	Absorber cooling water inlet temperature at time interval i
4	$t_{18,i-1}$	°C	Evaporator chilled water outlet temperature at time interval i-1
5	$t_{16,i-1}$	°C	Condenser cooling water outlet temperature at time interval i-1
6	$t_{12,i-1}$	°C	Generator hot water outlet temperature at time interval i-1
7	$t_{14,i-1}$	°C	Absorber cooling water outlet temperature at time interval i-1
8	$\overline{T}_{E,i-1}$	°C	Internal mean temperature of Evaporator at time interval i-1
9	$\overline{T}_{C,i-1}$	°C	Internal mean temperature of Condenser at time interval i-1
10	$\overline{T}_{G,i-1}$	°C	Internal mean temperature of Generator at time interval i-1
11	$\overline{T}_{A,i-1}$	°C	Internal mean temperature of Absorber at time interval i-1
12	$x_{sol,w,G,i-c2}$	kg_{Salt}/kg_{Sol}	Solution concentration of Absorber sump at time interval i-c2
13	$x_{sol,s,A,i-c1}$	kg_{Salt}/kg_{Sol}	Solution concentration of Generator sump at time interval i-c1
14	$\dot{m}_{sol,s,i-c1}$	kg/s	Strong solution mass flow at time interval i-c1
15	$x_{s,G,i-1}$	kg_{Salt}/kg_{Sol}	Equilibrium concentration in Generator at time interval i-1
16	$x_{s,A,i-1}$	kg_{Salt}/kg_{Sol}	Solution concentration of Generator sump at time interval i-1
17	$x_{w,G,i-1}$	kg_{Salt}/kg_{Sol}	Solution concentration of Absorber sump at time interval i-1
18	$x_{w,A,i-1}$	kg_{Salt}/kg_{Sol}	Equilibrium concentration in Absorber at time interval i-1
19	$M_{st,sol,G,i-1}$	kg	Total mass in Generator sump at time interval i-1
20	$M_{st,sol,A,i-1}$	kg	Total mass in Absorber sump at time interval i-1
21	Δt	s	Time period between time intervals i and i-1

Table 8.5. Output parameter of the dynamic model.

No.	Outputs	Unit	Description
1	$t_{18,i}$	°C	Evaporator chilled water outlet temperature at time interval i
2	$t_{16,i}$	°C	Condenser cooling water outlet temperature at time interval i
3	$t_{12,i}$	°C	Generator hot water outlet temperature at time interval i
4	$t_{14,i}$	°C	Absorber cooling water outlet temperature at time interval i
5	$\overline{T}_{E,i}$	°C	Internal mean temperature of Evaporator at time interval i
6	$\overline{T}_{C,i}$	°C	Internal mean temperature of Condenser at time interval i
7	$\overline{T}_{G,i}$	°C	Internal mean temperature of Generator at time interval i
8	$\overline{T}_{A,i}$	°C	Internal mean temperature of Absorber at time interval i
9	$\dot{m}_{v,G,i}$	kg/s	Vapour mass flow from Generator to Condenser at time interval i
10	$\dot{m}_{v,A,i}$	kg/s	Vapour mass flow from Evaporator to Absorber at time interval i
11	$x_{s,G,i}$	kg_{Salt}/kg_{Sol}	Equilibrium concentration in Generator at time interval i
12	$x_{s,A,i}$	kg_{Salt}/kg_{Sol}	Solution concentration of Generator sump at time interval i
13	$x_{w,A,i}$	kg_{Salt}/kg_{Sol}	Equilibrium concentration in Absorber at time interval i
14	$x_{w,G,i}$	kg_{Salt}/kg_{Sol}	Solution concentration of Absorber sump at time interval i
15	$\dot{m}_{sol,tb,G,i}$	kg/s	Solution mass flow after tube bundle in Generator
16	$\dot{m}_{sol,tb,A,i}$	kg/s	Solution mass flow after tube bundle in Absorber
17	$m_{st,sol,G,i}$	kg	Stored solution in Generator sump at time interval i
18	$m_{st,sol,A,i}$	kg	Stored solution in Absorber sump at time interval i
19	z_i	m	Height of solution level in Generator sump at time interval i
20	$\dot{m}_{sol,s,i}$	kg/s	Strong solution mass flow at time interval i
21	$p_{G,i}$	Pa	Generator/Condenser pressure at time interval i
22	$p_{A,i}$	Pa	Evaporator/Absorber pressure at time interval i
23	$M_{st,sol,G,i}$	kg	Total solution mass in Generator at time interval i
24	$M_{st,sol,A,i}$	kg	Total solution mass in Absorber at time interval i

Table 8.6. Constant parameters of the dynamic model.

No.	Constants	Unit	Value	Description
1	$r_{(pc)}$	kJ/kgK	2450	Evaporation enthalpy of water
2	$l_{(pc)}$	kJ/kgK	272	Solution enthalpy of LiBr/water solution
3	$(UA)_{E,ext}$	kW/K	2.9	External UA value of Evaporator
4	$(UA)_{C,ext}$	kW/K	5.2	External UA value of Condenser
5	$(UA)_{G,ext}$	kW/K	4.0	External UA value of Generator
6	$(UA)_{A,ext}$	kW/K	3.2	External UA value of Absorber
7	$(UA)_{E,\mathrm{int}}$	kW/K	3.9	Internal UA value of Evaporator
8	$(UA)_{C,\mathrm{int}}$	kW/K	8.7	Internal UA value of Condenser
9	$(UA)_{G,\mathrm{int}}$	kW/K	4.3	Internal UA value of Generator
10	$(UA)_{A,\mathrm{int}}$	kW/K	3.2	Internal UA value of Absorber
11	$\dot{m}_{sol,w}$	kg/s	0.0559	Mass flow of weak solution
12	$\dot{m}_{hw}$	kg/s	0.3322	Mass flow of hot water
13	$\dot{m}_{cw}$	kg/s	0.7462	Mass flow of cooling water
14	$\dot{m}_{chw}$	kg/s	0.808	Mass flow of chilled water
15	A_t	m²	$4.9*10^{-4}$	Cross area of solution tube (DN 25)
16	h_0	m	0.1	height between solution outlet at Generator and inlet at Absorber
17	$M_{st,sol,G,start}$	kg	0.24	Accumulated solution in Generator sump
18	$M_{st,sol,A,start}$	kg	0.19	Accumulated solution in Absorber sump
19	ς	-	2100	Resistance coefficient of solution heat exchanger and piping
20	c_1	-	67	time constant for solution flow Generator to Absorber
21	c_2	-	61	time constant for solution flow Absorber to Generator
22	$(Mc_p)_{E,ext}$	kJ/K	6.8	Cumulated heat capacity of Evaporator, external
23	$(Mc_p)_{C,ext}$	kJ/K	6.4	Cumulated heat capacity of Condenser, external
24	$(Mc_p)_{G,ext}$	kJ/K	9.0	Cumulated heat capacity of Generator, external
25	$(Mc_p)_{A,ext}$	kJ/K	9.0	Cumulated heat capacity of Absorber, external
26	$(Mc_p)_{E,\mathrm{int}}$	kJ/K	38.4	Cumulated heat capacity of Evaporator, internal
27	$(Mc_p)_{C,\mathrm{int}}$	kJ/K	38.2	Cumulated heat capacity of Condenser , internal
28	$(Mc_p)_{G,\mathrm{int}}$	kJ/K	82.2	Cumulated heat capacity of Generator , internal
29	$(Mc_p)_{A,\mathrm{int}}$	kJ/K	81.9	Cumulated heat capacity of Absorber , internal
30	η_{SHX}	-	0.9	Efficiency of solution heat exchanger
31	cp_w	kJ/kgK	4.19	Specific heat capacity of liquid water

32	cp_v	kJ/kgK	1.86	Specific heat capacity of water vapour
33	$cp_{sol,s}$	kJ/kgK	3.8	Specific heat capacity of strong solution
34	$\rho_{sol,s}$	kg/m³	1600	Density of strong solution

8.8 Energy balances of experiments with different solar circuit controls

Table 8.7. Thermal energy balances

Strategy	Date dd:mm:yy	Q_{gt} [kWh_{th}]	Q_B [kWh_{th}]	Q_{st} [kWh_{th}]	Q_G [kWh_{th}]	Q_E [kWh_{th}]	Q_C [kWh_{th}]	Q_{AC} [kWh_{th}]
STAN	10.08.04	244.5 ± 7.4	99.9 ± 5.0	-2.6	97.3 ± 5.9	62.4 ± 2.8	61.1 ± 3.3	170.4 ± 4.2
TDIFF	02.09.04	126.3 ± 5.4	47.6 ± 2.5	4.8	39.2 ± 2.2	23.6 ± 1.8	22.8 ± 2.3	68.0 ± 3.1
INSOL	09.09.04	188.5 ± 5.7	74.1 ± 3.7	5.2	64.8 ± 2.4	39.5 ± 1.9	38.1 ± 2.3	111.3 ± 2.9

Table 8.8. Electrical energy balances

Strategy	Date dd:mm:yy	$Q_{el,P1,P2}$ [kWh_{el}]	$Q_{el,P3,P4,P5a/b}$ [kWh_{el}]	$Q_{el,chiller}$ [kWh_{el}]	Q_{ct} [kWh_{el}]	t_{op} [h]	t_{wb} [°C]
STAN	10.08.04	1.8 ± 0.1	9.6 ± 0.1	0.8 ± 0.1	2.2 ± 0.1	7.4	19.0 ± 0.5
TDIFF	02.09.04	0.8 ± 0.1	4.8 ± 0.1	0.6 ± 0.1	0.7 ± 0.1	3.9	21.3 ± 0.5
INSOL	09.09.04	1.4 ± 0.1	6.6 ± 0.1	0.7 ± 0.1	0.8 ± 0.1	5.6	11.2 ± 0.3

Table 8.9. Calculated variables

Strategy	Date dd:mm:yy	$Q_{el,c}$ [kWh_{el}]	$Q_{ct,c}$ [kWh_{el}]	η_{wb} [-]	η_{sol} [-]	$\eta_{solar-cold}$ [-]	COP [-]	a_e [kWh_{th}/kWh_{el}]
STAN	10.08.04	1.8 ± 0.1	2.4 ± 0.1	0.9	0.41 ± 0.02	0.26 ± 0.01	0.64 ± 0.05	14.7 ± 0.7
TDIFF	02.09.04	0.7 ± 0.1	0.7 ± 0.1	1.0	0.38 ± 0.03	0.19 ± 0.02	0.60 ± 0.06	17.5 ± 1.9
INSOL	09.09.04	1.1 ± 0.1	1.5 ± 0.2	0.5	0.39 ± 0.02	0.21 ± 0.01	0.61 ± 0.04	15.4 ± 1.0

8.9 Contents of CD-ROM

The following documents have been included electronically on the attached CD-ROM due to reasons of space. All simulation source codes, TRNSYS decks and electronic libraries have been programmed by Paul Kohlenbach, except otherwise stated. Commercial use of these files is prohibited. They can however be used for non-commercial research purposes with special permission of the author. For permission and questions or comments please write to: *pkohlenbach@gmx.de*

The TRNSYS files for the steady-state simulations of the absorption chiller are explained as follows. They have been programmed using TRNSYS 15. The file 'trnlib.dll' needs to be copied into the main directory of TRNSYS, all other files can be copied into a different directory.

Main simulation program:

- Type177_DWM3.TPF

This file is the IISiBat file for the steady-state TRNSYS simulations. It simulates chiller operation at various rates of recirculation of the three-way valve DWM3. For the standard TRNSYS shell, the following deck file can be used.

- TYPE177_Phönix.dck

The main TRNSYS library with all types being used is included in the file '**trnlib.dll**'. The simulation yields and output file "**datadwm3.txt**" which contains the numeric results of all external chiller circuits.

Also included is the TRNSYS type 177 which simulates the Phönix absorption chiller in steady-state operation. The folder "Documentation of Type 177" contains the source code of the type as a pro-forma object file which can be included into your TRNSYS library. Also included is an exemplary IISiBat file to demonstrate the functionality. Further, the documentation for the type 177 is included in pdf format. All contents in this folder have been programmed by Albers.

8.10 Publication list

Part of the research contained in this thesis has been published in journals or presented at national and international conferences. The first two publications of the following list are directly related to this thesis, the other publications are joint productions of the research project at Phönix SonnenWärme AG.

Wiegand E., Kohlenbach P., Kühn A., Petersen S., Ziegler F. „Entwicklung eines Nasskühlturms kleiner Leistungsklasse für den Einsatz in Systemen zum Solaren Kühlen“. Published in KI Luft- und Kältetechnik 10/2005.

Kohlenbach P., Clauß, V. „Vergleich verschiedener Strategien zur Regelung einer solarthermischen Anlage für den Einsatzzweck Solares Kühlen“. Presented at 15th OTTI-Symposium Thermische Solarenergie, Bad Staffelstein, Germany, 2005.

Kühn A., Harm M., Kohlenbach P., Petersen S., Schweigler C., Ziegler F. „Betriebsverhalten einer 10 kW Absorptionskälteanlage für niedrige Antriebstemperaturen“. Published in KI Luft- und Kältetechnik 7/2005.

Kohlenbach, P., Tamm, O., Schweigler, C., Harm, M., Albers, J., Kühn, A., and Petersen, S. "Entwicklung eines Systems zur solaren Kühlung im kleinen Leistungsbereich." Presented at 14th OTTI-Symposium Thermische Solarenergie, Bad Staffelstein, Germany, 2004.

Kühn A., Petersen S., Ziegler F., Kohlenbach P., Schweigler C., Harm M. „Performance of a 10 kW solar driven absorption chiller“. Presented at the 5th ISES Europe Solar Conference EuroSun 2004, Freiburg, Germany

Kohlenbach P., Harm M., Kühn A. „Solar Cooling System with Low Driving Temperature”. Presented at the Int. Conference on Improving Energy Efficiency in Commercial Buildings (IEECB) 2004, Frankfurt, Germany

List of Figures

List of Tables